CRANFIELD UNIVERSITY

Cranfield Biotechnology Centre

Graphene Modified Electrodes for Enhanced Electrochemical Detection

Nicholas John Walch

PhD Thesis

Supervisors:

Prof. S P J Higson
Prof. F Davis

January 2016

Acknowledgements

The author would like to thank the following individuals for their assistance during the course of this research: First and foremost Prof Seamus Higson, Dr Frank Davis, Dr Stuart Collyer, and Dr Jo Holmes for their invaluable experience and knowledge, Prof Alexei Nabok and Dr Simon Turega of Sheffield Hallam University for their input and assistance, and for the generous use of their lab facilities, Dr Licia Dossi of Cranfield Defence and Security for NMR help in the first year of the project, Dr Dan Evans for helping me design experiments and to continue to enjoy what I was doing even when things were going badly, Prof Sam Tothill and Dr Zeynep Altintas for their help adjusting to research and scientific writing, Kevin Osborne for his invaluable NMR knowledge and expertise, the technical staff at both Hallam and Cranfield Universities for all of their assistance in and out of the lab.

Finally and perhaps most importantly I would like to thank my parents and family for their unending support, without which none of this would have been possible.

"The term is over: The holidays have begun.

The dream is ended: This is the morning"

– Aslan, The Last Battle by C S Lewis

Rationale for Research

The detection of biomarkers for the early diagnosis of disease and biomedical monitoring is of increasing importance in the field of medicine. Many platforms for such detection already exist, however the cost to the end user or health service provider is often high and the expertise required to perform analyses only confounds this. What is needed are inexpensive and robust ways to quantify biomarkers that will allow point-of-care diagnosis for patients.

Since a point-of-care system typically cannot rely upon a great amount of sample preparation prior to analysis can be performed, the sensor platform must be able to differentiate between the target analyte and any other species that might be present in the sample. In the case of DNA quantification the sensor must be able to detect all four nucleotide bases individually and simultaneously. This means that some variety of specificity enhancing binding ligand must be incorporated into the sensor platform.

Antibody based sensors are one of the current industry standards for detection of a wide array of different compounds. However the production method used to give rise to an antibody against a specific compound of interest is generally very expensive and time consuming. Additionally there is the problem of antibody stability and longevity. Because of this, non-biological ligands will be considered for implementation within the sensor platform.

Electrochemical detection was chosen as the technical basis for the new sensor platform. This is largely because it provides an inexpensive and robust detection method that is both quantitative and qualitative. However it is not without its drawbacks; only certain analytes can be detected in this way, if they are able to be oxidised or reduced by an electrical potential. This limitation, however, does partly solve the specificity problem that exists when analysing mixtures of biological components since most other species present in the mixture are not electrochemically active.

Screen-printed carbon electrodes were chosen as a transducer substrate, as they drive the cost of the sensor down further. However a decreased electron transfer resistance at the electrode surface is preferable because it lowers the potential requirement for redox transformations to occur. Carbon is typically not an ideal electrode material, but the more conductive electrode surfaces (such as gold or platinum) are more expensive. Modification of the electrode surface with graphene will provide an inexpensive alternative to gold or platinum whilst offering a comparable performance.

Surfactant stabilised graphene will not only provide increased conductivity, but will also lower the surface tension of the sensor surface, resulting in greater surface contact and higher detection rates. Additionally lithographic graphene based electrodes have been shown to give simultaneous detection of all four nucleotide bases by a chromatography like separation of the peaks for each base molecule. However lithographic graphene is difficult to synthesise and requires the use of harsh chemicals. Therefore it was decided to investigate whether or not a similar effect could be observed using sonochemically produced graphene.

Calixarenes and resorcinarenes were chosen as binding ligands since they represent a non-biological binding ligand that is inexpensive to produce but can be modified extensively to subtly alter the binding kinetics. Strong guest-host binding has been demonstrated for complexes of these molecules with a variety of ligands, but *in-silico* modelling will be performed to design a suitable host molecule for this research. Water soluble calixarenes and resorcinarenes also have surfactant properties, with both hydrophobic and hydrophilic regions within the molecule. The surfactant properties can also be modified by changing upper and lower rim substituents. This particular characteristic of calixarenes and resorcinarenes will allow for their adsorption onto the surface of a graphene sheet, providing a perfect binding site for analyte molecules.

Abstract

The ability to inexpensively and reliably detect organic compounds is important across a multitude of different areas of science. Benzene ring functional groups are found in a wide variety of biological molecules, (such as amino acids, DNA nucleotide bases and blood based components). The qualification and quantification of these compounds in a sample has been achieved by techniques such as high performance liquid chromatography (HPLC), gas chromatography (GC), mass spectrometry (MS) and nuclear magnetic resonance (NMR), amongst others. These techniques, however, often require cumbersome, expensive equipment along with exhaustive sample preparation techniques and are thus not necessarily suitable for portable *in-situ* analysis of these compounds.

This thesis details the fabrication and characterisation of graphene modified electrodes that show an increased sensitivity towards biomolecular compounds such as dopamine, amino acids, and DNA. The graphene was synthesised using a novel semi-automated method which was performed using a bespoke apparatus designed to alleviate the labour involved in synthesising graphene by the sonochemical method. The method involved pumping an aqueous solution of the surfactant into a solution of graphite in water which was under constant sonication.

When used in an electrochemical system employing cyclic voltammetry the graphene modified electrodes showed not only a lower limit of detection in all cases, but also a shift in peak position which allowed for simultaneous quantification of mixtures of compounds. This could not be achieved with screen printed carbon electrodes alone as different peaks often occur at similar potentials, making it difficult or impossible to quantify these compounds individually. Slower scan rates can often give rise to separate peaks, however this adds time to the experiment which is not necessary with graphene modification.

The binding interactions of novel resorcinarene molecules were also predicted by molecular modelling techniques and then confirmed using NMR binding experiments. The resorcinarene was tested against a range of different analytes and showed a degree of specificity. The interaction between the two surfactant molecules and the graphene surface was also analysed to determine whether or not the resorcinarene molecules could be adsorbed onto graphene to produce a viable, molecularly specific electrode surface.

Table of Contents

List of Abbreviations

4NDP	4-nondecylpyridine
AC	Alternating Current
AFM	Atomic Force Microscopy
ASV	Absorptive Stripping Voltammetry
ATR	Attenuated Total Reflection
BR	calix[4]benzylresorcinarene
BR-	o-sulfonato calix[4]benzylresorcinarene
BR+	o-triethylammoniummethyl calix[4]benzylresorcinarene
BRDEA	o-diethylaminomethyl calix[4]benzylresorcinarene
BSA	Bovine Serum Albumin
CBS	Complete Basis Set
CCSD	Coupled Cluster Singles and Doubles
COSY	Correlation Spectroscopy
CTAB	Cetyl Trimethylammonium Bromide
CV	Cyclic Voltammetry
ddNTP	Dideoxynucleotide Triphosphate
DDR	calix[4]dodecylresorcinarene
DDR-	o-sulfonato calix[4]dodecylresorcinarene
DDR+	o-triethylammoniummethyl calix[4]dodecylresorcinarene
DDRDEA	o-diethylaminomethyl calix[4]dodecylresorcinarene
DEPT	Distortionless Enhancement by Polarisation Transfer
DLS	Dynamic Light Scattering
DNA	Deoxyribose Nucleic Acid
DPV	Differential Pulse Voltammogram
DSC	Differential Scanning Calorimetry
EDOT	3,4-ethylenedioxythiophene
EDX	Energy Dispersive X-Rays
EIS	Electrochemical Impedance Spectroscopy
FT	Fourier Transform
GABA	Gamma Aminobutyric Acid
GADock	Genetic Algorithm Docking Engine
GC	Gas Chromatography
HARP	High Aspect Ratio Process
HMBC	Heteronuclear Multiple-Bond Correlation Spectroscopy
HPLC	High Performance Liquid Chromatography
HSQC	Heteronuclear Single-Quantum Correlation Spectroscopy
ICP	Intrinsically Conducting Polymer
IR	Infrared
LB	Langmuir Blodgett
LBL	Layer-by-Layer
LC	Liquid Chromatography

LCD TV	Liquid Crystal Display Television
LS	Langmuir Schaefer
MALDI	Matrix Assisted Laser Desorption Ionisation
MM	Molecular Mechanics
MP2	Møller–Plesset Perturbation Theory
MS	Mass Spectrometry
NMR	Nuclear Magnetic Resonance
NOESY	Nuclear Overhauser Effect Spectroscopy
p	para (substitution)
P3OT	poly(3-octylthiophene-2,5-diyl)
PAH	Polyallylamine Hydrochloride
PANI	Polyaniline
PBS	Phosphate Buffered Saline
PCR	Polymerase Chain Reaction
PCS	Photon Correlation Spectroscopy
PEDOT	Poly-3,4-ethylenedioxythiophene
PEI	Polyethyleneimine
PM3	Parameterised Model Number 3
PPMMA-DMA	poly(methylmethacrylate-decylmethacrylate)
PPy	Polypyrrole
PSA	Prostate Specific Antigen
PSS	Polystyrene Sulfonic Acid
QM	Quantum Mechanics
RNA	Ribose Nucleic Acid
ROESY	Rotating Frame Nuclear Overhauser Effect Spectroscopy
RPM	Rotations Per Minute
SAM	Self-Assembled Monolayer
SCX4	p-sulfocalix[4]arene
SDF	Structural Data File
SDS	Sodium Dodecyl Sulfate
SEM	Scanning Electron Microscopy
SNP	Single Nucleotide Polymorphism
SPCE	Screen-Printed Carbon Electrode
SPR	Surface Plasmon Resonance
tert	Tertiary
TIRE	Total Internal Reflection Ellipsometry
TMS	Tetramethyl Silane
TNT	Trinitrotoluene
TOCSY	Total Correlation Spectroscopy
tRNA	Transfer Ribose Nucleic Acid
UFF	Universal Force Field
UV	Ultraviolet
VOC	Volatile Organic Contaminants
ZPVE	Zero Point Vibrational Energy

List of Figures

List of Tables

List of Publications

During the course of this PhD project several articles and conference posters have been published:

"*Enhancement of electrode performance by a simple casting method using sonochemically exfoliated graphene"* was published in Analytical Chemistry. It was based on the data given in Chapter 3 of this thesis. The text is given in Appendix 1 (Page 195).

"Characterisation of thin films of graphene-surfactant composites produced via a novel semi-automated method" was published in The Beilstein Journal of Nanotechnology. It was based on the data given in Chapter 2 of this thesis. The text is given in Appendix 2 (Page 211).

"Semi-automated sonochemical synthesis of graphene by continuous addition of aqueous surfactant" was presented at the 14th European Conference on Organised Films in 2015. It was based on the data given in Chapter 2 of this thesis. The design is given in Appendix 3 (Page 231).

Chapter 1 Introduction and Literature Review

1.1 Introduction

Sensors incorporating graphene or conducting polymers as a conductive base and calixarenes as a binding ligand will be investigated to see if an increase in sensitivity and selectivity can be gained. To explore the range of applications which are suitable for the implementation of calixarene based sensors, this research will focus on three separate groups of compounds that are of interest; blood based components, nucleotide bases, and amino acids. The chosen analytes are discussed here along with a rationale for why a new detection method is required. In addition to this, the relatively new conductive material graphene will be investigated to determine whether this provides a better conductive substrate than the more traditional conducting polymers. A combination of approaches will be employed, including cyclic voltammetry, long period fibre grating, the modification of tapered optical fibres and spectrophotometry.

1.2 Nucleotide Bases

The genetic information of all known lifeforms on earth is made up of five different nucleotide bases; adenine, thymine, guanine and cytosine (DNA) and uracil (RNA). The structures of these compounds are such that hydrogen bonds will only form between adenine and thymine or guanine and cytosine. Hydrogen bonds will also form between adenine and uracil, but this only occurs during transcription of DNA to RNA as the newly formed RNA strand is single-stranded. The structures of the nucleotide bases and the hydrogen bonding involved are shown in Figure 1.1.

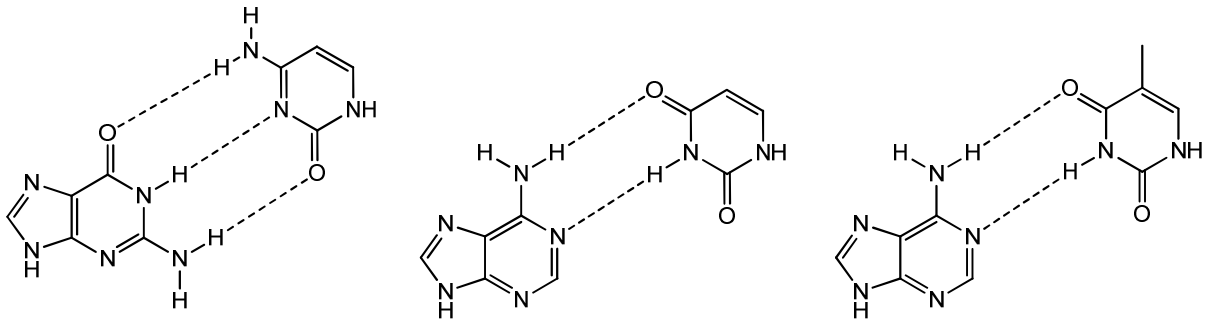

Figure 1.1 *– The structures of the nucleotide bases and the pairing interactions via hydrogen bonding. Cytosine & guanine and adenine & thymine in a DNA strand, and adenine & uracil in an RNA strand.*

This selective hydrogen bonding is essential during DNA replication to guarantee that the new strands are formed correctly and hence that proteins formed during translation have the correct sequence. However despite this in-built error prevention method it has been estimated that between 0.1 – 1% of nucleotides are misincorporated into a growing DNA strand (Johnson, Washington, Prakash, & Prakash, 2000). These mutations are often harmless, but they can occasionally result in the alteration of a triplet code, causing the wrong amino acid to be incorporated into a protein during translation. This can lead to a dysfunctional protein, which can be involved in the pathology of many different disease states in humans.

As such the detection of these single-nucleotide polymorphisms (SNPs) has become an important tool in the diagnosis of genetic diseases. There are a number of different approaches to this, including denaturing HPLC, which compares target DNA to wild type. This is done by preparing two strands of DNA by PCR (between 50 – 100 base pairs); one containing the sample from the patient and the other from a known un-mutated source. These two strands are then denatured and allowed to re-anneal, forming homo-duplexes (where the DNA strands match perfectly) and hetero-duplexes (where the presence of an SNP causes a loop like structure in the DNA where the hydrogen bonds don't form correctly). The HPLC column has a different affinity for homo and hetero duplexes (caused by the different relative melting points) and so the hetero-duplexes (with a lower melting point) will not be retained

by the column to the same degree as the homo-duplexes. The chromatogram will show the presence of two distinctly different components if an SNP is present, compared to the single component observed when the sample is identical to the wild type. Mass spectrometry can then be used to identify the specific polymorphism involved (Premstaller & Oefner, 2003).

Primer extension by PCR can also be used to detect SNPs. A DNA primer is annealed to the template DNA just before the SNP location. The polymerase enzyme then adds a dideoxynucleotide triphosphate (ddNTP) which, due to the lack of a hydroxyl group, terminates the chain formation after a single nucleotide addition. The nucleotide added to the antisense strand will be complimentary to the erroneous nucleotide in the sense strand. The new nucleotide can be identified using mass spectrometry or fluorescent methods. The specific point mutation can then be identified by comparison with wild type (Bayes & Gut, 2012).

All five nucleotide bases exist as redox couples, and as such can be detected electrochemically. The challenge is that the peak current on a cyclic voltammogram occurs in roughly the same place for all of the bases, and so distinguishing between different nucleotides in a mixture is impossible by conventional methods. This challenge has been overcome by using graphene modified electrodes to separate out the peaks for the different nucleotides. This allows for the detection of SNPs in short, single stranded DNA fragments. In a study by Zhou, Zhai, & Dong, (2009) single-stranded DNA fragments of 9 base pairs were analysed using cyclic voltammetry and differential pulse voltammetry. Four different strands were analysed, with different point mutations. The voltammograms of the mutated strands were overlaid with that of the wild type and this showed the mutations by a reduction in peak current for one peak and an increase in peak current for another (Figure 1.2).

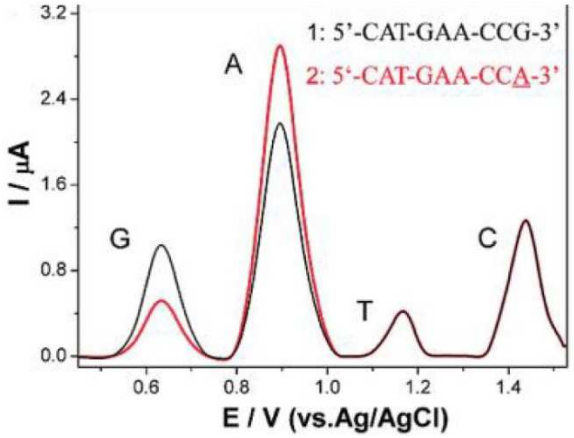

Figure 1.2 *– Differential pulse voltammogram (DPV) showing a point mutation SNP (G – A). The change in current between the two peaks may differ due to the relative difference in oxidation/reduction that occurs for different bases*(Zhou *et al*., 2009).

1.3 Blood Based Components

The ability to accurately quantify components in blood serum is of interest to medical science for the diagnosis of disease. A problem exists in that blood serum contains many different components, which can make the individual quantification of a single component impossible without either separating it out chromatographically or using an affinity ligand, such as an antibody. However both of these techniques add time and expense to the analysis.

Electrochemistry using graphene modified electrodes could provide a platform for simple, simultaneous detection of three potential components of blood serum, since they are components which are electrochemically active. These components are ascorbic acid, uric acid and dopamine, the structures of which are shown in Figure 1.3.

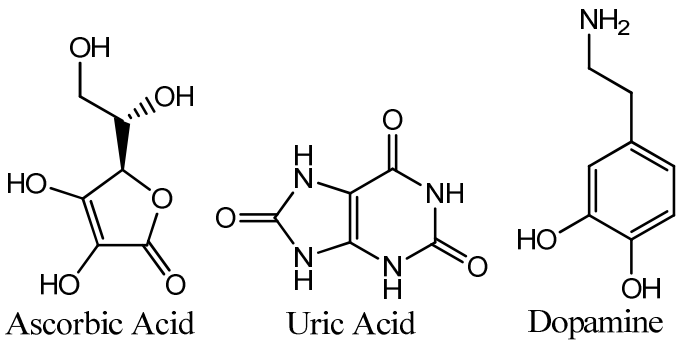

Figure 1.3 *– The structures of three electrochemically active compounds found in blood serum; ascorbic acid, uric acid and dopamine.*

Ascorbic acid, commonly known as Vitamin C, is an essential component of diet in humans. This is due to its activity as co-factor in many different enzymatic pathways, including the biosynthetic pathway of collagen. Collagen deficiency is one of the causes for certain symptoms of scurvy (Phillips & Yeowell, 1997). Additionally the antioxidant activity of ascorbic acid helps to prevent oxidative damage of DNA. In a study by B. M. Lee, Lee, & Kim, (1998) it was shown that the oxidative stress effect of smoking on DNA was lowered by 18.1% by daily intake of Vitamin C (500 mg) when compared with a placebo control. In healthy individuals the concentration of Vitamin C in blood plasma should be between 26.1 - 84.6 μmol L^{-1}, however levels will vary with dietary intake (W. Lee, Roberts, & Labbe, 1997).

Uric acid is a by-product of the breakdown of the purine nucleotide bases adenine and cytosine. In healthy individuals the concentration of uric acid in blood plasma should be between 147 – 466 μmol L^{-1} (Das, Borah, Ghose, & Choudhury, 2014). Due to the relatively low water solubility or uric acid (~360 μmol L^{-1} at 20^{o}C) a high blood plasma concentration can result in precipitation of solid uric acid, typically in the joints, causing a type of arthritis called gout. Other conditions such as hypertension and liver damage have also been associated with a high blood uric acid concentration (Heinig & Johnson, 2006). A low serum concentration of uric acid has also been associated with increased incidence of multiple sclerosis. This is due to the function of uric acid as a natural scavenger for peroxynitrite, a known cause of the disease (Rentzos *et al*., 2006).

Dopamine is a neurotransmitter involved in the transmission of nerve impulses across synapses in the brain. Outside of the brain, dopamine acts as a local chemical messenger. Increased levels of dopamine in the blood have been linked to hypotension, increased urine production and a decrease in insulin production. A deficiency of dopamine in the brain causes diseases such as restless leg syndrome, attention deficit disorder and Parkinson’s disease.

These conditions are often treated by either dopamine or dopamine analogues which have the same physiological effects as dopamine (Schmidt & Reith, 2005). Therefore the monitoring of dopamine levels is important for both diagnoses of dopamine related conditions as well as therapeutic drug monitoring after treatment for one of these conditions has begun. In healthy individuals the concentration of dopamine in blood plasma should be between 0.04 - 4.5 nmol L^{-1}.

1.4 Amino Acids

Amino acids are the basic monomer units used to create proteins in living organisms. Chemically they contain an amine group and a carboxylic acid group joined by a single carbon. The other groups on this carbon determine things like hydrophobicity, acid/base nature and electrochemical properties. The ability to detect amino acids in biological samples is important due to their vital biological function both in the synthesis of proteins and other biological molecules such as the use of glutamic acid as a precursor in the synthesis of gamma aminobutyric acid (GABA), which is an important neuroinhibitory chemical involved in nerve impulse regulation (Farokhcheh & Alizadeh, 2014). Other healthcare implications of amino acid detection are the use of amino acids as biomarkers for diseases such as renal cell carcinoma (Mustafa *et al*., 2011), ischaemic stroke (Gao *et al*., 2013), type 2 diabetes mellitus, stage 1 and 2 chronic kidney disease and cardiovascular disease (Batch, Hyland, & Svetkey, 2014). Amino acids can also be considered as a pollutant, with an imbalance of the abundance of the different compounds having an effect on aquatic ecosystems and water cycles (Samy, Robinson, & Hays, 2011).

Only three of the 23 proteinogenic amino acids exhibit electrochemical activity; phenylalanine, tryptophan and tyrosine (Figure 1.4), and as such detection of most of these cannot be carried out electrochemically without derivitisation.

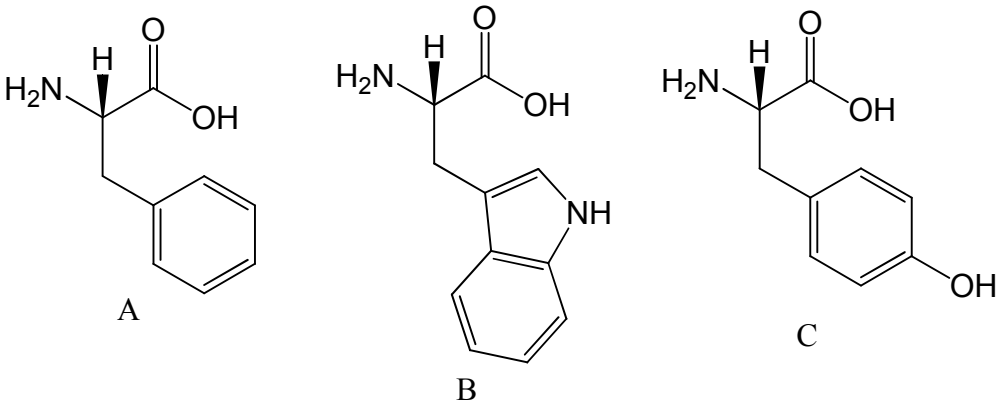

Figure 1.4 *– Chemical structures of the three electrochemically active amino acids; (A) phenylalanine, (B) tryptophan and (C) tyrosine.*

It has previously been demonstrated (Arena *et al.*, 2006; Muthu Mareeswaran, Prakash, Subramanian, & Rajagopal, 2012) that amino acids will bind to some calixarenes (Section 1.5) with high binding strength. Little selectivity between different amino acids was observed, however, and therefore specific detection of amino acids using only calixarenes as detection ligands is potentially not feasible. However in analyses where specific binding is not required, such as chirality detection, calixarenes are an ideal for concentrating the analyte at the surface of an electrode.

1.4.1 Amino Acid Chirality

The general structure of an amino acid includes a carbon with 4 different substituents; a carboxylic acid, a primary amine, a hydrogen and a variable group dependant on the amino acid. All amino acids (except for glycine where the variable group is another hydrogen) are therefore chiral. Amino acids used in protein synthesis are all the L form, with the D form only found in racemic mixtures produced by organic synthesis from non-chiral precursors. If the natural pool of amino acids was not limited to a single isomer, then the number of potential configurations of any given protein would be 2^n (where n is the number of amino acid residues in the protein). If this were true in the case of human insulin (a protein containing 52 amino acid residues) then there would be over 4.5×10^{15} subtly different

products from the translation of the insulin gene with a different stereoisomer of each amino acid in the chain. Whilst some of the incorrect products might still have some biological activity, it is likely that the majority of them would not. To avoid this variability in a protein being translated, the tRNA which carries the amino acid to the ribosome will only bind to the L form. In addition, the biological synthesis of amino acids always yields the L form.

Every organism on earth relies on amino acids for the construction of proteins. It has been suggested that amino acids might not have originated on earth and were in fact delivered to this planet by asteroid impacts many millions of years ago. Evidence based on contemporary findings of amino acids in more recent meteorite samples has shown that essential ingredient of life does exist elsewhere in the universe (Cronin & Pizzarello, 1999; Tewari, Paliwal, & Venkatakrishna, 2002). The discovery of extra-terrestrial amino acids might not indicate life, however, as it has been shown that amino acids can be formed naturally by UV irradiation of ice obtained from a meteor containing the base elements (Bernstein, Dworkin, Sandford, Cooper, & Allamandola, 2002). The amino acids made during this study, like those formed during organic synthesis from non-chiral precursors, are a racemic mixture of both stereoisomers. If it can be shown that a sample of extra-terrestrially acquired amino acids have a greater proportion of one or other stereoisomer, then it is very likely that a biological organism is responsible for their synthesis. This method is being used to determine if life has ever existed on Mars using analytical techniques such as GC-MS (Bada, Glavin, McDonald, & Becker, 1998; Bada & McDonald, 1996; McDonald & Bada, 1995). Both the Viking 1 & 2 landers in 1976 were fitted with GC-MS analysers to detect the presence of organic molecules, however none were found above the ppb level. Since then the feasibility of both GC-MS and HPLC based analytical platforms has been evaluated for future studies. The main issue with both is that since the analysis is of solid samples, solvents and in the case of GC-MS a carrier gas, must also be transported along with the equipment, which in itself is very

expensive. This puts up the cost of a specific mission and also limits the number of samples and the area that can be analysed, since it is not financially viable to send more than one probe at a time. A cheaper and less complicated alternative would allow for multiple probes to be sent to the same planetary body at the same time which would increase the sample size and the likelihood of a positive result.

1.5 Calixarenes and Resorcinarenes

Two types of binding ligands examined in this research are calixarenes and resorcinarenes. Calixarenes are cyclic molecules composed of multiple (4 – 20) para-substituted phenol residues. The arrangement of these phenols is such that the hydroxyl groups are orientated down and inwards (the endo rim) and the para-substituents are orientated up and outwards (the exo rim). The whole structure resembles a Greek vase, which gives rise to the nomenclature; calix (a Greek word meaning vase or chalice) and arene (referring to the phenol residues contained within the molecule). Calixarenes have been described as "molecular baskets" because of their ability to interact with other molecules via the binding pocket formed by the outwardly orientated exo rim. The para-substituents of the phenol residues provide some degree of specificity for binding and the size of the binding pocket (determined by the number of phenol residues), also determines the type of molecule which is able to bind (Gutsche, 2008).

Calixarene nomenclature consists of three pieces of information; firstly the *para* substituent (prefixed by a lowercase letter *p*), secondly the number of units composing the ring (given in square brackets: [n]) and finally the type of unit composing the ring structure (phenol "arene", resorcinol "resorcinarene"). For example, a calixarene containing four para-tertiary butyl substituted phenol residues would be *p-tert*-butylcalix[4]arene. Calixarenes are also divided into minor and major classifications, with the major calixarenes containing an even number of phenol residues and the minor calixarenes containing an odd number. This

nomenclature denotes the relative ease of synthesising odd and even number calixarenes by the various methods listed in Section 1.5. The major calixarenes, consisting of the cyclic tetramer, hexamer and octamer, can be readily synthesised in laboratory reactions on either large scale or small scale. However, the minor calixarenes consisting of the cyclic pentamer and heptamer are not as simple to produce in the same yield as the major calixarenes. A comparable yield can be achieved for these calixarenes, but the synthetic pathway is more complex and demanding. The structures of the three major and two minor calixarenes are shown in Figure 1.5. Other calixarenes, with [n] larger than 8 are not shown, but can be synthesised. They comprise cyclic structures with between nine and twenty para-substituted phenol residues (Gutsche, 2008).

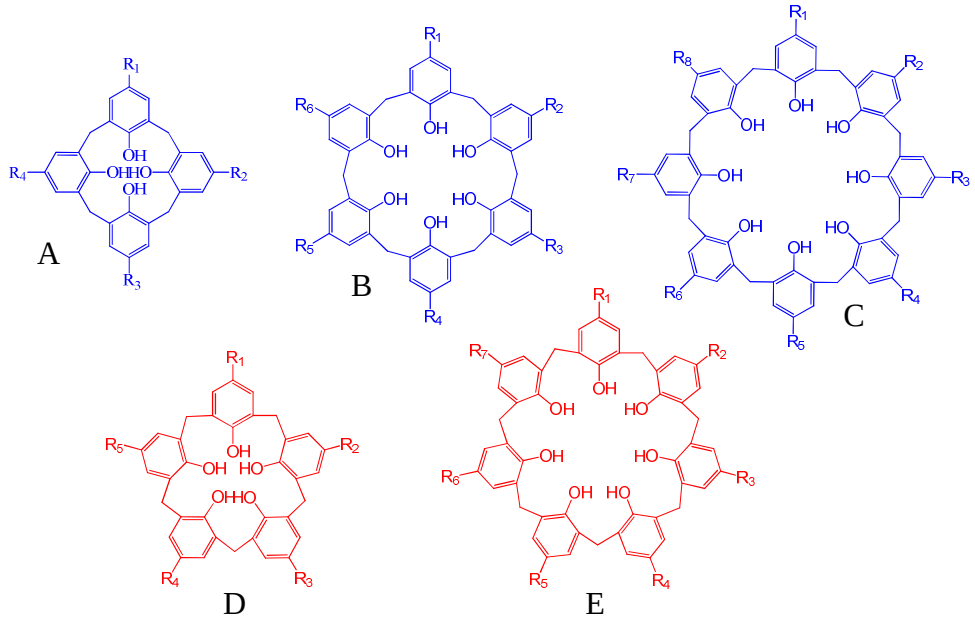

Figure 1.5 *– The structures of the major calixarenes, (A) the tetramer, (B) hexamer and (C) octamer (blue), and the minor calixarenes, (D) pentamer and (E) heptamer (red).*

The discovery of calixarenes is a long and interesting story. The first step was carried out by Adolph von Baeyer in 1872 with his work on the reaction of phenol and formaldehyde. The result of the base catalysed reaction between these two chemicals was shown to be a red-brown resin which Baeyer described as being “tar like” in nature. Baeyer was unable to

find a practical use for this material, however, and so he did not continue the research (Baeyer, 1872).

In 1902 Leo Hendrik Baekeland began performing research building on that of Baeyer. Baekeland hypothesised that by careful control of the base catalyst a more uniform and controllable material could be produced which could be marketed as a commercial product. In 1907 Baekeland patented the procedure for making what he called “Bakelite”. This was the first commercially available synthetic plastic (Gutsche, 2008).

One problem with Bakelite is that, like many plastics, it is a cross linked structure. Due to the –OH group in the phenol being an electron releasing group, the benzene ring is activated and further substituents are directed into the *ortho* and *para* positions. This gives rise to the cross-linked polymer structure shown in Figure 1.6. A cross linked structure is problematic when trying to create a macromolecular structure with a cavitand for guest-host interactions.

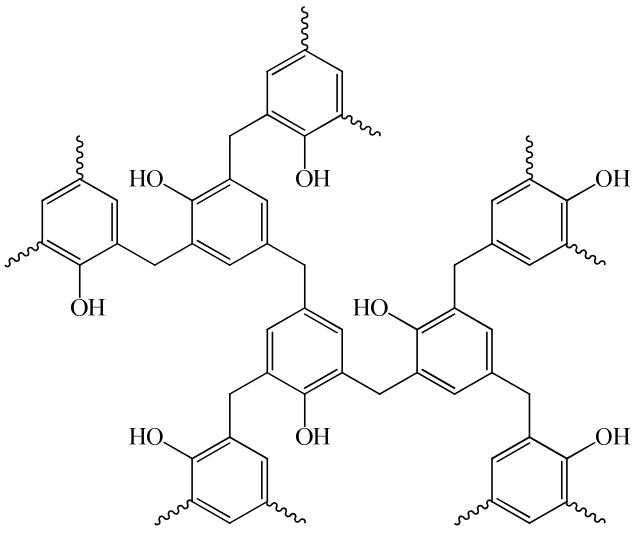

Figure 1.6 *– A potential structure for a section of a highly cross-linked poly-phenol compound synthesised by base catalysis of the reaction between phenol and formaldehyde.*

In 1942 Alois Zinke and Erich Ziegler experimented with blocking the *para* position of the phenol with either an electron withdrawing group, which would block the *para* position, deactivate the ring and direct further substituents to the *meta* position (with respect to itself),

or a weaker electron releasing group, which would block the *para* position, and activate the benzene ring. This activation would not lead to *ortho* substitution (with respect to itself), however, as the hydroxyl group would represent a stronger electron releasing group, hence further substituents would be added into the *ortho* position with respect to the hydroxyl group (Zinke & Zeigler, 1941).

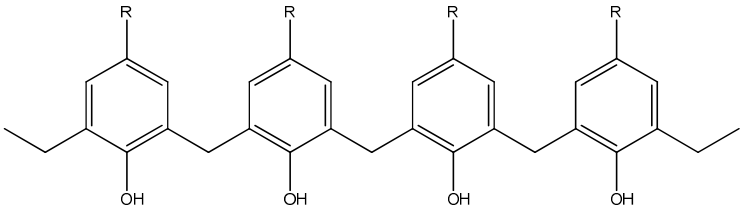

Figure 1.7 *– A linear polymer chain comprised of four para-substituted phenol residues. The R group in each case blocks the para position with respect to the hydroxyl and ensures subsequent reactions occur in the desired place* (Zinke & Zeigler, 1941).

In their paper, Zinke and Ziegler proposed a synthesis method (Section 1.1.1.1) which yielded a crystalline product with empirical formula $C_{11}H_{14}O$. They deduced, due to the lack of reaction with HBr, that this compound did not contain ether groups, but they did not propose a structure for the compound until a further publication (1944) where the cyclic structure of p-tert-butylcalix[4]arene was shown for the first time (Figure 1.8).

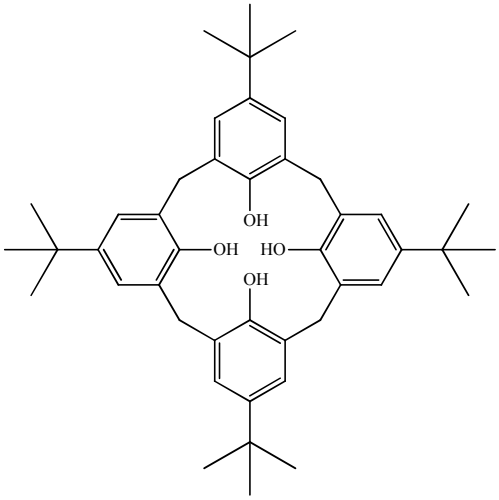

Figure 1.8 *– The cyclic structure of p-tert-butylcalix[4]arene proposed by Zinke and Zeigler (1944).*

This cyclic structure was not confirmed by Zinke and Ziegler, as the technology to resolve structural information from crystalline products using X-Ray diffraction was still in its infancy in 1944. Instead, two British chemists working for Bakelite would confirm the structural hypothesis. Hayes and Hunter (1958) used the relatively new technique of IR spectroscopy to show a 1,2,4,6 tetra-substitution pattern on each aromatic ring. This information coupled with the known empirical formula showed that the cyclic structure was feasible.

It was not until the 1970's that Gutsche discovered the ability of calixarenes to bind to other molecules (termed a guest-host interaction). Gutsche and his team synthesised p-tert-butylcalix[4]arene by two different methods. It was found that p-tert-butylcalix[4]arene possessed "a striking ability" to form guest-host complexes with other molecules. Among the molecules tested chloroform, benzene and toluene were demonstrated to bind very strongly. Binding affinity was such that guest molecules could only be removed by extended heating at high temperatures and low pressures (Gutsche, Dhawan, No, & Muthukrishnan, 1981).

Since the work of Gutsche in 1981, there have been over 400 examples in the literature of calixarenes for sensing applications. Calixarene based sensors have been used to detect a wide variety of analytes. Both gases and solutions have been analysed, with common analytes ranging from metal ions, such as copper (Qazi, Ocak, Ocak, & Memon, 2013), sodium (Wujcik, Blasdel, Trowbridge, & Monty, 2013), lead (Guziński, Lisak, Kupis, Jasiński, & Bocheńska, 2013) and calcium (Georghiou *et al*., 2013); volatile organic compounds (Topliss, James, Davis, Higson, & Tatam, 2010); DNA (Qin, Liu, Hong-Bo, Li-Na, & Xiaoya, 2013); gases (Md Yasin, Iyer, & Raston, 2013; Tsue *et al*., 2008) and amino acids (Hassen *et al*., 2007).

1.5.1 Synthesis Methods

Over the decades since they were first isolated, many different methods for synthesising calixarenes have been devised and compared. The different methods fall into two major categories; single-step procedures and multi-step procedures. The multi-step procedures are then further divided into convergent and non-convergent. Convergent syntheses involve synthesising two separate parts of the molecule and then reacting them together to give a cyclic molecule; this process will be further explained in Section 1.1.1.4. Non-convergent procedures involve synthesising the molecule step-wise as a chain which is then cyclised; this process will be further explained in Section 1.1.1.4. Within these different types of methods are several procedures developed by individual chemists which involve different mechanisms and reagents. In this section the different methods will be defined and discussed.

1.1.1.1 Zinke-Cornforth One-Step Synthesis

The Zinke-Cornforth procedure was originally devised by Zinke and Ziegler and set out in their paper of 1944. It was then adopted by John Cornforth and modified for use in his work with treating tuberculosis (Cornforth, Hart, Rees, & Stock, 1955). The first part of the procedure involves mixing an equimolar amount of the para-substituted phenol compound and a 12.3 M aqueous solution of formaldehyde with a 0.045 molar equivalent (with respect to the phenol) amount of NaOH to act as the catalyst. This reaction mixture is heated for 2 hours at 110 – 120^{o}C until a thick viscous mass is produced. This mass is called the "precursor" and contains the product of interest as well as other polyphenol compounds. This precursor material is then refluxed with diphenyl ether for a further 2 hours before being cooled and filtered. The crude product is then recrystallized from toluene to give a white crystalline solid with a melting point between 342 – 344^{o}C at a yield of approximately 50%. The mechanism for the base catalysed reaction is described by Gutsche (2008) and is shown in Figure 1.9. By the one-step synthetic method, the poly-phenol chain will continue to grow

until cyclisation occurs. This is why calixarenes of different sizes will form from the same reaction.

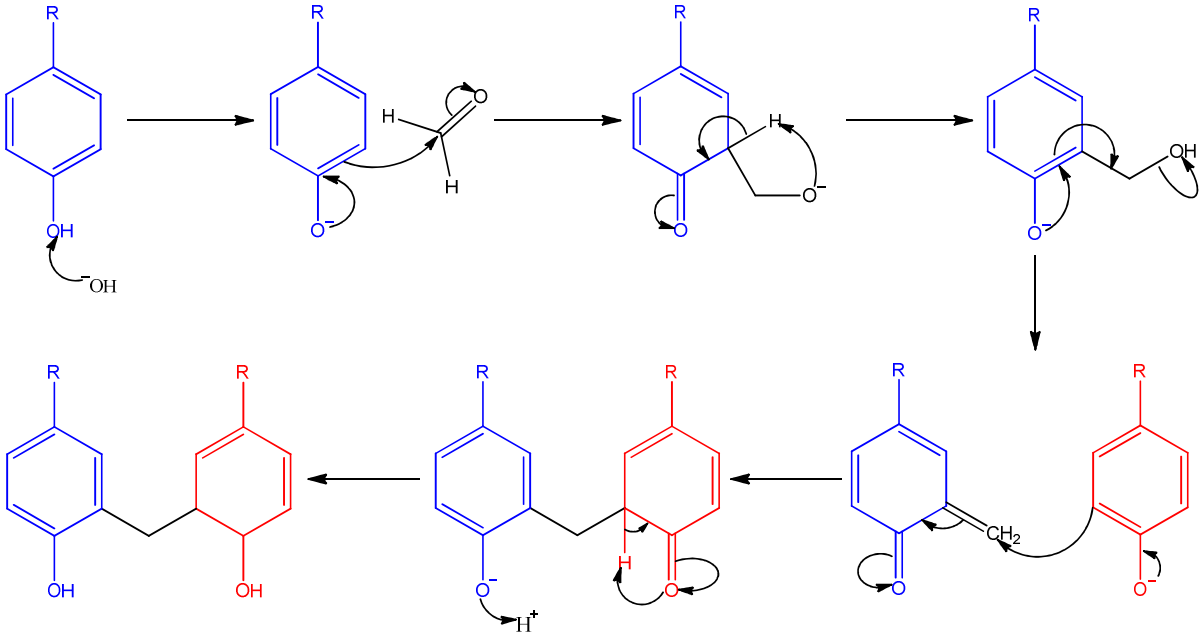

Figure 1.9 *– The mechanism of base-catalysed synthesis of calixarenes described by Gutsche* (2008).

In the original Zinke-Ziegler method the inefficient neutralisation step resulted in a small amount of base remaining in the mixture. This caused significant differences in the ratio of the different cyclic products. To combat this, the amount of base added at the beginning of the synthesis was carefully calibrated by Cornforth to give the optimum percentage yield of the cyclic tetramer. Later, somewhat serendipitously, the research group led by Gutsche discovered that if the concentration of base was vastly increased, only the calix[6]arene would form (Gutsche *et al.*, 1981). This led them to examine the relationship between the amount of base and the ratio between the cyclic tetramer and the cyclic hexamer products. This relationship is shown in Figure 1.10.

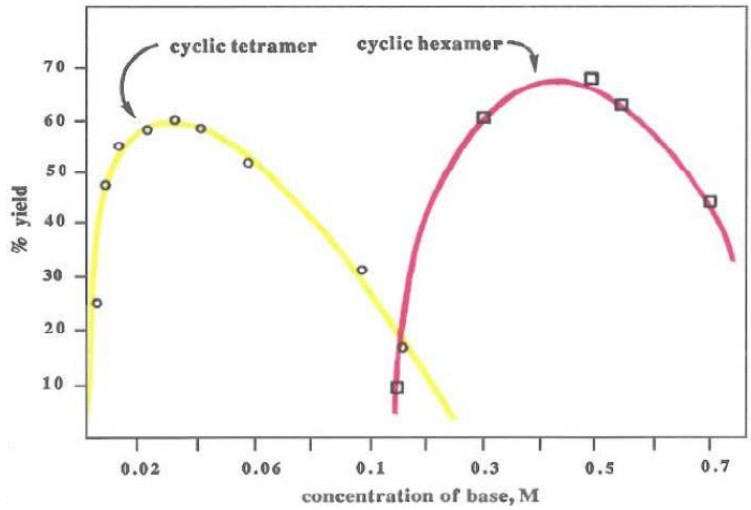

Figure 1.10 *– The relationship between the initial concentration of base and the product formed* (Gutsche *et al*., 1981).

1.1.1.2 Petrolite and Modified Petrolite One-Step Synthesis

Since the Zinke-Cornforth procedure, a number of different single-step methods have been devised for calixarene synthesis. Perhaps the most common of these is the Petrolite procedure. The Petrolite procedure was discovered as a result of the quality control investigation into the main product of the Petrolite Corporation. Using a very similar method to that of Zinke, Petrolite produced a poly-phenol demulsifier for treating crude oil; but the impurities created during the manufacturing process were a cause for concern, and so the manufacturing procedure was reviewed. The chemists performing the review were aware of the work of Zinke and Ziegler with cyclic polyphenols and, spotting a similarity between the impurities they were studying and the products described by Zinke, perfected and patented what is now known as the Petrolite procedure.

A mixture containing dimethylbenzene, a para-substituted phenol, polyoxymethylene and amount of NaOH equal to 0.03 molar equivalents with respect to the para-substituted phenol is refluxed for 4 hours. The reaction mixture is then cooled, filtered and recrystallized from chloroform to give a 60 – 65% yield of a white crystalline solid with a melting point of 418 - 420^{o}C (Gutsche & Munch, 1990).

The Petrolite procedure gives the cyclic octamer. The cyclic hexamer, as well as being obtained from the Zinke-Cornforth procedure with an increased amount of base, can also be synthesised using a modified Petrolite procedure.

A mixture of a para-substituted phenol, a 12.7 M aqueous solution of formaldehyde and an amount of KOH equal to 0.34 molar equivalents with respect to the para-substituted phenol is heated for 2 hours until a light yellow viscous precursor is formed. This precursor is then dissolved in dimethylbenzene and refluxed for 3 hours. The product is then cooled, filtered and neutralised before being recrystallized from a chloroform methanol mixture to give an 80 – 85% yield of a white crystalline solid with a melting point between 380 – 381^{o}C (Gutsche, Dhawan, Leonis, & Stewart, 1990).

1.1.1.3 One Step Synthesis of Calix[5]arene

Synthesis of the major calixarenes, the cyclic tetramer, hexamer and octamer, can be easily carried out in the laboratory on a small scale or large scale with substantial yields. However the minor calixarenes, the cyclic pentamer and hexamer, are more difficult to synthesise by single step methods (Gutsche, 2008). A single step process for synthesis of p-tert-butylcalix[5]arene was developed by Dumazet *et al* (1997) which involves opening up the ring of a calix[4]arene and inserting a new monomer. The process was reported to yield 32% of the cyclic pentamer as well as producing the cyclic hexamer and octamer as minor products.

An equal molar amount of calix[4]arene and p-tert-butylphenol (2.35 mmol) was dissolved in 30 ml of tetralin. The mixture was then stirred and heated to approximately 60^{o}C, until it became clear, at which point potassium hydroxide (100 ml, 4 M, 0.4 mmol) was added and the solution turned yellow in colour. The reaction mixture was then heated to 190^{o}C which was maintained for 4 hours. The colour of the solution changed from yellow to orange and

then to a dark red-brown. The solvent was removed and then the product was dissolved in chloroform acidified with HCl, washed three times with water and then refluxed with acetone to dissolve impurities. The purified product was then filtered from the acetone, and contained a mixture of the cyclic pentamer, cyclic hexamer and cyclic octamer. The filtrate was then concentrated and chilled to -40^{o}C to yield more product from solution.

Sodium hydroxide was also investigated as the catalyst for this reaction. The product yield in this case was only 11.3 %, as opposed to the 32% yield obtained from a potassium hydroxide catalysed reaction. Dumazet *et al*. (1997) hypothesised that this was because the cation from the base catalyst plays a part in the reaction by acting as a template for the cyclic molecule to form around.

1.1.1.4 Hayes-Hunter Non-Convergent Multi-Step Synthesis

The one step synthetic pathways can be used to produce calixarenes with relatively high yields. However the para-substituents of each phenol residue will be the same. In addition to this, with the exception of calix[5]arene (Section 1.1.1.3), only the major calixarenes can be synthesised by the one step methods. If the desired product contains phenol residues with different substituents or has to be a minor calixarene, then a multi-step method should be adopted for synthesis. The Hayes-Hunter method (1958) was adopted and modified by Kämmerer *et al* (1978) and used to produce numerous different cyclic polyphenol compounds containing either five, six or seven phenol residues para-substituted with either methyl or *tert*-butyl groups. The procedure occurs according to the base catalysed mechanism given in Figure 1.9, as well as acid catalysed condensation polymerisation. The starting *p*-substituted phenol is prepared by blocking one of the *ortho* positions by halogenation. This is so that alkylation will only occur at one site on the molecule. The reaction pathway for the Hayes-Hunter synthesis is given in Figure 1.11.

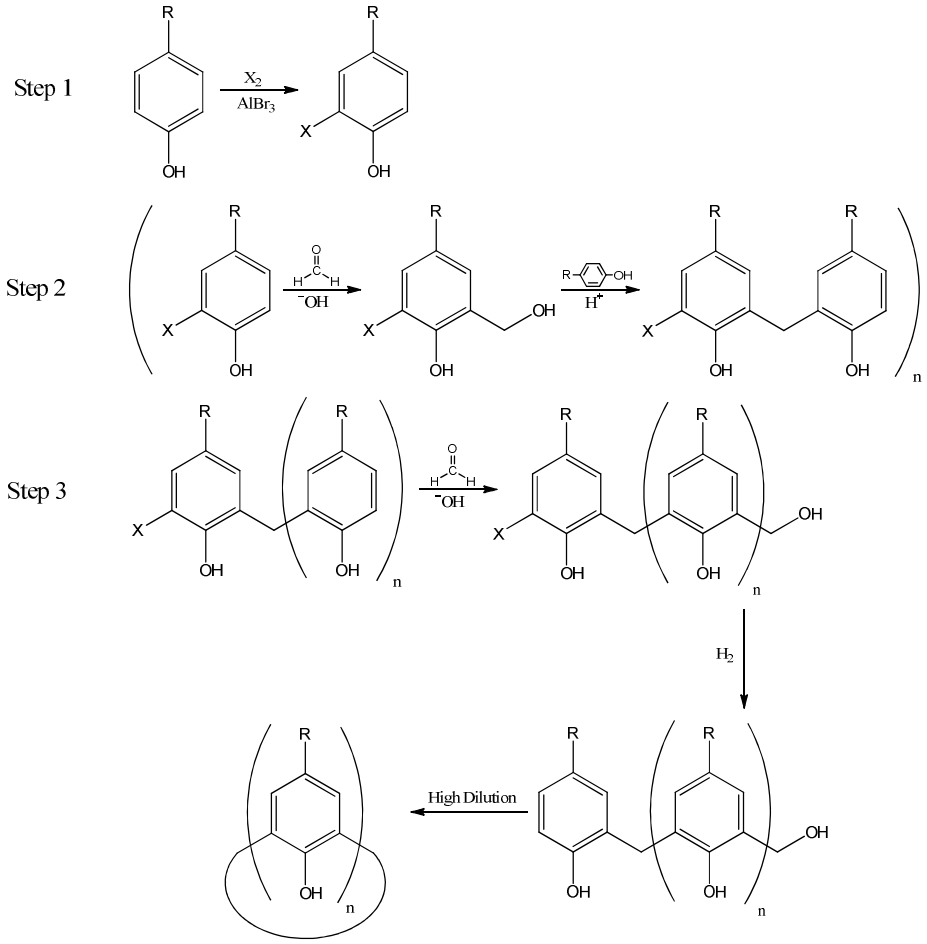

Figure 1.11 *– The stepwise synthesis of calixarenes devised by Hayes and Hunter. Reproduced from No & Gutsche* (1982).

The advantage of this type of synthesis is that it can be used to produce calixarenes of any size and the para-substituents can be tailored to the specific application. This makes the products considerably more versatile than those made by single-step synthetic methods. The two disadvantages are that the procedure is considerably more time consuming than a single step method, and the yields obtained are often extremely low, depending on the number of phenol residues to be added.

1.1.1.5 Convergent Multi-Step Syntheses

With the aim of reducing the number of steps involved in synthesis and increasing the yield, Böhmer, Marschollek and Zetta (1987) developed a convergent method which involved

separate synthesis of polyphenol fragments which are then condensed together to form a cyclic structure (Figure 1.12).

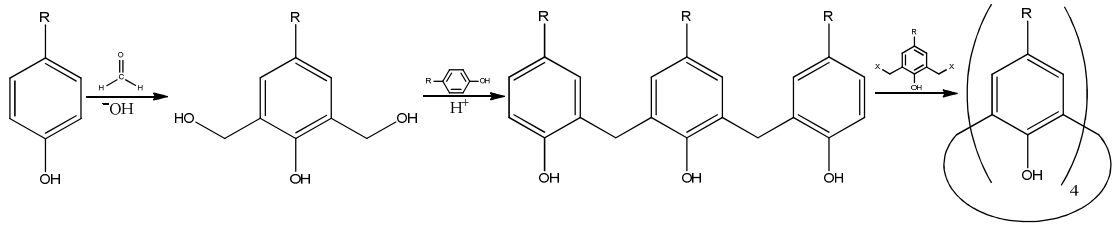

Figure 1.12 *– The "3 + 1" convergent multi-step synthesis of calixarenes which allows for the addition of different substituents to each phenol residue ($R^1R^2R^1R^3$)* (Böhmer, Marschollek, *et al*., 1987).

This type of synthesis was described by Böhmer as a "3 + 1" synthesis. The advantage of this is that it is far less complex than the Hayes-Hunter method. However the disadvantage is that the para-substituents cannot all be different in a calixarene produced by this method, with at least two having to be the same. Another method, the "2 + 2" method, allows for complete heterogenicity with respect to the phenolic residues para-substituents.

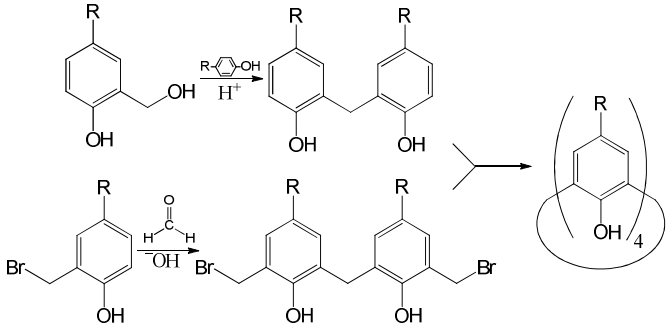

Figure 1.13 *– The "2 + 2" convergent multi-step synthesis of calixarenes which allows for the addition of different substituents to each phenol residue ($R^1R^2R^3R^4$)* (Böhmer, Merkel, & Kunz, 1987).

1.1.1.6 Synthesis of Resorcinarenes

Resorcinarenes are similar to calixarenes, but instead of being cyclic polyphenols they are cyclic polyresorcinols. Resorcinol contains two *ortho/para* directing hydroxyl groups. This means that the *para* position with respect to one of the hydroxyl groups will be in the *ortho* position to the other and vice versa. As such these positions will be doubly activated. The

carbon between the two hydroxyl groups will also be doubly activated as it is in the *ortho* position with respect to two strongly activating electron releasing groups. Addition does occur at this position, but the product is not preferred as it is less stable than the major product (Durairaj, 2005).

Resorcinarenes are seen primarily as the cyclic tetramer as this is the lowest energy conformation. They are made by an acid catalysed condensation of resorcinol and an aldehyde, which can contain a substituent to give functionality to the molecule. Once the ring is formed, it can be further derivatised by either adding groups to the carbon in between the two hydroxyl groups, which is now highly reactive as the only activated site left on the benzene ring, or by reacting with the hydroxyl groups directly. The mechanism by which resorcinarenes are formed is given in Figure 1.14.

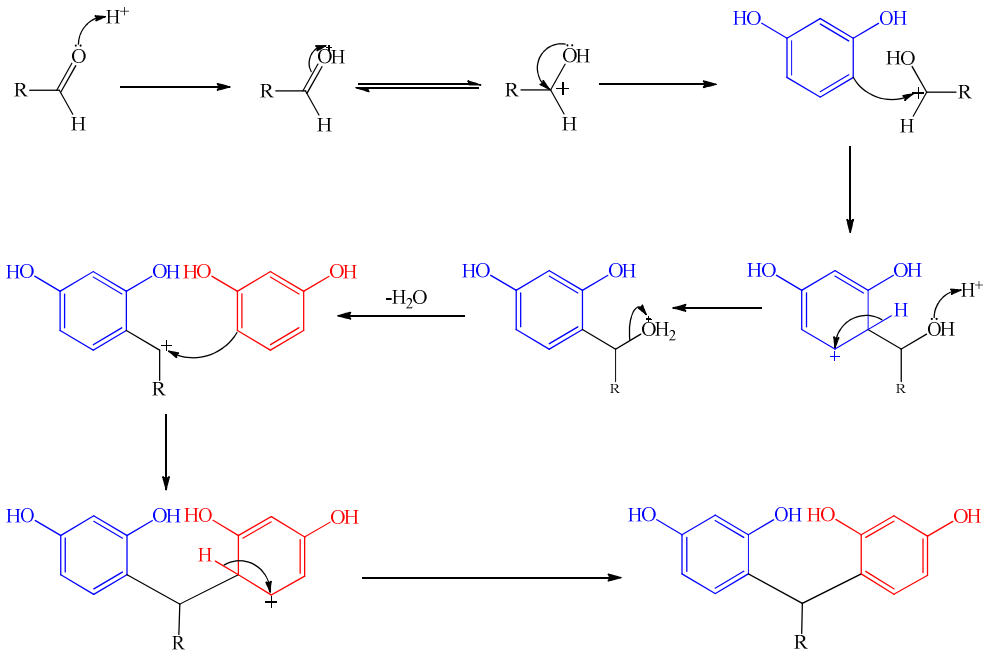

Figure 1.14 *– The mechanism of acid-catalysed synthesis of resorcinarenes described by Gutsche* (2008).

A method for the synthesis of calix[4]resorcinarene was published by Aoyama, Tanaka and Sugahara (1989). A solution of resorcinol and the desired aldehyde in equimolar amounts (0.23 mol) was prepared in ethanol and 12 M HCl was added as a catalyst. This was

then sparged of oxygen by bubbling nitrogen through the solution and then refluxed for 10 hours. The mixture was then cooled to room temperature and the precipitate filtered from the solution. Subsequent precipitate was recovered in small amounts by adding water to the permeate. The precipitate was then washed with hot water before being recrystallized twice from chloroform and twice from a mixture of hexane-acetone. The final yield was approximately 50%. This is the method that was adopted for the synthesis of the resorcinarene in Chapter 4.

1.1.1.7 Solvent-Free Syntheses of Resorcinarenes

A green chemistry method is reported in literature which can be used to synthesise resorcinarenes without the presence of a solvent. Roberts *et al*. (2001) being the earliest example of this method uses a 1:1 molar ratio of resorcinol and the desired coupling aldehyde and a catalytic amount (5% by moles) of *p*-toluenesulfonic acid. The reactants were placed into a mortar and ground vigorously with a pestle. A viscous paste is formed after a few seconds of grinding which solidifies upon further grinding. The red solid product was then left to stand for 1 hour before being washed with water and then recrystallized from hot methanol to yield a pink coloured solid. The study uses 6 different benzene containing aldehydes and reports yields of between 80 – 96%.

Other examples in literature using this method include Firdaus *et al*. (2008) and Karami *et al*. (2012). Firdaus used 4-hydroxy-3-methoxybenzaldehyde (vanillin) giving a yield of 52% and 4-methoxybenzaldehyde giving a yield of 63%. Karami also studied the formation of a resorcinarene using 4-methoxybenzaldehyde, obtaining a yield of 80 %. Products were also obtained using 8 other varieties of substituted benzaldehydes giving yields of between 78 - 95 %. In the Karami study the *p*-toluenesulfonic acid catalyst was replaced by tungstate sulfuric acid in a ratio of 10 % by moles.

The atom economy of this process should be 98 % with only one mole of water being produced from every coupling reaction. This would mean the procedure fits one of the criteria of green chemistry. However the reported atom economy was much lower, at 48 %, which is due to the loss of product during the recrystallization stage as well as any by-products (such as dimers, trimers & substitution at the 2 position instead of the 4 position) that are produced by the reaction. However the lack of solvent, low energy costs, small amount of catalyst and reduced time when compared to other methods mean that this synthesis method can still be classed as "green chemistry".

1.5.2 Calixarene Guest-Host Interactions

The usefulness of calixarenes comes largely from their ability to form guest-host interactions as previously mentioned. There are a number of different types of interactions, involving both the delocalised π electrons in the benzene ring of the phenol residues and also intermolecular forces caused by the *para* substituents. The *para* substituents will only give rise to ionic and Van-der-Waals interactions, depending on the relative polarity of the guest molecule, as well as hydrogen bonding. These types of interaction are relatively simple and easy to explain. However the benzene ring interactions with the guest molecule are more interesting and complex. These interactions are categorised into π-stacking, π-polar and π-cation, and are explained in more detail below.

Depending on the nature of the molecules involved, multiple interactions can take place. For instance in the case of the guest-host complex formed between the amino acid phenylalanine and *p*-sulfocalix[4]arene, there might be hydrogen bonds formed between the carboxylic acid group on the guest and the sulfonic acid *para* substituent on the calixarene host. In addition to this, there might be π-stacking interactions between the benzene ring in the amino acid's side

chain and the benzene rings of the calixarene. A combination of all of the interactions involved gives rise to the unique binding affinity of a specific guest-host interaction.

1.1.1.8 π-Stacking

π-stacking, also known as π-π stacking, is an interaction between two benzene rings. This type of interaction has been reported as being involved in the stabilisation of proteins, DNA and also in the guest-host interaction of calixarenes. There are three conformations of the π-π interaction termed planar sandwich, T-shaped and parallel displaced conformations (Figure 1.15).

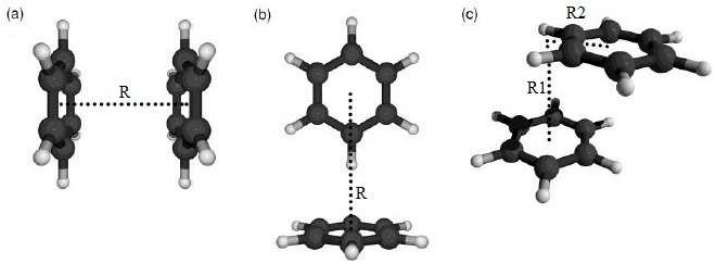

Figure 1.15 *– The three potential conformations of a π-π interaction. R represents the distances between the molecules. (a) planar sandwich, (b)T-shaped & (c) parallel displaced* (Sinnokrot, Valeev, & Sherrill, 2002).

The distance between the two benzene molecules has been measured by a number of different research groups (Hobza, Selzle, & Schlag, 1994, 1996; Jaffe & Smith, 1996; Sinnokrot *et al*., 2002). The distance between the two molecules in a dimer depends on the particular conformation that they are in. The studies used molecular modelling, and the average intermolecular distances are 3.92 ± 0.18 Å (planar sandwich), 4.98 ± 0.15 Å (T-shaped). 3.50 ± 0.1 Å (parallel displaced, R1) and 1.68 ± 0.11 Å (T-shaped, R2).

The binding energies were also shown to be different depending on the conformation. Multiple different methods for assessing binding energy were used; Møller–Plesset perturbation theory (MP2), coupled cluster singles and doubles (CCSD), complete basis set (CBS) & zero point vibrational energy (ZPVE). The published binding energies have a

greater standard deviation than the intermolecular distances from the same papers. This is due to discrepancies between how the different methods assess binding energy. The values are as follows; 1.76 ± 1.48 kcal mol^{-1} (planar sandwich), 2.29 ± 1.38 kcal mol^{-1} (T-shaped) and 2.93 ± 2.14 kcal mol^{-1} (parallel displaced). The data shows that the T-shaped and the parallel displaced conformations are the most energetically favourable.

1.1.1.9 Quadrupole Moment of Benzene

This energetic favourability can be explained by the quadrupole moment of benzene, where a positive or negative charge exists above and below the ring with an oppositely charged area in the middle. The region in the middle has a larger area than the charged area above and below and as such the molecule has four poles (above, below and at either side), hence quadrupole. Therefore the planar sandwich conformation is only favourable in dimers where the polarity of one quadrupole has been inverted, for instance in hexafluorobenzene.

The quadrupole effect is also responsible for the other two types of π interactions; π-cation and π-polar. In π-polar interactions the positively charged region above and below the ring or in the middle (dependant on the polarity of the quadrupole) interacts with the δ^- charge on the electronegative atom of a polar bond in a similar fashion to hydrogen bonding. In π-cation a positive charge on a metal ion or other positively charged ion interacts with a negative charge in either location on the quadrupole. The quadrupole moment of benzene is shown in Figure 1.16.

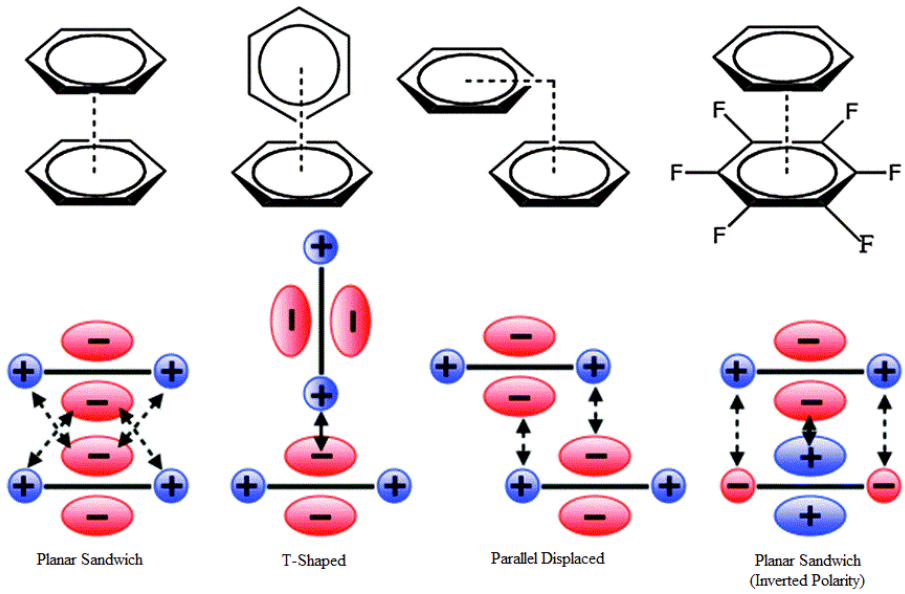

Figure 1.16 *– The quadrupole moment of benzene showing why the T-shape and parallel displaced conformations of benzene dimers are more energetically favourable then the planar sandwich* (Matthews, Welton, & Hunt, 2014).

In a study by Sunner, Nishizawa, & Kebarle, (1981), the binding energy of potassium to benzene was shown to be higher than the binding energy of potassium to water, 19.2 kcal mol^{-1} and 17.9 kcal mol^{-1} respectively, showing that π-cation interactions can be stronger than hydrogen bonding. The highest binding energy was reported for Li^{+} ions to benzene with a binding energy of 38.3 kcal mol^{-1} (Taft *et al*., 1990) which is roughly a whole order of magnitude higher than those reported for π-stacking interactions showing that these types of interaction are stronger.

1.5.3 Calixarene Conformations

Due to the large polyaromatic structure of calixarenes and the various intramolecular forces involved there are multiple different conformations that a given calixarene will adopt. The number of potential conformations, as well as the most energetically favourable of these conformations, is determined by the number of phenol residues in the calix as well as the *para* substituents. The conformation of the calixarene is vitally important for the function as either an enzyme mimic or binding ligand. The conformation is also important in predicting

binding affinities. If a model is used where the calixarene is in a conformation other than the most energetically favourable, then the predicted binding energy will be inaccurate. In addition to this, the flexibility of the calixarene molecules allows for changes in the conformation in solution. Therefore not all of the molecules will be in the same conformations. This can make modelling calixarenes accurately *in-silico* a difficult task (Section 1.5.4).

1.1.1.10 Calix[4]arenes

Potential conformations of calixarene tetramers are fairly limited when compared to the other major calixarenes. With limited rotation, the only way that the tetramer can alter its conformation is by changing the orientation of one or more of the phenol residues (upwards or downwards with respect to the *para* substituent). This gives rise to four different structural conformations; cone, partial cone, 1,3-alternate and 1,2-alternate (Figure 1.17).

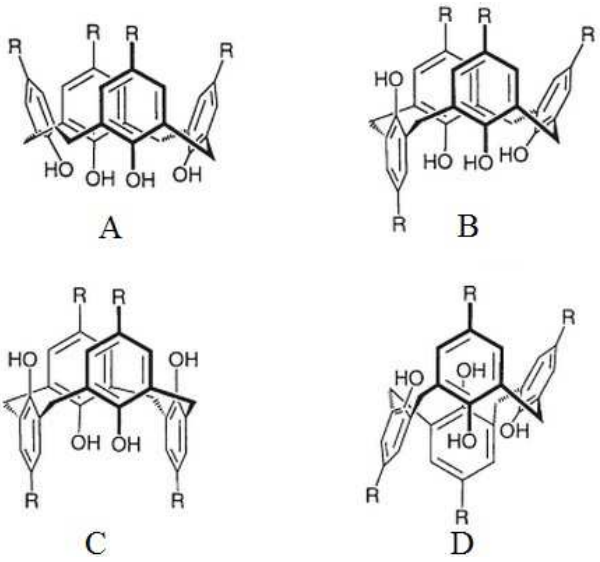

Figure 1.17 *– The four conformational states of the calixarene tetramer (u = upwards orientation, d = downwards orientation); (A) Cone (u,u,u,u), (B) Partial Cone (u,u,u,d), (C) 1,3-Alternate (u,d,u,d) & (D) 1,2-Alternate (u,u,d,d)* (Gutsche, 2008).

In the solid state the tetramer adopts the cone conformation. This has been confirmed by X-Ray crystallography performed on a 1 : 1 complex of *p-tert*-butylcalix[4]arene and toluene (Andreetti, Ungaro, & Pochini, 1979) .

With standard calixarenes the u/d notation can easily be used to denote conformations. However for calixarene derivatives such as ethers and esters a priority based nomenclature must be used. A reference phenol residue is chosen according to the Cahn-Ingold-Prelog nomenclature rules, which is then designated as “up”. The orientation of other groups is then given relative to this. The order in which the phenol residues are listed are again relative to the nomenclature rules, with the orientations given in order from highest to lowest priority (Gutsche, 2008).

1.1.1.11 Calix[6]arenes

With two more phenol residues than the tetramer, the hexamer adds another potential orientation to each given phenol group. In addition to up (u) and down (d), the possibility now exists for the phenol to be orientated outwards (o) or inwards (i) with respect to the para substituent. Steric hindrance will not allow for a fully outwards or inwards orientation, however, so an approximate 45^{o} angle is adopted. This means that an additional parameter must be added to the naming system to denote this.

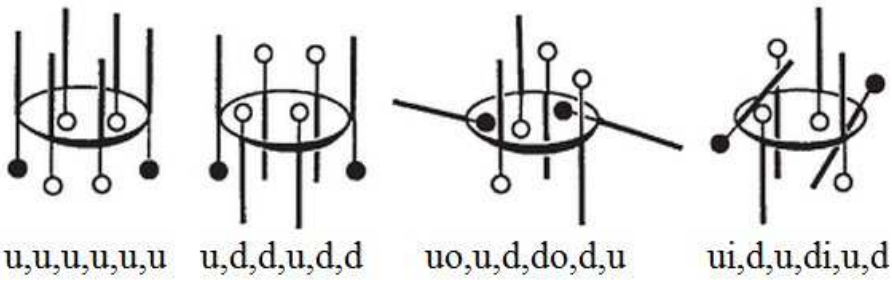

Figure 1.18 *– Four potential conformations of a hexameric calixarene to show the orientation nomenclature; (u) upwards, (d) downwards, (o) outwards and (i) inwards. The circle represents the hydroxyl group* (Gutsche, 2008).

Several different conformations of calix[6]arene have been described in literature; distorted cone, compressed cone, partial cone, double partial cone, winged, 1,2,3-alternate, 1,3,5-alternate and distorted 1,2,3-alternate (Gutsche, 2008). In a solid state, the conformation of a calixarene hexamer depends on the solvent from which it is crystallised. When a

non-polar solvent is used the hydrogen bonding holds the calixarene into the pinched cone conformation (ou,u,uo,uo,u,uo). When the calixarene is crystallised from a polar solvent the hydrogen bonding in solution is between the calixarene and the solvent rather than intramolecular hydrogen bonding. Therefore when the solvent is removed the resultant structure is the distorted 1,2,3-alternate structure (u,u,uo,d,d,do). These structural differences were discovered using X-Ray crystallography (Wolfgong *et al*., 1996).

1.1.1.12 Calix[8]arenes

The calixarene octamer exists in five common conformations; pleated loop, twisted loop, pinched loop, inverted double cone and 1,2,3,4-alternate. The most energetically favourable conformation in solution is difficult to predict and remains unclear. Specialist NMR techniques can be used to determine the actual conformation for a given guest, host and solvent combination. COSY, NOESY and ROESY NMR spectroscopy can be used to distinguish between two conformations by looking at the splitting patterns of the methylene group peaks. In certain conformations the methylene hydrogens the asymmetry will cause the methylene hydrogens to have a splitting effect on each other, giving a double doublet instead of a singlet. With increased temperature the peaks will merge into a singlet, showing that the conformation has changed (Figure 1.19).

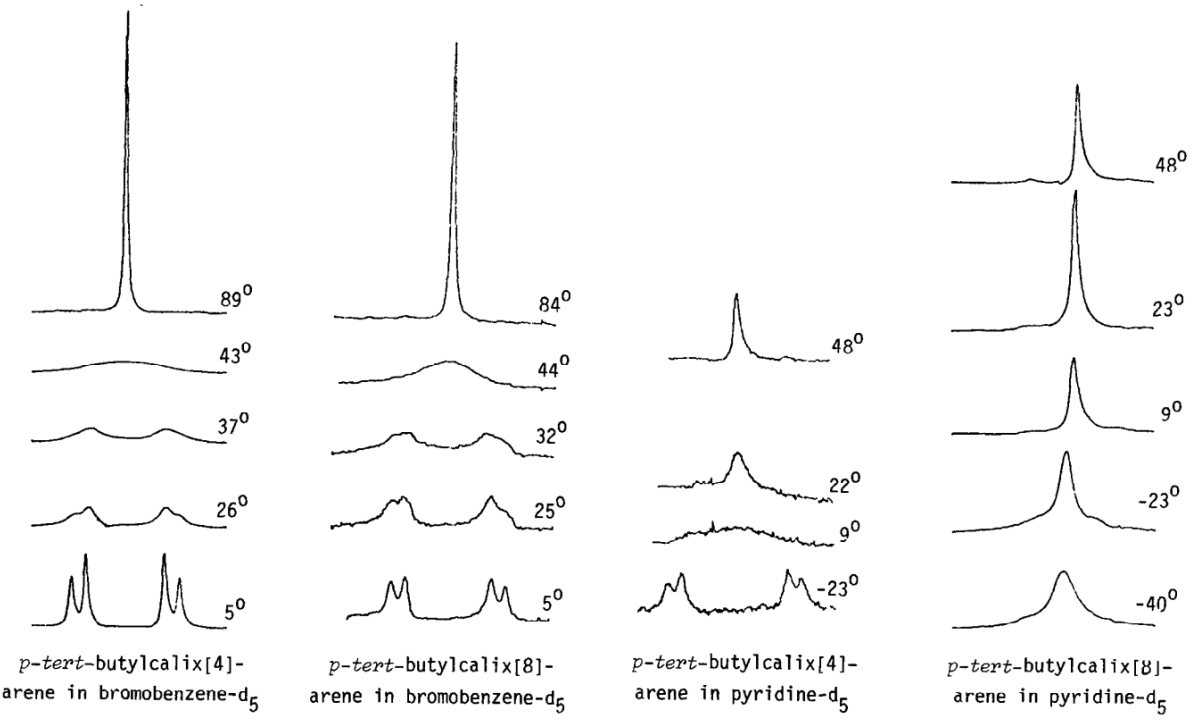

Figure 1.19 *– Temperature dependant NMR spectra showing the splitting of the methylene peaks in different conformations arising from different solvents* (Gutsche, 2008).

In the solid phase the octamer has been shown by X-Ray diffraction to adopt a pleated loop conformation (Gutsche, Gutsche, & Karaulov, 1985; Harrowfield, Ogden, Richmond, & White, 1991). However a subsequent study where the same calixarene, *p-tert*-butylcalix[8]arene, was complexed with eight pyridine molecules adopted a twisted conformation (Czugler, Tisza, & Speier, 1991). The 1,2,3,4-alternate conformation (Harrowfield, Ogden, & White, 1991) and the inverted double cone conformation (Perret, Bonnard, Danylyuk, Suwinska, & Coleman, 2006) have also been reported in literature.

1.5.4 Molecular Modelling of Calixarenes

Molecular modelling, sometimes called *in-silico* modelling is a tool that uses computer algorithms to assess the binding strength between two molecules. It is described in more depth in Section 1.8. In terms of the guest-host interaction of calixarenes, molecular modelling has been used to assess binding before any synthesis has been performed. This allows for selection of an appropriate calix to bind a specific analyte. The first example of

this technique being used to model the guest-host interactions of calixarenes is that of Grootenhuis *et al.* (1990). The results of the *in-silico* analysis agreed with the data obtained by other methods, with the exception of a discrepancy in the predicted most stable conformation of one of the calixarenes. Discrepancies like this led to questions as to whether or not molecular modelling was an appropriate tool for future work on calixarene interactions (Gutsche, 2008).

Despite the questions over accuracy and possible validity, this method has been used to model complexes of calixarenes with a number of different analytes including metal ions (Kane, Fayne, Diamond, Bell, & McKervey, 1998; Kane, Kincaid, Fayne, Diamond, & McKervey, 2000; Lawal *et al*., 2009), alcohols (Ghoufi, Morel, Morel-Desrosiers, & Malfreyt, 2005) and amino acids (Arena *et al*., 2006; Zielenkiewicz, Marcinowicz, Poznanski, Cherenok, & Kalchenko, 2005). Binding energy studies conducted *in-silico* can be verified using techniques such as NMR or absorbance titrations and differential scanning calorimetry (DSC).

Another application of molecular modelling in the study of calixarenes is to predict the most energetically favourable conformation. It is important to know this even in binding studies because the binding energy can differ vastly from the actual value if the calixarene is not in the correct conformation. Some examples in literature of this application of modelling techniques are (Lawal *et al*., 2009; Patra *et al*., 2013; Regnouf-De-Vains, Cartier, Fenet, & Pellet-Rostaing, 2005). Accuracy of conformational modelling might not be reliable as the conformation of a calixarene can depend on the solvent that is present. Although some molecular modelling packages allow for calculations to be run in the presence of a solvent, this still might be a source of error. Conformational studies using *in-silico* modelling can be verified using other methods such as NMR or X-Ray crystallography.

1.5.5 Current Uses of Calixarenes

Since their conception in the early part of the 20th century, calixarenes and other closely related compounds such as resorcinarenes and thiacalixarenes (where a sulfur atom is used to link the phenol residues instead of a methylene group), have been used extensively in a wide variety of different areas. Their ability to form guest-host complexes with a wide variety of different compounds allows for their usage in an array of analytical techniques, and the presence of a binding pocket gives them the ability to mimic the catalytic activity of some enzymes. The current examples in literature of uses for this family of compounds are discussed here.

1.1.1.13 Enzyme Mimics

The application of calixarenes to the field of enzyme mimics was considered as early as the 1970's (Gutsche, 2008). The aim was to find a cyclic compound that could be easily synthesised in the laboratory, as opposed to cyclodextrins which can only be isolated from natural sources. The basket-like shape of calixarenes proved to be more applicable to the use as enzyme mimics than the disc shaped crown ethers, which were also considered.

A modern example of this application is the use of a resorcinarene derived compound as an enzyme-mimic catalyst for the Menshutkin reaction. The Menshutkin reaction is used to convert tertiary amine salts into quaternary amine salts and was selected by Purse, Gissot and Rebek (2005) for their work on designing an effective enzyme-mimic catalyst. The tertiary amine used was quinuclidine, an ethylene bridge containing compound with a tertiary amine. The reactant chemicals were shown to bind into the cavitand of the resorcinarene and the rate of reaction was increased. The structure of the resorcinarene is shown in Figure 1.20.

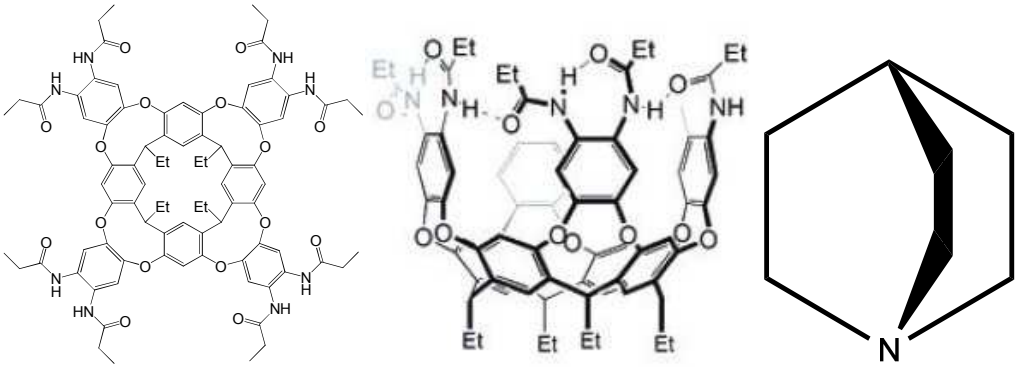

Figure 1.20 *– (A) Primary structure of the resorcinarene based enzyme-mimic, (B) Secondary structure showing the 3D cavitand formed when intramolecular hydrogen bonding occurs & (C) The structure of quinuclidine* (Purse, Gissot, & Rebek Jr., 2005).

The so-called "deep cavitand" was created by adding a bulky benzene ring containing compound after initial synthesis of the resorcinarene. The secondary groups are added across two adjacent resorcinol residues, adding strength to the natural "basket" shape. In addition the hydrogen bonding between different units creates a deep binding pocket which facilitates the reaction. The investigation found that using these materials as an enzyme mimic allowed the reaction to proceed 1.6 x 10^3 times faster than it normally would without catalysis. The catalytic effect of the resorcinarene on the Menshutkin reaction of quinuclidine was dependant on the electrophile, but some improvement on the rate of reaction was seen with all of the electrophiles tested (Purse *et al*., 2005).

1.1.1.14 HPLC Stationary Phase

High performance liquid chromatography (HPLC) has long been used as a separation technique for analysing mixtures of compounds with similar but slightly different properties. All chromatographic techniques rely on two separate phases (stationary and mobile) between which the analytes contained within a sample move based on properties such as polarity and/or volatility (for example in gas chromatography). In HPLC, the stationary phase is generally in the solid state. Silica is commonly used as the basis of an HPLC stationary phase, often with a secondary group bonded to the surface to change the properties of the

stationary phase. Traditionally this is something which is non-specific, such as a C_{18} chain which changes the polar surface of the silica into a non-polar surface. However the literature is reporting examples of molecules capable of forming specific interactions, which allow for detection of individual species from a sample containing closely related compounds that are unable to be resolved using traditional chromatographic methods. Some examples of molecules detected by calixarenes in this manner include toxic metals (Durmaz *et al*., 2013); tobacco specific N-nitrosamines (L. Wang *et al*., 2013) and drug molecules (Mokhtari & Pourabdollah, 2012).

The benefit of using a calixarene bonded solid phase over a traditional molecular recognition ligand such as an antibody or an imprinted polymer is that these can often bind their targets too strongly, and thus the target analyte may never be eluted from the column. A calixarene, due to the weaker interaction and broader selectivity will fail to do this, instead giving separation of the components by semi-specific, reversible interaction.

1.1.1.15 Ionic and Molecular Detection

An ion selective electrode is able to distinguish between different ions in a heterogeneous mixture of ions in solution. The difficulty with this task is that the specificity of the electrode cannot be based solely on size exclusion and in this context, for example, a hydrogen ion is smaller than a sodium ion. Any size exclusion based electrode for sodium ions will therefore not be able to distinguish between sodium and hydrogen ions.

The use of calixarenes and related cyclic poly-aromatic compounds as ionophores is well reported in the literature. Where other types of ion-selective electrodes might rely on size exclusion filtration to select specific ions for interaction with an electrode, calixarenes allow for direct detection. This is achieved by incorporating them directly into the electrode surface. Guest-host interactions are then detected between the ions and the calixarene.

Specificity is increased as ions with an incorrect radius (either larger or smaller than the desired analyte) for successful binding will not trigger a sensor response. This technique has been used to detect metal ions, such as lead(II) (Guziński *et al*., 2013), holmium(III) (Singh & Rani, 2012) and sodium (Jayakannan, Babourina, & Rengel, 2011), as well as complex ions such as neostigmine (El-Kosasy, Nebsen, Abd El-Rahman, Salem, & El-Bardicy, 2011) and rivastigmine (El-Sayed, 2014). The guest-host complexes in these applications are formed by π-cation interactions, which is an interaction between the electron rich face of the benzene ring and the electron deficient cation.

In a similar application, calixarenes have been incorporated into electrochemical sensors for molecular detection of non-ionic molecules. This application also relies on the ability of calixarenes to form guest-host complexes. Due to the abundance of benzene molecules present in the calixarene structure, the molecules which are best suited for detection by calixarenes are those which also contain benzene ring structures. These will complex by π-stacking interactions, with the π-electrons in each benzene ring interacting with each other in a number of different conformations. Calixarenes can also be used to bind and detect polar molecules. This is partly due to the hydroxyl group in each phenol residue, and also due to the ability of benzene to form π-polar interactions. In a similar way to π-cation interactions, the electron rich face of the benzene ring will attract the δ^+ pole of a permanent dipole. Calixarenes have been used to detect a wide variety of different analytes employing these different modes of interaction. Volatile organic compounds (Topliss *et al*., 2010); purine and pyramidine nucleic acid bases (Qin *et al*., 2013); gases (Md Yasin *et al*., 2013; Tsue *et al*., 2008) and amino acids (Hassen *et al*., 2007) are some of the literature examples of compounds that can be detected by calixarene based sensors. Tables 1.1 and 1.2 show a number of molecules used in current research and the calixarenes and resorcinarenes (respectively) that have been used to detect them.

Table 1.1 *– Current research involving calixarene based sensors.*

Reference	Calix Number	Substituent	Analyte(s)
(Qin *et al.*, 2013)	4	Various Azides	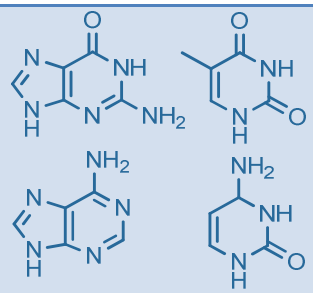
(Tsue *et al.*, 2008)	7	*t*-butyl	O=C=O
(Md Yasin *et al.*, 2013)	8	Phosphonic Acid	H-H
(Hassen *et al.*, 2007)	4	*t*-butyl and Benzene	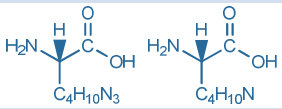
(F. Zhang *et al.*, 2013)	4	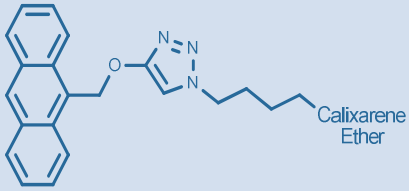	
(Schazmann, Alhashimy, & Diamond, 2006)	4	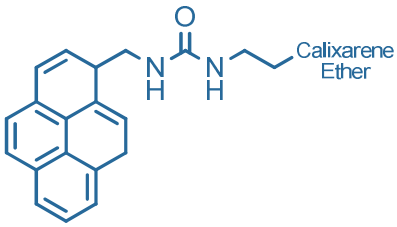	Cl^-

NB, where an ether is specified the substituent is bonded to the molecule via the hydroxyl, not via the *p*-substituent group on the phenol.

Table 1.2 *– Current research involving resorcinarene based sensors.*

Reference	Calix Number	Substituent	Analyte(s)
(Topliss *et al.*, 2010)	4	Undecane	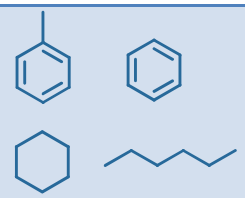
(Hassen *et al.*, 2007)	4	Undecane	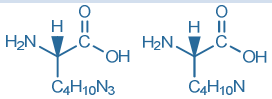
(Menon, Modi, Pandya, & Lodha, 2013)	4	Sulphonate	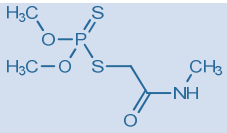
(W. Wang, Zhu, & Yan, 2013)	4	Butane	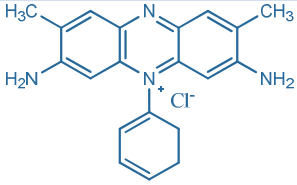
(Dickert, Bäumler, & Stathopulos, 1997)	4	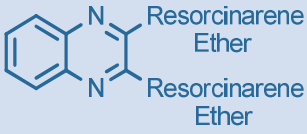	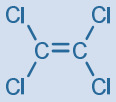
(He *et al.*, 2002)	4	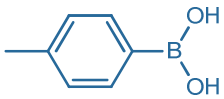	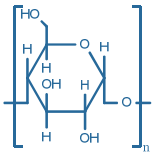

NB, where an ether is specified the substituent is bonded to the molecule via the hydroxyl, not via the R group on the methylene linkage.

1.6 Conducting Polymers

An alternative to the graphene based modifications used later in this research is conducting polymers. A conducting polymer is a polymer which is able to conduct an electrical current. These can be divided into redox polymers and electron-carrying polymers. Since their original conception, synthetic polymers have been used in the field of electronics as insulators. This singular approach to the application of plastics was challenged in the 1970's by the work of Heeger, MacDiarmid and Shirakawa (1977) who showed that by exposing

polyacetylene film to a halogen gas they could increase its conductivity by over seven orders of magnitude. This research was the beginning of the field of conducting polymers.

Further work on these novel conducting materials showed that certain polymers exhibited electrically conductive properties either when partially oxidised or partially reduced. The addition of anionic dopants (such as the halogens used by Heeger, MacDiarmid and Shirakawa) into the polymer was also investigated since it was imagined that these negatively charged species could be utilised to transmit the electrical charge, mimicking free electrons in a metallic conductor.

Conducting polymers have been applied to a wide variety of different applications including but not limited to photovoltaic cells (Hu, Zhang, & Zhu, 2014), organic-based light emitting diodes (Wu, Li, Wu, & Guo, 2014), semiconductors (Mohamoud, 2008), printed electronics (Rost, 2005) and biosensor applications (Ekabutr, Chailapakul, & Supaphol, 2013; Pesavento, D'Agostino, Profumo, Biesuz, & Alberti, 2014; Winther-Jensen, Kerr, & Winther-Jensen, 2014). A comprehensive review of the application of conducting polymers to the field of analytical science was performed by Collyer, Davis and Higson (2010).

1.6.1 Redox Polymers

A redox polymer is defined as a polymer which contains separate and isolated redox sites which can be independently oxidised or reduced. These redox sites can either be covalently attached and incorporated into the polymeric structure or held by electrostatic interactions. The mechanism by which the current is conducted is known as electron exchange or electron hopping, where the electrons are passed between adjacent redox sites.

Covalently attached redox groups can either be contained within the chain or exist as "pendant" groups branching off the main chain. In either case, the principle mechanism of conduction is the same. Figure 1.21 shows a schematic of how this occurs.

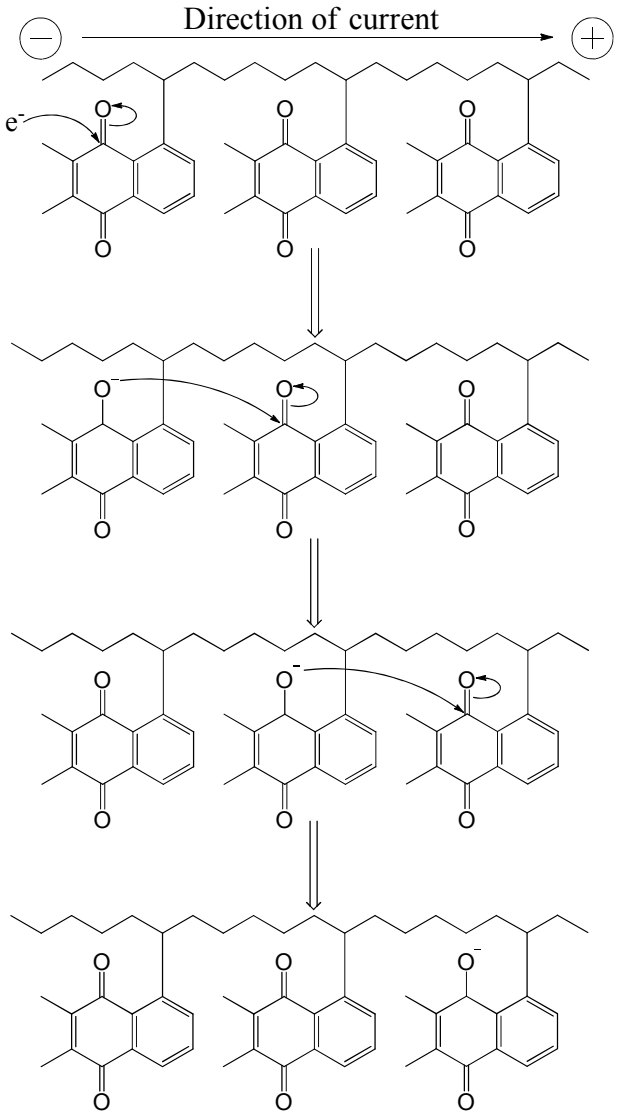

Figure 1.21 *– Schematic showing the mechanism of conduction in a redox polymer (polyvinyl napthoquinone). The curly arrows show the mechanism of conduction by movement of oxygen and electrons* (Inzelt, 2012; Manecke, 1974).

The arrows in Figure 1.21 show the movement of electrons towards the positive terminal by reduction of a double bonded oxygen in a carbonyl. Once oxidized, the negative charge is attracted to the electron deficient double bonded structure of an adjacent carbonyl and the charge moves across. The negative charge moves down the chain onto subsequent monomer residues, thus conducting a charge along the polymer chain. This is made possible by the slightly acidic nature of the hydroxyl groups yielded when quinone is converted into hydroquinone by keto-enol tautomerism (Inzelt, 2012).

1.6.2 Intrinsically-Conducting Polymers

The more common form of conducting polymer is the intrinsically conducting polymer (ICP). The reason that most polymers (for instance polyethene) are insulating is that all of the outer shell electrons in the molecule are sp^3 hybridised. This means that the energy level of each electron is equal, and each electron is involved in bonding. In order for a polymer to be able to conduct, the electrons in the carbon chain must be sp^2 hybridised as shown in Figure 1.22.

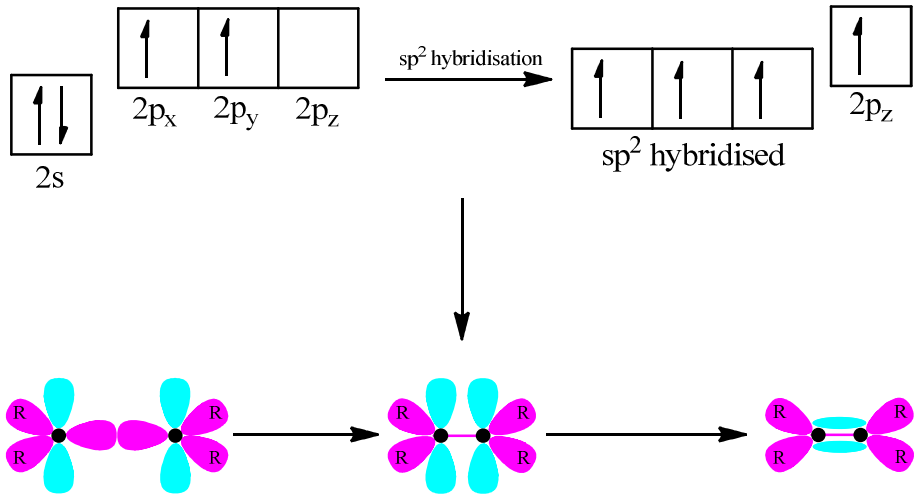

Figure 1.22 *– Diagrammatic representation of the sp^2 hybridisation of electrons in a double bonded carbon structure. σ-bonding orbitals are shown in magenta and π-bonding orbitals are shown in cyan.*

The advantage of this structure over an sp^3 hybridised structure is that there are a large number of electrons which can move if given the opportunity by an adjacent electron deficient environment. When the polymer is doped with an oxidising agent, some of these π-electrons are removed and the remaining electrons are delocalised, creating these electron deficient environments (carbocations). This allows for a structure with alternating double and single bonds to change conformation, with the double bonds switching between carbon atoms in the chain (Feast, Tsibouklis, Pouwer, Groenendaal, & Meijer, 1996). This movement is demonstrated in Figure 1.23.

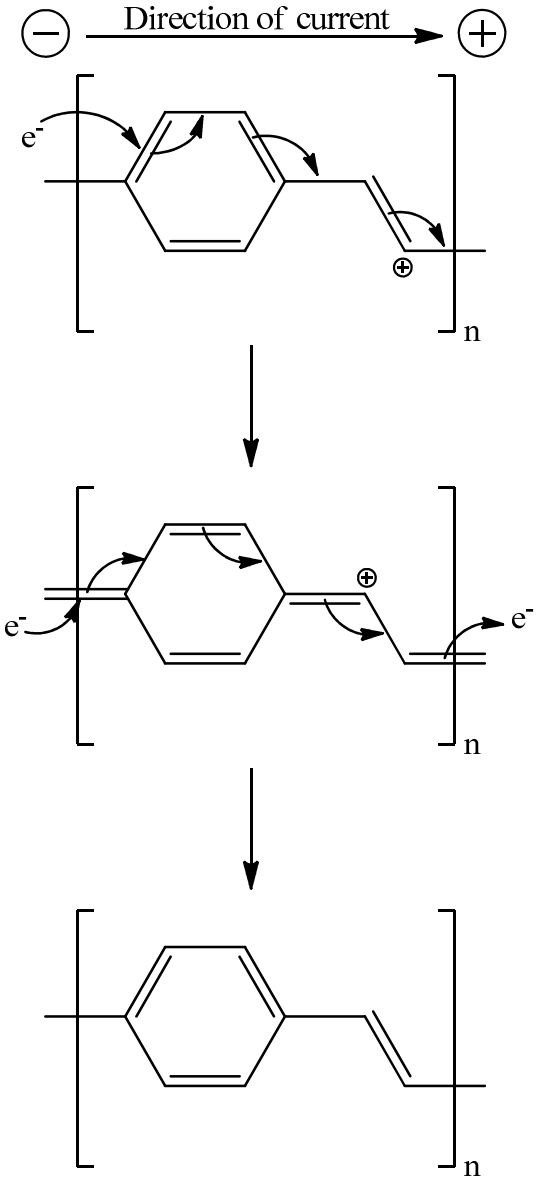

Figure 1.23 *– Schematic showing the mechanism of conduction for a p-doped intrinsically-conducting polymer (polyphenylene vinylene). The movement of electrons towards the positive terminal causes the carbocation to move towards the negative terminal.*

This type of polymer will not conduct an electrical charge without a dopant, since the electrons require an electron deficient region to move into. Some conducting polymers contain functional groups which are able to yield a positive charge under certain conditions. These are known as “self-doping” polymers. The concept of doping is discussed below.

1.6.3 Doping

Doping is the process of adding a compound or compounds to a polymer which will not be involved in the polymerisation process but will change the physical or chemical properties of the end product. The concept is similar to that of doping an inorganic semiconductor, such as silicon. The result is a considerable increase in electrical conductivity even when only very small amounts of dopant are added. The difference with polymer doping is that the dopant must either partially oxidise (p-doping) or partially reduce (n-doping) the polymer chain to allow for the movement of electrons. In both cases a counter ion must be present to preserve overall neutrality of the polymer. Using polyacetylene $(CH)_n$ as an example, the two different doping methods are represented in Equations (1.1 (1.2.

$$(CH)_n \longrightarrow [(CH)^{x+}]_n + (x)e^-$$

$$[(CH)^{x+}]_n + (x)A^- \longrightarrow [(CH)^+ A^-_x]_n \qquad (1.1)$$

Electrons are removed (Oxidation)

$$(CH)_n + (x)e^- \longrightarrow [(CH)^{x-}]_n$$

$$[(CH)^{x-}]_n + (x)M^+ \longrightarrow [(CH)^{x-} M^+_x]_n \qquad (1.2)$$

Electrons are added (Reduction)

Equations to show the p-doping (oxidation) and n-doping (reduction) of a conducting polymer (polyacetylene) to increase electrical conductivity (MacDiarmid, Mammone, Kaner, & Porter, 1985).

In practice the charges given in the equation will not be a whole number. This is because they will not be present on all residues in the polymer, so when showing repeating units of monomer, the charge displayed is shown as a ratio of charge to each repeating unit. The degree to which the polymer is oxidised or reduced depends on the dopant used. In a study by MacDiarmid *et al* (1985) investigated different dopants for both p-doping and n-doping of polyacetylene. Firstly, they noted that without a dopant the two isomeric forms of the polymer exhibited significantly different conductivities; with the *cis* isomer showing a

conductivity of 1.7×10^{-9} S cm^{-1} and the *trans* isomer showing a conductivity of 4.4×10^{-5} S cm^{-1}. But as soon as a dopant was added the observed conductivities were similar regardless of which isomer was used as the starting material. This is due to the fact that isomerisation takes place during the doping process, and so a mixture of *cis* and *trans* residues will be present along the length of the polymer chain. Furthermore, the team reported a greater increase in conductivity when using oxidising dopants, where the maximum conductivity shown was 1.2×10^{3} S cm^{-1} when arsenic pentafluoride was used as the p-dopant, giving a doped polymer with the empirical formula $[(CH)^{0.1+}(AsF_5)^{-}_{0.1}]$. When a reductive dopant was used the maximum conductivity was shown to be 2×10^{2} S cm^{-1} when lithium naphthalide was used as the n-dopant, giving a doped polymer with the empirical formula $[\ Li^{+}_{0.2}(CH)^{0.2-}]$. The team used a dopant ratio of 1 : 1 (dopant : monomer).

1.6.4 Types of Conducting Polymers

A number of conjugated polymers have been suggested for use as "synthetic metals" due to their ability to conduct electricity when either partially oxidised or partially reduced. The three which are mentioned most often in literature are; poly-3,4-ethylenedioxythiophene (PEDOT), which has been described in over 1000 journal articles; polypyrrole (PPy), which has been described in over 2500 journal articles; and polyaniline (PANI), which has been described in nearly 4000 journal articles. Since these polymers are the most common, they will be discussed below. This approximated data is based on a search using the online journal library database Scopus.

1.1.1.16 Poly-3,4-ethylenedioxythiophene (PEDOT)

Poly-3,4-ethylenedioxythiophene, abbreviated to PEDOT, is the polymerised form of the monomer 3,4-ethylenedioxylthiophene. PEDOT is optically transparent, highly stable and easy to manufacture in bulk. The optical properties coupled with the electrical conductivity make this polymer ideal for use in liquid crystal display televisions (LCD TV). It also has

potential applications in the area of biosensors, especially if electrical and optical detection methods are to be used simultaneously (Groenendaal, Jonas, Freitag, Pielartzik, & Reynolds, 2000). The structures of both the monomer and the polymer repeating unit are show in Figure 1.24.

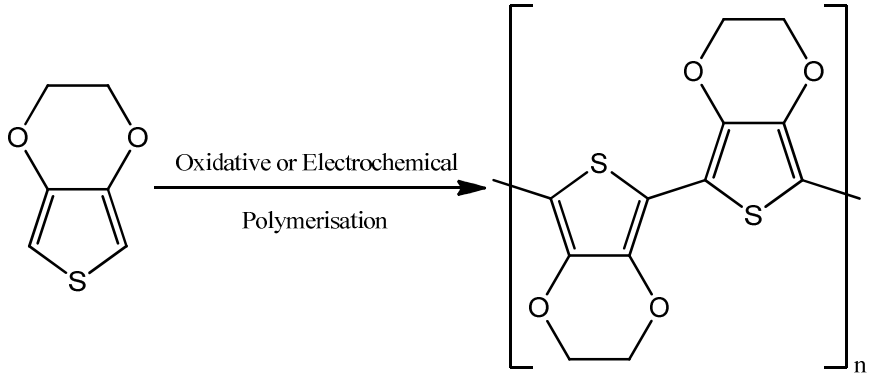

Figure 1.24 *– Formation of the conducting polymer poly-3,4-ethylenedioxythiophene from 3,4-ethylenedioxythiophene by either the oxidative or electrochemical polymerisation method.*

The mechanism by which 3,4-ethylenedioxythiophene polymerises to form a polymer is not conclusively agreed upon, but it has been suggested by Andersson *et al* (1994) that the mechanism involves the formation of a radical cation. The proposed mechanism is shown in Figure 1.25 below.

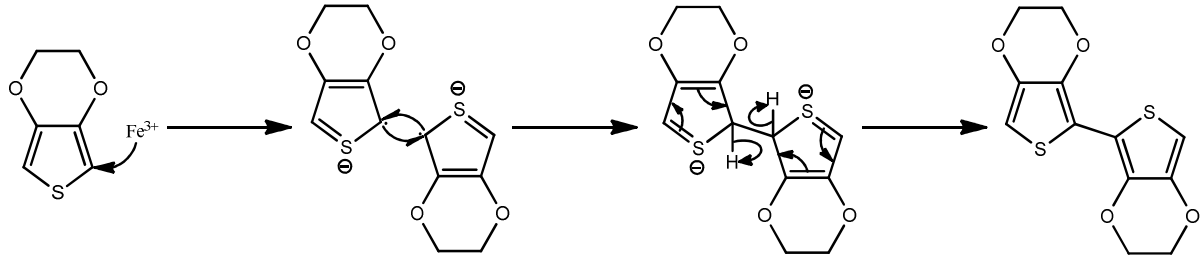

Figure 1.25 *– The mechanism of polymerisation of 3,4-ethylenedioxythiophene described by Andersson et al (1994).*

Electrical conduction in PEDOT occurs according to the mechanism of an intrinsically-conducting polymer described in Section 1.6.2. As such doping is required in order to make the polymer conducting. A number of different dopants have been described in

literature for use with PEDOT; ferrocene carboxylic acid and ferricyanide (Nie *et al*., 2013); dimethyl sulfoxide, dimethyl formamide and tetrahydrofuran (J. Y. Kim, Jung, Lee, & Joo, 2002); polyoxymethylene tridecyl ether (Ouyang *et al*., 2002); methane sulfonic acid, naphthalene sulfonic acid and *p*-toluene sulfonic acid (S. H. Yu *et al*., 2013); ethylene glycol, nitromethanol, glycerol and other such organic solvents with multiple hydroxyl groups present (Ouyang, 2013).

An issue with PEDOT arises, when being used as a sensor in aqueous based systems, from the inherent hydrophobicity of the polymer. This is a problem since there will be a repulsive force between the polymer surface and the aqueous phase which might prevent or limit the interaction of the analyte with the sensor. In order to limit this preventative force, PEDOT is often complexed with another polymer which lowers its hydrophobicity. Polystyrene sulfonic acid (PSS) is used for this purpose, and forms a strong ionic interaction with the PEDOT. PSS itself acts as a mild dopant due to the proton donating capability of the sulfonic acid group (Guo, Jian, Lin, Zhu, & Zhu, 2013; Ouyang, 2013).

1.1.1.17 Polypyrrole (PPy)

Polypyrrole (PPy) is the polymerised form of the monomer pyrrole. Polypyrrole is yellow in its pure form and becomes blue/black when a dopant is added. Films composed of polypyrrole are mechanically unstable, becoming increasingly more brittle when doped, but they are thermally stable up to 300^{o}C. However doped polypyrrole heated above 150^{o}C will start to lose its conductivity as the dopant evaporates. Polypyrrole is insoluble in organic solvents, but swelling of the polymeric matrix will occur to varying degrees depending on the solvent used (Vernitskaya, 1997). The structures of both the monomer and the polymer repeating unit are shown in Figure 1.26.

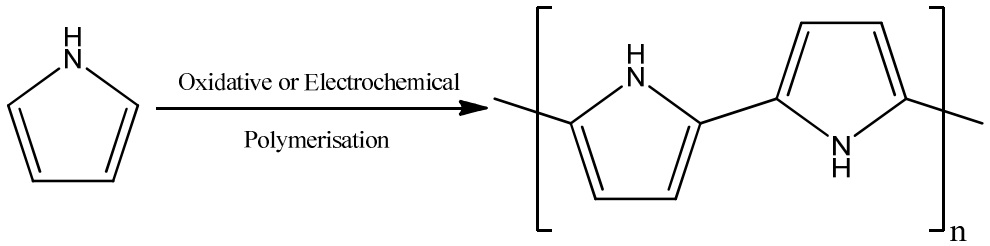

Figure 1.26 *– Formation of the conducting polymer polypyrrole from the pyrrole monomer by either the oxidative or electrochemical polymerisation method.*

The polymerisation mechanism for oxidative polymerisation is given in Figure 1.25. Polypyrrole can also be produced by electrochemical methods, where a voltage of 0.8 V is applied to a solution containing the monomer and a polymer chain will form and precipitate out of solution (E. H. Yu & Sundmacher, 2007). The mechanism of electrochemical polymerisation is given in Figure 1.27.

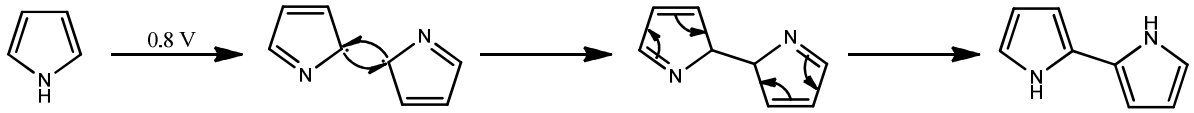

Figure 1.27 *– The mechanism of polymerisation of pyrrole described by* (Dong & Ding, 1987).

Polypyrrole is primarily classed as an intrinsically-conducting polymer and therefore is not conductive in its pure form, requiring a dopant for electrical conductivity (Vernitskaya, 1997). Anionic dopants that have been used include; tetrathiomolybdate (Belanger, Laperriere, & Gravel, 1990); tetrachloroferrate (Hahn, Stanchina, Gajda, & Vogelhut, 1986); ferrocyanide (S. Lee, Han, & Paik, 1993); metal pthalocyanines and porphyrins (Reynolds, Pyo, & Qiu, 1994); ferrocenesulfonates (S. Lee *et al*., 1993); and quinonesulfonates (Zinger, 1989).

The increase in conductivity of polypyrrole is greatest when larger anionic species are used as the dopant. For example, doping with tosylate ions gives a polymer with a conductivity of between 89 – 121 S cm^{-1} compared with a polymer doped with fluoroborate, which has a

conductivity of 2 – 2.5 S cm^{-1}. This is likely due to the polymer having to swell to incorporate the larger ion (Vernitskaya, 1997).

1.1.1.18 Polyaniline (PANI)

Polyaniline (PANI) is the polymerised form of the monomer aniline. It exists in three distinct forms; fully reduced (leucoemeraldine), partially oxidised (emeraldine) and fully oxidised (pernigraniline). The oxidation occurs at the nitrogen which is found between each benzene residue in the polymer. In the oxidised form the nitrogen is part of a double bonded system and in the reduced form the nitrogen is saturated. In emeraldine, the partially oxidised form, the nitrogens in adjacent repeating units alternate between protonated and unprotonated (Chiang & MacDiarmid, 1986; Feast *et al*., 1996). The structures of the monomer and the three forms of the polymer are shown in Figure 1.28.

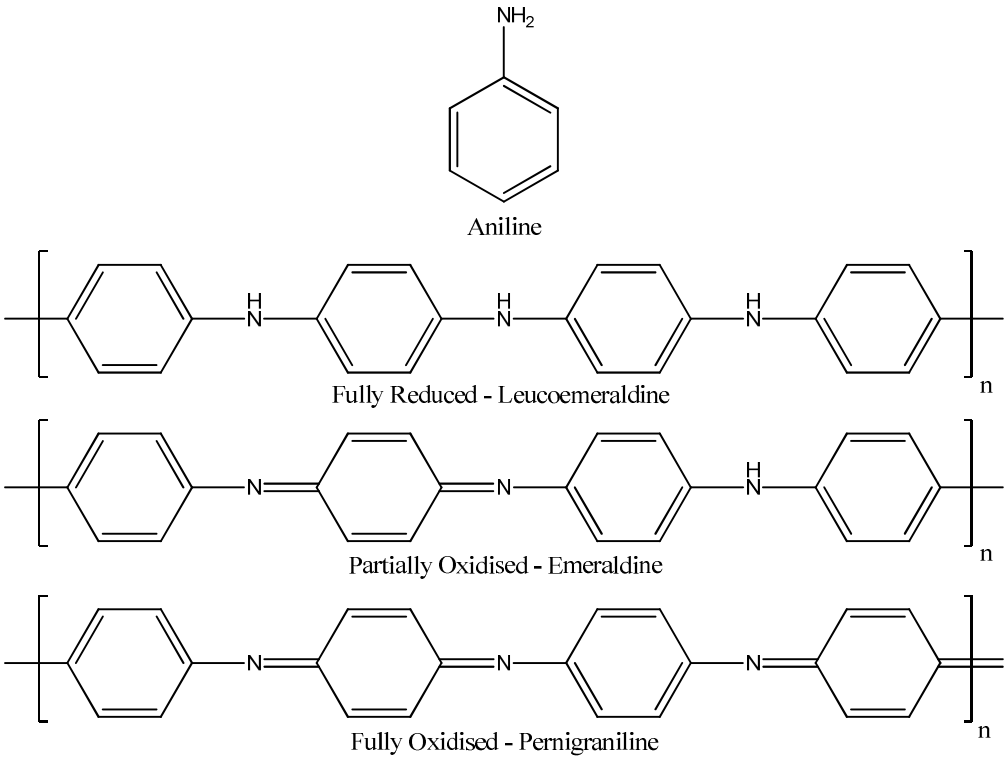

Figure 1.28 *– The structures of the monomer aniline and the three oxidation states of polyaniline* (Feast *et al*., 1996).

Of the three oxidation forms of polyaniline, leucoemeraldine and pernigraniline are poor conductors of electricity even upon doping with an acid. Emeraldine, on the other hand, becomes highly conductive upon doping. In this case the doping protonates the lone pair on the nitrogen, freeing the molecule to conjugate between the diaminobenzene and the diaminoquinone state, thus allowing conduction to occur (MacDiarmid, 2001).

Emeraldine has been produced by partial oxidation of leucoemeraldine using a variety of different oxidising agents such as; chlorine gas, nitrosonium hexafluorophosphate, iron(III) chloride, tin(IV) chloride and tetracyanoquinodimethane (Ray *et al*., 1989). Doping is then achieved by addition of a strong acid which protonates the nitrogen atoms in the polymer chain (MacDiarmid, 2001). The resultant doped emeraldine form of polyaniline can also be achieved by oxidative doping of leucoemeraldine, for example with chlorine or nitrosonium hexafluorophosphate (Ray *et al*., 1989).

When partial oxidation occurs a colour change is observed from white to blue. A further colour change, from blue to green, is observed upon doping. If the polymer becomes fully oxidised then it will become blue/black and will no longer conduct electricity. This colour changing capacity of polyaniline has been used as an electrochromic sensor. In a study by L.-M. Huang, Chen, & Wen, (2006) polyaniline was doped with DL-camphor-10-sulfonic acid and exhibited a change in colour between from pale yellow (-0.5 V) to dark blue (+2.5 V). The colour change is induced by electrochemical oxidation/reduction of the polyaniline between the three oxidation states.

1.6.5 Sensor Applications of Conductive Polymers

In the field of analytical detection there are numerous techniques which detect changes in electrical current caused by oxidation and reduction at an electrode. This change in current occurs as a result of the electrode donating or removing electrons to a charged species in

solution. The ability of a bare carbon electrode to pass on a charge is increased by the application of a conductive polymer. Therefore the detection is enhanced in one of two ways; either the threshold voltage for oxidation or reduction changes, with peak pairs moving closer together, or the maximum current at the peak is increased. Often both of these effects can be observed.

There are many examples in literature of conducting polymers being used for sensor applications. Because of the conductive nature, these sensors are not limited to electrochemical and electroanalytical techniques but also encompass other types of sensors such as tilt sensors (Castano, Winkelmann, & Flatau, 2010) and pressure sensors (Carvalho & Radwin, 1996; Choong *et al*., 2014). Since this research will deal with conductive polymers for electroanalytical chemistry, however, only these applications will be discussed below.

A study by Taryba and Lamaka (2014) used poly(3-octylthiophene-2,5-diyl) (P3OT) as a conductive polymer base to create a pH electrode. The advantage of the new electrode over the traditional pH electrode was the lack of glass or liquid in its construction which made the older style electrodes fragile. Selectivity for H^+ ions on the new electrode was achieved by using a selectively permeable membrane constructed of poly(methylmethacrylate-decylmethacrylate) (PMMA-DMA) with ionophores of 4-nondecylpyridine (4NDP). The microelectrode was created by depositing the various layers onto a needle-like shaft made from a platinum/iridium alloy using a layer-by-layer dipping method. The needle was insulated using 2-chloro-1,4-dimethylbenzene with the exception of the tip, which was coated with gold. A layer of P3OT was then deposited to a thickness of 0.2 – 0.6 nm. The ion-selective membrane was deposited by dipping the coated electrode into a solution of PMMA-DMA (0.5 – 10 %) and 4NDP (3 %) in xylene. The optimised membrane was tested against samples of various pH showing a range of pH 2 – 12. The electrode showed a linear,

Nernstian response between these values and the response was only slightly affected by the presence of a NaCl impurity, with readings only 3.5% higher than in pure buffered samples.

A flexible sensor for detecting volatile organic compounds (VOCs) was produced using two different conductive polymers; polyaniline (PANI) and poly(3,4-ethylenedioxythiophene)-poly(styrene-sulfonate) (PEDOT:PSS) as a conductive base (T. Kim & Kwak, 2012). The polymers were coated onto various membranes composed of polypropylene, polytetrafluoroethylene, cellulose ester, cellulose acetate or high density polyethylene. The newly fabricated sensors were then exposed to a saturated atmosphere of acetone and the change in resistance across the polymer film was measured. The PANI based sensor showed a higher resistance change in the presence of acetone than the PEDOT:PSS based sensor (5 % and 0.3 % respectively). The VOCs tested were acetone, chloroform, benzene, cyclohexane and hexane at concentrations between 100 – 500 mg L^{-1}, with the sensor demonstrating highest sensitivity for acetone. The best membrane base was shown to be cellulose ester, with a PANI coating showing a resistance change of 35.6 % ± 10.4 in the presence of acetone.

Glucose biosensors have been part of diabetes monitoring for some time, but the electrodes used in the electrochemical detection are historically based on platinum. Even more modern electrodes incorporate precious metals into a carbon paste (Newman & Turner, 2005). This makes them expensive, and since they are only single use electrons this makes blood glucose monitoring an expensive medical procedure. A glucose sensor based on conductive polymers was developed by Wang, Chen & Ho (2013). This sensor consists of nanobeads composed of branched polyethyleneimine bound to ferrocene, which acts as a redox mediator, glucose oxidase, which converts glucose into gluconolactone, and PEDOT:PSS, which binds the other constituents together and increases the electrode surface area. The nanobeads are then immobilised onto the surface of a carbon electrode which transmits the charge to be detected. The current is generated as a result of the oxidation of glucose by the glucose oxidase

enzyme. The liberated electrons are transferred to the electrode, causing a current which can be measured. The sensor was tested against a range of glucose concentrations between 0.5 - 10 mmol L^{-1} showing a good response which was almost linear. Results also show that the sensors incorporating PEDOT:PSS to increase the surface area did have a higher current response than those without. Furthermore, the sensor was tested against other compounds found in blood such as uric acid, dopamine and ascorbic acid. These tests show a very low cross reactivity (less than 10%). Reviews on the subject of conductive polymer based biosensors have been published by Ates (2013) & Park *et al*. (2014).

1.7 Graphene

Graphene, first isolated in 2004, is a 2D arrangement of carbon atoms which are linked together by sp^2 hybridised bonds similar to those found in benzene. Each carbon atom is geometrically trigonal planar and has π-electrons which are delocalised above and below the plane of the sheet. This delocalisation coupled with the low thickness of the sheet gives graphene unique electrical and optical properties which make it very useful in both the fields of electronics and electrochemistry (Novoselov *et al*., 2004).

Graphene is described as a semimetallic semiconductor. This is because in its pure isolated form it is slightly less conductive than a metal. The maximum conductivity of a single sheet of graphene is 1×10^2 S cm^{-1} (J. Liu *et al*., 2012). Composites containing multiple layers of graphene as well as other components can have conductivities between 1×10^3 and 2×10^4 S cm^{-1} (De & Coleman, 2010). This conductivity is caused by the slight overlap in the conduction and valence bands. This makes graphene a zero-gap semiconductor, as opposed to most semiconductors which have a band gap. The conductivity can be reduced to make it a true semiconductor by adding monofunctional or bifunctional molecules as spacers between individual sheets of graphene (Figure 1.29). These spacing molecules can either be covalently

attached or can interact via π-π stacking. Using this method, the conductivity of graphene can be reduced to as low as 1 mS cm^{-1} (J. Liu *et al*., 2012).

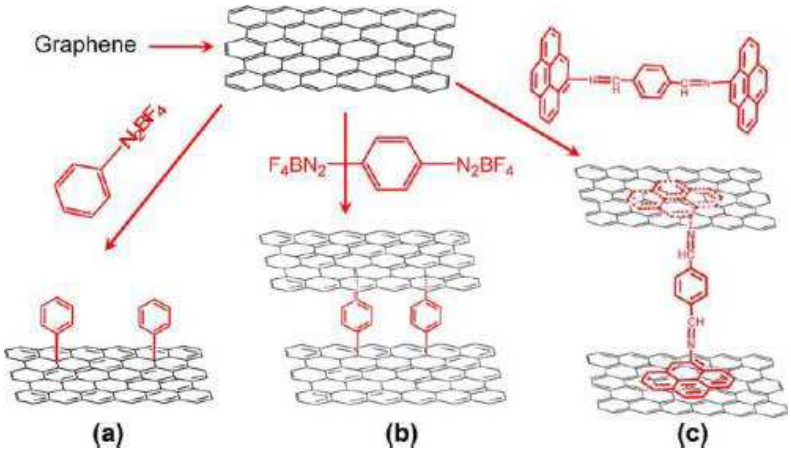

Figure 1.29 *– Post synthesis modification of graphene to change conductivity. (a) Covalent modification with monoaryl diazonium salts. (b) Covalent modification with bifunctional aryl diazonium salts. (c) π-π stacking of graphene with a bipyrene terminal molecular wire* (J. Liu *et al*., 2012).

Conduction in a graphene sheet occurs according to a similar method as an intrinsically-conducting polymer as shown in Figure 1.23. However, unlike an intrinsically-conducting polymer, graphene does not require a dopant in order for conduction to occur. A study by Schedin *et al.* (2007) showed that even at high concentrations of anionic dopant the conductivity of graphene is not significantly affected. Cationic dopants, however, have been shown to decrease the conductivity of graphene. A 20-fold reduction in conductivity was observed when graphene was doped with potassium (Chen *et al*., 2008).

Graphene has already been utilised in a multitude of different sensing applications considering this is still a relatively new material. The advantage to using graphene as a conductive base for biosensors is that has a relatively low background noise (a flatter baseline signal) and a high conductivity than screen printed carbon alone. This means that the signal to noise ratio will be higher for a smaller signal, meaning that that the signal will stand out more, allowing for the detection of much lower concentrations of analyte than with comparable materials. It has been hypothesised that suspended graphene sensors are more

effective than silica supported sensors because charges at the surface of the silica act as charge traps and external scattering forces which reduce the electron carrying capacity of the graphene (Cheng, Li, Li, Zhou, & Fang, 2010).

1.7.1 Sensor Applications of Graphene

A highly sensitive sensor for prostate specific antigen (PSA), a biomarker used for the detection of prostate cancer, was developed by Zhang, Li and Cui (2012) using a suspended graphene technique. In this technique, multiple layers of graphene were deposited between two gold electrodes onto a SiO_2 / Si support and each separated from the next by an insulating polymer layer. When complete, the SiO_2 layer was removed using HF and the Si layer etched away with SF_6. The capture antibody (anti-PSA) was immobilised onto the graphene and the biosensor was then ready to use. The analyte was quantified by measuring the change in conductivity of the graphene with increasing concentration of PSA. The construction of this sensor chip is shown in Figure 1.30.

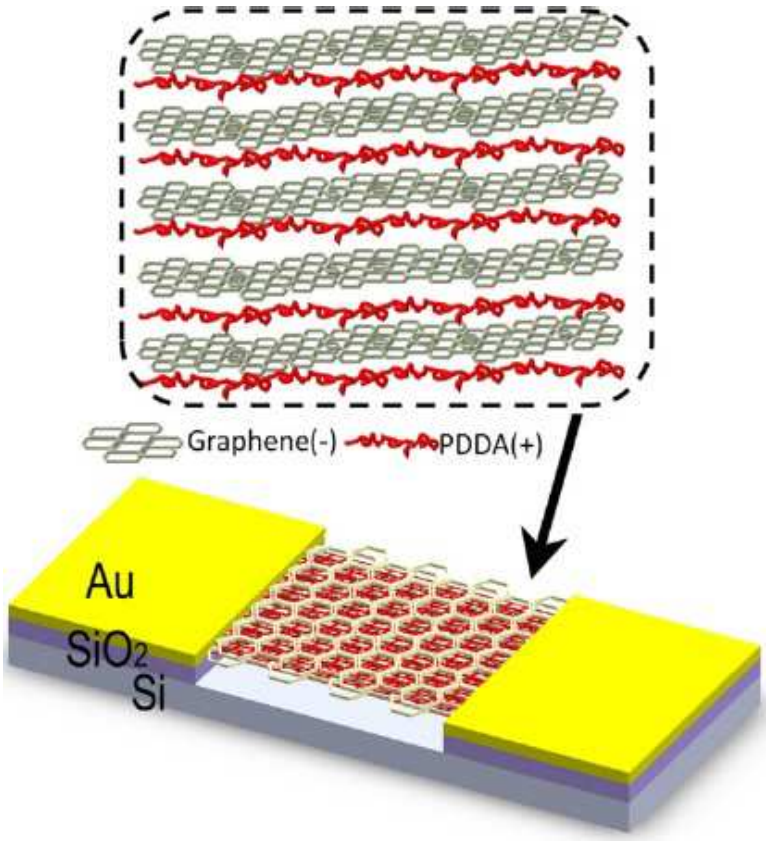

Figure 1.30 *– A suspended graphene sensor chip for detection of prostate specific antigen as a cancer diagnosis tool* (B. Zhang *et al*., 2012).

A biosensor for the detection of glucose was reported by Shan *et al* (2009) using graphene and the enzyme glucose oxidase. Unlike previous systems for measuring blood glucose levels (Clark Jr. & Lyons, 1962), which relied on the indirect detection of oxygen reduction or oxidation of H_2O_2 at an electrode as a measure of enzyme activity, this sensor system was able to detect the enzyme activity directly. This was achieved by direct electron transfer from the enzyme to the graphene sheet during glucose oxidation. It was reported that using this method the glucose concentration was linear up to 14 mmol L^{-1}, with the expected blood glucose level in a healthy individual being between 4 – 6 mmol L^{-1}, making this a potential future application for *in-situ* glucose testing. The upper limit of the sensor could have been increased by enclosing it in a membrane. A comprehensive analysis of the history of glucose bio-sensing was published by Newman & Turner (2005).

A graphene based immunosensor was developed by Liu *et al*. (2011) for the specific detection of viruses. The sensor was fabricated by functionalising the graphene layer with 1-pyrenebutyric acid. This was then used to couple an anti-rotavirus antibody to the sensor surface via N-hydroxysuccinamide facilitated amide formation. The remainder of the graphene surface was then blocked with bovine serum albumin (BSA) to prevent any non-specific binding. The rotavirus detection was then performed using cyclic voltammetry in an electrolyte solution containing $K_3Fe(CN)_6$ and KCl. The cyclic voltammogram showed a reduction in peak current and an increase in the peak voltage when in the presence of the rotavirus pathogen when compared to a blank. A control was also performed using variola virus. A reduction in peak current was observed, but it was not as pronounced as with the rotavirus.

One of the interesting effects of graphene on cyclic voltammetry is its ability to change the position of reduction / oxidation peaks on a voltammogram. The reduction and oxidation peak for a specific analyte can be closer together when a graphene coated electrode is used. This effect of graphene is the basis for research by Kim *et al*. (2010) where a graphene coated electrode was used to detect dopamine in the presence of ascorbic acid. Dopamine is an important neurotransmitter and its detection is therefore required. However detecting dopamine in blood samples can be difficult because of other electrochemically active compounds present which oxidise or reduce at similar voltages. It was discovered that the graphene coated electrode caused the voltage peak for ascorbic acid to move from 0.092 V - 0.024 V. The peak for dopamine, however, was unaffected. This separation effect allows for accurate determination of dopamine concentration within a mixed solution such as a blood sample.

1.7.2 Production Methods

Since its conception in 2004, many different methods for producing graphene have been discussed in literature (Soldano, Mahmood, & Dujardin, 2010). These methods range from mechanical techniques such as exfoliation and sonication to chemical techniques such as reduction of graphite oxide or the heating of a carbon containing compound to deposit a graphene sheet on a solid support. The various methods for graphene production will be discussed here.

1.1.1.19 Mechanical Exfoliation from Graphite

Mechanical exfoliation of graphene from graphite was the first production method used by the original researchers who discovered graphene in 2004. The procedure involves repeatedly peeling off layers (mesas) of graphene from highly ordered crystalline graphite. Graphite is essentially many layers of graphene held together by Van-der-Waals forces. It exhibits some similar properties to graphene, although the conductivity is not as efficient since the electron flow has a greater volume of material to flow into.

Preparation of graphene was performed using scotch tape and the newly prepared films were shown by electron microscopy to be only a few atomic layers of graphene thick. Single layer graphene was also produced by this method. The team fabricated metallic field-effect transistors from the few-layer and the single layer graphene flakes which proved to be switchable between a 2D electron gas state, via the ability of electrons to move freely in only two dimensions, to a 2D hole gas state, where there are no electrons. This effectively allowed the conductivity to be switched on and off by a voltage gate (Novoselov *et al*., 2004).

This technique is fundamentally flawed in that it cannot be used to consistently produce single layer sheets of graphene. Despite the fact that few-layer graphene sheets exhibit very

similar properties to those of single layer graphene it cannot be considered to be true graphene.

1.1.1.20 Epitaxial Growth of Graphene

Epitaxis is the process of depositing a crystalline layer onto a crystalline solid without covalent interaction between the layers. One method of doing this is to heat a silicon carbide (SiC) wafer to a high temperature and under a low pressure in the presence of an inert noble gas (argon) which will control the sublimation process of the SiC to give solid carbon. A graphene sheet is then formed with the dimensions of the original wafer (Sutter, 2009).

Another epitaxial production method is the chemical vapour deposition of carbon onto a flexible metal sheet. The metal sheet acts as a catalyst which, under a high temperature and low pressure, ensures that the newly liberated carbon forms a monolayer of graphene instead of some 3-dimensional structure. The other benefit of this is that once the catalyst is completely covered the reaction will cease, meaning that only a single layer of graphene can form. A study by Bae *et al* (2010) used copper as the metal substrate and methane as the carbon source. They were able to produce a sheet of graphene with a diagonal length of 30 inches, which was incorporated into a touch screen device.

The benefit of this method over others is that it is able to produce a large sheet of continuous graphene where other methods tend to yield far smaller flakes instead. This is useful if the intended application is flexible electronics, where a screen composed of small flakes of graphene might not be as transparent as one composed of a single sheet.

1.1.1.21 Reduction of Graphite Oxide

Chemical reduction of graphite oxide made by mechanical exfoliation (Section 1.1.1.19) has been described by Stankovitch *et al* (2007). Graphite oxide is intrinsically non-conductive because there are fewer sp^2 hybridised bonds compared with graphene. As mentioned above

(Sections 1.6.2 and 1.7) sp^2 hybridisation is necessary for electrical conduction in graphene because of the delocalisation of the p-orbitals within the graphene sheet. By chemically reducing the oxygen containing groups in the graphite oxide (epoxides, hydroxyls and carboxylic acids) a sheet of graphene was produced.

The graphite oxide was prepared by reaction of graphite powder with a mixture of sodium nitrate, sulfuric acid and potassium permanganate as described by Hummers and Offeman (1958). Graphite oxide consists of multiple sheets of oxidised graphene. This was then converted into graphene by chemical reduction using hydrazine hydrate. The graphite oxide was dispersed in water and sonicated until the solution became clear. The reductant was then added and the solution heated under reflux for 24 hours. As the graphite oxide was reduced, the newly formed graphene was precipitated out of solution as a black solid. This was then washed with methanol and dried. The structure of graphite oxide is shown in Figure 1.31.

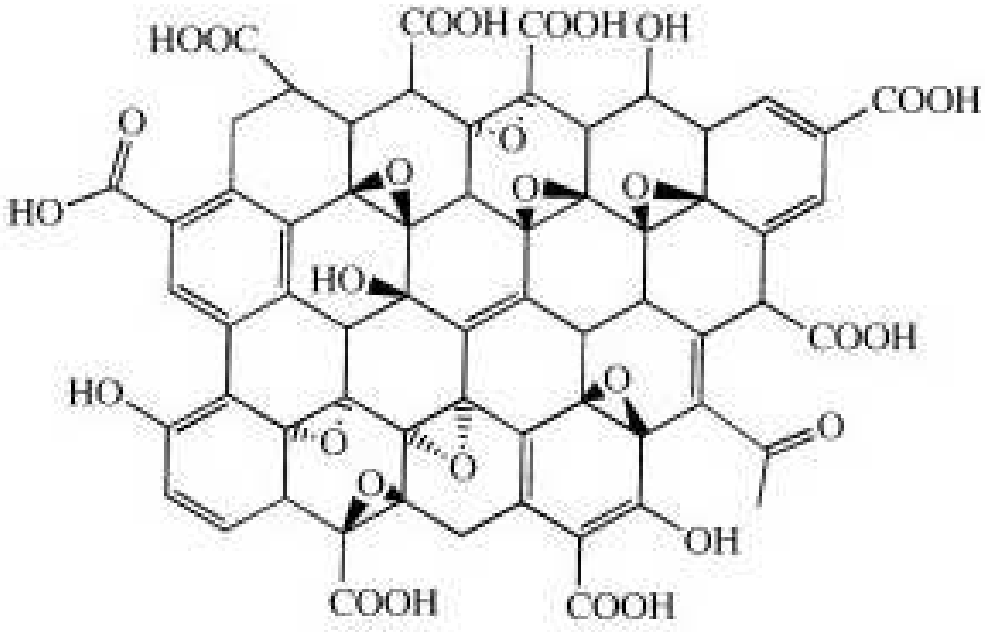

Figure 1.31 *– Typical structure of graphite oxide showing the different types of polar groups on above and below the plane of the graphene sheet* (Jerew, 2013).

The presence of polar groups above and below the plane of the graphite layer allows for hydrophilic interaction between the water and the graphite oxide sheets. This separation causes the newly formed sheets of graphene to be single layer sheets. Conductivity of the graphene was shown to be approximately 20 S cm^{-1}.

1.1.1.22 Sonication of Graphite

Graphene can be produced by sonication of a solution of graphite powder in the presence of an appropriate surfactant. The sonication was performed for 5 minutes at a power of 60 W, which was sufficient to disaggregate the individual graphite layers. The surfactant in solution forms a monolayer around the newly disaggregated graphene preventing the Van-der-Waals interaction from reforming and so the graphene remains as single layers. This process is shown in Figure 1.32.

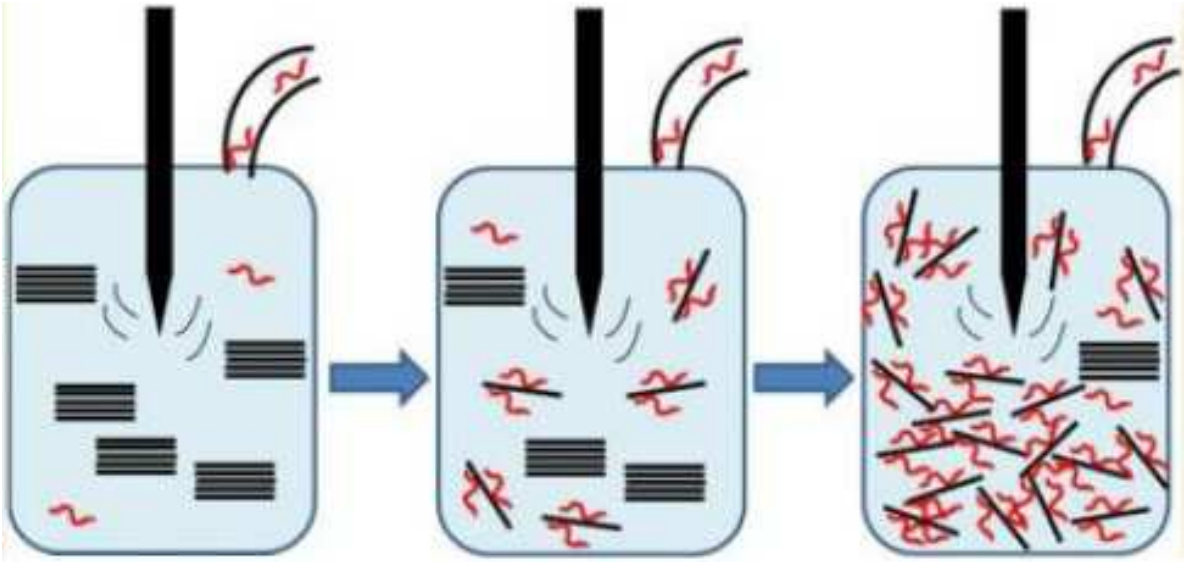

Figure 1.32 *– Production of graphene by sonication of graphite in solution with a surfactant* (Notley, 2012).

The concentration of surfactant was found to influence the final concentration of graphene. Notley (2012) investigated the effect of increasing surface tension given by different concentrations of surfactant on the concentration of the final product. The study showed that the concentration of product plateaus at a surface tension of 41 mJ m^{-2}, which is also the

surface free energy of graphene. At this surface tension the amount of surfactant in solution is sufficient to surround any graphene sheets that are formed during sonication, and so the product yield is not increased by addition of further surfactant. Transmission electron microscope images show predominantly single layer graphene flakes of between 100 - 200 nm in size (Notley, 2012). Different surfactants were investigated, with the highest product yield being obtained using Synperonic® F 108 (10.23 mg ml^{-1} of graphene). The graphene suspension was purified by membrane dialysis through a 100 kDa cellulose membrane to remove the surfactant and any other impurities. Each solution was then centrifuged at 1500 x G for 5 minutes to remove larger aggregates before use.

Similar methods have also been described by other groups, but with significantly lower yields; 0.01 mg ml^{-1} (Hernandez *et al*., 2008), 2.21 mg ml^{-1} (Alzari *et al*., 2011) and 5.33 mg ml^{-1} (Nuvoli *et al*., 2011).

1.8 Molecular Modelling

Determination of expected complexation energy of guest-host complexes can be determined using computer modelling. Molecular modelling or *in-silico* modelling is becoming a very useful tool in the field of drug development. The basic principle behind it is that instead of having to do many rounds of complex *in-vitro* and *in-vivo* assays in order to test the binding affinity of a new drug which is being developed, the binding strengths of different ligands can be simulated using known binding characteristics. This allows potentially thousands of different ligands to tested against a particular receptor which has been identified as playing a key role in a particular disease of interest without having to go through the lengthy process of synthesising each one and testing it against the target receptor (Meyer, Swanson, & Williams, 2000; Nikiforovich, 1994).

Binding energy has the units kCal mol^{-1}, where the lower the energy the higher affinity the binding between the two species, as this represents a more stable structure. This can also be

represented as a binding constant (K), or in kJ mol^{-1}. Conversion between kCal and kJ can easily be done since 1 kCal is equal to 4.186 kJ. A correlation graph between binding constant and binding energy in kCal mol^{-1} can be seen in Figure 1.33.

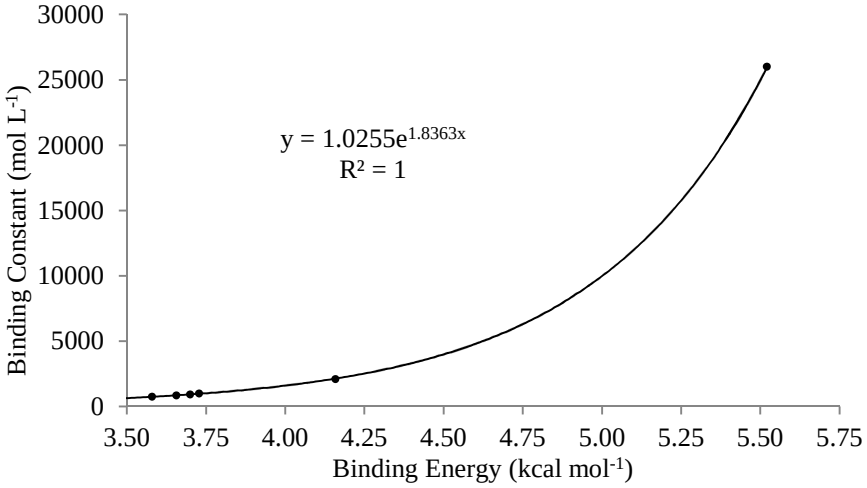

Figure 1.33 *– The correlation between the binding constant (K) with the units of mol* L^{-1} *and the binding energy in kCal* mol^{-1} *for a complex formed between one or more molecules. Made using data obtained from Mareeswaran et al.* (2012).

The reverse application of this method is to design a receptor around a target molecule. In this mode, the LeapFrog algorithm of the molecular modelling software SYBLL is used to simulate annealing between the target molecule and a virtual library of 20 of the common proteinogenic amino acids. This method was used by Heurich, Altintas & Tothill (2013) to produce a novel protein ligand for ochratoxin A, a mycotoxin that has been identified as a potential carcinogen. The software simulated annealing between the ochratoxin and the amino acid library, producing a list of binding energies for each amino acid.

Once the LeapFrog algorithm had determined the amino acids with the highest binding affinity to the target, the DREAM-mode of the software (using the “tailor” option) was used to create new protein fragments of between 3 and 5 amino acid residues in length. The binding energies of these new protein fragments was then assessed by the software and the top five fragments were then manually modified by either addition of amino acids or

dimerization. The SYBLL software then performed a simulated anneal between each of these fragments and the binding energies were recorded. In addition to the relative strength of the binding energy involved in the complex, other aspects of the suggested peptides were considered such as length of peptide strand and hydrophobicity of the resultant protein. All aspects of the suggested ligands were considered and two novel protein structures were selected to be synthesised (Figure 1.34); these novel peptides were not the peptides with the highest binding affinity as these were not feasible in solution. A compromise had to be reached to give successful binding (Heurich *et al*., 2013).

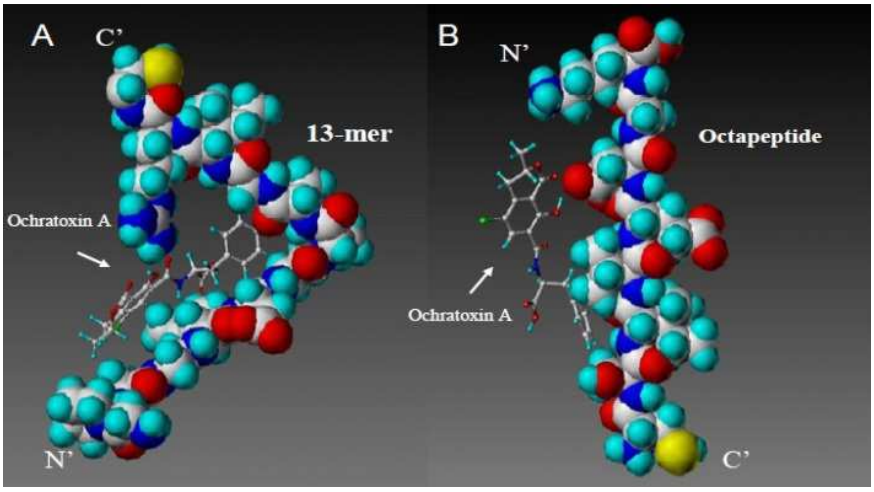

Figure 1.34 *– Screenshot of a simulated anneal between two novel peptides and ochratoxin A performed by the LeapFrog algorithm of molecular modelling software SYBLL* (Heurich *et al*., 2013).

Another example of this process is *in-silico* modification of the enzyme Kemp eliminase KE70 demonstrated by Khersonsky *et al*. (2011). In the study, the computationally designed enzyme was modified by insertion of amino acids deemed to improve the catalytic activity of the enzyme as well as random mutagenesis. In 9 rounds of computational analysis, a new form of the enzyme was created with greater than 400 times catalytic activity than the original design.

1.8.1 Concepts in Molecular Modelling

There are many different types of algorithms and concepts within the field of molecular modelling which must be understood before *in-silico* studies can be fully utilised. These will be briefly explained below.

Molecular mechanics (MM) & quantum mechanics (QM) are two different methods for calculating the energy contained within a bonded or non-bonded system. The calculation takes into account the change in bond energy caused by things like orientation, bond lengths & angles, hydrogen bond length and Van-der-Waals interaction. The difference between MM and QM is that that MM uses standard bond lengths and angles to calculate the lowest energy structures. In QM all of these parameters are calculated using the Schrödinger equation and therefore the conclusion of a structure energy minimisation is closer to the actual conformation. Because the MM energy minimisation algorithms do not take into account the electrons these methods tend to be faster. Also, since the number of parameters used is lower than for a QM method, there is no limit on the number of atoms that a molecule can have. In reality both of these methods can be used. When a molecule is roughly drawn, an MM method can be used to "clean up" the structure, before a more thorough QM method is used to give a more finely tuned conformation (Hehre, 2003).

In molecular modelling a genetic algorithm can be used to determine binding energy. The algorithm works by altering the way a ligand and a receptor fit together either by orientation of the ligand or flexibility (by bond rotation) of the ligand and/or receptor. Each of these different simulated bindings is called a pose. The algorithm calculates the binding energy of each pose, taking into account the number and length of hydrogen bonds as well as any Van-der-Waals forces between the ligand and the receptor, and then compares this to the binding energy of the previous pose. If the binding energy is lower, i.e. the binding is stronger, then the new pose is accepted. If not then it is rejected and a new pose is analysed.

In this way the algorithm gradually improves the strength of the binding in a similar fashion to Darwinian evolution, hence the name. The algorithm will stop when it reaches the end of an allowed number of iterations or it fails to reduce the binding energy any further. This type of method will give the lowest possible binding energy for a ligand and a receptor. But whether or not this energy is comparable to the actual value depends on a number of factors such as conformations of the ligand and receptor and the presence of different solvents. Most molecular modelling software packages allow for a simulated anneal to be performed in the presence of different solvents so that these effects can be observed. A popular application of a genetic algorithm is the Monte Carlo method, which repeats random calculations multiple times to gain data which can then be analysed for trends (Haupt & Haupt, 2004).

A phenomenon within the field of molecular modelling that can lead to incorrect results is the local minimum effect. A local minimum occurs when the ligand gets stuck in a pose that is of a low energy but not the lowest possible energy (Figure 1.35).

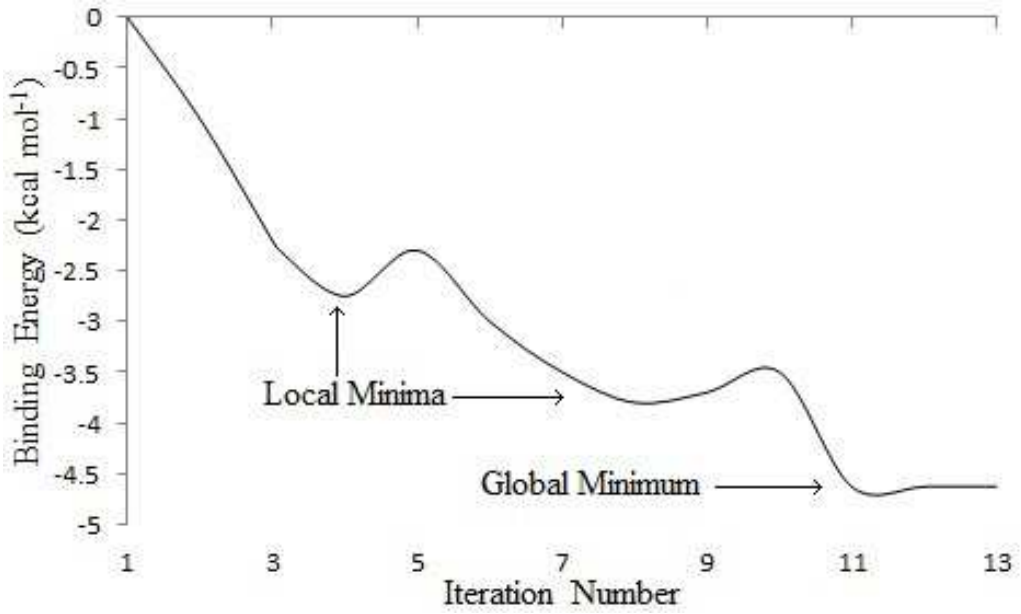

Figure 1.35 *- The concept of a local minimum in molecular dynamics showing how an energy minimisation or binding energy calculation can give an incorrect result.*

If the resolution of the software is too low then a Monte Carlo algorithm will not allow the ligand to move out of this pose because to do so it would have to adopt a higher energy

conformation (Schelstraete, Schepens, & Verschelde, 1999). Resolution in this context refers to a number of different parameters. Convergence energy is the maximum energy change between two consecutive poses at which the software will determine it has reached the lowest possible energy. Grid resolution is the distance between two points on the grid which is used to position a guest and host molecule during a simulated anneal. The mutation rate, in a genetic algorithm, is the rate at which the guest molecule is changed with each successive iteration.

1.9 Analytical Techniques

In order to detect the formation and dissociation of a guest-host complex between the calixarene and the analyte an analytical technique must be used. Numerous techniques exist for the quantitative and/or qualitative analysis of analytes in solution via specific binding interactions. Surface plasmon resonance, quartz crystal microbalance and chromatographic techniques are well described in literature as being reliable and reproducible for both qualitative and also quantitative analysis of mixtures. However, they are not practical for a portable low cost and low maintenance application since they require expensive equipment, large volumes of solvents and other miscellaneous solutions to perform analysis. Potential sweep voltammetry techniques, such as cyclic voltammetry, would be more suited, since they are able to directly detect analytes in solution without the need for excessive sample preparation.

1.9.1 Nuclear Magnetic Resonance Spectroscopy

Nuclear magnetic resonance (NMR) spectroscopy utilises the magnetic properties of certain atomic nuclei, including but not limited to ^{1}H, ^{13}C, ^{15}N and ^{31}P, to determine the presence and position of certain functional groups within a molecule. As described later (Section 1.1.1.23) NMR can also be used to determine binding energy in guest-host complexes. The NMR effect occurs when the nucleus of an atom is subjected to a constant magnetic field which

causes the nuclear spin to align. This alignment is then countered by the application of a radio frequency pulse at a given frequency and perpendicular to the magnetic field. This causes a resonance in the nucleus which can be detected. It is then amplified and converted into a digital signal which is used to create the NMR spectrum (Keeler, 2010).

The frequency of the resonance is dependent on the frequency of the magnetic field and thus to make interpretation and comparison of spectra less complicated a chemical shift scale is adopted. The chemical shift scale gives the position of a peak relative to a known compound, which will always be the same regardless of the strength of the magnetic field. The reference compound in the case of ^{1}H and ^{13}C NMR experiments is tetramethyl silane (TMS). The chemical shift can be converted into actual frequencies for mathematical calculations if necessary. Nuclei in different regions within the molecule can behave in subtly different ways when subjected to the radio frequency pulses. This is caused by the presence of electronegative species such as nitrogen and oxygen in the molecule and their position relative to the nucleus in question. This is called the deshielding effect, and it results in nuclei in a more electronegative environment showing more towards the left of the spectra, whereas nuclei with little or no proximity to an electronegative element will give peaks closer to that given by the reference (Keeler, 2010).

In addition to the chemical shift, peaks on a ^{1}H NMR spectrum also have splitting patterns. A splitting pattern is caused by the spin of adjacent nuclei of the same type. Since the spin state can be “up” or “down” this means that the combination of a dual-nuclear spin can either be the same or in opposite directions (up-up / down-down or up-down). These different spin states will give slightly different resonance frequencies, giving rise to a split peak. Peak splitting is helpful when interpreting a spectrum because it gives information about relative position of the groups which give rise to a peak. For example, in a ^{1}H NMR spectrum a group that gives a doublet peak is next to a carbon with only one hydrogen on it. A group that gives

a quadruplet peak is next to a carbon with three hydrogens on it. The number of peaks that a particular hydrogen environment will generate is calculated by the n+1 rule, where n is the number of adjacent hydrogens. A similar phenomenon can be observed in ^{13}C NMR, where peak splitting is caused by the number of protons on the carbon. Here the number of peaks is equal to n+1, where n is the number of hydrogens attached (Keeler, 2010).

Since an ^{1}H NMR experiment can only detect ^{1}H nuclei and not ^{2}H a hydrogen containing solvent that would normally flood the spectrum with an unwanted signal can still be used, but in its deuterated form. If a hydrogenated solvent were to be used, the signal would be so strong that the signals from the sample would not be visible. A deuterated solvent with dissociable protons, such as D_2O, can also be used to exchange any dissociable hydrogens in the sample with deuterium atoms. This allows these protons to be highlighted when compared to a non-exchanged sample or removed completely to clean up a cluttered spectrum.

1.1.1.23 Advanced NMR Techniques

While traditional NMR techniques may be used for the structural determination of small simple molecules, for interpretation of spectra for larger and more complicated molecules, there are a number of advanced techniques to that can be used.

Correlation spectroscopy (COSY) is a 2-dimensional technique where a correlogram is produced by irradiating the sample at the frequency of a peak. This causes the peak and any other peaks which represent a nucleus in an adjacent environment to be highlighted by the software. This is performed sequentially until all peaks in a spectrum have been analysed. The results are then combined into a graphical representation which is easier to interpret than a one dimensional spectrum. Two ppm scales are shown at right angles to each other and peak correlations are shown in the space between them. Since the irradiated peak and any adjacent peaks are all highlighted the correlogram is symmetrical and a diagonal line can be

used to determine peak correlation (Figure 1.36). Only directly adjacent nuclei can be identified by a COSY spectrum.

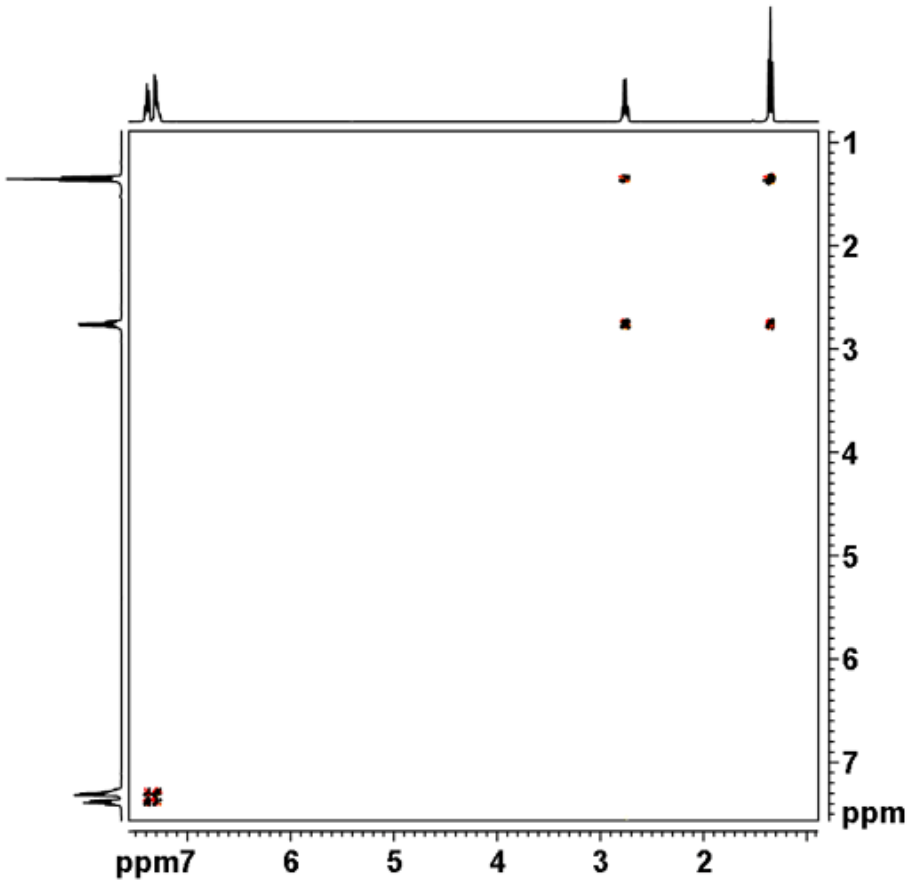

Figure 1.36 *– The correlation spectroscopy (COSY) spectrum for ethylbenzene showing how adjacent peaks are highlighted by the technique.*

A similar technique called total correlation spectroscopy (TOCSY) can be used in conjunction with a COSY spectrum. This technique not only shows directly adjacent nuclei, but also nuclei in the same spin system. A spin system in the context of a TOCSY experiment is defined as a group of similar nuclei environments separated by a hetero atom, for instance in the polyamide backbone of a protein where two carbon atoms are separated by a nitrogen. The two carbon atoms and anything bonded to them make up a spin system (Bruch, 1996).

Another type of NMR correlation spectroscopy is heteronuclear single-quantum correlation spectroscopy (HSQC). In this type of spectroscopy the 2-dimensional aspect of the

correlation is provided by an NMR spectrum of a different nucleus. This works in a similar way to the COSY spectroscopy. The sample is irradiated at a frequency corresponding to a peak. This causes an effect on the peaks representing any nucleus bonded directly to the nucleus shown by the first peak. This is useful in complex molecules because it will show peaks from a ^{1}H NMR and a ^{13}C NMR which represent the same part of the molecule. As with COSY, HSQC only shows atoms linked by a single bond. There is a similar technique called heteronuclear multiple-bond correlation spectroscopy (HMBC) which is able to identify atoms within the same spin system (Bruch, 1996).

Nuclear Overhauser Effect Spectroscopy (NOESY) is another form of correlation spectroscopy only instead of highlighting nuclei which are bonded to each other it shows nuclei which are spatially close to each other (within 5 Å). This type of NMR study is useful for binding studies since it will show what parts of the guest and host molecules are close to each other. It is also useful in studying the conformations of calixarenes as some nuclei are only close enough to each other to give a NOESY signal in certain conformations. This technique utilises the nuclear Overhauser effect, which allows spin polarisations to transfer from one nuclear spin populations to another so long as they are within 5 Å of each other (Bruch, 1996).

A technique which is useful for interpretation of complex ^{13}C NMR spectra is distortionless enhancement by polarisation transfer (DEPT). This technique uses a polarised radio frequency signal to produce the resonance in the nuclei of the sample. The result of this polarisation is that only certain carbon nuclei (dependent on the number of hydrogens attached) will show. There are three types of DEPT experiment; 45^{o}, 90^{o} & 135^{o}. Each angle will highlight different types of carbons. DEPT-45^{o} will show all carbons with protons attached (i.e. primary, secondary and tertiary). This will eliminate any quaternary carbons from the spectra. DEPT-90^{o} only shows tertiary carbons (CH) with all others being omitted.

DEPT-135^{o} is a little more complicated with primary (CH_3) and tertiary carbons showing as normal, but secondary (CH_2) carbon peaks will show as negative peaks. Combining a DEPT-90^{o} and DEPT-135^{o} spectrum will distinguish which of the positive peaks are tertiary. A DEPT-45^{o} can then be compared to a standard ^{13}C NMR to identify any quaternary carbons. With individual peaks categorised as primary, secondary, tertiary and quaternary, they can be more easily assigned to carbons in a molecule (Bruch, 1996).

The binding of a guest and a host molecule to form a guest-host complex can also be observed by NMR. When two molecules bind together by Van-der-Waals, the nuclei of the atoms involved in the binding become more shielded in NMR terms. This can be observed by the shifting of a peak on the NMR spectrum when compared to the spectrum for the unbound sample.

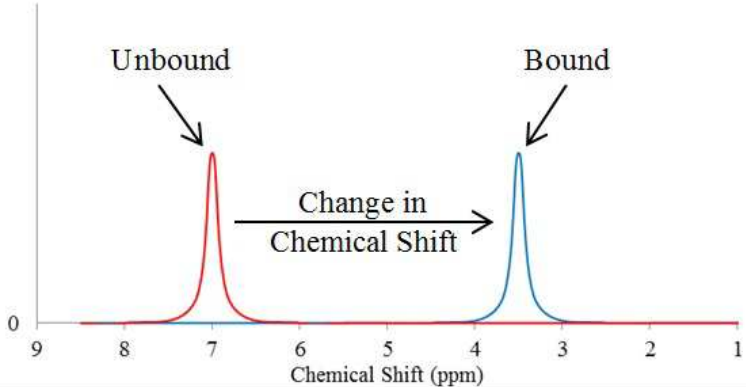

Figure 1.37 *– The effect of intermolecular binding on the position of a peak in an NMR spectrum showing the unbound position (left) and bound (right).*

An NMR titration can be performed where the guest and the host molecules are combined in varying quantities up to a 1:1 ratio (assuming that the binding is 1:1). The peak shifting in relation to the concentration change can then be used to determine binding energy. In addition to this, NMR binding studies can also show exactly where on the molecule the binding has occurred. This is because only the peak which represents a nucleus involved in the binding will shift as a result of the interaction. Once identified the atom or atoms involved can be used to build up a picture of how the binding occurs as well as any conformational

change imposed on the host by the binding (Akita, Matsui, & Yamamoto, 2014; Hayashi, Ujihara, & Kohata, 2004; Sheff, Lucius, Owens, & Gray, 2011).

1.9.2 Infra-Red, and Raman Spectroscopy

Infra-red (IR) spectroscopy is a vibrational technique that uses light absorption at different frequencies to determine the functional groups and bonds present within a sample. For the purposes of this research IR spectroscopy will be used to determine the structure of the new resorcinarene compounds. Raman spectroscopy will be used to determine that graphene had been successfully produced. The technique utilises the scientific principle that certain bonds will vibrate as they absorb a specific frequency or a specific frequency range of light in the infra-red spectrum of light (typically between 400 – 4000 cm^{-1}). The IR spectrometer works by first creating an interferogram consisting of all frequencies in the desired range. This interferogram is then passed through the sample, which will absorb certain frequencies whilst letting others pass through. The transmitted light is then translated back into individual frequencies using Fourier transform and plotted as a function of transmittance against frequency. The specific absorbance of different functional groups creates characteristic bands. This allows for structural information about the molecule to be determined, however direct comparison with IR spectral databases is required for accurate molecular identification.

There are a number of different types of absorption that can be seen, and these are characteristic of the type of vibration that occurs. Three common types of vibration leading to adsorption are as follows; symmetrical stretch, asymmetrical stretch, and bend. These vibrations occur when particular bonds (for example C-H) absorb energy at a specific frequency. Most bonds are capable of more than one type of vibration, and therefore there is often more than one band to indicate the presence of a particular functional group.

IR spectroscopy is useful in organic synthesis to determine whether or not a reaction has been successful by comparing the spectrum of the product with that of the reactants and/or intermediate products and looking for the disappearance of characteristic absorbance bands. An example of this is the disappearance of the peak representing the carbonyl when synthesising resorcinarenes by the condensation of resorcinol and an aldehyde. Another use of IR spectroscopy is to verify the removal of solvents used in production, such as water. Water has a characteristic absorption at around 3500 cm^{-1} and can often be difficult to remove from hygroscopic material. However since there are a number of different functional groups that absorb in this region it is necessary to look at the shape of the absorbance as well as the specific frequencies.

A similar technique called Raman spectroscopy involves passing a beam of monochromatic light through a sample and scattering of the incident beam occurs. The scattering is inelastic, meaning that it does not return to its original state after it passes through the sample. This means that small changes in the frequency of the transmitted light can be detected and used to determine certain properties of the sample. Unlike IR spectroscopy Raman shows not only what bonds are present in the sample but also gives information about the intermolecular forces involved. This makes it ideal for detecting whether or not the Van-der-Waals forces in graphite have been sufficiently broken down to form graphene.

1.9.3 Dynamic Light Scattering

One of the techniques used in this research to determine the size of the graphene particles is dynamic light scattering. Dynamic light scattering (DLS) or photon correlation spectroscopy (PCS) is a technique which relies on Brownian motion, the random movement of particles or molecules within a liquid or gas, to determine the size of particles smaller than a micrometer. Brownian motion of a particle is caused by the movement of adjacent solvent molecules. The friction between the particle and the solvent also effects this movement, and the larger the

particle the greater the force of friction and so the slower the movement. The basic components of a DLS spectrometer are a He-Ne laser, a lens and a photo detector. The data obtained by the photo detector is then extrapolated by a photon correlator (Goldburg, 1999).

The measurement is taken by passing a coherent monochromatic beam of light through the sample. Upon coming into contact with a suspended particle with a diameter smaller than the wavelength of light, the beam is scattered by an equal amount in all directions by Rayleigh scattering (Goldburg, 1999; Malvern Instruments, 2012). The speed of movement of the particles is then detected as they pass through the path of the light beam and this data can be translated to give the hydrodynamic diameter of the particle using the Stokes-Einstein equation (1.3).

$$d(H) = \frac{kT}{3\pi\eta D} \qquad (1.3)$$

The Stokes-Einstein equation for measuring particle size by DLS (Malvern Instruments, 2012)

The terms in this equation are as follows:- the hydrodynamic diameter of the particle (d(H)), the Boltzmann distribution constant (k), the absolute temperature of the sample (T), the solvent viscosity (η) and the translational diffusion coefficient (D).

1.9.4 Total Internal Reflection Ellipsometry

Total internal reflection ellipsometry (TIRE) is an optical technique which can be used to measure the dielectric properties of a thin film. It can be used to characterise a number of different surface properties such as composition, doping level and electrical conductivity. In this research TIRE will be used to determine film thickness of deposited graphene thin films. The technique relies on the surface plasmon resonance (SPR) phenomenon, where energy from an incident beam of plane polarised light hitting the surface of a metal causes electromagnetic waves known as surface plasmon polaritons to propagate through the metal.

The SPR effect occurs at the boundary between the metal and the air/solvent and as such it is highly sensitive to alterations in the surface.

The amount of light energy absorbed is dependent on a number of factors; the thickness of the metal layer (which remains constant), the angle of incidence of the plane polarised light and the composition of the metal surface. Changes in the composition of the surface can therefore be determined by altering the angle of incidence to maintain maximum light absorption by the surface. The typical apparatus for TIRE is shown below.

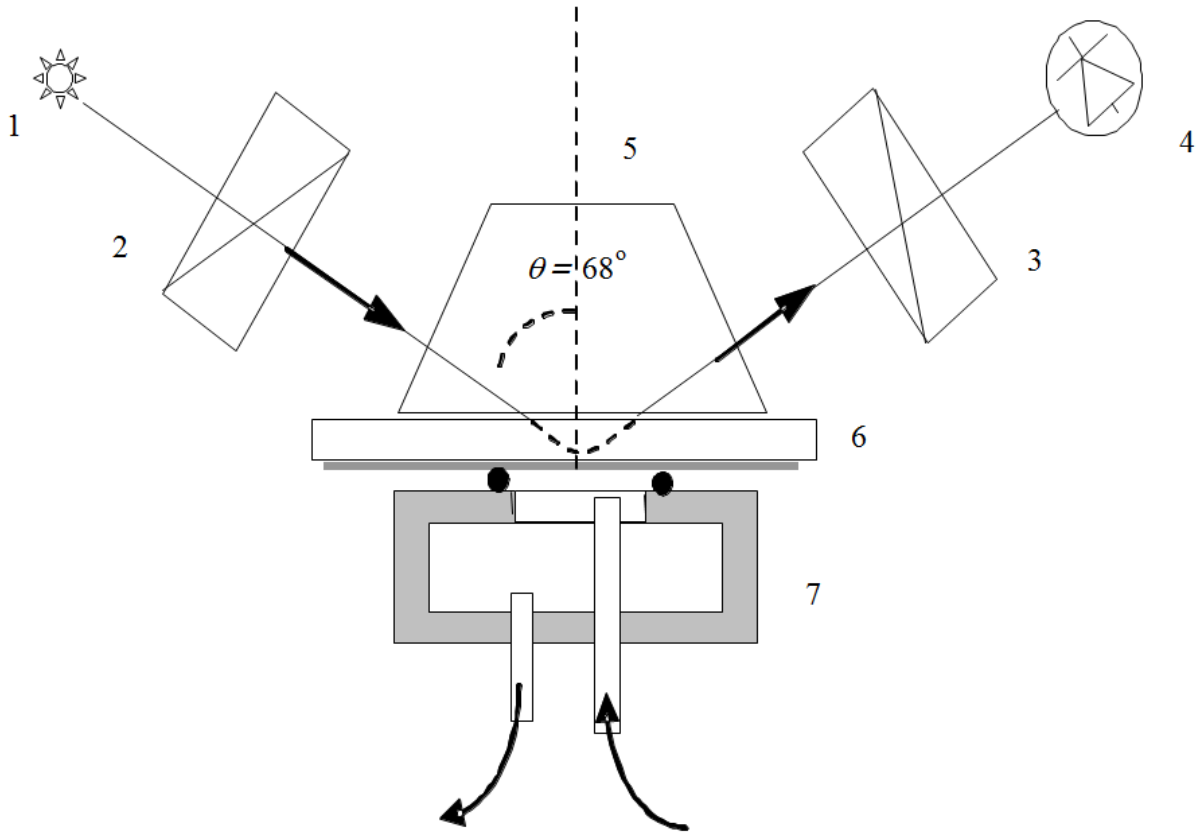

Figure 1.38 – Typical apparatus setup for a total internal reflection ellipsometer comprising white light source (1), polariser (2), analyser (3), photodetector array (4), 68◦ prism (5), Cr/Au coated glass slide (6), reaction cell (7).

Unlike traditional SPR, however, TIRE can detect changes in the polarity of the detected light. This can make the technique up to 10 times more sensitive to surface changes than

SPR. Additionally it allows for the thickness of surface layers to be determined by fitting the data to previously defined parameters. This makes it a useful technique for monitoring deposition of a sample onto a substrate by Langmuir-Blodgett, Langmuir-Schaefer, or Layer by Layer deposition.

1.9.5 Differential Scanning Calorimetry

Differential scanning calorimetry (DSC) is an analytical technique which is used to measure phase changes (melting / evaporation) in a sample. It can be used to determine the energy involved in a calixarene or resorcinarene guest-host complex. The measurement is taken by heating the sample and a reference at the same time and with the same amount of energy. The amount of energy required to increase the temperature of the sample compared to the reference is recorded and plotted onto a graph. As a phase transition occurs, a positive or negative peak will be seen representing the change in heat flow as that transition occurs. The change in heat flow is calculated by subtracting the heat flow in the sample chamber from the heat flow in the reference chamber (or vice-versa depending on the equipment used). An example of a DSC curve is shown in Figure 1.39.

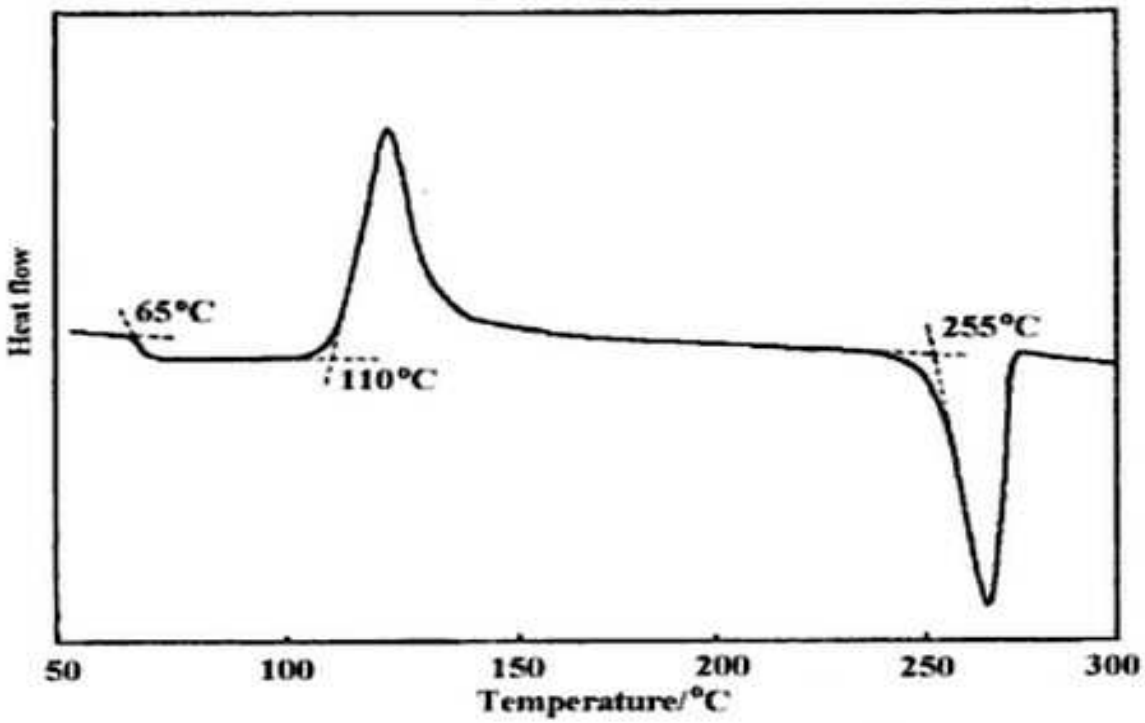

Figure 1.39 *– The thermal analysis curve for poly(ethylene terephthalate) analysed by DSC. The three phase transitions shown are as follows; (left) glass transition (T_g), (middle) crystallisation (T_c) and (right) melting temperature (T_m)* (Pungor, 1995).

Whether a phase transition will give a positive or negative peak is dependent on the instrument that is used for the analysis. The convention is to represent exothermic transitions as positive peaks, with endothermic transitions showing as negative peaks. The area under the curve for each peak can be used to calculate the enthalpy change associated with a particular phase transition via Equation(1.4.

$$\Delta H = K \times A \qquad (1.4)$$

The equation used to calculate the enthalpy change of a phase transition in DSC where ΔH is the enthalpy change, K is the calorimetric constant of the calorimeter and A is the area under the curve (Pungor, 1995).

DSC is commonly used to characterise polymers and determine the relevant transition temperatures for a new polymer material. However another application is for binding studies, typically of proteins (Celej, Dassie, González, Bianconi, & Fidelio, 2006; Wasylewski, 2004), but the process could be used to assess the binding energy involved in a calixarene

guest-host complex. The dissociation of a guest-host complex involves the breaking of intermolecular forces in the same way as melting. Therefore the specific binding energy, or the amount of energy required to overcome the binding, is the same as the enthalpy change. If this value is given in Joules then a conversion can be used to give the binding energy in kCal mol^{-1}, which is more convenient for comparison to a value calculated from an *in-silico* model (Section 1.8).

This technique has been used to analyse the thermal properties of some calixarenes and their guest-host complexes. Hajipour, Habibi & Ruoho (2010) funtionalised poly(acrylic acid) with a calix[4]arene derivative for the purposes of detecting toxic heavy metals. The functionalised polymers were analysed using DSC to determine their binding affinity. The study showed that the modified polymers had a greater affinity for their target than the unmodified control polymer. Safina *et al*. (2013) used DSC to measure the enthalpy change associated with the collapse of a guest host complex formed between *tert*-butylcalix[6]arene and organic solvents / mixtures of organic solvents. The binding energy involved in each complex was then calculated from the area under the DSC curve. Kunsági-Máté *et al*. (2005) studied the inclusion complexation of *p*-sulfocalix[6]arene with *p*-nitrophenol using DSC. The study showed the complexation had a ratio of 1:1, with a strong binding energy. However the measured Gibbs free energy of complexation is small, resulting in a complex with low stability.

1.9.6 Absorptive Stripping Voltammetry

Absorptive stripping voltammetry (ASV) is similar to cyclic and linear voltammetry in that the output is a graph of current against voltage. In ASV, however, the analyte is first adsorbed into the electrode surface during a preconcentration step and then oxidised or reduced as the potential is ramped between two predefined values. This technique is useful

for the analysis of metal ions, and due to the preconcentration step it can be used to quantify lower concentrations than conventional cyclic or linear voltammetry.

1.9.7 Cyclic Voltametry

Cyclic voltammetry is a dynamic electrochemical technique that involves measuring the current flowing in an electrochemical cell when a potential is ramped from one potential to another and then back again to the starting potential. A non-polarisable reference electrode provides a potential to allow the working and counter electrodes to be polarised with respect to this reference potential.

In cyclic voltammetry, the voltage applied to the electrodes is swept between two values (V_1 and V_2) with a triangular waveform. The current is then measured and used to generate a voltammogram. Both of these are shown in Figure 1.40.

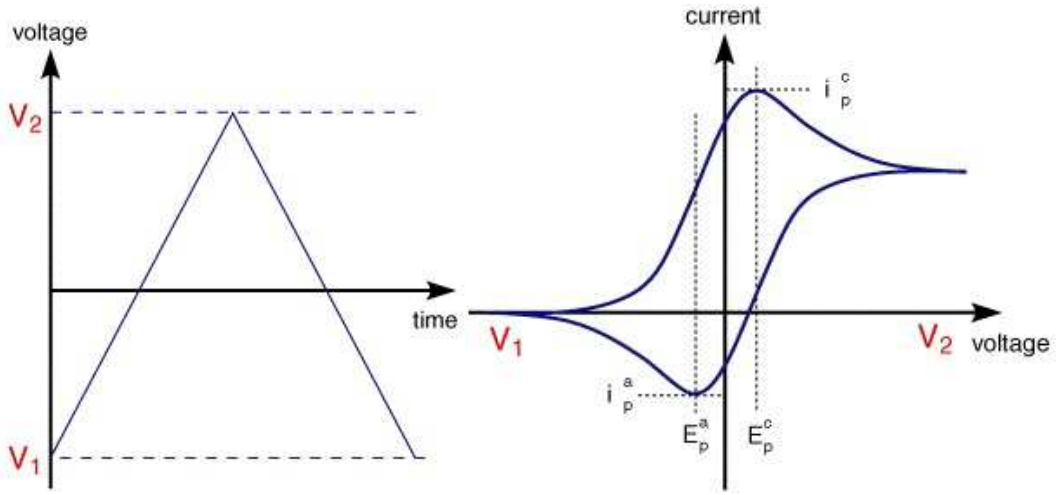

Figure 1.40 *– The triangular waveform of the voltage sweep used to generate a cyclic voltammogram (left) and the shape of a cyclic voltammogram (right) (University of Cambridge, 2013).*

The terms shown in Figure 1.40 are; anode potential (E_p^a), anode current (i_p^a), cathode potential (E_p^c) and cathode current (i_p^c). For a reversible redox reaction (for example the conversion of Fe^{3+} to Fe^{2+} and vice versa) the current on both the oxidation peak (forward sweep) and the reduction peak (reverse sweep) will have a ratio of 1. Furthermore, an

increase in the scan rate will affect both peaks simultaneously. When the scan rate is increased, the peak current will increase but the peak voltage will remain in the same position.

This increase in current is caused by the size of the diffusion layer. In electrochemistry, the diffusion layer can be thought of as the area of the analyte solution immediately adjacent to the electrode with the thickness dependant of a number of factors. The diffusion layer contains a concentration gradient of the analyte which is quantified. It is therefore, due to oxidation/reduction by the electrode, the area in which the concentration of the analyte is different from that in the bulk solution. As the scan rate increases the thickness of the diffusion layer decreases because the analyte has less time to diffuse close enough to the electrode for a reaction to occur. The amount of analyte diffusing towards the electrode is known as the flux, and is directly proportional to the measured current since the analyte is directly involved in the electron transport from the electrode.

In summary, as the scan rate increases, the diffusion layer decreases. This means that there is a smaller distance for the analyte to diffuse to the electrode and so flux increases, causing an increase in the measured current. The effect of the scan rate on the voltammogram is shown in Figure 1.41.

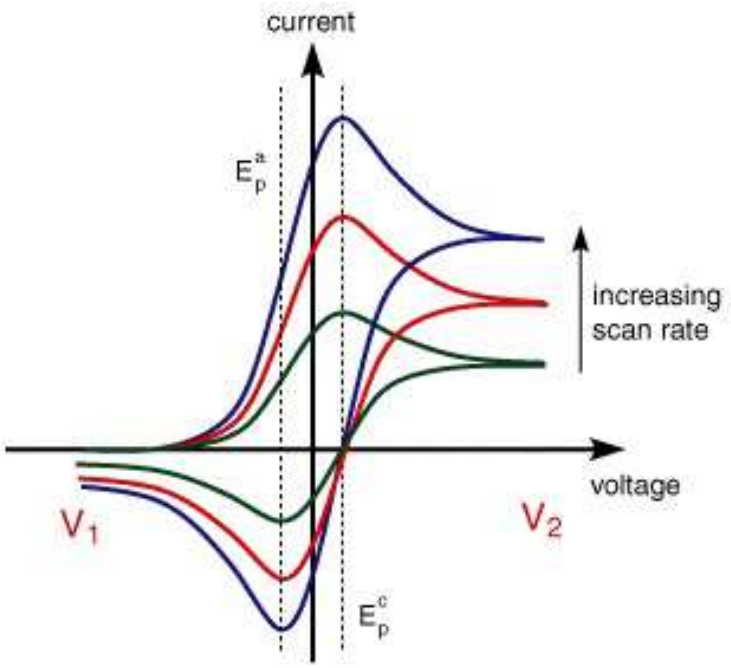

Figure 1.41 *– Effect of the scan rate on the appearance of a cyclic voltammogram for a reversible redox reaction (University of Cambridge, 2013).*

The shape of the voltammogram between E_p and the switching voltage (the voltage at which the direction of the sweep is reversed) can also be explained by the diffusion layer effect. As the oxidation/reduction at the electrode reaches its maximum rate a concentration gradient builds up in the diffusion layer. This apparent drop in concentration forces a slower rate of electron transfer, since there is a diminished quantity of analyte for conversion at the electrode surface. At higher scan rates the peak current increases which corresponds to a greater rate of analyte conversion making the concentration gradient at the surface of the electrode larger. This means that the drop in current between the peak and the voltage at which the sweep is reversed is more pronounced at higher scan rates.

Cyclic voltammetry can be used as both a qualitative and also a quantitative technique. The voltage required to cause oxidation will be different depending on the analyte. Therefore the position of the peak current can be used to give qualitative information when compared to a known value. This is classed as semi-qualitative because, as with a retention value in a chromatographic technique, it cannot be assumed that the two compounds are the same on the

basis of the peak current. Quantitative information can be gained by comparing the peak current value to a calibration curve. Care must be taken when doing this, because as already discussed the peak current value can be distorted by increasing or decreasing the scan rate.

1.9.8 Electrochemical Impedance Spectroscopy

Electrochemical impedance spectroscopy (EIS), also known as dielectric spectroscopy, is used to analyse the dielectric properties of a material. A dielectric material is an electrical insulator which, when exposed to an alternating electric current, takes on the properties of a semiconductor. The alternating electric current causes a polarisation effect within the electrode surface, whereby positive charges are orientated towards the field and negative charges orient away from the field. This alters the electrical field within the material by creating an internal field different to the external field. The result is that the impedance of the material from which the electrode surface is composed changes dependant on the frequency of the applied alternating electrical current measured in Hertz (Hz).

Dielectric spectroscopy measures the impedance of a material over a range of frequencies. This data is then plotted as either a Bode plot, with impedance on the y axis and frequency of the alternating electrical current on the x axis, or a Nyquist plot, with capacitance (a measure of charge build-up between two conducting plates separated by and insulator) on the y-axis (Z``) and impedance (the resistance of a circuit to an alternating electrical current) on the x-axis (Z`). The Nyquist plot takes the form of a semicircle whereas the Bode plots are sigmoidal curves. An example of the different plots is given in Figure 1.42.

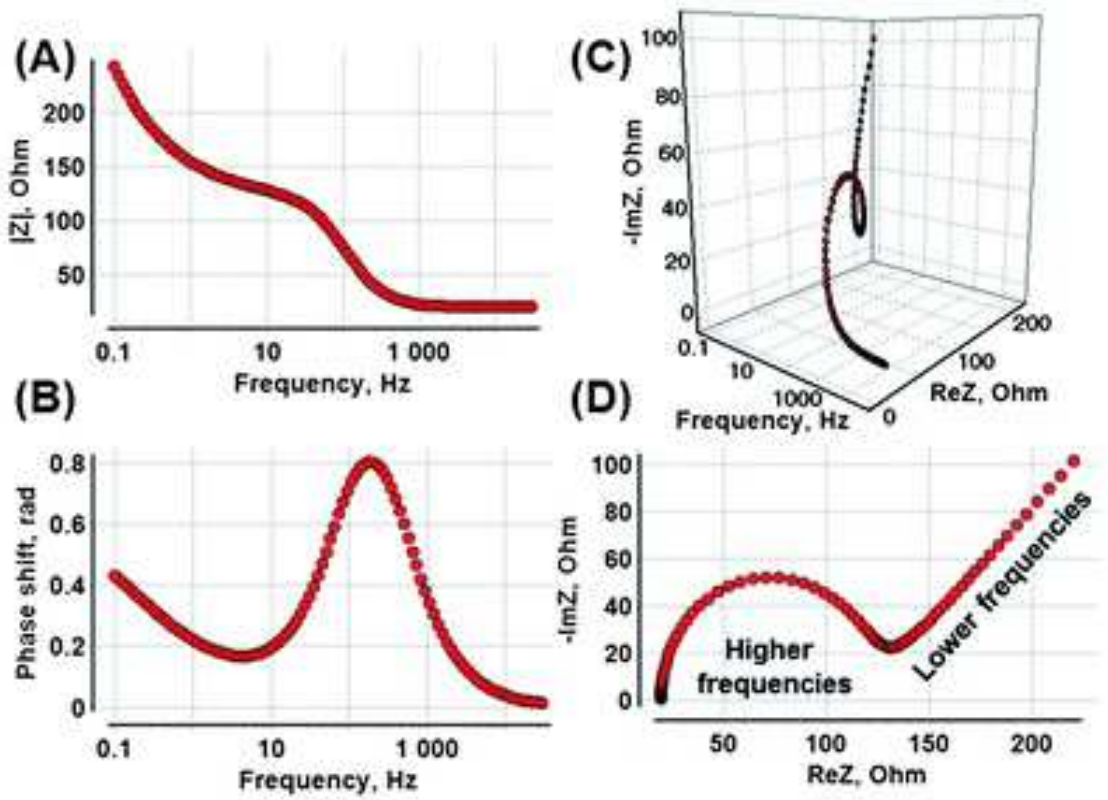

Figure 1.42 – *Different data plots for a dielectric spectroscopy experiment; (A) Bode plot of impedance, (B) Bode plot of phase angle, (C) a 3D representation of a Nyquist plot showing frequency, (D) a standard Nyquist plot (Bandarenka, 2013).*

The Nyquist plot can be used to measure the electron transfer between the electrode surface (composed of the material being studied) and the media in which is it is conducted. Ferro/ferricyanide solution is often used as it readily switches between the oxidised and reduced forms and can be used as a standard to compare different surfaces. Electron transfer measurements are obtained by extending the Nyquist plot to complete the semicircle then measuring the diameter of that semicircle. This shows the resistance to electron transfer for a given electron surface. Figure 1.43, below, depicts a representation of a Nyquist plot comparison between two different electrode surfaces analysed in 10 mM ferro/ferricyanide. From the figure it can be seen that graphene offers far less resistance (3.18 kΩ) to the electron transfer than the bare carbon electrode (168.5 kΩ). This plot shows that the graphene modified electrode offers enhanced conductivity compared with the carbon (Langford, 2013).

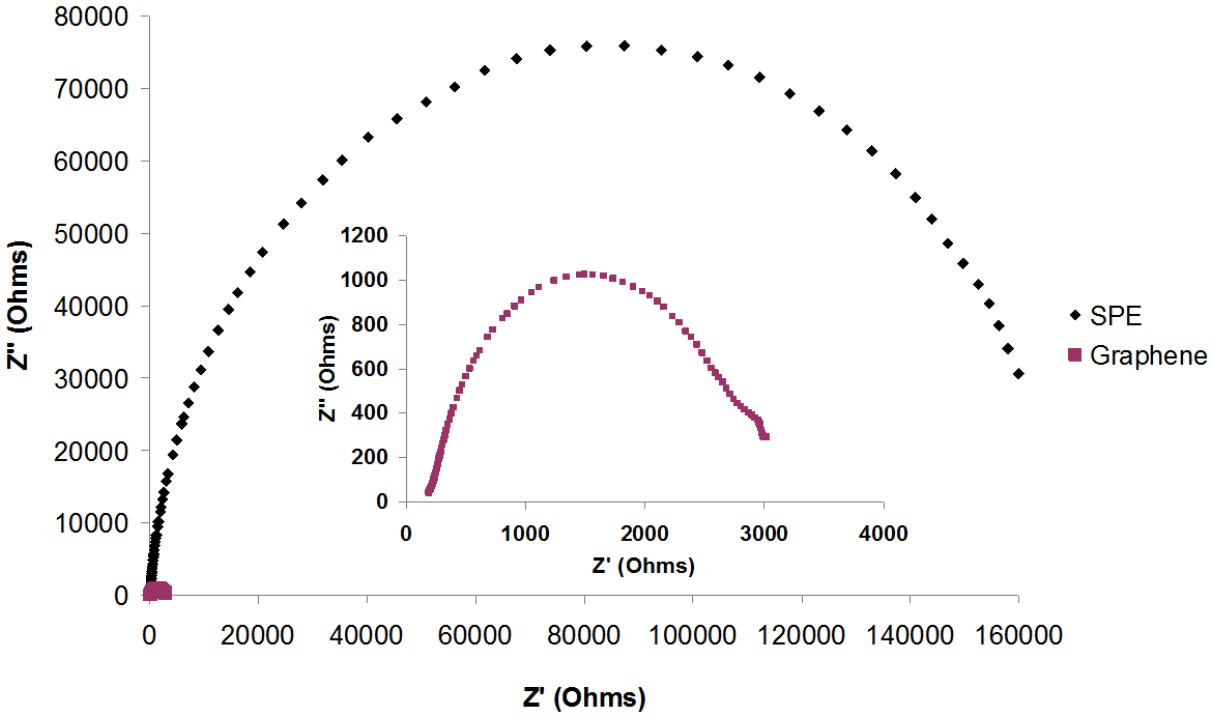

Figure 1.43 *– Nyquist plot showing the difference in electron transfer resistance between a screen printed carbon electrode (SPE) and an SPE coated with graphene* (Langford, 2013).

The higher values of Z`` (capacitance) essentially represent a higher charge at the electrode surface. This is relative to impedance, which is the resistance of an electrical system to alternating current. As the impedance increases the charge build-up, or capacitance, of the surface increases to a point where it passes on that charge to the analyte in solution. This is why a sharp drop is shown in capacitance as the impedance continues to rise.

A Bode plot of frequency against impedance can also be used to characterise the conductivity of the material. When comparing two different electrode surfaces, the starting impedance shows the comparative conductivity of the two surfaces. An example of this is shown in Figure 1.44.

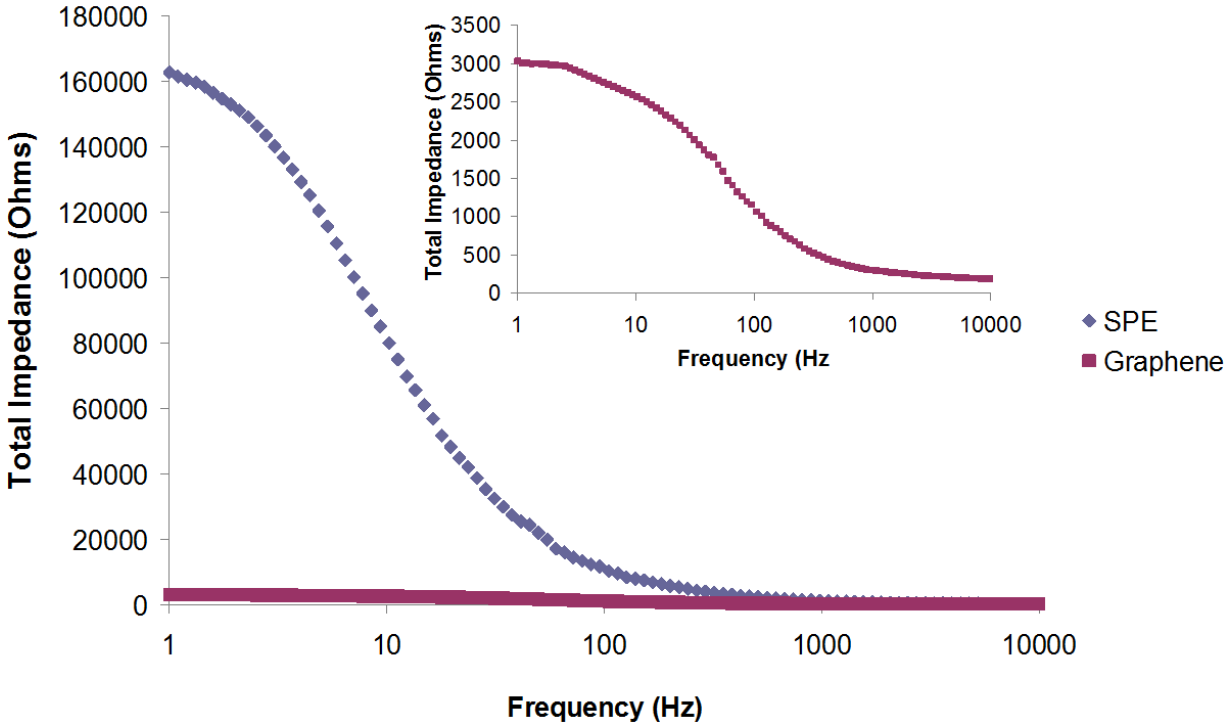

Figure 1.44 *– Bode plots of impedance against frequency for comparison of a screen printed carbon electrode (SPCE) and a graphene coated electrode with ferri/ferrocyanide as the analyte* (Langford, 2013).

In this example it is clear that the graphene coated electrode exhibits much lower impedance than the bare carbon electrode. This shows that graphene is a better facilitator of electron transfer than screen printed carbon alone.

1.9.9 Langmuir-Blodgett Films

Langmuir-Blodgett (LB), named after physicists Irving Langmuir and Katherine Blodgett, is a technique involved in the study of thin films and monolayers. Langmuir-Blodgett techniques will be used in this research to prepare thing graphene and resorcinarene films for study. A Langmuir-Blodgett trough consists of a volume of water with a known area, a moving barrier and a sensor to measure surface pressure in millipascals (mPa). The compound being studied is dissolved in a solvent that will not mix with the water and spread very carefully onto the surface of the water without penetrating the water surface. If the water surface is broken then the solvent can drop to the bottom or the compound can simply

dissolve in the water. The concentration should be low enough so as to form only a single diffuse layer. Once the solvent has evaporated, the barrier is moved across the water surface, compressing the patches of monolayer into a single continuous monolayer. As this compression occurs the surface pressure begins to rise until the monolayer becomes unstable. At this point the monolayer will collapse, either by forming a bilayer on the surface or dissolving in the sub-phase. The monolayer collapse is accompanied by a sharp drop in surface pressure. The maximum pressure that a monolayer will reach before collapse is dependent on the molecule being studied. If a known concentration is used, and the molecular weight of the compound is also known, then the area per molecule can be calculated using the area of the monolayer at its maximum pressure.

Langmuir-Blodgett films can be produced for a number of different reasons. One of the most popular is for depositing a single layer or a controlled multi-layer coating into a substrate for studies using other methods (such as infra-red spectroscopy or elipsometry). There are two common methods for doing this. In both methods the monolayer is compressed to a specific surface pressure, which is maintained throughout the experiment. This is achieved by constant compression of the monolayer in response to any pressure drop. The compressed monolayer can then be transferred by either the Langmuir-Blodgett technique or the Langmuir-Shaefer technique.

In Langmuir-Blodgett deposition, the substrate is dipped into the water vertically and then withdrawn. This technique causes a layer to be deposited on the way down and the way up, and the layer is deposited onto both sides of the substrate. A variation on this technique is to lower the substrate into the water before compression of the monolayer. In this way withdrawing the substrate through the compressed monolayer will give a single layer onto both sides of the substrate.

There are three different possible types of LB deposition known as X-, Y-, and Z-type deposition. X-type deposition is where deposition occurs on the down stroke only resulting in a monolayer with the hydrophilic surface facing outwards. Y-type deposition is where deposition occurs on both the upward and the downward stroke, resulting in the formation of a bilayer. Z-type deposition is where deposition occurs on the upward stroke only resulting in a monolayer with the hydrophobic surface facing outwards. In both x- and z- type deposition it is possible to form a bilayer, however the mechanism by which this occurs is not fully understood (Peng, Ketterson, & Dutta, 1988).

The Langmuir-Shaefer (LS) technique for depositing a monolayer involves dipping the substrate horizontally into the trough, touching it gently against the surface of the water. The substrate is then removed from the surface, leaving a monolayer deposited onto only one side. Pressure is more important for this technique, as if the monolayer is not sufficiently compressed it will just move out of the way when the substrate makes contact and it will not be deposited successfully.

The choice of technique depends on the type of coating that is required as well as the desired orientation of molecules on the surface. Since this technique only works effectively with amphiphilic molecules, it stands to reason that the monolayer will be composed of molecules all standing with the hydrophobic regions pointing upwards away from the water. Therefore, a single layered deposition by the Langmuir-Blodgett method will provide a coating with the hydrophobic area of the monolayer exposed, whereas deposition by the Langmuir-Shaefer method will give a monolayer with the hydrophilic area exposed.

1.10 Aims and Objectives

1.10.1 Project Aims

The principle aim of this research is to develop a sensor or sensors comprising resorcinarenes with a conductive base of graphene for detection of various compounds; electrochemically active amino acids (tyrosine, tryptophan, and phenylalanine), blood based components (dopamine in the presence of other electrochemically active species such as acorbic acid and uric acid), and nucleotide bases (adenine, thymine, guanine, cytosine, and uracil).

The sensor platform will use a technical basis of electrochemistry in the form of cyclic voltammetry. Additionally to create a novel semi-automated method for synthesis of graphene by sonochemical exfoliation that will facilitate the production of graphene-surfactant complexes.

1.10.2 Project Objectives

In order to achieve the above stated goals the research project is designed to meet the following objectives:

- To design and build a bespoke apparatus for the semi-automated synthesis of surfactant stabilised graphene.
- To create and characterise composites of graphene stabilised by a positively or negatively charged ionic surfactant.
- To investigate the fabrication of thin films of graphene-surfactant complexes using Langmuir-Blodgett and electrostatic layer-by-layer assembly.

- To optimise the fabrication and electrochemical capabilities of the newly created composite materials in terms of starting material concentration and electromotive force of the deposited material on an electrode surface.
- To analyse the detection capabilities by cyclic voltammetry of the above mentioned composites using tyrosine, tryptophan, phenylalanine, dopamine, ascorbic acid, uric acid, adenine, thymine, guanine, cytosine, and uracil.
- To design a resorcinarene based binding molecule using molecular modelling techniques to act as a selective binding ligand for adsorption onto graphene sheets.
- To synthesise the above mentioned resorcinarene and validate the *in-silico* model using NMR spectroscopy.

Chapter 2 Production and Characterisation of Graphene

2.1 Introduction

Since its initial discovery and development by Novoselov *et al*. graphene has been of great interest to the scientific community due to its interesting optical and electrical properties. Graphene is defined as a single layer of sp^2 hybridised carbon with no 3^{rd} dimension. The double bonded structure of graphene is responsible for the electrical properties of the material as the movement of π-bonds between adjacent carbon atoms can be used to transmit an electrical current. Because of this electrical activity in particular, graphene is being examined as a base material in a number of different applications including sensor applications, for use in flexible electronics and graphene based printable inks for printed electrical circuits.

Graphene has reportedly been produced in a number of different ways. The method chosen for this research is by sonochemical exfoliation in water in the presence of a surfactant, as reported by Notley *et al*. This method was chosen for a number of reasons; firstly, it does not require the use of hazardous chemicals such as sodium nitrate, sulfuric acid, potassium permanganate and hydrazine hydrate, which are used in the oxidation of graphite to graphite oxide and then reduction to graphene. Secondly it guarantees single-layer or few-layer graphene, rather than the potential for larger products or graphene sheets with an uneven size distribution that might be produced in other techniques such as mechanical exfoliation (the "scotch tape" method). The sonochemical method was carried out using a semi-automated apparatus designed specifically for the purposes of this research.

The properties of newly synthesised graphene should be determined before its application to these new technologies. The presence of graphene can be verified using Raman spectroscopy, with characteristic peaks showing at 1324 cm^{-1} and 1612 cm^{-1} in addition to the peak at 1576 cm^{-1} in pure graphite. The size of the graphene flakes can be determined using dynamic light scattering (DLS). Size and shape of graphene flakes can be further examined using

scanning electron microscopy (SEM) and atomic force microscopy (AFM). Concentration of graphene in solution can be determined using UV/Vis spectroscopy and applying the Beer-Lambert law, where the extinction coefficient of graphene in solution is 13.9 mg ml^{-1} cm^{-1} at 650 nm as reported by Fan *et al*. Stability of monolayer membranes can be studied using Langmuir-Blodgett films. The Nuclear Overhauser effect, which is present in nuclear magnetic resonance (NMR) spectroscopy, can be used to determine the amount of contact between the surfactant and the graphene sheet. This is achieved by observing peak shifting which occurs when two nuclei are within 5 Å of each other. These techniques will be used to determine the quality of the newly synthesised graphene.

In this chapter a semi-automated technology of graphene production by sonochemical exfoliation of graphite in the presence of ionic surfactants is described in detail. The composite graphene-surfactant materials produced were characterised with NMR and Raman spectroscopy to confirm the formation of graphene. Thin films of graphene composites were deposited using the techniques of Langmuir-Blodgett (LB) and electrostatic layer-by-layer (LBL) deposition. Films composed of these new graphene composite materials were then characterised using SEM, AFM, and spectroscopic ellipsometry. The study of SPR in gold films coated with graphene using total internal reflection ellipsometry was carried out for the first time.

The graphene produced in this section will subsequently be utilized as an electrode coating, to be applied to screen printed carbon electrodes. These electrodes will then be used to enhance the detection of compounds by a combination of electrochemical detection methods such as cyclic and linear voltammetry. This chapter forms the basis for a journal article in the Beilstein Journal of Nanotechnology. At the time of printing this article was accepted for publication but not yet released.

2.2 Materials

Graphite powder and sodium dodecyl sulphate (SDS) were obtained from Fisher Scientific (Loughborough, UK). Cetyl trimethylammonium bromide (CTAB) was obtained from Sigma-Aldrich (Poole, UK).

Ultra-pure (18 MΩ cm^{-1}) water was produced using a Milli-Q water purification system obtained from Millipore (Tokyo, Japan). Freeze drying was performed using a ScanVac CoolSafe freeze dryer from Labogene (Lynge, Denmark). Langmuir-Blodgett films were prepared using a NIMA Langmuir-Blodgett trough (NIMA Technology, Coventry, England). Nuclear magnetic resonance spectroscopy was performed on an Ascend 400 NMR spectrometer running TopSpin analysis software (Bruker, Billerica, Massachusetts, USA). Atomic force microscopy was performed using a Nanoscope IIIa (Digital Instruments (Bruker), Billerica, Massachusetts, USA). Sonication of graphite was performed using a UP50H Ultrasonic Processor (Hielscher Ultrasonics, Teltow, Germany). Pumping of aqueous surfactant was performed using a Gilson peristaltic pump (Gilson Scientific Laboratory Supplied, Hessle, UK). Spectroscopic ellipsometry was performed using an M2000 ellipsometer (J. A. Woollam, Lincoln, USA).

2.3 Automated Sonochemical Exfoliation of Graphene

Two different surfactants were used to synthesise graphene-surfactant complexes; sodium dodecyl sulphate (SDS) and cetyl trimethylammonium bromide (CTAB). Firstly the surfactant solutions were prepared by dissolving in water. The SDS solution was made to a concentration of 462.9 mg ml^{-1} while the CTAB solution concentration was made up to 49.7 mg ml^{-1}. These solutions were prepared and then placed into a water bath heated to 50^{o}C to aid dissolution.

Once dissolved, the surfactant solution was placed into the surfactant reservoir of the synthesiser. This solution was then pumped into the reactor via a peristaltic pump during synthesis at a rate of 35 μL min^{-1} giving an addition rate of 16.2 mg min^{-1} for the SDS and 1.74 mg min^{-1} for the CTAB. The addition rate was crucial to maintain a surface tension of 41 mJ m^{-2}, which is both the optimum surface tension for graphene production and also the surface free energy of graphene. The graphite suspension (10 - 50 %) was then placed into the reactor, and sonicated continuously for 120 minutes at a power of 50 W. A total of 3.15 ml of surfactant solution was added in each case over the course of the synthesis. The sonication step was carried out in a high aspect ratio process (HARP) fume cabinet, as an aerosol containing potentially harmful graphene nanoparticles is produced at this stage. A schematic diagram of this apparatus is shown below (Figure 2.1).

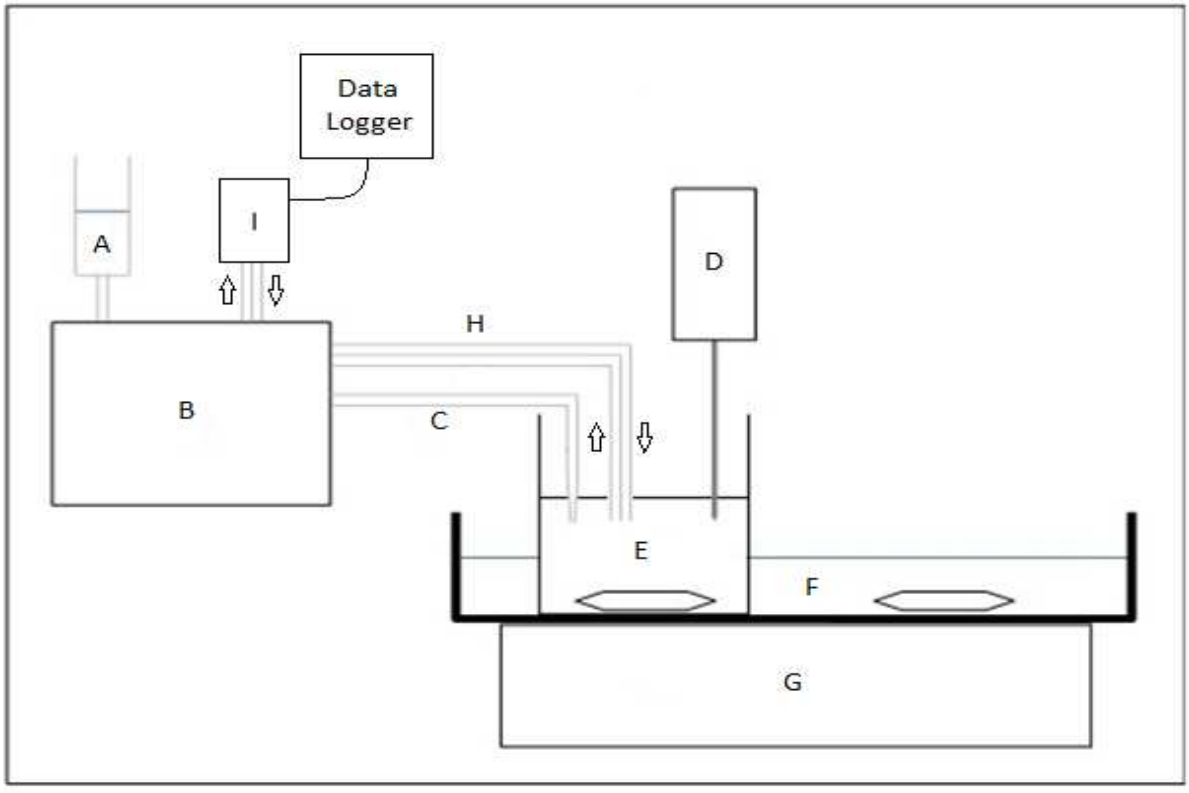

Figure 2.1 *- A schematic diagram of the apparatus used to synthesis graphene. (A) surfactant solution, (B) peristaltic pump, (C) heat, (D) ultrasonic probe, (E) reactor, (F) water, (G) magnetic stirring unit,(H) sampling loop, and (I) photometric flow cell.*

The apparatus was designed to alleviate the time constraints of the Notley method. In that method, solid surfactant must be added every 5 minutes whilst continuous sonication is carried out. This method with its continuous addition of aqueous surfactant eliminates the need for constant supervision of the process as well as providing the reproducibility of automation. This is only semi-automated, however, as full automation would require the monitoring of surface tension throughout the synthesis as well as automatic adjustments to the surfactant flow rate to maintain this at the required level of 41 mJ m^{-2}.

2.4 Methods

In this section the methods for the production, characterisation and usage of graphene will be described.

2.4.1 Production of Graphene-Surfactant Complexes

The function of the apparatus (schematic shown in Figure 2.1) for the production of graphene is explained thusly. The aqueous suspension of graphite powder is placed into the reactor (E). The graphite is kept in suspension throughout the procedure using a magnetic stirrer (G). The ultrasonic probe (D) operating at a power of 50 W, penetrates approximately 1 cm into the graphite suspension. The surfactant solution (A) is pumped into the reactor via a peristaltic pump (B). The reservoir containing the surfactant and the tubing carrying it to the reactor are heated to 50^{o}C in a water bath (C) to prevent precipitation of the surfactant from solution in the tubing. A water trough (F) is used as a heat sink to dissipate any heat produced in the reactor during synthesis, as the tip of the ultrasonic probe can reach temperatures of up to 100^{o}C during continuous operation. The heat sink is stirred continuously, also using the magnetic stirrer (G), to maximise cooling efficiency.

A sampling loop (H) continuously cycles the liquid contents of the reactor through a photometric flow cell (I) which determines the concentration of graphene by measuring absorbance at 650 nm. The concentration data is then recorded using a data logger.

Upon completion of the 120 minute cycle, the contents of the reactor were removed and placed into a 50 ml centrifuge tube and spun at 3500 RPM for 20 minutes. The supernatant was then removed and the pellet (containing mostly unreacted graphite as well as some precipitated graphene) was re-suspended in 40 ml of deionised water. This was then centrifuged at 3500 RPM for 20 minutes. This process was repeated until no more graphene was contained in the supernatant. If a dry sample was required, then the graphene suspension was frozen and then placed into a freeze dryer (Labogene) for 3 – 4 days (depending on the sample size) and then subsequently into a vacuum oven at 70^{o}C overnight to remove all traces of water.

2.4.2 Initial Characterisation of Graphene Solutions

Before freeze drying the graphene solutions were first analysed by UV/vis spectrophotometry and dynamic light scattering to determine their concentration and particle size respectively. The concentration of the graphene solutions was determined by recording the absorbance of the graphene at 650 nm and multiplying by the extinction coefficient (13.9 mg ml^{-1} cm^{-1}) according to the Beer-Lambert law. The average particle size was also estimated by diluting the sample to give a particle count rate of approximately 200 counts per second by the analyser.

2.4.3 Spectroscopic Analysis of Graphene

Graphene from the third graphite washing step onwards was collected together and dried as detailed above (Section 3.4.1). The first wash and the initial supernatant were not used for spectroscopic analysis because they contained large amounts of unbound surfactant that

would interfere with results. The graphene-surfactant complex used for analysis contained 50% graphene and 50% surfactant. This was the highest obtainable purity.

Raman spectroscopy was performed using an InVia Raman Microscope (Renishaw) with a wavelength of 532 nm. The dry graphene powder was pressed between two glass microscope slides which were gently rubbed together to form a very thin layer of powder. The Raman spectrum was then measured between 100 – 3200 cm^{-1}. A control was performed using graphite powder for comparison.

NMR spectroscopy was performed using an Ascend 400 NMR Spectrometer (Bruker). For the NMR sample great care was taken to ensure that all of the water was removed before analysis. This is because the surfactant's polar head group is capable of binding water molecules which are not removed by freeze drying alone. The graphene samples were then dissolved in D_2O and the NMR spectrum was recorded. Due to the fact that this was a stabilised suspension not a true solution 32 scans were performed to get a good quality spectrum. The spectrum of the surfactants alone was also recorded for comparison.

2.4.4 Analysis of Graphene Monolayers and Multilayers

The electrical properties of graphene are best observed when a single layer (monolayer) of graphene is used. This is because the electron flow is confined to a 2 dimensional plane and therefore the loss of electrons in the 3rd dimension does not occur. There are numerous ways to deposit coatings onto a substrate; layer-by-layer, spin coating, sputter coating etc. However all of these techniques do not necessarily provide a monolayer. To obtain a true monolayer (i.e. with no molecular third dimension) a Self-Assembled Monolayer (SAM) could be used which relies on semi-irreversible interactions of molecules with a surface (e.g. a SAM formed by the interaction of thiolated molecules with gold). The Langmuir-Blodgett technique is a technique which is used to create a monolayer of an amphiphilic molecule (containing of both

hydrophobic and hydrophilic regions) by interaction on a water surface. This is not strictly a SAM since the interaction is fully reversible. This technique is described in more detail in Section 3.4.4.1.

The stability of these films must then be analysed in terms of their optical properties, electrical properties and physical/mechanical properties. The various techniques and methods used for this are described here.

2.4.4.1 Preparation of a Langmuir-Blodgett Film

Both composite materials obtained, e.g. Graphene(+)CTAB and Graphene(-)SDS, were soluble in water due to the presence of ionic groups, NMe_3^+ and SO_3^- respectively. Yet, the presence of alkyl chains and π-systems facilitated their solubility in chloroform, hence the use of Langmuir-Blodgett (LB) technology (Nima 610 trough) was possible for thin film deposition. The standard LB procedure was applied; a solution of graphene(+)CTAB in chloroform (1 mg ml^{-1}, 100 μL) was spread onto the surface of deionised water (Millipore). Surface pressure was then recorded using a Wilhelmy plate based sensor. Because of the unknown ratio of graphene / surfactant within the complex the area per molecule (or repeated unit) was difficult to calculate, so the actual area was presented, in units of cm^2. Typical surface pressure vs. area diagrams of graphene-surfactant composites were used to show the formation of a stable monolayer on the water surface, similar to that found for classical amphiphilic compounds. Consecutive compressions of the monolayer were performed to test the durability of the monolayer and to show any potential losses of material caused either by the monolayer collapse or dissolving of the material in water.

The surface pressure of the compressed monolayer was measured, and the pressure at which collapse of the monolayer occurred was noted. A lower pressure was then chosen for deposition by Langmuir-Blodgett and Langmuir-Schaefer methods onto either a glass

microscope slide or a silicon wafer. For this deposition the monolayer was continually compressed via a feedback circuit so that the surface pressure was kept constant throughout the procedure. Different surface pressures were used for different depositions. Deposition was confirmed by a drop in the surface area of the monolayer coinciding with the movement of the substrate.

2.4.4.2 Electrostatic LbL deposition

Graphene multi-layered structures were created using a simple technique of electrostatic layer-by-layer (LbL) deposition, a well-established technique developed first for poly-electrolytes and later adapted for deposition of other objects, i.e. nanoparticles, biomolecules (proteins, antibodies, enzymes, DNA, etc.). Multilayered films of graphene were deposited onto gold coated glass microscope slides by alternating layers of a graphene-surfactant with oppositely charged polyelectrolytes, e.g. graphene(+)CTAB layers alternated with polyanionic layers of polystyrene sulfonate sodium salt (PSS), while graphene(-)SDS was alternated with layers of polycationic species such as polyallylamine hydrochloride (PAH) or polyethyleneimine (PEI). Alternating layers of graphene(-)SDS and graphene(+)CTAB was also attempted. The films were deposited by consecutive dipping of gold coated glass or silicon wafers into solutions of the above chemicals (1 mg ml^{-1}) in deionised water. An incubation time of 20 minutes was used to allow for each subsequent layer to stick to the previous layer. Gold coated glass slides were also functionalised with cystamine hydrochloride to make the surface positively charged with the intention of strengthening the first deposited layer. The mutlilayered films obtained were then characterised with scanning SEM combined with EDX (energy dispersing X-ray) elemental analysis (SEM NOVA) and AFM.

3.4.4.3 Atomic Force Microscopy

Graphene was deposited onto a silicon chip by the Langmuir-Schaefer method whilst maintaining a constant monolayer surface pressure of 25 mPa, as determined by analysis of the monolayer stability, or the layer by layer method at a concentration of 1 mg ml^{-1}. Regardless of the deposition method, the silicon chip was then washed by immersion in deionised water to remove any unbound surfactant from the chip surface. The chip was then left to air dry, as drying with a stream of nitrogen appeared to remove the graphene from the surface. The dry chip was then placed into the AFM (Nanoscope IIIa, Digital Instruments) which was operated in tapping mode, using Veeco cantilevers with silicon nitride tips having a radius of less than 10 nm, with the automatic scan assist regime. The operating frequency was approximately 75 kHz. The typical scan rate was 1 Hz. Oscillation amplitude 2 dimensional images were recorded and then the Bruker software was used to create pseudo 3 dimensional images and to perform line analysis. Phase images were also recorded, where the contrast of the image was related to the hardness of the material surface.

2.4.4.4 Ellipsometry Studies

Ellipsometry was performed according to techniques reported by Azzam and Bashra (2003). UV-vis spectra of graphene-surfactant samples are featureless showing almost constant absorbance over the spectral range of 350 - 800 nm, while the main absorption band of graphene lies in UV at about 280 nm. Therefore, optical properties of novel graphene-surfactant composites were studied via spectroscopic ellipsometry using an M2000 ellipsometer (J. A. Woollam) operating in the 370 - 1000 nm spectral range. The measurements were performed on graphene-surfactant films deposited onto different substrates, i.e. glass microscope slides, silicon wafers, and gold-coated glass microscope slides.

The thickness values (*d*) and dispersions, e.g. spectra, of refractive index and (*n*) and extinction coefficient (*k*) of graphene films can be found by fitting the obtained spectra to a model using dedicated J.A. Woollam software. In this particular case, the simplest model of the reflecting system consisted of the following four layers: (1) Si substrate (optical parameters of which, e.g. dispersion functions of *n* and *k*, are taken from J.A. Woollam library of materials); (2) the layer of native oxide (SiO_2) which is typically present on the surface of Si; (3) the deposited layer of PAH/graphene(-)SDS; and (4) the ambient layer, e.g. air. The fitting was then performed by calculating the values of Ψ and Δ at every spectral point using the Fresnel equations for the above reflecting system, and then comparing the calculated spectra with the experimental ones by calculating the error function. One of the least square techniques was used to minimize the error function; the values of *d*, and dispersions of $n(\lambda)$ and $k(\lambda)$ for the unknown layer, at which the minimum achieved, is the outcome of the fitting.

The fitting for the thickness of the native SiO_2 layer was performed first using the data for the bare Si substrate. The parameters of SiO_2 layers obtained were then fixed for consecutive fittings. For fitting ellipsometry data of graphene layers several possible models were considered and tried; the best results were achieved using a simple model of Lorentz oscillator available in the J.A. Woollam data analysis software which is given below (Equation (***2.1***) as a dispersion function of a complex dielectric permittivity $\varepsilon(h\nu)$:

$$\varepsilon(h\nu) = \varepsilon_{1\infty} + \sum_k \frac{A_k}{E_k^2 - (h\nu)^2 - jB_k h\nu} \qquad (2.1)$$

where $\varepsilon_{1\infty}$ is the dielectric permittivity at infinitive frequency, E_k , A_k , and B_k are, respectively, the position, amplitude, and half-width of *k*-Lorenzian peak; there could be a number of peaks from 1 to *k*.

The best fit was obtained with the use of a single Lorenzian oscillator with the following parameters: $\varepsilon_{1\infty} = 1.31$; $E_k = 0.625\,eV$; $A_k = 1.759\,(eV)^2$; $B_k = 3.86\,eV$.

2.4.4.5 TIRE study

The surface plasmon resonance (SPR) phenomenon was studied using the method of total internal reflection ellipsometry (TIRE). The TIRE experimental set-up was built based on a J.A. Woollam M2000 spectroscopic ellipsometry instrument in which the light is coupled into a thin gold film deposited on glass through a 68^o prism providing total internal reflection conditions. The cell attached underneath allows measurements in different media. Scans were performed between wavelengths from 400 – 1000 nm. The advantage of using TIRE is in 10-fold sensitivity enhancement as compared to traditional SPR (Tompkins, 2005).

The samples were constructed by electrostatic LbL deposition (Section 3.4.4.2) of PEI and graphene(-)SDS on chromium/gold coated glass microscope slides. The results, in terms of Ψ and Δ, were plotted against incident light wavelength. Spectra of Ψ resemble a traditional SPR curve with the maximum angle corresponding to conditions of total internal reflection of light, while the minimum angle is the SPR itself. The spectra of Δ, which do not exist in traditional SPR and represent a new phase angle related characteristic, show a sharp drop near the resonance wavelength.

In the model for TIRE data fitting the top layer (ambient) was glass (BK7); the chromium/gold layer, which was fitted separately, and the parameters for this were kept constant for subsequent data fittings. For the PEI/graphene(-)SDS film the substrate was water since the reaction cell was filled with water. Fitting was not as easily achieved as with conventional ellipsometry and the best results were achieved when using a random fit for graphene layers.

2.5 Results and Discussion

The results from the graphene research are discussed here. These include the production and characterisation by various techniques, such as dynamic light scattering, nuclear magnetic resonance spectroscopy, Ramen spectroscopy, Langmuir-Blodgett monolayer techniques, atomic force microscopy, and spectrophotometry.

2.5.1 Initial Characterisation of Graphene Solutions

Graphene(-)SDS was produced and the absorbance was measured at 650 nm. By applying the Beer-Lambert law with an extinction coefficient of 13.9 mg ml^{-1} cm^{-1} the concentration of graphene in solution obtained from each surfactant at varying initial graphite concentration was calculated. The graphene concentration relative to the initial graphite concentration is shown in Figure 2.2.

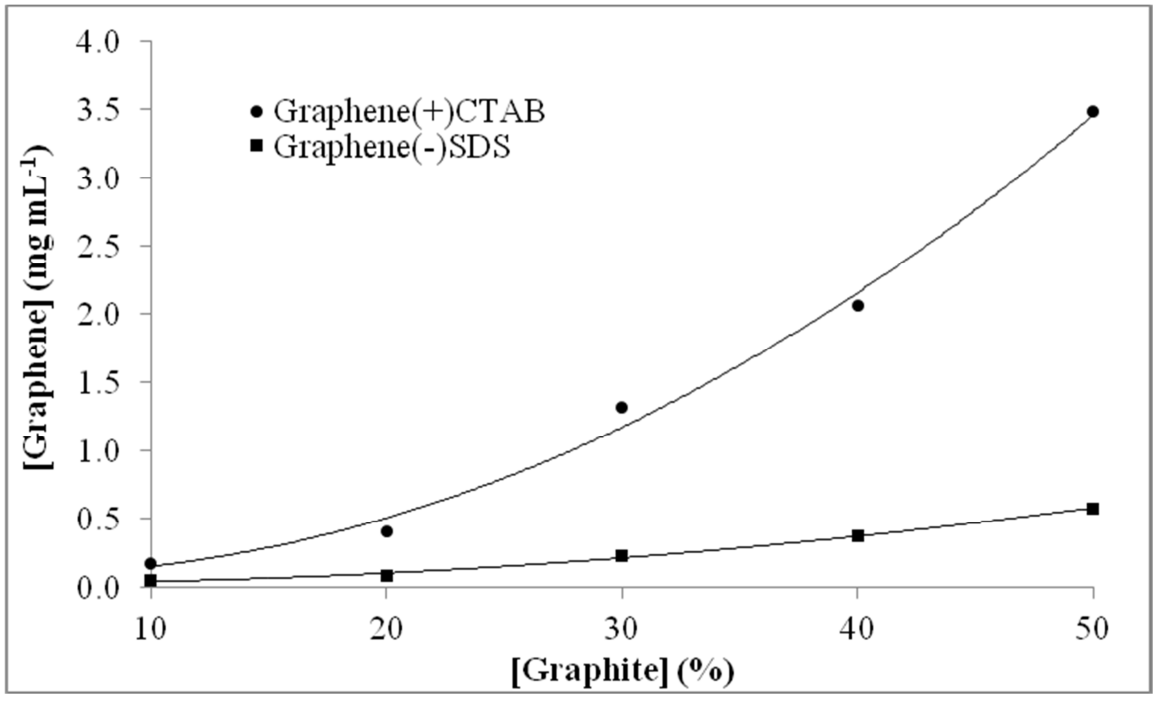

***Figure 2.2** - Effect of initial graphite suspension concentration in water on final graphene concentration after sonication for 120 minutes in the presence of different surfactants.*

The average particle size of each composite material was also determined by dynamic light scattering (DLS). The results are shown in Figure 2.3.

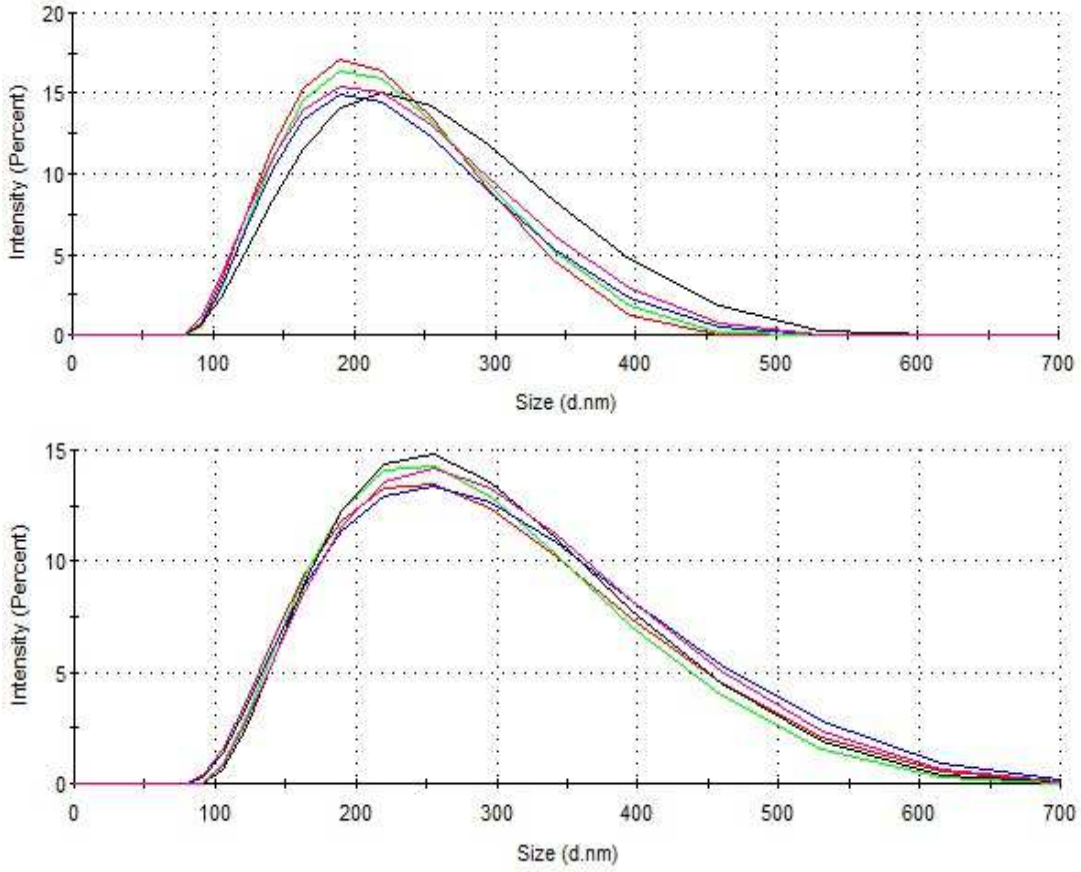

Figure 2.3 – *Dynamic light scattering results for graphene(-)SDS and graphene(+)CTAB showing a particle size of 214.2 ± 10.4 nm (with a polydispersity index of 0.405 ± 0.037), and 264.5 ± 4.967 nm (with a polydispersity index of 0. 264 ± 0.023) respectively.*

The results show that the graphene sample produced using CTAB contained slightly larger graphene flakes and also had a lower standard deviation and polydispersity than SDS stabilised graphene. This suggests that the size distribution within the positively charged graphene is lower than that of the negatively charged graphene. It is likely that the size distribution of flakes within any given graphene sample will be large. This is because (even assuming cuboidal particles of relatively uniform size) the plane of the graphene sheets within graphite is unlikely to be perpendicular to the flat face of the particle. A possible explanation for the smaller particle size in the graphene(-)SDS could be the lower efficacy of SDS as a surfactant compared with the CTAB. This would also explain the lower concentration of graphene being produced with this surfactant, since the starting concentration of graphite and the surface tension of the water is the same in the synthesis of

both samples. The lower efficiency of the SDS as a surfactant might cause the slightly larger flakes of graphene to fall out of suspension during centrifugation, whereas the CTAB is able to hold these larger flakes in suspension throughout the procedure.

2.5.2 Spectroscopic Analyses of Graphene

The sample was analysed using Raman microscopy to determine the presence of graphene and by nuclear magnetic resonance spectroscopy to analyse the interaction between the surfactant and the graphene surface. The results are given below. Raman microscopy was performed at Birmingham University in collaboration with Dr Isaac Chang and Dr Shei. Nuclear magnetic resonance was performed at Sheffield Hallam University in Collaboration with Dr Simon Turega.

2.5.2.1 Raman Spectroscopy

Figure 2.4 shows intense peaks at 1350 cm^{-1} (D) and 1620 cm^{-1} (G & D`). Additionally the peak labelled 2D is slightly broader, between 2650 – 2700 cm^{-1}. This is indicative of graphene flakes with a high number of edge defects (Huang *et al.*, 2013).

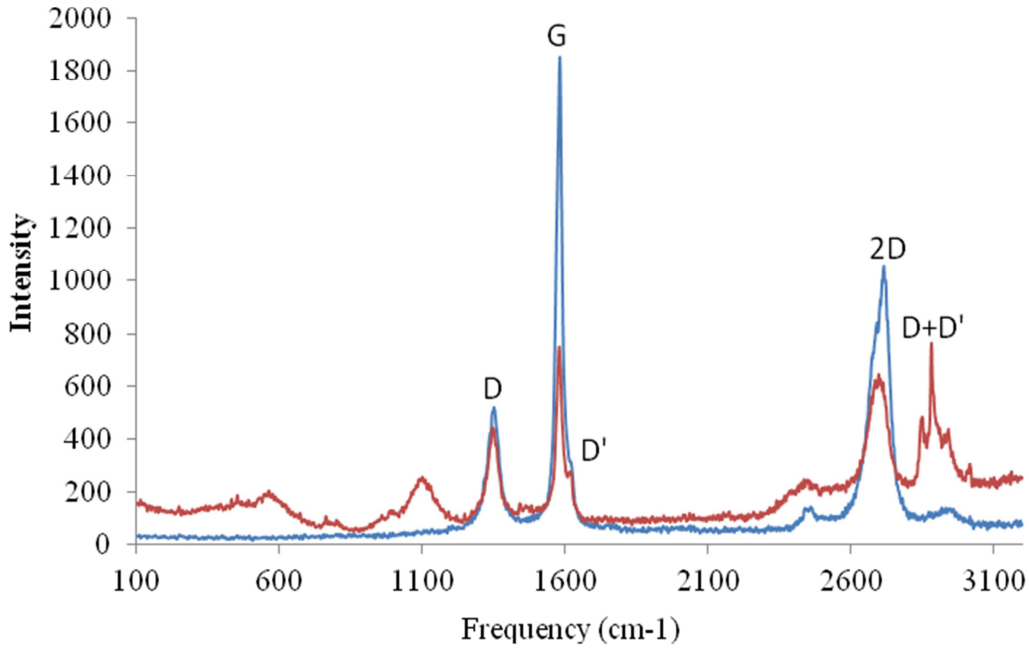

Figure 2.4 *- The Raman spectrum of surfactant stabilised graphene (red) compared with the spectrum of graphite (blue).*

The G band is present in all sp^2 hybridised carbon materials, and is caused by stretching of the C-C bond. The reduction in intensity in the graphene spectrum compared with the graphite spectrum is caused by the reduced number of layers. The D and D' bands are caused by disorder in the graphene flakes. The D' band is present when there are surface defects, such as charging or other impurities adsorbed onto the surface. The D band is caused by edge defects such as a "zig-zag" or "chair" shape on the edge. Edge defects provide an enhancement to electrochemical systems by increasing the total capacitance of the electrode surface. Both the D & D' are not present in pristine graphene with straight edges.

The 2D band is also present in many sp^2 hybridized systems and can be used to estimate the number of layers. However the intensity is also dependant on the excitation laser frequency and so cannot be solely relied upon.

2.5.2.2 Nuclear Magnetic Resonance Spectroscopy

The ^{1}H-NMR of the graphene-surfactant complex, when compared to the ^{1}H-NMR of the surfactant alone, shows a change in the chemical shift of peaks representing hydrogens involved in the complexation interaction (Figure 2.5). The data shows a peak shift towards the left for almost every peak. This is a shielding effect caused by the delocalised electrons in the graphene sheet which only occurs when the proton is in close proximity (less than 5 Å) and involved in Van-der-Waals interactions. This suggests that the hydrophobic chains of each surfactant lie flat against the graphene sheet with the exception of carbon-1 (the carbon attached directly to the polar head group), which is pulled away from it by the polar head group and therefore does not undergo as much of a shielding effect in the SDS-graphene complex.

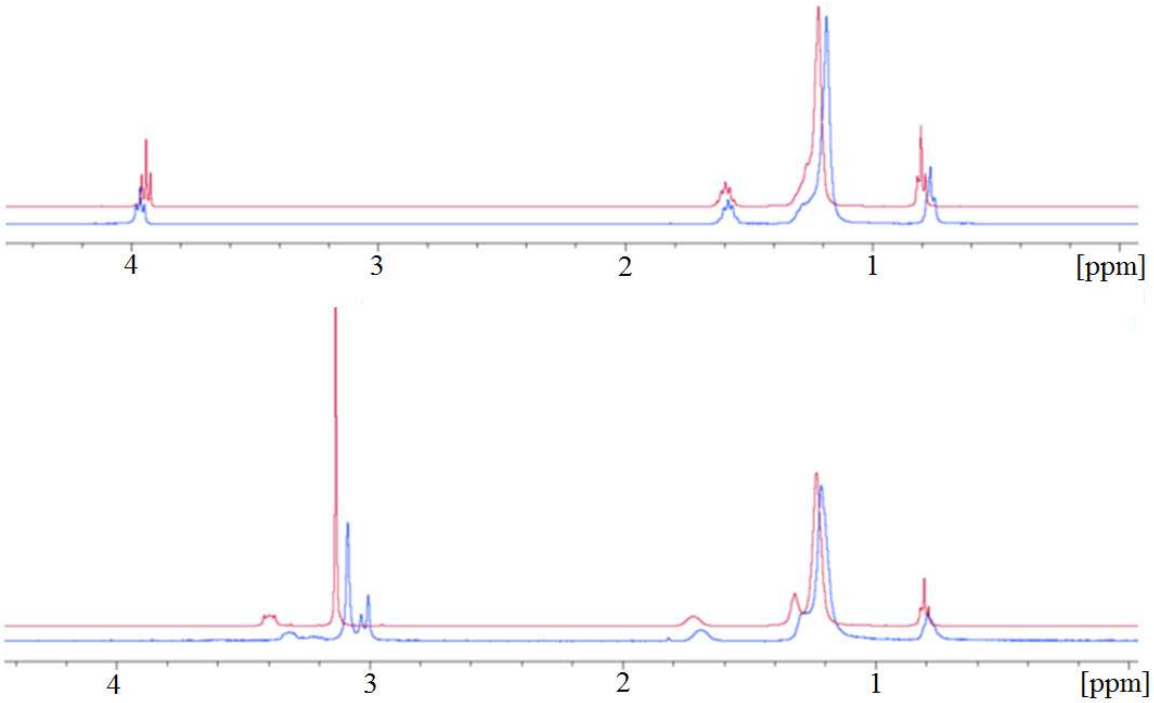

Figure 2.5 *- The ^{1}H-NMR of the graphene-surfactant complexes (blue) for SDS (top) and CTAB (bottom) stabilized graphene compared with the surfactant alone (red).*

Additionally, for the CTAB-graphene complex, two of the methyl groups on the quaternary amine are interacting with the graphene sheet. This is shown by the splitting of the peak representing them into three peaks. This interaction causes the CTAB to lie much flatter against the graphene than SDS, resulting in the polar head being pulled closer to the sheet. This is why the peak for carbon-1 in the CTAB-graphene complex is displaced further towards the left than its equivalent in the SDS stabilised graphene.

The peak representing carbon-1 in SDS (at around 4 ppm) is shifted downfield by complexation with the graphene. This means that the protons are deshielded by the presence of the graphene. Since the carbon-sulfur bond is polar the electron density around the carbon atom is already lower than it would normally be if it were in a carbon-carbon bond. Repulsion between the graphene and the sulfate group could cause lengthening of the carbon-sulfur bond. This could in turn lead to a lower electron density around the proton nuclei responsible for the shift in this peak.

3.5.3 Analysis of Graphene Monolayers

The monolayers produced using Langmuir-Blodgett techniques were analysed by various techniques such as spectrophotometry, atomic force microscopy and total internal reflection spectroscopy. The data from these analyses is presented here. This work was performed at Sheffield Hallam University in collaboration with Professor Alexei Nabok.

2.5.3.1 Preparation of a Langmuir-Blodgett Film

The graphene(-)SDS monolayer that was formed collapsed at a much lower surface pressure than its positively charged counterpart. This meant that deposition was not possible. However, as shown by the decompression and subsequent second compression cycle in Figure 2.6, the compound on the water surface did aggregate into a monolayer. This is obvious by the fact that the surface pressure drops below the initial surface pressure after the compound was spread onto the water surface and also the gradient of the second curve compared to the first.

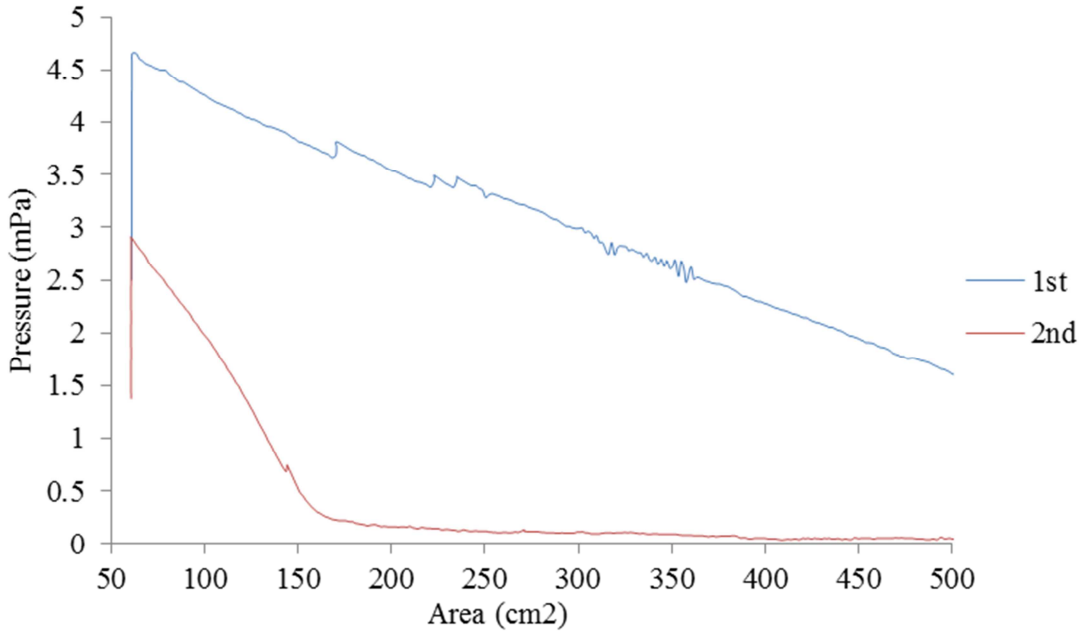

***Figure 2.6** – Langmuir-Blodgett film of graphene(-)SDS showing the change in surface pressure associated with reducing area for two consecutive compression cycles.*

The monolayer collapse at 3 & 4.5 mPa respectively could be due to either the graphene composite dissolving into the water sub-phase or the monolayer folding to form a bilayer or a multilayer. Given that the negative charges on the graphene should repel each other and the surface pressure value did not rise higher than 5 mPa it is more likely that the compound has dissolved into the sub-phase. This could be due to the shorter carbon chain on the SDS compared with that of CTAB (12 and 16 carbons respectively), making the graphene(-)SDS more soluble than the graphene(+)CTAB. Greater solubility of the graphene(-)SDS could also be due to the slightly smaller size of these graphene flakes.

In contrast to this, the graphene(+)CTAB sample formed a stable monolayer up to 30 mPa (Figure 2.7). Four repeat cycles were performed, with cycles 2, 3 & 4 being almost identical and cycle 1 only differing from these by a small amount which is expected during an initial compression. The monolayer finally starts to collapse at approximately 30 mPa. In this case the monolayer collapse could be due to either monolayer folding or the graphene dissolving into the sub-phase, however further investigation is required to be certain of the exact cause.

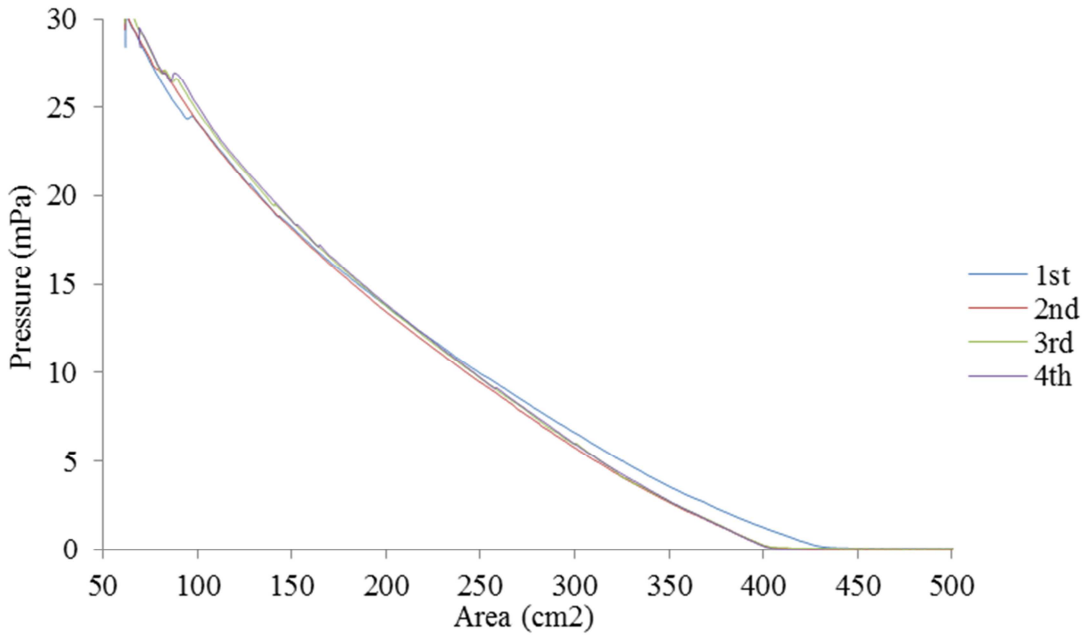

***Figure 2.7** – Langmuir-Blodgett film of graphene(+)CTAB showing the change in surface pressure associated with reducing area for four consecutive compression cycles.*

Deposition was then performed at 25 mPa. This surface pressure was chosen in order to guarantee a single layer of graphene was deposited. This cannot be guaranteed at higher surface pressures as the monolayer might have started to collapse, forming bilayers or multilayers.

The graphene monolayer was deposited onto a glass slide by the Langmuir-Blodgett method, with 60 deposition cycles being performed. The Langmuir-Blodgett trough was set to maintain the surface pressure at 25 mPa by continuous compression. Figure 2.8 shows the deposition process with the surface area of the monolayer decreasing (blue) as the glass slide moves through it (red) with 30 mm being fully submerged.

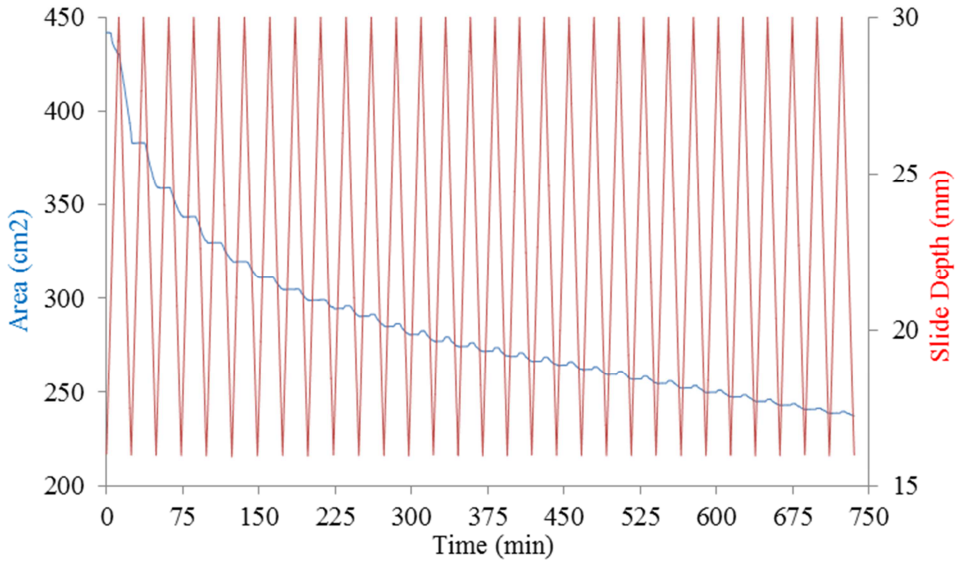

Figure 2.8 *– The deposition of graphene(+)CTAB monolayer onto a glass microscope slide by the Langmuir-Blodgett method showing change in area to maintain a surface pressure of 25 mPa.*

This deposition method has the potential to yield 60 layers of graphene on each side of the glass slide. However from the data obtained during the deposition it is clear that less than this is deposited. The surface area of the monolayer decreases whenever the amount of material in the monolayer is reduced. This occurs because the monolayer must be compressed to maintain the required surface pressure. It is clear from the data that this only happens on the upward movement of the glass slide, as the meniscus of the water causes the monolayer to

follow the slide out of the water. In the field of Langmuir-Blodgett films, this type of deposition is known as Z-type deposition. This means that only 30 monolayers will be deposited onto each side of the slide.

The fact that this occurs on the upward and not the downward movement, however, means that the reduction in surface area is more likely due to deposition rather than due to the graphene dissolving into the sub-phase. For the first eight deposition cycles there is no change in surface area on the downward movement of the slide, however subsequent cycles show a rise in surface area as the slide is moved downwards. This suggests that the intermolecular forces holding the deposited graphene onto the slide are less than those keeping the monolayer in contact with the surface, and so the deposited graphene begins to peel away from the slide and re-join the monolayer. This could be due to the repulsion between the growing positive charge on the slide caused by previous deposition and the graphene being deposited. This is supported by the fact that as the deposition cycles continue the decrease in the surface area for each successive cycle is decreased.

The graphene monolayer was also deposited as a single layer onto a silicon chip, as shown in Figure 2.9, for analysis by atomic force microscopy (AFM). The surface area decrease between 29 & 32 minutes shows the deposition of the monolayer and corresponds to the surface area of the substrate.

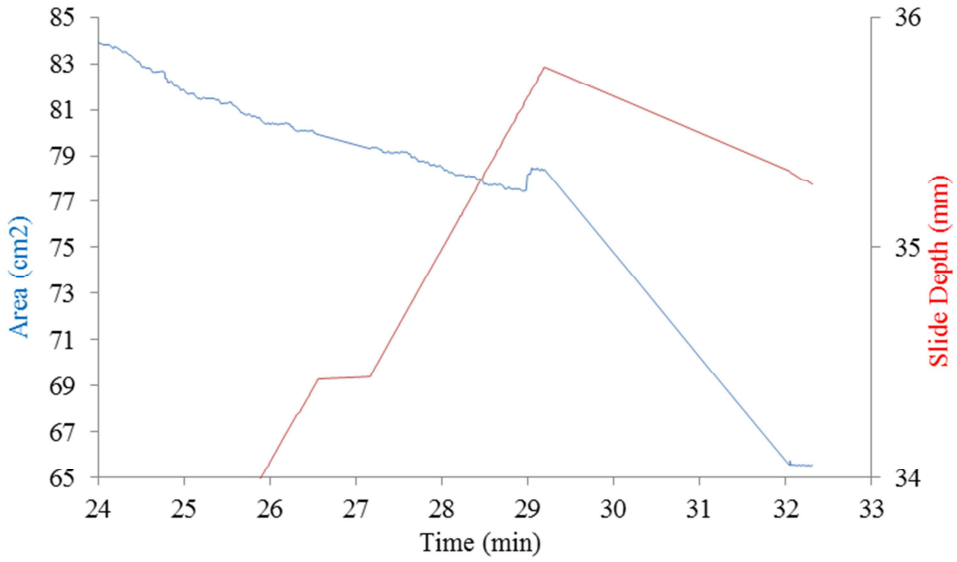

Figure 2.9 *- Deposition of graphene(+)CTAB monolayer onto a silicon chip by the Langmuir-Schaefer method showing change in area (blue) to maintain a surface pressure of 25 mPa during deposition (slide position shown in red).*

2.5.3.2 Layer-by-Layer Deposition of Graphene

The increase in size with each successive layer of graphene as determined by ellipsometry is shown in Figure 2.10.

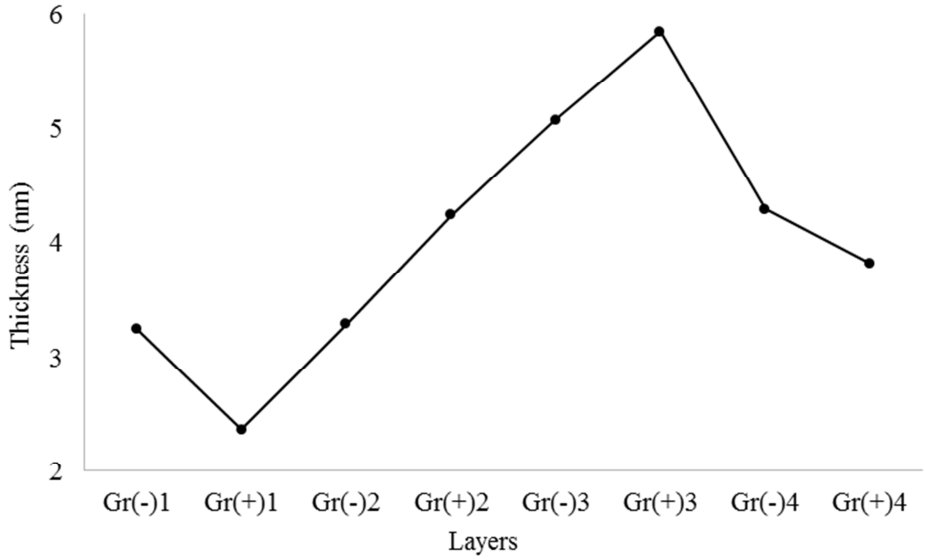

Figure 2.10 *– The increase in coating thickness on a silicon chip coated with alternating layers of graphene(-SDS) and graphene(+)CTAB and analysed by ellipsometry.*

The decrease in coating thickness between layers one and two could be due to the instability of the first layer in this method. And since the silicon chip is not charged, the electrostatic

forces between the deposited layer and the graphene in solution are greater than those holding the layer immobilised onto the surface. The next five layers are deposited giving a linear increase in coating thickness with each successive layer. The slope of this linear portion of the graph gives a layer thickness of 0.87 nm per layer. This layer thickness is less than that of a bilayer of CTAB of SDS (approximately 4 – 5 nm) which shows that the surfactant's hydrophobic chains lie flat on the graphene surface, which is confirmed by NMR (Section 2.5.2.2). After layer number six the coating begins to collapse, with a decrease in coating thickness as the graphene layers start to peel off. This is a similar phenomenon to that observed in the Langmuir-Blodgett deposition of 60 layers, where the deposition of graphene was most effective for the first eight deposition cycles. This again could be due to the electrostatic interaction between the deposited graphene and the graphene in solution being stronger than the attraction integrating each layer into the coating. As the coating thickness increases, the number of layer-layer interfaces increases and thus the likelihood of one of these interfaces breaking is greater.

Attempts at depositing thin films of graphene(+)CTAB using a traditional LB process, e.g. vertical dipping and withdrawing the substrate through the monolayer, were not successful since the transfer ratio was poor. The first withdrawal yielded about 60 %; then the layer was shown to peel off during subsequent dipping cycles. The overall transfer ratio by area (when substrate surface area was compared with loss of monolayer area) was 10 – 20 %. The most significant cause of this was poor adhesion of the first graphene layer to hydrophilic substrates. This could be improved in future work via the use of substrates with surface modifications which either enhance the surface charge or make the surface more hydrophobic. Much better results were obtained using the horizontal lifting method known as Langmuir-Shaefer (LS) deposition; where the hydrophilic substrate is held horizontally to the assembled monolayer and then lowered slowly to gently touch water surface; the monolayer

is then transferred onto the substrate surface. Only a single layer of graphene(+)CTAB could be deposited by LS deposition. Attempts to deposit multilayers by the LS technique failed, as the deposited layers began to peel off upon consecutive depositions.

2.5.3.3 Atomic Force Microscopy

Organised monolayer films obtained in this fashion were then characterised by AFM. A typical AFM image of graphene(+)CTAB flakes deposited onto a piece of silicon wafer using LS method is shown in Figure 2.11. The larger scale image (a) shows a number of irregularly shaped graphene(+)CTAB flakes with gaps between; the flakes were sometimes shown to overlap, forming double and sometimes triple layers. Image (b) shows, a pseudo 3D image of a flat individual flake of about 500 nm in size with another smaller flake lying on top.

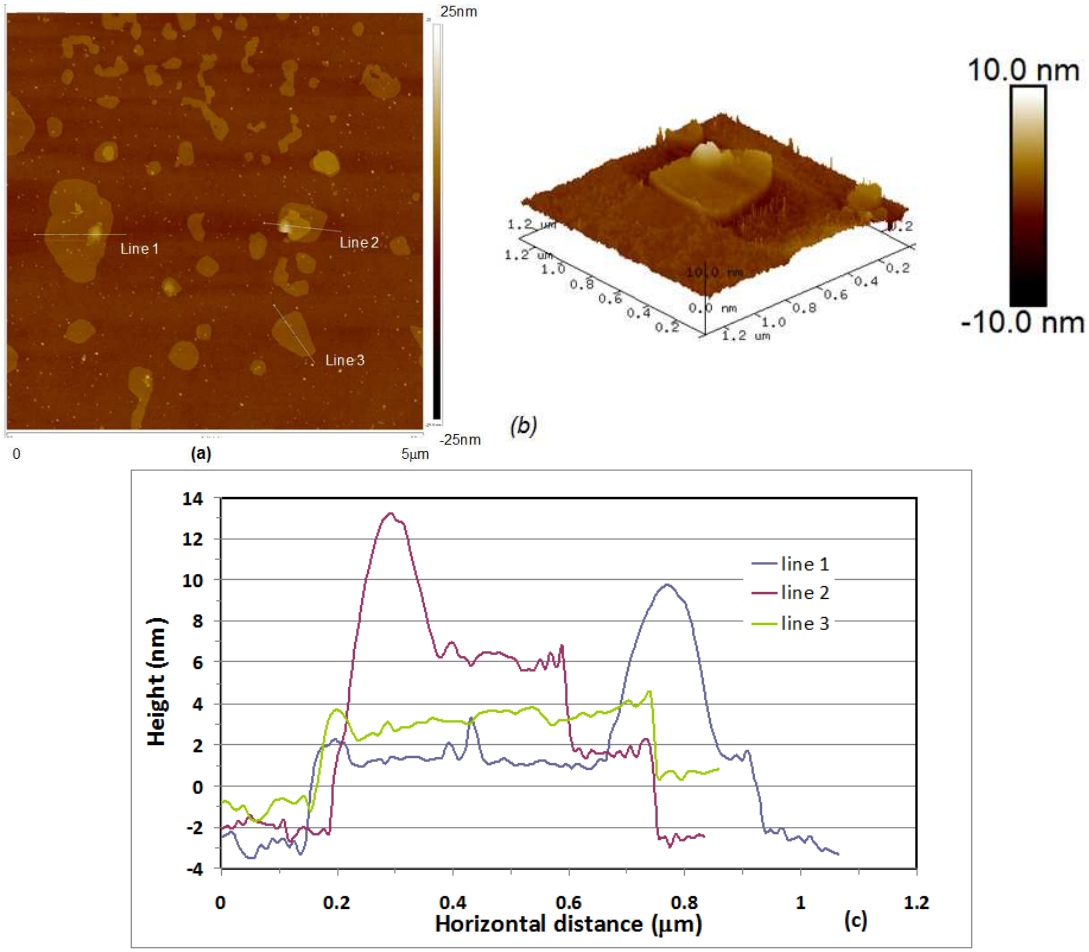

Figure 2.11 – *AFM images of the same sample of a graphene(+)CTAB layer deposited onto a silicon substrate using the LS method: (a) 2D image 5 µm; (b) pseudo-3D image of individual graphene flake. (c) Sectional analysis of the image in (a).*

Sectional analysis of AFM image along the lines shown, allows for an estimation of the graphene(+)CTAB flake thickness at 2 nm, which is significantly higher than the reported thickness of pristine graphene of 0.355 nm. The obtained value of 2 nm for an individual graphene(+)CTAB is likely due to the presence of surfactant molecules, CTAB in this case.

It is clear from these images that the surface coverage is not complete. Additionally the graphene flakes were seen to change position and shape during scanning, suggesting poor adhesion to the silicon surface. This could potentially be overcome in future work by using silicon wafers modified with silanised surface coatings for sample deposition.

Much better results (in terms of adhesion and surface coverage) were obtained by using a simple technique of electrostatic layer-by-layer (LbL) deposition. Multilayered films of graphene were deposited onto gold coated glass microscope slides by alternating layers of a graphene-surfactant with oppositely charged polyelectrolytes, e.g. graphene(+)CTAB layers alternated with polyanionic layers of polystyrene sulfonate sodium salt (PSS), while graphene(-)SDS was alternated with layers of polycationic species such as polyallylamine hydrochloride (PAH) or polyethyleneimine (PEI). Alternating layers of graphene(-)SDS and graphene(+)CTAB was also attempted. The mutlilayered films obtained were then characterised with scanning SEM combined with EDX (energy dispersing X-ray) elemental analysis (SEM NOVA) and AFM.

Not all alternating combinations worked well, however. For example, the most promising combination of graphene(+)CTAB with graphene(-)SDS was not successful, while the alternation of graphene(+)CTAB with PAH (or with PEI) proved to be the most optimal. Deposition on glass or silicon samples was performed by electrostatic adsorption of PAH (or PEI) for 20 - 30 min followed by dipping into a solution of graphene(-)SDS for 10 - 15 min. This sequence was repeated several times with a typical incubation time of 10 - 15 min.

Figure 2.12 shows an SEM image of alternating layers of PAH and graphene(-)SDS deposited onto a silicon substrate. Separate flakes are clearly visible, the largest of which is approximately 30 μm across. EDX spectral analysis (b) performed on a flake show a dominating peak of carbon while on the empty space (c) silicon is the dominant peak. This shows, that the graphene flakes consist predominantly of carbon, with a few trace elements.

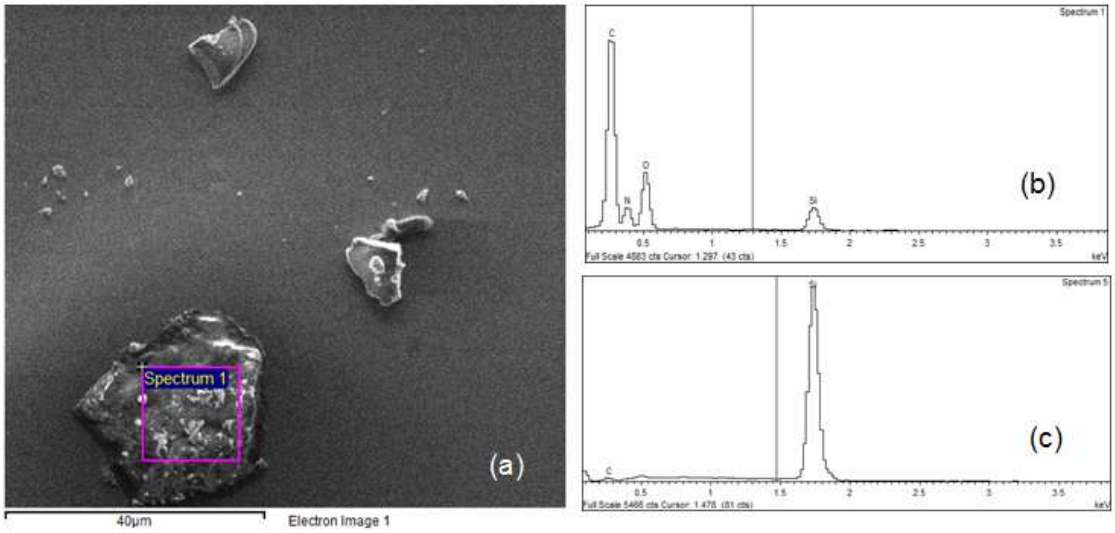

Figure 2.12 *- (a) SEM image of PAH/graphene(-)SDS layer on a silicon surface; (b) EDX spectra recorded on a graphene flake, and (c) an empty space.*

Deposition of the first few layers gives a less than optimal coverage. The reason for this is likely poor adhesion between layers of graphene(-)SDS and PAH. Deposition of subsequent layers greatly improves the coverage by overlapping adjacent graphene flakes.

Adhesion between graphene and substrate was greatly improved when using a stronger polycation such as PEI. The AFM image of graphene(-)SDS deposited onto a layer of PEI in Figure 2.13 shows far better surface coverage. However it can be seen that graphene flakes overlap and form double and, in some cases, triple layers.

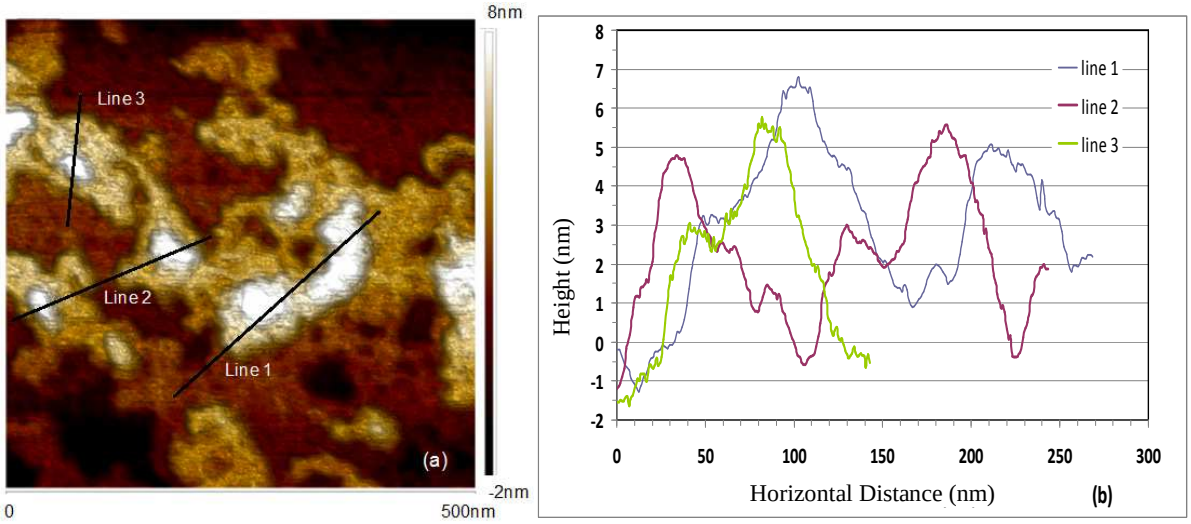

Figure 2.13 *- (a) AFM image (tapping mode) of a PEI/graphene(-)SDS film, and (b) a corresponding sectional analysis.*

Sectional analysis performed on the sample shows the double and triple layers, and shows the thickness of a single flake at approximately 2.5 nm. This is a somewhat higher than that for Langmuir-Schaefer deposited films; the difference could potentially be caused by the presence of PEI layer.

2.5.3.4 Spectroscopic Ellipsometry Study

Ellipsometry measurements were performed on graphene-surfactant films deposited on different substrates, i.e. glass microscope slides, silicon wafers, and gold-coated glass microscope slides. Typical spectra of ellipsometric parameters Ψ and Δ (representing, respectively, the ratio of amplitudes and phase shift of p- and s- components of polarized light) of graphene(-)SDS deposited on silicon by alternation with PAH are shown in Figure 2.14.

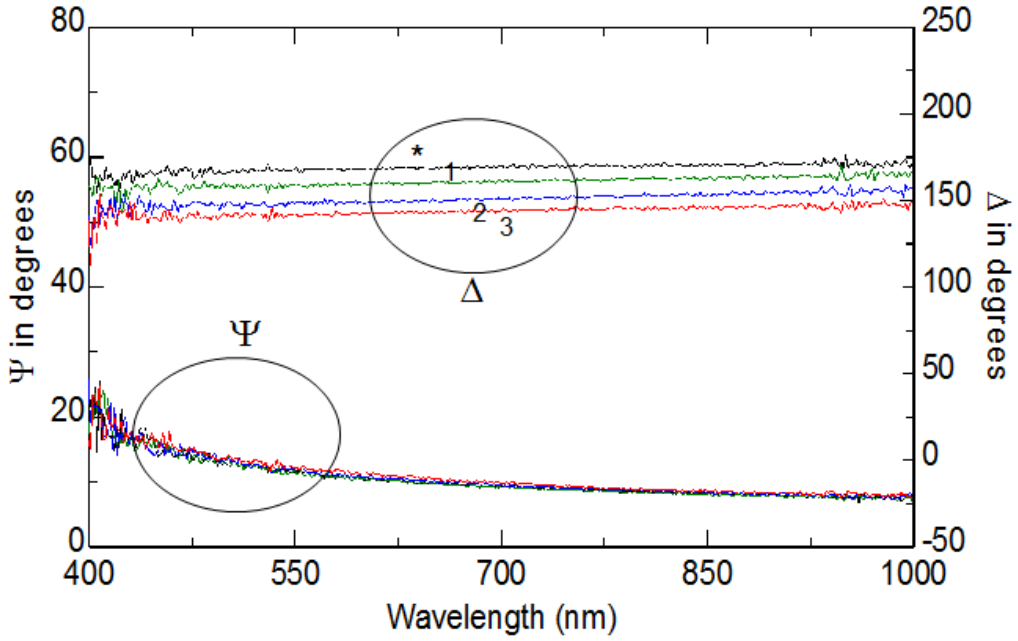

Figure 2.14 *- Spectra of ellipsometric parameters Ψ and Δ recorded on a bare silicon surface (*) and on deposited PAH/graphene(-)SDS films. Numbers 1, 2, and 3 indicate the number of bilayers deposited.*

It can be seen from the ellipsometry data that all Ψ spectra are the same regardless of surface deposition, while Δ spectra shift downwards upon deposition of bilayers of PAH/graphene(-)SDS.

For analysis of graphene multilayers deposited by the layer-by-layer method, spectroscopic ellipsometry measurements were carried out on samples after each layer was deposited. The results of this are shown in Figure 2.15. Similarly to previous experiments, Ψ spectra were not changed much while Δ spectra were shifted downwards upon deposition of graphene layers. The ellipsometry data fitting was performed in a similar manner as described above. The data shows that the deposition is not consistent, possibly because of poor adhesion between graphene layers.

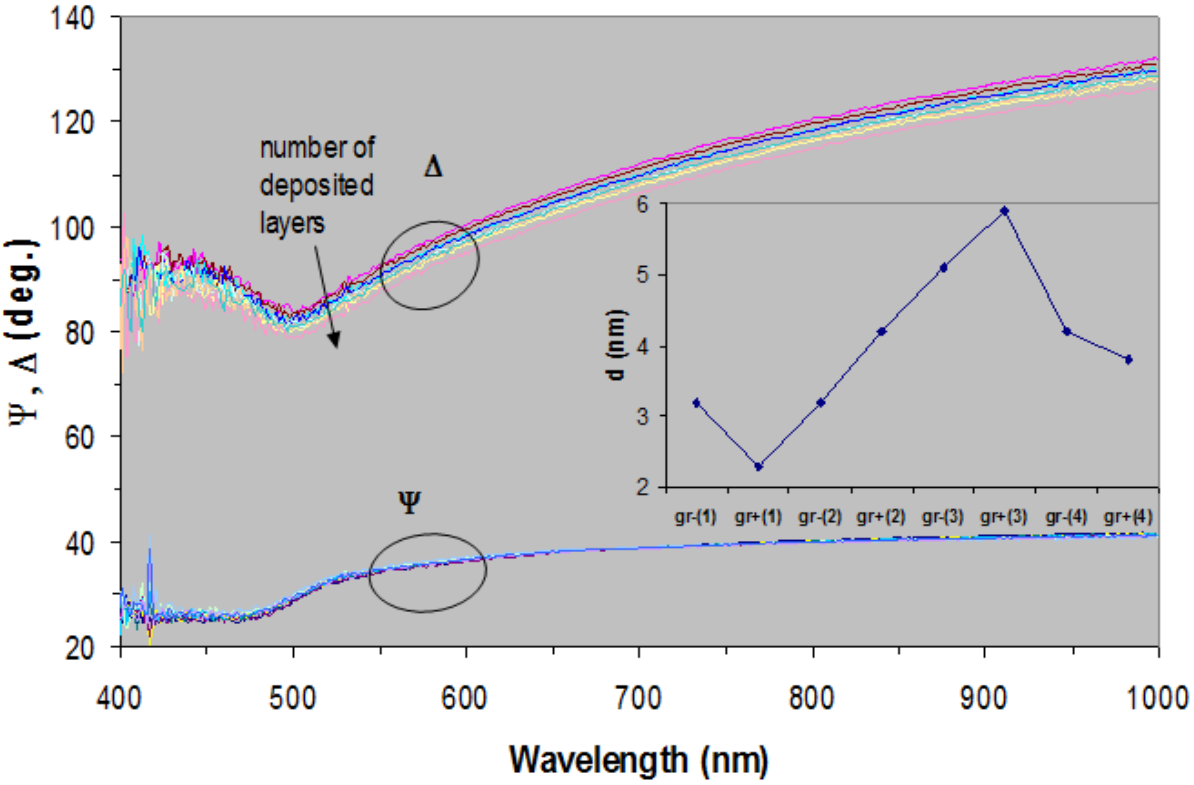

Figure 2.15 *- Ψ and Δ spectra of graphene films deposited on chromium/gold coated glass slides by alternation of graphene(-)SDS and graphene(+)CTAB. The arrow indicates the increase in the number of deposited layers. The inset shows the variation of the film thickness on the number of graphene layers deposited.*

As mentioned above, the best results were obtained using PEI (rather than PAH) as a binding layer alternating with graphene(-)SDS. The ellipsometry spectra in Figure 2.16 are recorded on samples of PEI/graphene(-)SDS deposited on glass and gold-coated glass, respectively.

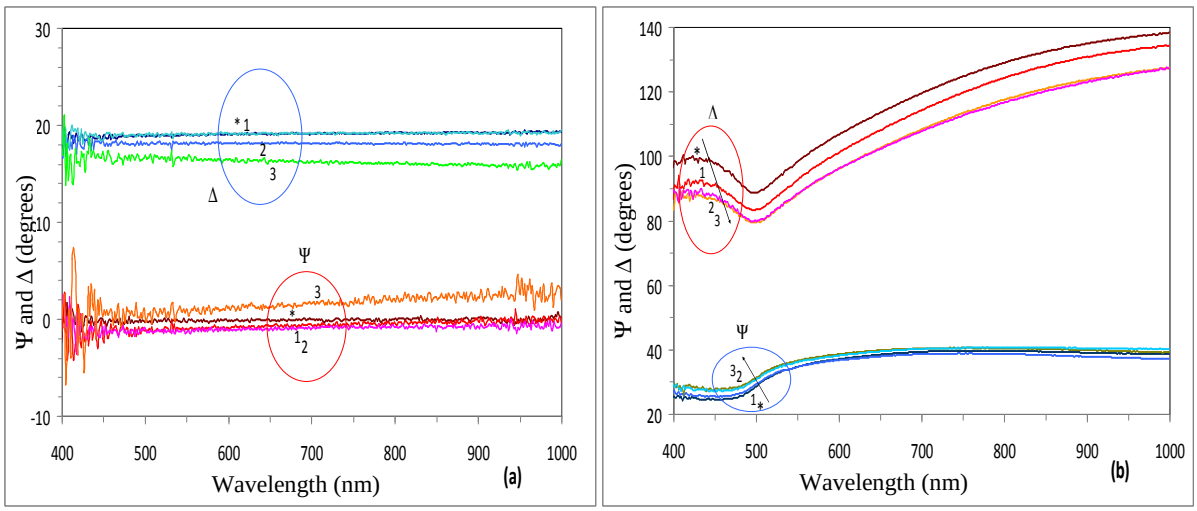

Figure 2.16 *- Ψ and Δ spectra of PEI/graphene(-)SDS films deposited on (a) glass and (b) gold coated glass. Arrows show the increase in the number of layers deposited.*

Fitting of the data in Figure 2.16 was carried out using a three layer model with the substrates being glass or chromium/gold coated glass. As before the graphene layers were modeled by Lorentz oscillator. The results show a consistent increase in the films thickness upon deposition of bilayers of PEI/graphene(-)SDS with the thickness increment of 2.5 nm which is similar to what was observed directly with AFM.

The ellipsometric spectra for graphene deposited on glass (Figure 2.17a) did not show any specific features, such as plasmonic peaks related to light absorption, and the behavior of the graphene layer was consistent with a dielectric material. This correlates well with featureless absorption spectra of graphene in a visible range and the known fact that plasmon band of graphene lies in UV range at about 280 nm. In contrast to that the data in Figure 2.17*b* shows the features related to absorption by surface plasmons but they are attributed to gold films; the layers of graphene did not alter this much, merely causing a small shift of Ψ and Δ spectra.

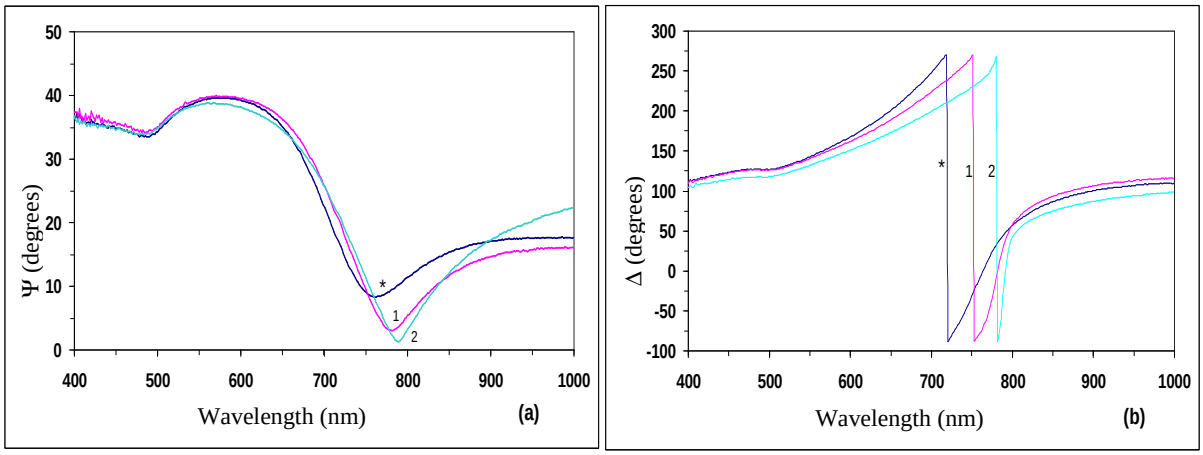

Figure 2.17 *- TIRE spectra of (a) Ψ, and (b) Δ recorded on a bare gold-coated glass slide (*) and after deposition of bilayers of PEI/graphene(-)SDS. Numbers 1, 2, and 3 indicate the number of bilayers deposited.*

2.5.3.5 TIRE study

The results obtained from the total internal reflection study are shown in Figure 2.17 as spectra of Ψ and Δ. Deposition of graphene layers made the SPR minimum shift to a larger

wavelength on the Ψ spectra while causing an additional phase shift on Δ spectra. The enhancement of the SPR peak due to the deposition of graphene layers is observed for the first time. It is interesting to note that graphene itself does not show plasmonic behavior in the visible spectral range as was proven by ellipsometry measurements in Figure 2.15 - Figure 2.17. At the same time the interaction of π-electrons in graphene and free electrons in gold may lead to the enhancement of SPR in gold layers. The thickness increment values were approximately 2.5 nm, similar to the previous experiments using traditional (external reflection) ellipsometry.

2.6 Conclusion

A simple semi-automated technique for graphene production by aqueous sonochemical exfoliation of graphite in the presence of ionic surfactants, e.g. CTAB or SDS, was developed. Full automation could be potentially achieved by adding surface tension sensors to control the amount of surfactant being added to the reactor, thus maintaining a constant and optimum surface tension. The formation of individual graphene flakes and the interaction of alkyl chains of the surfactants with graphene were, respectively, confirmed with Raman spectroscopy and NMR measurements.

The two different graphene-surfactant complexes produced (graphene(+)CTAB and graphene(-)SDS) appeared to be soluble in water and thus suitable for electrostatic LbL deposition. Both compounds were also found to be amphiphilic and soluble in chloroform, hence it was also possible to form stable monolayers on the water surface. Thin films of the above graphene composites were deposited onto different solid substrates, i.e. silicon, glass and gold-coated glass, using either electrostatic LbL, LB, or LS deposition techniques. SEM and AFM study showed that LB or LS films of graphene(+)CTAB had poor surface coverage and adhesion to the substrate. Electrostatic LbL deposition of graphene by alternation of

graphene with oppositely charged polyelectrolytes was much more promising in these aspects. Several combinations of materials were tried including the alternation of graphene(+)CTAB and graphene(-)SDS. The best results were achieved by alternation of graphene(-)SDS with PEI. AFM study allowed the estimation the thickness of an individual graphene-surfactant flakes of about 2 - 2.5 nm.

The spectroscopic ellipsometry study of graphene thin films gave similar values for the thickness of the graphene-surfactant composite layer. While the dispersions of refractive index and extinction coefficient were modelled by a single Lorenzian peak lying in far IR region, the absorption peak of graphene at approximately 280 nm was outside the spectral range (370 – 1000 nm) of the ellipsometric instrument. Interesting results were obtained when studying the SPR effect in gold films coated with a few layers of graphene using the technique of total internal reflection ellipsometry (TIRE). Although graphene itself shows no spectral features associated with plasmon oscillations in the above spectral range, in TIRE experiments the deposition of graphene layers on gold progressively enhanced the plasmon resonance on Ψ-spectra and caused an extra phase shift on Δ-spectra. This phenomenon can be explored in future work for enhancing the performance of SPR-based bio-sensors.

Chapter 3 Electrical and Electrochemical Properties of Graphene

3.1 Introduction

Graphene has been shown to display a wide range of interesting properties; such as high mechanical durability, optical transparency, high surface area, and good electrical conductivity (Davis, F., personal communication, 2014). It is the high surface area and its electrical properties that make graphene a potential candidate material for enhancing the performance of electrochemical sensors. It has been demonstrated that modification of glassy carbon electrodes with graphene leads to an increase in oxidation peak currents and the lowering of oxidation potentials. Electrochemical impedance measurements show a much lower charge transfer resistance for graphene modified electrodes compared with screen printed carbon electrodes.

Another important field of research under investigation is the development of sensors for the direct detection of small biomolecules without the use of enzymes. Graphene makes an ideal candidate for these electrochemical sensors because of its enhanced electro-catalytic effects and fast electron transfer kinetics observed in comparison to those possible with traditional inexpensive sensor materials such as screen printed carbon. This chapter focusses on detection of three different groups of compounds as follows.

Dopamine is most widely investigated, because its concentration can be directly linked to a number of clinical conditions. Of particular interest is the development of a dopamine electrochemical sensor that can selectively distinguish dopamine even in the presence of uric acid and ascorbic acid, which have overlapping voltammetric responses. Direct oxidation of the five bases in DNA and RNA can also be detected with separate peaks being obtained for each base in short strands of both single and double-stranded DNA, and RNA. Of the 20 proteinogenic amino acids, three are electrochemically active; phenylalanine, tyrosine, and tryptophan. These compounds give oxidation and reduction peaks that overlap, however

resolution of these peaks might be achieved with the application of graphene to an electrode surface.

The graphene produced in the previous section (Chapter 2) will be utilised as an electrode coating to be applied to screen printed carbon electrodes. These electrodes will then be used to enhance the detection of compounds by a combination of electrochemical detection methods such as cyclic and linear voltammetry. These are dynamic electrochemical techniques that involve measuring the current flowing in an electrochemical cell when a potential is ramped between two potentials. A non-polarisable reference electrode provides a potential to allow the working and counter electrodes to be polarised with respect to this reference potential.

In this chapter a range of electrochemical techniques will be used to characterise the graphene modified electrodes and determine whether or not they offer a significant advantage over standard screen printed carbon. In cyclic voltammetry, the potential applied to the electrodes is swept cyclically between two values (V_1 and V_2) with a triangular waveform. In linear voltammetry, the voltage is swept from one value to another, without a return sweep being performed. In both potential techniques the current is then measured and used to generate a voltammogram.

In electrochemical impedance spectroscopy an alternating electrical voltage applied to the electrode surface causes a polarisation effect, whereby positive charges are orientated towards the field and negative charges orient away from the field. This alters the electrical field within the material by creating an internal field different to the external field. The result is that the impedance of the material from which the electrode surface is composed changes dependant on the frequency of the applied alternating electrical current measured in Hertz (Hz). This data can then be plotted as a semi-circular Nyquist plot, which can be used

to determine the resistance to electron transfer at the electrode surface. This chapter forms the basis for a journal article published in Analytical Chemistry (Walch *et al*., 2015).

3.2 Materials

Sodium dodecyl sulphate (SDS) and the five nucleotide bases (adenine, thymine, guanine, cytosine, and uracil) were obtained from Fisher Scientific (Loughborough, UK). Cetyl trimethylammonium bromide (CTAB), the three electrochemically active amino acids (phenylalanine, tyrosine, and tryptophan), and the blood based compounds (dopamine, uric acid, and ascorbic acid) were obtained from Sigma-Aldrich (Poole, UK).

Ultra-pure (18 MΩ cm^{-1}) water was produced using a Milli-Q water purification system obtained from Millipore (Tokyo, Japan).

3.3 Methods

In this section the methods for the fabrication of graphene modified electrodes an the characterisation of their electrochemical properties will be described.

3.3.1 Electrochemical Impedance Spectroscopy of Graphene

The resistance to electron transfer of the deposited graphene samples at different concentration was investigated using electrochemical impedance spectroscopy. The graphene was deposited (5 μL) onto the surface of a screen printed carbon electrode. The electrode was then left to air dry for 1 hour. When the graphene suspension had dried the electrode was washed with deionised water to remove any surfactant that was not bound to the graphene surface. The concentrations of graphene(-)SDS and graphene(+)CTAB deposited onto the elecrodes were 0.05, 0.10, 0.14 & 0.17 mg ml^{-1}. Control electrodes of SDS (150 mg ml^{-1}) and CTAB (49.7 mg ml^{-1}) were also prepared, as well as a blank unmodified electrode for comparison. The electrodes were then placed into a solution of ferri/ferrocyanide (5 mM) in PBS (0.01 mM, pH 7.4) and Nyquist plots were recorded. The data was recorded between

1 and 10000 Hz on a logarithmic scale. In total 100 measurements were taken for each electrode. The data was collected and a semicircle was extrapolated from the Nyquist plot, the diameter of the semicircle being equal to the electron transfer resistance (Katz & Willner, 2003). This reading was taken three times to allow an average and standard deviation to be calculated.

3.3.2 Deposition and Electrochemistry of Graphene

The graphene solution was used to enhance the detection of analytes by the electrochemical technique cyclic voltammetry. This was achieved by depositing the graphene directly onto the electrode. A screen printed carbon electrode with two working electrodes and a counter electrode (composed of carbon and a reference electrode composed of silver/silver chloride) was cut from the sheet and washed with deionised water to remove any dust or contamination that might have accumulated. Then an aliquot of graphene solution (5 μL) was pipetted carefully onto the surface of the left hand side working electrode taking care to cover the electrode evenly and completely. The electrode was then left to air dry for 1 hour. When the graphene suspension had dried the electrode was washed with deionised water to remove any surfactant that was not bound to the graphene surface. The optimum graphene concentration for deposition was determined experimentally by performing a concentration scout. Electrodes were prepared using a range of different graphene concentration (0.05, 0.1, 0.14 & 0.18 mg ml^{-1}) and then used to detect dopamine (1 mM, 10 ml) in phosphate buffered saline (PBS) solution in water (10 mM, pH 7.4) by cyclic voltammetry. The electrode used consisted of two working electrodes, one of which was left unmodified and used as a blank for comparison. The resulting peak position and current intensity were recorded and used to determine the optimum concentration.

Once the optimum concentration had been determined, the optimum scan parameters were determined. The potentiostat was not cycled beyond -1.1 – 1.1 V for any experiment unless

necessary for separation as a wider scan range would cause electrolysis of the water in the sample, which is not insignificant. Where such a range could not be avoided the sample was first purged of oxygen by sonication under vacuum. Different scan rates (2 - 50 mV s^{-1}) were tried to determine which would give the best separation of more than one compound in a mixture.

3.3.3 Resolution of a Mixture of Compounds

Mixtures of different classes of compounds were prepared and then analysed using cyclic voltammetry to determine if the graphene electrodes produced a voltammogram with better peak resolution for different compounds when compared with the unmodified electrodes. Three different mixtures were prepared; blood based compounds, nucleotide bases, and amino acids. The mixture of blood based compounds contained dopamine (45 μM), ascorbic acid (75 μM) and uric acid (60 μM) in PBS (10 mM, pH 7.4). This experiment was based on the work of Xiao *et al*. (2014). The nucleotide base mixture contained adenine, thymine, guanine, cytosine and uracil (1 mM) in PBS (10 mM, pH 7.4). The amino acid mixture contained phenylalanine, tyrosine, and tryptophan (1 mM) in PBS (10 mM, pH 7.4).

The blood based compound mixture was analysed using cyclic voltammetry between -1 – 1 V with a sweep rate of 25 mV s^{-1}. The nucleotide base mixture was analysed by linear voltammetry between 0 – 1.7 V at a sweep rate of 2 mV s^{-1}. Faster sweep rates were also performed, however optimal resolution was achieved at the lower rates. Linear voltammetry was chosen in this case because the high potential damaged the electrode surface and as such cyclic voltammetry was not an appropriate technique. The amino acid mixture was analysed using cyclic voltammetry between -1 – 1 V, however no resolution was achieved between compounds even at low sweep rates by the graphene coated electrodes and the voltammograms looked similar to those produced using unmodified screen printed carbon electrodes.

For all of these experiments the electrodes were prepared as mentioned above, using negatively charged graphene (graphene(-)SDS) at a concentration of 0.19 mg ml^{-1}. These parameters were determined to be optimum during the initial experiments.

3.3.4 Detection of Aqueous Metal Ions

Previous work (Langford, 2013) also used graphene modified electrodes were also used to detect certain metal ions in aqueous solution. This work is described as an example of other uses of surfactant stabilised graphene.

A solution of lead, copper, and mercury ions (1 ppm) was analysed using absorptive stripping voltammetry between -0.8 – 0.4 V. Electrodes modified with both positively and negatively charged (graphene(+)CTAB and graphene(-)SDS respectively) were used to detect the metal ions and an unmodified screen printed carbon electrode was also used for comparison.

3.3.5 Electrochemistry of Conducting Polymer Films

The efficacy of graphene coated electrodes was compared to that of three conducting polymer films; poly aniline (PANI), poly pyrrole (PPy), and poly (3,4-ethylenedioxythiophene) (PEDOT). This was done in order to show whether or not the graphene modified electrodes offered an advantage over currently available technology.

Electrodes were prepared by cycling the potential between -0.5 – 0.7 V in the presence of the monomers. Aniline, pyrrole and 3,4-ethylenedioxythiophene (EDOT) solutions were prepared at a concentration of 0.01 mol L^{-1} in water, with a concentration of 0.1 mol L^{-1} polystyrene sulfonate (PSS) as a dopant. Electrodes with different film thicknesses were prepared by varying the number of cyclic voltammetry cycles. Film thicknesses of 5, 10, and 20 cycles were prepared for analysis of the effect of film thickness on electrode conductivity.

Once prepared, the electrodes were analysed using electrochemical impedance spectroscopy to determine the resistance to electron transfer at the electrode surface. Each electrode was analysed under open circuit potential from 1 – 10000 Hz at 10 mV. Scans were performed in 5 mmol L^{-1} ferri/ferrocyanide solution in PBS buffer. Nyquist plots were recorded and the resistance calculated for each film thickness.

3.4 Results and Discussion

The results of the electrochemical analysis of compounds using graphene modified electrodes will be discussed here.

3.4.1 Electrochemical Impedance Spectroscopy

The alternating current (AC) impedance was measured to determine the resistance to electron transfer at the electrode surfaces. The lower the resistance to electron transfer the more effective the electrode surface is at oxidizing/reducing chemical compounds by electrochemistry. The electron transfer resistance at various concentrations of graphene(-)SDS and graphene(+)CTAB is shown in Figure 3.1. Ferri/ferrocyanide (5 mM) was used as an electron transfer mediator.

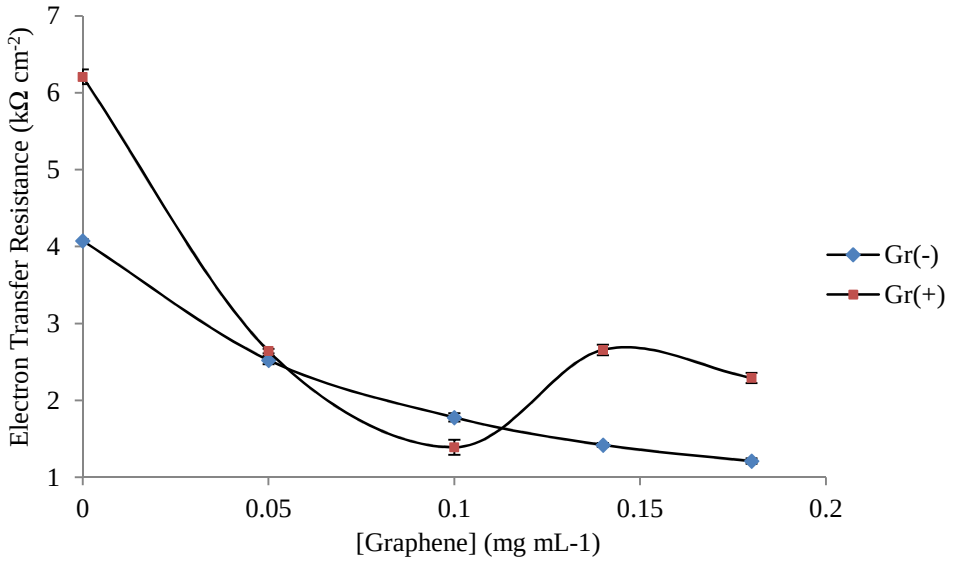

Figure 3.1 *– The electron transfer resistance for graphene(-)SDS and graphene(+)CTAB coated electrodes at different concentrations. Ferri/ferrocyanide (5 mM) was used as the charge transfer medium.*

The data shows that there is a difference in electron transfer resistance at different concentrations of both graphene samples. However the optimum concentration, defined by the minimum electron transfer resistance in each case, is different for different graphene polarities. The pattern is mirrored in the results of the concentration scouting by cyclic voltammetry shown in Section 3.4.2.1, with the graphene(+)CTAB showing a lower optimum concentration than the graphene(-)SDS.

The Nyquist plots of resistance and reactance for both graphene samples at their optimum concentration are shown, as well as an unmodified screen-printed carbon electrode for comparison. The results show a considerable decrease in resistance with the graphene coated electrodes. The electron transfer resistivity for the unmodified carbon electrode was 45.92 ± 0.123 kΩ, whilst the electrodes modified with graphene(-)SDS and graphene(+)CTAB showed values of 1.78 ± 0.056 kΩ and 2.29 ± 0.068 kΩ respectively, giving an approximate 20-fold decrease in resistance to electron transfer at the electrode surface when modified with graphene. The graphene(-)SDS showed a slightly lower resistance than the graphene(+)CTAB, suggesting that it is more active and better facilitates electron transfer, and is therefore a more effective surface for electrochemistry.

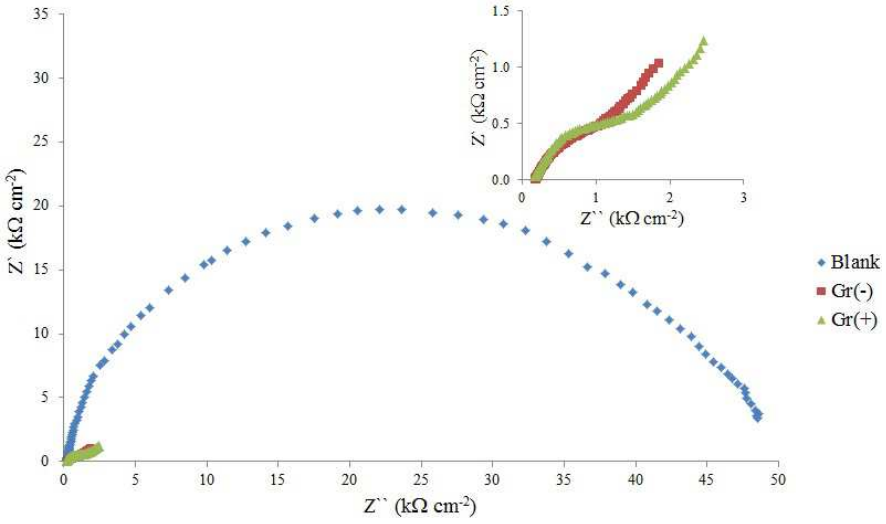

Figure 3.2 *– Nyquist plots for graphene(-)SDS and graphene(+)CTAB at the optimum concentration for minimal electron transfer resistance compared to a blank screen printed carbon electrode in ferri/ferrocyanide.*

The shape of the graph after the curved potion can also be used to characterise the surface. The unmodified electrode continues in an almost perfect semi-circle, showing that the rate limiting step is the electron transfer at the surface. However the rise in reactance after the curved portion for the graphene samples shows that the rate limiting step is the diffusion of analyte to the electrode, causing an increase in surface charge at the electrode surface. This is indicative of an electrode surface with a high conductivity and/or favourable electron transfer characteristics. Additionally the gradient of the linear portion of the graphs show that the rise in surface charge is greater for the graphene(-)SDS, showing it to be a better conductive surface than the graphene(+)CTAB.

3.4.2 Deposition and Electrochemistry of Graphene

Once fully characterised, the graphene samples were used to modify screen printed carbon electrodes for electrochemical detection. The optimum concentration for each type of graphene was found by cyclic voltammetry and then the ability of each sample to resolve the detection of various mixtures of compounds was assessed.

3.4.2.1 Concentration Scouting

The concentration at which maximum resolution was achieved between two adjacent peaks representing different compounds was determined by cyclic voltammetry using dopamine (1 mM) as the analyte.

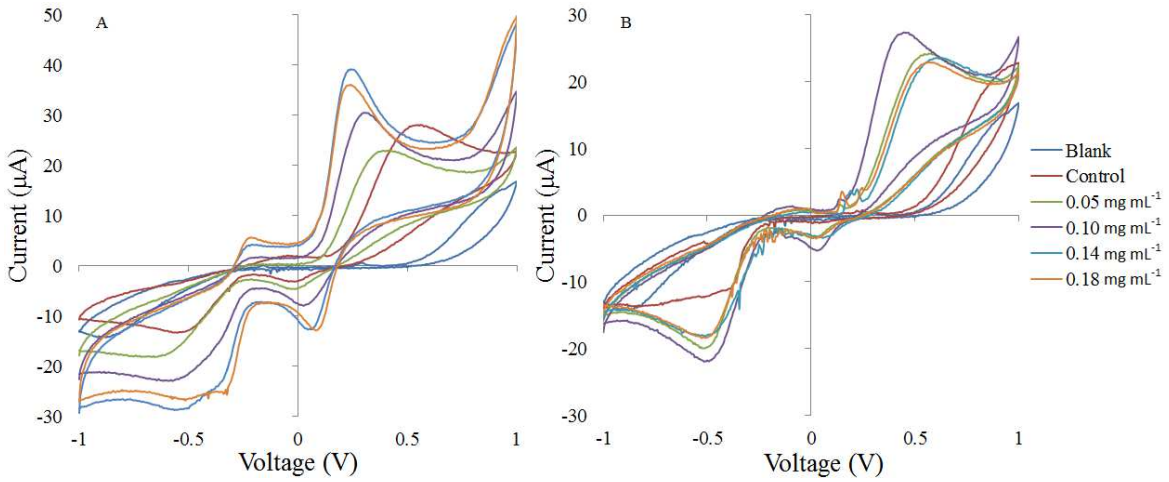

Figure 3.3 *– Cyclic voltammograms for dopamine (1 mM) using a screen printed carbon electrode modified with graphene(-)SDS (A) and graphene(+)CTAB (B) at different concentrations. A control experiment where the electrode was modified with saturated surfactant solution alone is also shown.*

The data shows a shift in the peak position with increased graphene concentration at the electrode surface. This is due to an increase in the electromotive force between the electrode and the analyte, which is a function of the decreasing electron transfer resistance. Additionally, the peak current increases with an increased concentration of graphene. This is due to more analyte being oxidised/reduced at the electrode surface as the conductivity relative to the blank electrode increases.

The peak position and intensity also changes when surfactant alone is used to modify the electrode. This is due to the lowering of the hydrophobicity of the electrode surface, allowing for better contact between the electrode surface and the aqueous solvent in which the dopamine is dissolved. Also, since charged surfactants are used in this study, the charge at the electrode surface could attract analytes of the opposite polarity leading to higher conversion rates. This observation is supported by the relative effectiveness of the SDS and CTAB on the conversion of analyte in the control experiments. Since the analyte (dopamine) carries a positive charge it will be attracted to the negative charge caused by residual SDS on the electrode surface and repelled by residual CTAB. This electrostatic effect could also

influence the effectiveness of the different graphene polarities as electrode coatings for cyclic voltammetry. However the effects of the surfactant were much less than those of the graphene composites, even though much higher concentrations of surfactant were used.

The optimum concentration for each graphene sample was determined as that which caused the maximum peak shift and current intensity Figure 3.4. The optimum concentrations selected for future work with graphene(-)SDS and graphene(+)CTAB were 0.15 mg ml^{-1} and 0.90 mg ml^{-1} respectively.

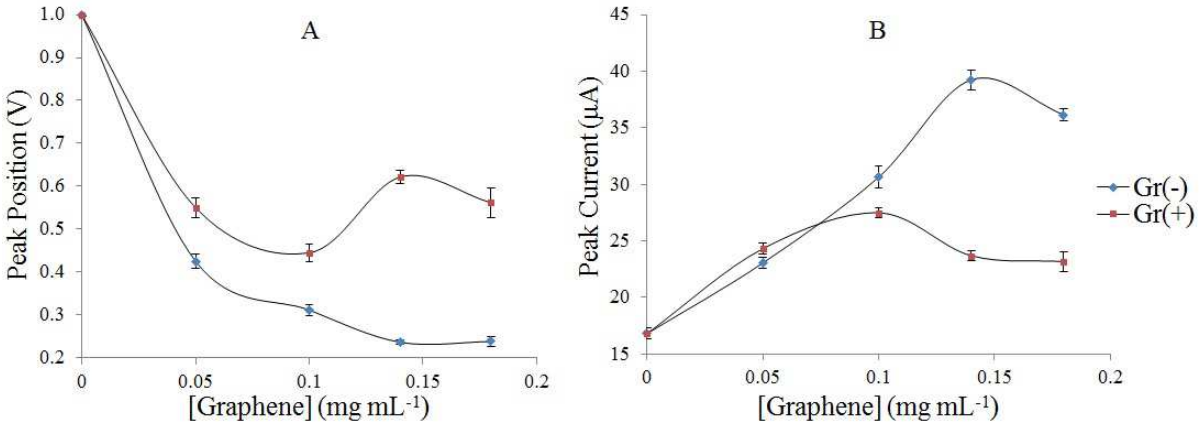

Figure 3.4 *- A comparison of the peak voltage (A) and peak current (B) at different concentrations of graphene(-)SDS and graphene(+)CTAB.*

3.4.3 Resolution of a Mixture of Compounds

Screen printed carbon electrodes were modified with graphene(-)SDS and graphene(+)CTAB at the optimum concentrations determined in Section 3.4.3. These electrodes were then used to detect mixtures of compounds with the hope of resolving adjacent peaks representing different compounds. The mixtures of compounds fell into three classes; nucleotide bases (adenine, thymine, guanine and cytosine, 1 mM), blood based components (dopamine, uric acid and ascorbic acid, 45 µM, 60 µM & 75 µM respectively), and electrochemically active amino acids (phenylalanine, tyrosine and tryptophan, 1 mM).

The resolving power of graphene(-)SDS for a mixture of the four nucleotide bases detected by linear voltammetry is shown in Figure 3.5

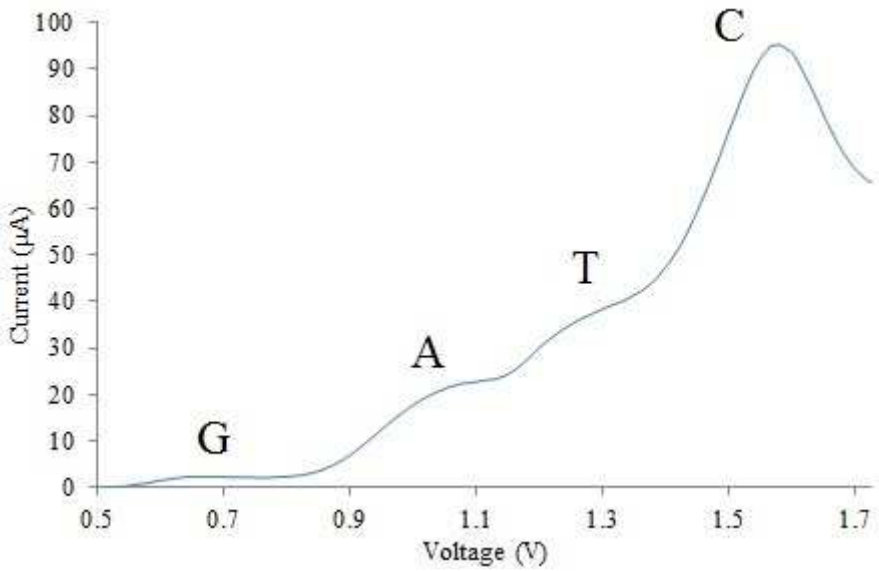

***Figure 3.5** – Linear voltammogram for a mixture of (A) adenine, (T) thymine, (G) guanine & (C) cytosine (1 mM) in PBS (0.01 mM, pH 7.4) on an electrode modified with graphene(-)SDS at a scan rate of 2 mVs.*

The peaks for guanine, adenine and cytosine are fairly well resolved on a graphene coated electrode when compared with a blank screen printed electrode (Figure 3.6), each beginning to plateau before the next peak begins. The characteristic drop in current usually observed with cyclic and linear voltammetry is not observed in this case due to the slow scan rate. The thymine peak is not fully resolved at this scan rate, however.

The different compounds in the mixture can be quantified, however each peak cannot be looked at in isolation. Since the position of a peak in terms of voltage should be considered a threshold voltage at which conversion of analyte begins, the current of a peak has a cumulative effect on each successive peak as the current does not drop down to baseline after each peak. Also, despite the fact that all of the analytes are present in the mixture at the same amount, this is not reflected in the relative intensities of each peak.

Linear voltammetry instead of cyclic voltammetry was chosen in this case for two reasons. Firstly there is no reduction peak, as the oxidation of the nucleotide bases is irreversible. And

secondly the maximum voltage was so high that the electrode surface was destroyed and successive scans by cyclic voltammetry did not show any useful data.

A comparison between the resolving power of graphene(-)SDS and graphene(+)CTAB is shown in Figure 3.6. The two voltammograms are presented on different scales to allow for comparison of peak position despite the vast difference in the peak intensities.

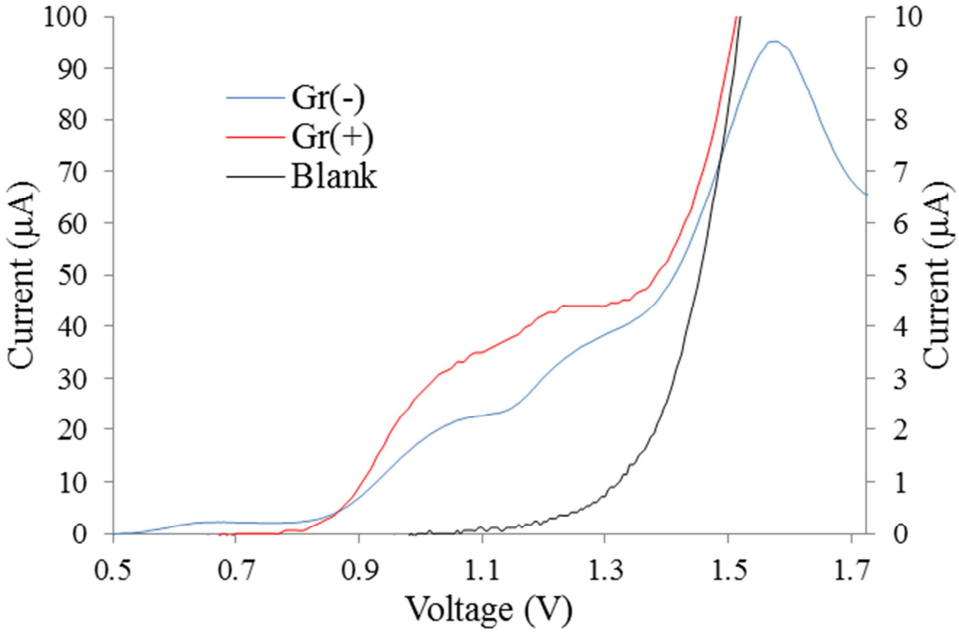

Figure 3.6 *– Comparison of the linear voltammogram for adenine, thymine, guanine and cytosine (1mM) on electrodes modified with graphene(-)SDS (blue, left scale) and graphene(+)CTAB (red, right scale). Data obtained using a blank unmodified electrode is also shown for comparison (black, left scale).*

The resolving power of the graphene(+)CTAB is far less than that of graphene(-)SDS with only three poorly defined peaks visible. The peaks for adenine and thymine have condensed into a single peak and are not distinguishable from one another. The peak representing guanine is of a similar relative intensity to the middle peak, but has not migrated as far with this graphene sample as with the other sample. The cytosine peak seems to have shifted further towards the left than with the graphene(-)SDS, however the peak does not level off, and in fact continues to increase until the electrode is destroyed at around 1.7 V. This is not shown as it would make the first two peaks difficult to see on the graph.

A similar pattern is seen when resolving the blood components; dopamine, uric acid and ascorbic acid. On the voltammogram recorded using graphene(-)SDS two peaks can be seen in the forward sweep (-1 – 1 V) and one very intense peak in the reverse sweep (1 – -1 V). The reverse peak is caused by the dopamine and the uric acid. Since it is a reducing agent, the ascorbic acid does not have a reduction peak, as oxidation of ascorbic acid is irreversible. The electrode modified with graphene(+)CTAB showed an improvement in resolution compared to the unmodified electrode, however the peaks are still poorly resolved and irreversible with only a single peak in the forward sweep. The reverse peak is still present, however intensities of all peaks compared with graphene(-)SDS is lower. The voltammograms are presented in Figure 3.7.

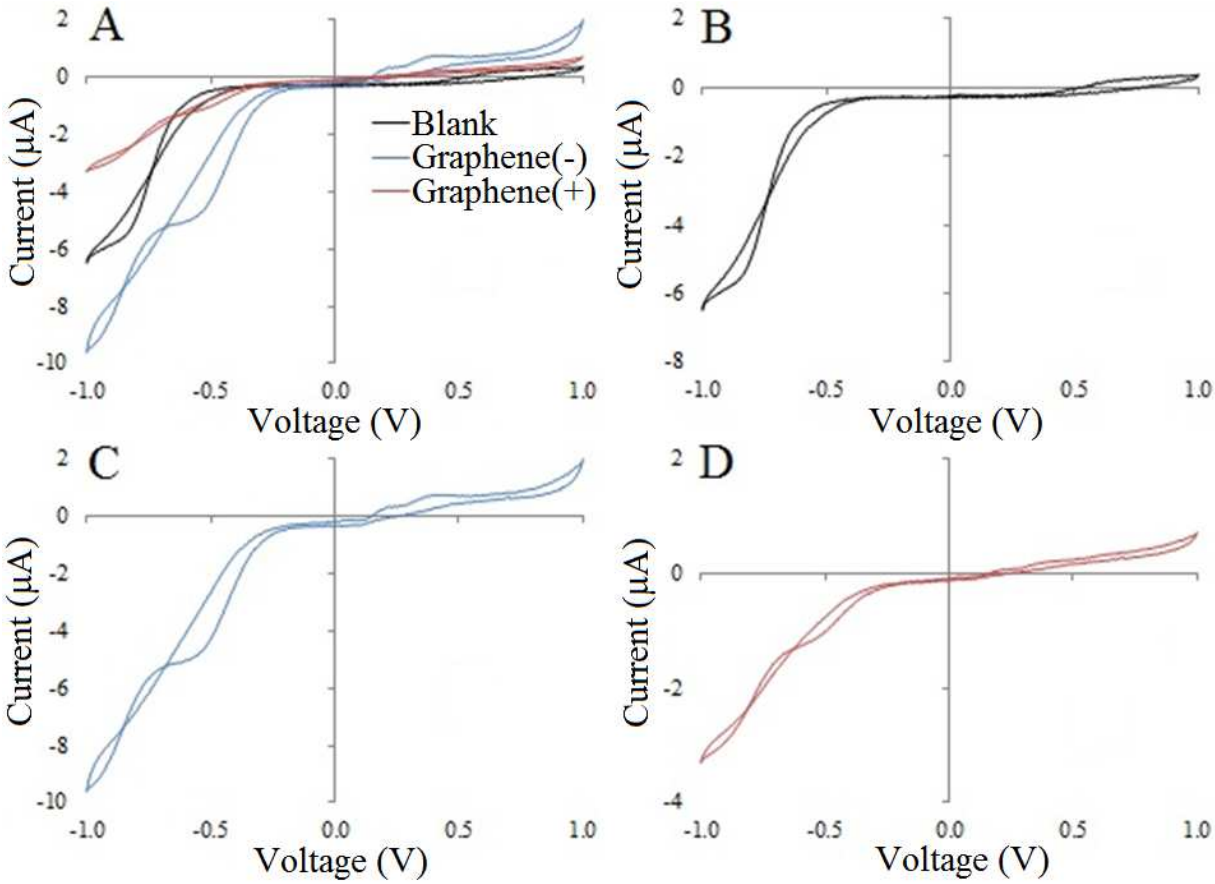

Figure 3.7 *– Cyclic voltammograms for a mixture of dopamine (45 µM), ascorbic acid (75 µM) and uric acid (60 µM) on an unmodified screen printed carbon electrode (B) and screen printed carbon electrodes coated with graphene(-)SDS (C) and graphene(+)CTAB.*

3.4.4 Detection of Aqueous Metal Ions

Other workers in our group have demonstrated an improved activity of graphene modified electrodes in heavy metal detection, specifically lead (from lead acetate), copper (from copper(II) chloride), and mercury (from mercury chloride). Examples of their results are included for comparison (Langford, 2013; Walch *et al*., 2015).

Electrodes were modified with either a positively or negatively charged graphene-surfactant complex (graphene(+)CTAB or graphene(-)SDS respectively) before being used to detect metal ions at a concentration of 1 ppm in water. The results are given in Figure 3.8.

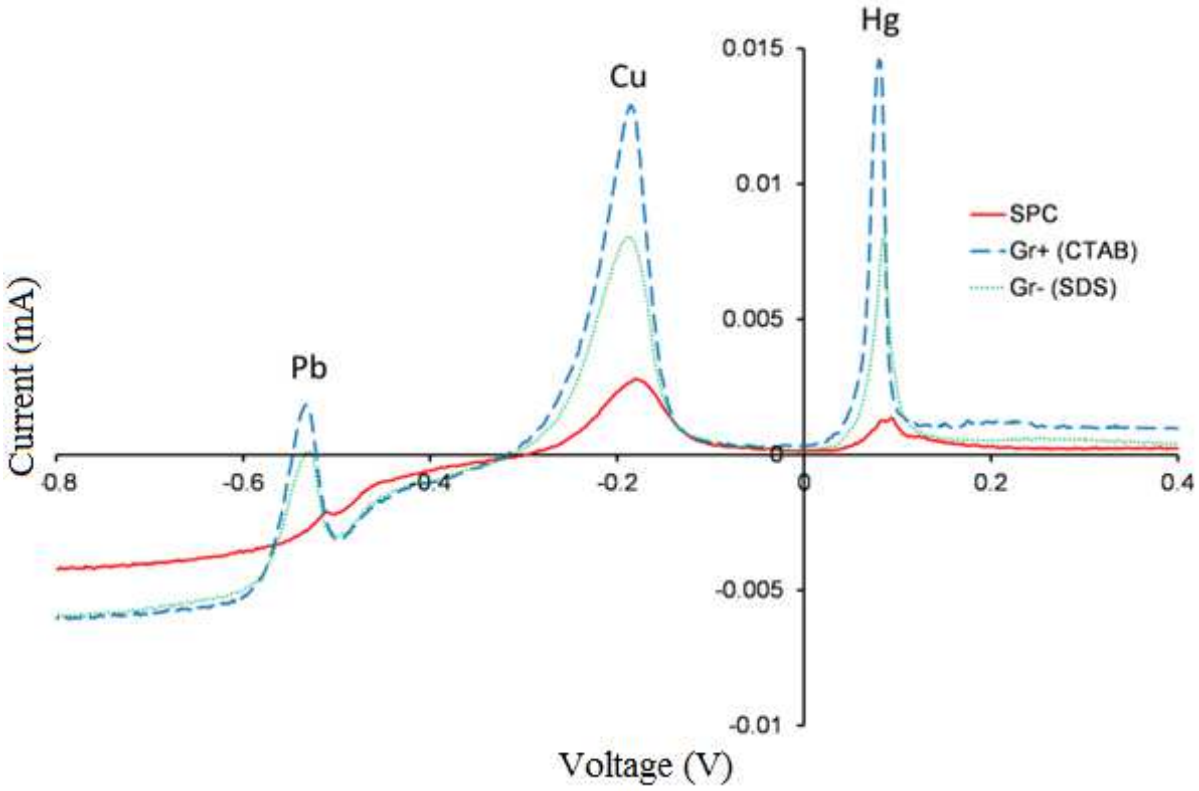

Figure 3.8 *– Absorptive stripping voltammogram of lead, copper, and mercury ions in water detected on a screen printed carbon electrode (SPCE), an SPCE coated with graphene(+)CTAB, and an SPCE coated with graphene(-)SDS* (Langford, 2013; Walch *et al*., 2015).

It is clear from the data that both the graphene(+)CTAB and the graphene(-)SDS offer significant advantages over screen printed carbon alone. However in this case the positively charged graphene shows the most increase in peak current. Peak voltage is similar (but not

wholly identical) for the two different graphene strains, however peak voltage caries significantly between coated and uncoated electrodes. This suggests a decreased resistance to electron transfer at the electrode surface. In the case of lead ions the screen printed carbon electrodes do not offer significant peak current to allow for detection. Therefore graphene modified electrodes could be utilised for detection of lead ions in aqueous solution.

3.4.5 Electrochemistry of Conducting Polymer Films

The graphene modified electrodes were compared with those modified with conducting polymers to determine if they offer an improvement over currently available technology. Figure 3.9 shows the successive polymerisation of poly(3,4-ethylenedioxythiophene) (a), polyaniline (b), and polypyrrole (c) for 20 cycles of cyclic voltammetry.

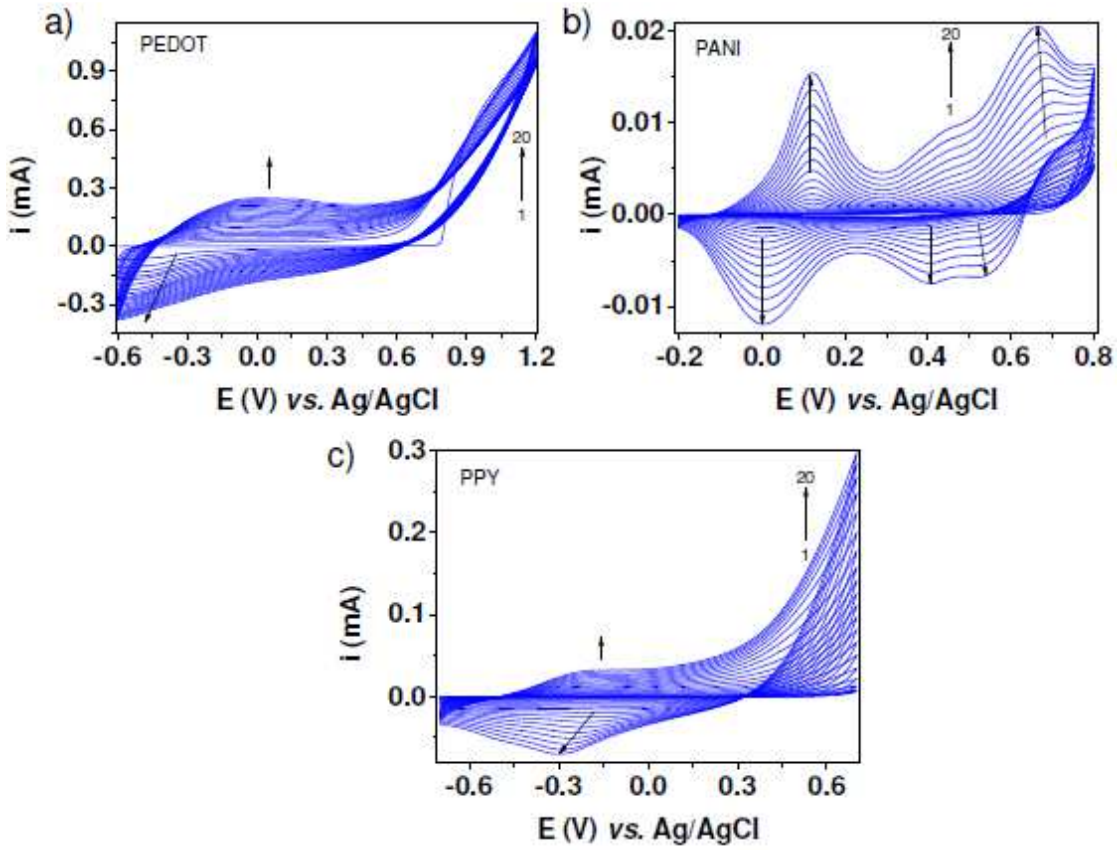

Figure 3.9 *– Electropolymerisation of a) PEDOT between -0.6 – 1.2 V, b) PANI between -0.2 – 0.8 V, and c) PPy between -0.7 – 0.7 V. Monomer concentration was 0.01 M and NaPSS (0.1 M) was used as a dopant. 20 Cycles were performed at a scan rate of 50 mV* s^{-1}.

In all cases the peak current increases with each successive deposition cycle. This is because the electrode surface is becoming more and more conductive as the conducting polymer layer gets thicker. All three voltammograms show both an oxidation and reduction peak. Deposition occurs in all cases on the oxidation peak, with the reduction peak showing reduction of the film. In the cases of PEDOT and PPy the peak voltage of the reduction peak is shifting towards the left with successive deposition cycles. This suggests that as the film thickness grows it becomes increasingly more difficult to reduce. These voltammograms also show a wide oxidation peak for PEDOT and PPy, which suggests that the deposition reactions for these polymers occurred at a slower rate compared with that of PANI, which shows a sharp peak in both the oxidation and reduction directions. The maximum current achieved for PANI is approximately ten times less than that of PEDOT and PPy, showing that the PANI film deposition was not as successful. This could be due to the fact that the pH chosen for deposition was pH 7.4 (using PBS as a buffer). PANI films are best deposited using a more acidic pH of around 2 – 3. Out of the three polymers that were analysed the highest peak current observed was that of PEDOT which is consistent with the results of the electrochemical impedance spectroscopy shown in Figure 3.10.

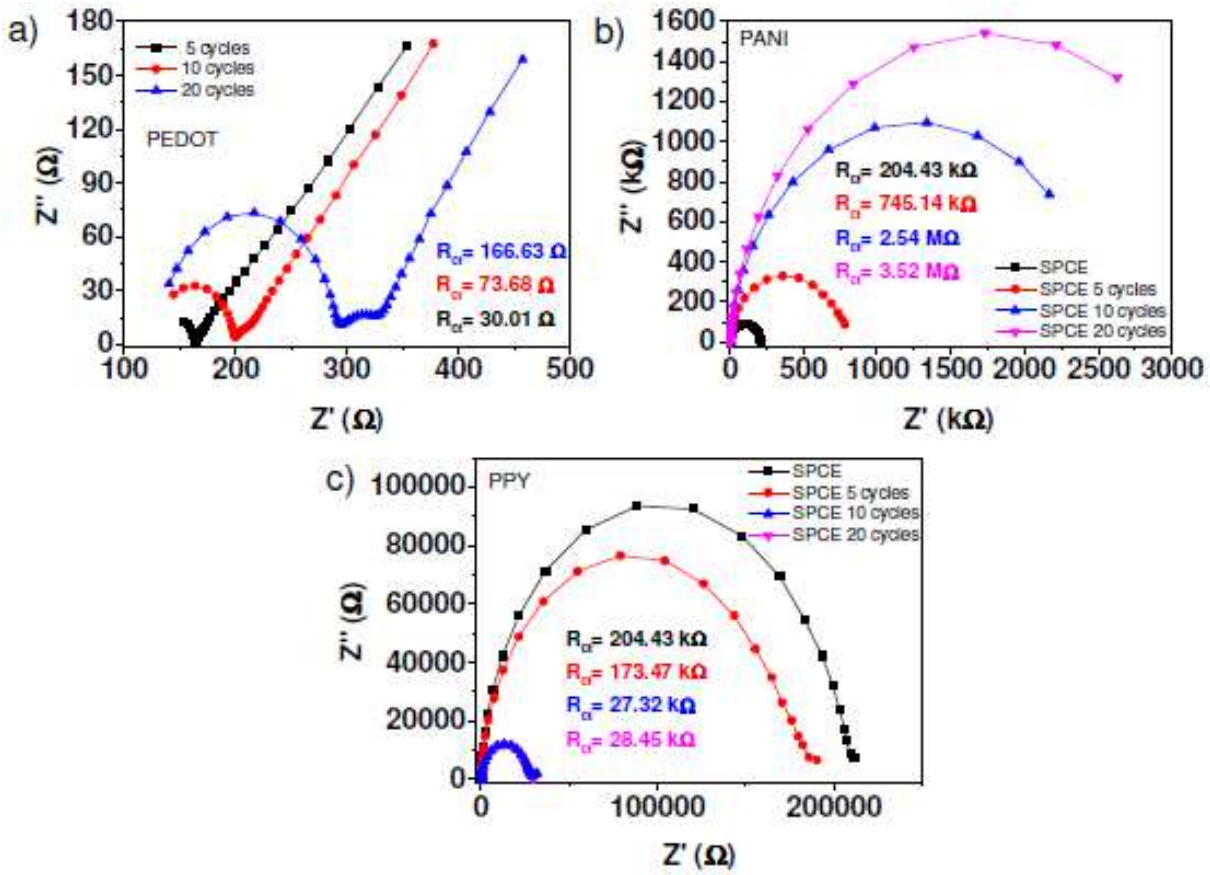

Figure 3.10 *– Electrochemical impedance spectroscopy in 5 mol L^{-1} ferro/ferricyanide under open circuit potential from 100 mHz – 100 kHz at 10 mV.*

With the electrodes modified with PEDOT and PPy films it is clear that resistance to electron transfer at the electrode surface is decreases with insulating layer thickness. This means that polymer film provides a better electrocatalytic surface than bare screen printed carbon alone, at least with respect to the ferri/ferrocyanide analyte used in the experiment. The PANI film shows an increase in resistance with successive deposition cycles, suggesting that the film deposited under the given conditions does not provide a good electrocatalytic surface towards the ferri/ferrocyanide analytes.

A comparison of the effects of increasing film thickness for all three conducting polymers is given in Figure 3.11.

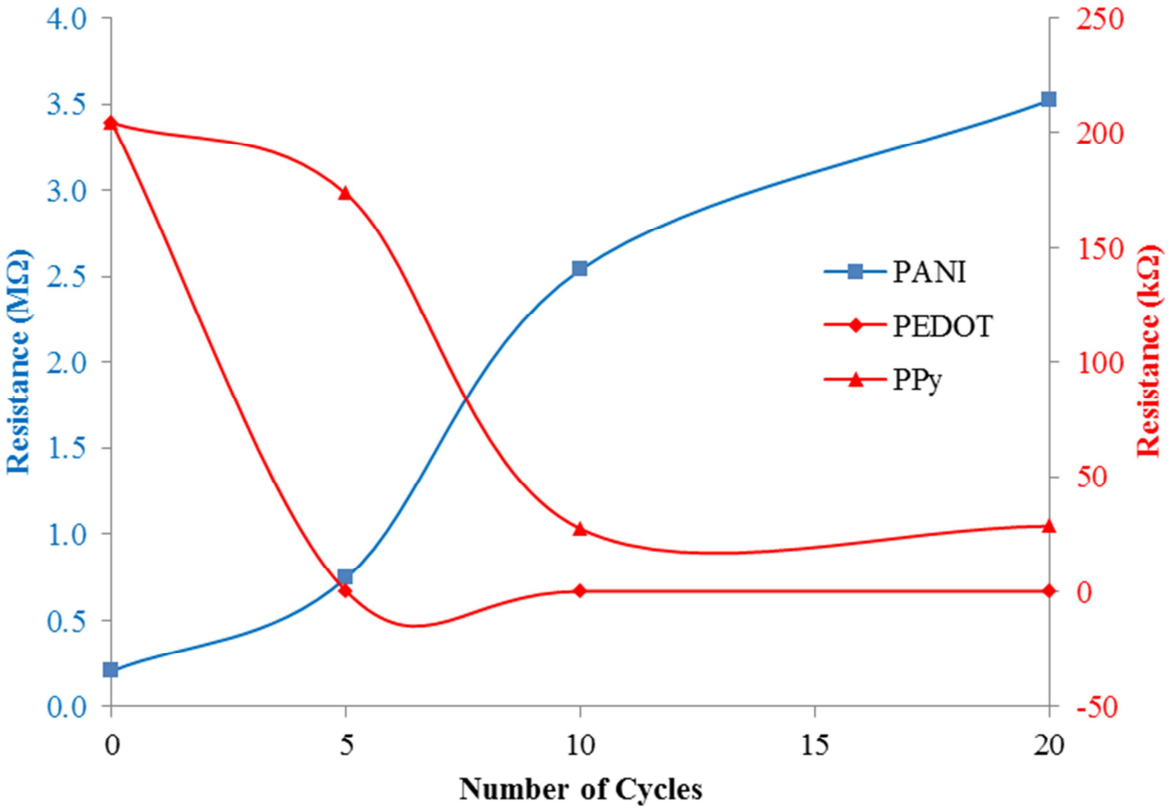

Figure 3.11 *– Comparison of the change in resistance to electron transfer with increasing film thickness for three different polymers; PANI (blue axis), PEDOT, and PPy (red axis). The film thickness was controlled by changing the number of cycles of cyclic voltammetry.*

The comparison in Figure 3.11 shows that there is a large decrease in resistance between 0 - 5 cycles in the PEDOT and 5 - 10 cycles in the PPy. After the sigmoidal part of the curve there is little decrease in the resistance of the electrode surface, with the lowest resistance achieved being 0.03 kΩ for PEDOT (20 cycles) and 27.32 kΩ for PPy (15 cycles). The curve for PANI shows a sharp increase in resistance between 5 – 10 cycles, but then resistance continues to rise between 10 – 20 cycles at a similar rate as between 0 – 5 cycles. The final resistance (after 20 cycles) for PANI was 3.52 MΩ, approximately 10 times greater than the unmodified electrode alone.

The polymer film with the lowest resistance to electron transfer (PEDOT, 20 cycles) is likely to perform the best out of all of the electrodes tested, since the electrocatalytic effect is highest. This means that the activation energy of any redox couple is reduced in the same

way as if a traditional catalyst was used. Unlike traditional catalysts, however, the electrocatalytic effect of an electrode surface is dependent on the redox couple in question.

3.5 Conclusions

In conclusion, the graphene modification of the electrodes showed a marked improvement, compared with screen printed carbon alone, in the resolution of peaks representing different components in a mixture allowing for simultaneous detection of these components without an initial separation step. Additionally an increase in peak current was observed, allowing for a lower limit of detection compared to an unmodified screen printed electrode.

The data obtained from both the electrochemical impedance spectroscopy and also the cyclic voltammetry showed that the graphene(-)SDS proved to be a better surface coating than graphene(+)CTAB. This observation is based on the gradient of the Nyquist plot after the circular portion as well as the minimum resistance to electron transfer obtained with this sample. Additionally, the greater resolving power of the graphene(-)SDS compared with graphene(+)CTAB for mixtures of compounds by electrochemical methods.

The comparison of graphene coating with conducting polymer films shows that graphene alone does not show a greater enhancement of the electrocatalytic effect of the electrode surface than conducting polymers. The lowest resistance to electron transfer observed for graphene was 1.3 kΩ, compared with 0.03 kΩ resistance observed for PEDOT. However the casting method for modifying a screen printed electrode with graphene is easier to perform than the electropolymerisation method for depositing a conducting polymer film. Additionally, surfactant stabilised graphene provides more scope for surface modification with binding ligands to provide greater specificity towards an analyte.

Chapter 4 Modelling and Synthesis of Resorcinarenes for Guest-Host Interactions

4.1 Introduction

Calixarenes are group of cyclic polyphenols which were first isolated by Zinke and Ziegler (1941). Calixarenes are of interest to the scientific community largely due to their ability to form guest-host interactions with other molecules. They contain a *para* substituent (with respect to the phenol hydroxyl group) which can influence these guest-host interactions. Each phenol residue also contains a hydroxyl which can be involved in hydrogen bonding, and a benzene ring which can be involved in π-bonding. These interactions are explained further in Section 1.1.1.8. These aspects of calixarenes make them a good choice for potential synthetic receptors. Theoretically there are thousands of different calixarenes that can be synthesised. Since there are a number of different parameters that can be varied, including; the *para* substituent on each phenol residue (including heterosubstituted calixarenes), the total number of phenol residues (typically 4 – 8), the bridging group between each phenol residue (which can be carbon, nitrogen or sulfur based) and any additional functionalisation applied to the hydroxyl groups. Since it is not feasible to screen each and every one of these possible combinations against a target *in-vitro*, an *in-silico* screening method is required. This will provide a way to assess binding and identify calixarenes with the highest binding affinity to be tested by other methods and used in research. The problem with such a method is that, since this is not what most commercially available molecular modelling packages are designed to do, the theoretical binding energies might not necessarily match those observed in practice. However there are a number of examples in the literature which use molecular modelling to predict the behaviour of calixarenes (Ghoufi *et al.*, 2005; Kane *et al.*, 2000; & Korchowiec *et al.*, 2010).

Resorcinarenes are a class of cyclic compounds composed of four or more resorcinol residues. They are produced by linking resorcinol molecules together by reaction with an aldehyde, and eventual cyclisation. Resorcinarenes, like calixarenes (their phenol containing

counterparts) have been of great interest to the scientific community since their discovery along with calixarenes in the late 19th century (Baeyer, 1872). This is largely due to the 3 dimensional structure that they adopt, which takes the form of a basket. This basket contains a space (called the cavitand) which has the ability to bind other molecules in guest-host interactions (Section1.5.2). These interactions have led to the use of calixarenes and resorcinarenes for a number of different purposes; including molecular recognition, HPLC stationary phases and even as enzyme mimics (Section 1.5.5).

The key components of a resorcinarene are; four benzene rings each with two hydroxyl groups in the *meta* position to each other and a bridging carbon between each ring. The variability between different resorcinarene compounds is brought about by derivatization at different points on the molecule. Firstly, the aldehyde used to create the bridging carbon linkage can greatly alter the resulting molecule as it can have almost any chain length as well as branching and functionality at the end of the chain. Secondly, the carbon atom between the two hydroxyls on the benzene ring is very reactive and can easily be functionalised. Finally, the hydroxyls themselves can be reacted to form an ether, ester or other functional group. These different functionalization methods of the basic resorcinarene structure alter the molecule in different ways. A longer aldehyde chain will make the resultant molecule more hydrophobic, functionalization of the middle carbon can have numerous effects on guest-host interaction and conformation and derivatization of the hydroxyls will remove the hydrogen bonding around the *exo* ring of the molecule, thus altering the final conformation. Information about the conformations of calixarenes and resorcinarenes can be found in Section 1.5.3.

Molecular modelling, also known as *in-silico* modelling, is a useful tool in various areas of modern science. It uses mathematical algorithms to simulate binding interactions between two molecules and asses the strength of binding. Molecular modelling allows preliminary

research to be done on a compound or protein of interest to save time during laboratory based studies. The use of molecular modelling for the discovery and high throughput screening of small organic molecules against protein receptor targets is well established in the literature as a tool of drug discovery (Siepmann & Siepmann, 2008; Clark, 2003; & Lengauer *et al.*, 2004). This technique essentially involves designing a small molecule to fit into a receptor of known structure and conformation. There are also examples in literature of the inverse procedure, where a synthetic receptor was designed around a ligand or target compound (Chianella *et al.*, 2006; & Nicholls *et al.*, 2009). Previous to the use of this software a "trial and error" approach would be used for this process.

If the data obtained from *in-silico* modelling is to be relied upon it must first be validated by another method to highlight any discrepancies between the mathematical model and reality. There are a number of different methods that can be used to determine the binding energy of a guest-host complex. In this study NMR spectroscopy (described in Section 1.9) will be used to validate the data from the *in-silico* model. The data obtained from these techniques will validate two different aspects of the model; firstly the DSC will show the actual binding energy between the guest and the host, which can then be compared to the theoretical values and secondly, the NMR titration will not only give an idea of the binding energy but will also show the orientation of the guest whilst bound to the host.

In this chapter novel resorcinarene molecules will be modelled *in-silico*, synthesised, and evaluated to verify predicted binding energy. Monolayer stability will also be assessed using Langmuir-Blodgett techniques to determine suitability for use in guest-host interactions on the surface of graphene. The method selected for synthesis is a procedure described by Mel'nikova *et al*. (2009). The parent resorcinarene was then further derivativatised using the Mannich reaction described by Matsushita & Matsui (1993).

4.2 Materials

Ethanol, toluene, methanol, cyclohexane chloroform, and sodium chloride were obtained from Fisher Scientific (Loughborough, UK). Phosphate buffered saline (PBS), p-sulfocalix[4]arene (SCX4), resorcinol, dodecanal and p-toluenesulfonic acid were all obtained from Sigma Aldrich (Poole, UK). Nitrogen gas was obtained from BOC gases (Manchester, UK). Molecular modelling was performed using ArgusLab, Planaria Software, USA.

Ultra-pure (18 MΩ cm^{-1}) water was produced using a Milli-Q water purification system obtained from Millipore (Tokyo, Japan). Freeze drying was performed using a ScanVac CoolSafe freeze dryer from Labogene (Lynge, Denmark). Langmuir-Blodgett films were prepared using a NIMA Langmuir-Blodgett trough at Sheffield Hallam University (NIMA Technology, Coventry, England). Nuclear magnetic resonance spectroscopy was performed on an Ascend 400 NMR spectrometer running TopSpin analysis software (Bruker, Billerica, Massachusetts, USA).

4.3 Methods

The various methods used in this chapter will be described here. NMR IR and Mass Spec analyses were performed at Sheffield Hallam University on samples prepared in the biomedical research centre.

4.3.1 Molecular Modelling

Molecular models of four novel resorcinarene molecules were prepared using ArgusLab (Planaria Software). The virtual resorcinarene molecules were minimised to the lowest energy conformation by first using the molecular mechanics (MM) universal force field (UFF) algorithm (1000 iterations, convergence at 0.1 kcal mol^{-1} $Å^{-1}$) to “clean up” the molecular geometry. A more accurate minimisation was then obtained using the quantum

mechanics (QM) parameterised model number 3 (PM3) algorithm (1000 iterations, convergence at 0.1 kcal mol^{-1} $Å^{-1}$). The optimised structure was then set as a binding site and the file was saved. Ligand structures were prepared in the same way as above, except that the MM/UFF algorithm only required 100 iterations. The ligand structures were then defined as ligands and the files were saved.

A Monte Carlo based simulated anneal was performed to assess the binding strength of each guest host complex. A Monte Carlo method involves the software forming a complex between the guest and the host entities multiple times in a simulated anneal and measuring the binding energy involved. The specific algorithm used in the simulated anneal was the genetic algorithm docking engine (GADock) within the ArgusLab software. GADock is named as such because it mimics natural evolution, with changes in orientation and bond rotation giving different binding energies. Changes are not random, however, and a new conformation will only be adopted if it is more energetically favourable than the previous one. In each simulation the grid resolution was set to 0.1 Å and the ligand was set to flexible. The advanced settings were as follows: Population size (50), maximum generations (5000), elitism (5), mutation rate (0.2), crossover rate (0.8) and convergence (0.1 kcal mol^{-1}).

Each guest host complex simulated was performed 100 times and a binding energy was given by the software. This was achieved by creating a ligand database using the MolConvert function of Marvin Beans (ChemAxon software). MolConvert is a command prompt based tool that allows for creation of a structural data file (SDF) from molecules in the .mol format. Each ligand was placed into the database 100 times, giving a total of 100 simulated anneals for each guest/host pair.

4.3.2 Solid-Phase Synthesis of Parent Resorcinarenes

The parent resorcinarenes were synthesised by condensation reaction between resorcinol and an aldehyde (benzaldehyde or dodecanal) using an acid catalyst by a solid phase method (Roberts *et al*., 2001). This was achieved by combining resorcinol and the aldehyde in equal molar amounts (50 mmol) and a catalytic amount (equal to 5 % of the other reactants) of *p*-toluenesulfonic acid (2.5 mmol). The reactants were placed into a mortar and ground with a pestle for 2 – 3 minutes until the product became too hard to grind. The product was then left at room temperature for 1 hour to fully react and harden. Nitrogen was use to keep the product away from oxygen in an effort to minimise oxidation of the product.

Once hardened, the product was dissolved in cyclohexane (20 ml) to assist in removal from the mortar. Next, as much cyclohexane as possible was removed by evaporation under nitrogen and the resultant oily product was then re-dissolved in methanol (20 ml). This was then poured into a saturated saline solution in water (500 ml), causing a slightly pink solid to precipitate out and rise to the surface. Addition of more NaCl to the water caused further precipitation of the solid. The precipitate was collected and frozen before being placed into a freeze dryer overnight. The result was a dry slightly pink powdered solid which was used in further work.

4.3.3 Liquid-Phase Synthesis of Parent Resorcinarenes

The parent resorcinarenes were also synthesised by condensation reaction between resorcinol and an aldehyde (benzaldehyde or dodecanal) using an acid catalyst in ethanol (Aoyama *et al*., 1989). This was achieved by combining resorcinol and the aldehyde (230 mmol) and concentrated hydrochloric acid (37 ml) at 0^{o}C. The round bottomed flask was then purged with nitrogen to remove all oxygen from the reaction chamber. A constant atmosphere of nitrogen was maintained throughout the synthesis. The reaction mixture was then refluxed overnight.

The reaction mixture was cooled, and then filtered. Any remaining product that remained in the supernatant was then precipitated by addition of water. The grey solid product was then washed thoroughly with hot water, then with methanol. The purified product obtained an off-white powder. This was dried thoroughly under vacuum. The vacuum was required because efforts to dry the powder through heating alone caused discolouration of the product.

4.3.4 Amination via the Mannich Reaction

The Mannich reaction was used to functionalise the new resorcinarene by aminomethylation of the carbon in the *ortho* position to both hydroxyl groups on each benzene ring in the molecule. The parent resorcinarene tetramer (0.1 mmol) was dissolved in a mixture of ethanol : toluene (1:1, 20 ml) and diethylamine (0.5 mmol) was added along with paraformaldehyde (0.5 mmol). The mixture was then placed into a sealed glass bottle (50 ml) and left at room temperature for 72 hours. The dark red glassy solid was then recovered from solution by evaporation of the solvent.

4.3.5 Sulfonation via the Mannich Reaction

The sulfonate groups were added in a similar fashion. The parent resorcinarene (0.1 mmol) was dissolved in a mixture of ethanol : water (1:1, 20 ml) and sodium sulfate (0.5 mmol) was added along with formaldehyde (0.5 mmol). The mixture was placed into a covered glass bottle (50 ml) and placed into a heated water bath. The sulfonation reaction was carried out under reflux for 12 hours. After the reaction had completed the reaction mixture was acidified with HCl causing a colour change from dark red to dark yellow. The product was then precipitated by addition of acetone. Further purification was then performed by dissolving the product in water and then precipitating out in a greater volume of methanol. The resulting precipitate was then dried completely under vacuum before further analysis. For this product discolouration did not occur when dried at room pressure, however it was noticed during

analysis that solvent remained in the sample even after several days of incubation at 70^{o}C, likely due to the complex forming nature of these types of compounds.

4.3.6 Analysis of Novel Resorcinarenes

Once the resorcinarene molecules had been synthesised and the weights had been recorded they were characterised using NMR spectroscopy, Langmuir-Blodgett techniques and tensiometry to determine structure and surface activity.

4.3.6.1 Solubility and Surface Activity

The compounds were dissolved in deionised water at 70^{o}C to their maximum solubility. The resulting solutions were then cooled to room temperature and filtered to remove any undissolved particulates. The solutions were then placed individually into a glass dish and the surface was cleaned using an aspirator to remove any dust or other surface contaminants. The surface tension was then measured using a Du Noüy ring based tensiometer platform.

A 1 ml sample of each solution was then placed into a pre-weighed Eppendorf tube, frozen using liquid nitrogen and placed into a freeze drier overnight. The freeze dried sample was then dried under vacuum to remove any further traces of water that might have remained after freeze drying. The Eppendorf was then weighed again to determine the mass of resorcinarene within the 1 ml sample.

4.3.6.2 NMR Spectroscopy

Nuclear Magnetic Resonance (^{1}H, ^{13}C, ^{13}C-DEPT, and HSQC) spectra were obtained using a Bruker Ascend 400 NMR spectrometer running TopSpin analysis software.

The derivatised and parent resorcinarene samples (5 mg) were dissolved in D_2O or deuterated methanol, acetonitrile or chloroform (dependant on their solubility) in 7.0 ml glass vials. The

solutions were then filtered into 5 mm NMR sample tubes to remove any undissolved particulates.

The NMR spectrometer was then set up to scan for ^{1}H nuclei with 32 scans per sample. A higher than normal number of scans was chosen for a variety of reasons. Foremost that the high molecular weight of the sample would likely cause peak broadening, and also a number of alternative conformations might exist, giving rise to smaller peaks within the spectrum which might not be as visible with a lower number of scans due to background noise. Water suppression was utilised, as some water might have remained in the sample, as well as the possibility of contamination in the D_2O.

4.3.6.3 Complex visualisation by NMR

Nuclear Magnetic Resonance (1H, 13C, 13C-DEPT, HSQC) spectra were obtained using a Bruker Ascend 400 NMR spectrometer running TopSpin analysis software.

Complexes were prepared by combining the host resorcinarene (o-sulfonato calix[4]resorcinarene) with 6 different host molecules (adenine, uracil, phenylalanine, tyrosine, ascorbic acid, and dopamine). All complexes were prepared with a 10 times excess of host molecule to give a greater chance of total complexation. The samples were then dissolved in D_2O and analysed. The autosampler was used for these samples as the peak positioning is more accurate than manual operation.

When all samples had been analysed the spectra were compared with those obtained from the guest and host molecules alone, without complexation. The shift in peak position was recorded and used to show binding between guest and host.

4.3.6.4 Infra-Red Spectroscopy

Infra-red spectroscopy was performed using a Bruker Alpha FT-IR spectrometer with an attenuated total reflection (ATR) platform. The resorcinarene samples were first dried at 70^{o}C under vacuum for 72 hours to remove all traces of water and any other solvents that might have remained from the synthesis. A small sample of the dried powder was then placed onto the ATR platform so that the diamond crystal was covered. Pressure was then applied to the sample using the ATR platform top piece. Readings were then taken between 450 - 5000 cm^{-1} to measure the transmittance of the sample at different frequencies.

4.3.6.5 Langmuir-Blodgett Isotherms

The Langmuir-Blodgett films were prepared using a Langmuir-Blodgett trough (NIMA). The trough was filled with water until the level of the water was just above the top of the trough. The resorcinarene samples were then dissolved in chloroform (1 mg ml^{-1}) and spread gently onto the surface of the water taking care not to penetrate the surface of the water. In total 100 μL of resorcinarene solution was spread onto the surface. Once the solvent had evaporated the barrier was moved across the surface of the water, compressing the monolayer. The surface pressure was measured along with the area of the monolayer. The barrier speed was such that the monolayer area decreased by 50 cm^2 per minute.

The surface pressure of the compressed monolayer was measured, and the pressure at which collapse of the monolayer occurred was noted. A lower pressure was then chosen for deposition by Langmuir-Blodgett and Langmuir-Schaefer onto either a glass microscope slide or a silicon wafer. For this deposition the monolayer was compressed using a continuous feedback mechanism so that the surface pressure was kept constant (40 mPa) throughout the procedure. Deposition was confirmed by a reduction in the surface area of the monolayer coinciding with the movement of the substrate.

4.4 Results and Discussion

The results from the novel resorcinarene synthesis are discussed here. These include the yield determination, spectroscopic analysis, Langmuir-Blodgett isotherm data, compound solubility and surface activity. The results from the resorcinarene modelling research will also be discussed here. These include the *in-silico* modelling of the guest-host interactions of four novel resorcinarene compounds with various analytes and the validation of the computer model by comparison of theoretical binding energies to actual binding energies obtained from differential scanning calorimetry.

4.4.1 Molecular Modelling

The modelling was performed as specified in Section 4.3.1 and the data was compared to find the best resorcinarene for binding the analytes. The sign on the binding energy has been inverted to make the data easier to interpret. The results are shown in Figure 4.1.

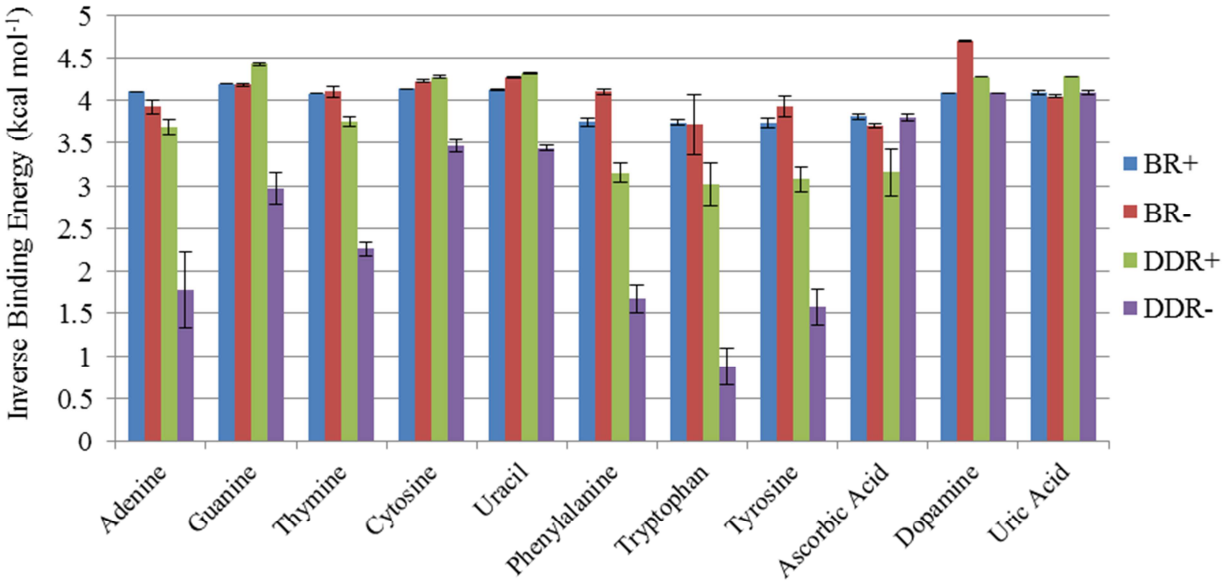

Figure 4.1 *– Computer simulated binding data for interactions of the nucleotide bases, amino acids and blood based biomarkers with some resorcinarene molecules; calix[4]benzylresorcinarene (BR) & calix[4]dodecylresorcinarene (DDR), with either a sulfonic acid (-) or a quaternary amine (+).*

The data shows that the calix[4]benzylresorcinarene derivatives both bind all of the analytes with a similar binding energy regardless of the R group in the *ortho* position on the benzene

rings. This is likely due to the fact that the benzene groups attached to the bridging carbon groups interact with each other by π-stacking causing a distortion of the cavitand. This results in a wider cavitand, with two of the benzene rings (1 & 3) at approximately 90^{o} to the other two (2 & 4). This means that the binding is less sterically hindered and stronger binding can occur. However this distortion of the cavitand results in a lower specificity (Figure 4.2).

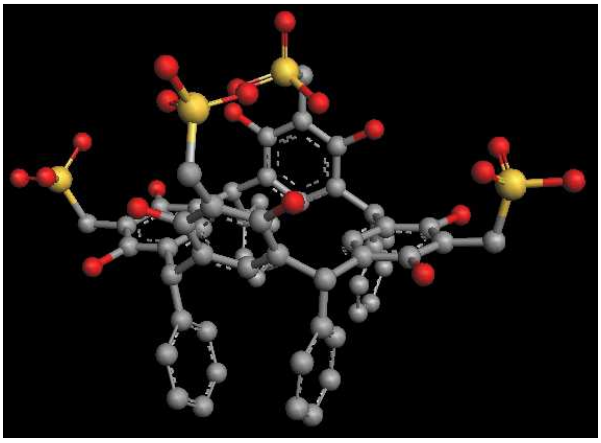

Figure 4.2 *– The 3D structure of o-sulfonato calix[4]benzylresorcinarene showing the distorted cavitand caused by the π-π interactions of the benzene groups.*

The calix[4]dodecylresorcinarene derivatives do not have such strong interaction between the R groups on the bridging carbon, with only Van-der-Waals forces and no π-interactions. This provides a better formed cavitand and allows for more specific interactions with the guest molecules. The quaternary amine derivative shows less specificity, but still a greater specificity than with its calix[4]benzylresorcinarene counterpart. The sulfonic acid derivative of the calix[4]dodecylresorcinarene shows the greatest specificity of all four resorcinarenes, however with the lowest binding energy.

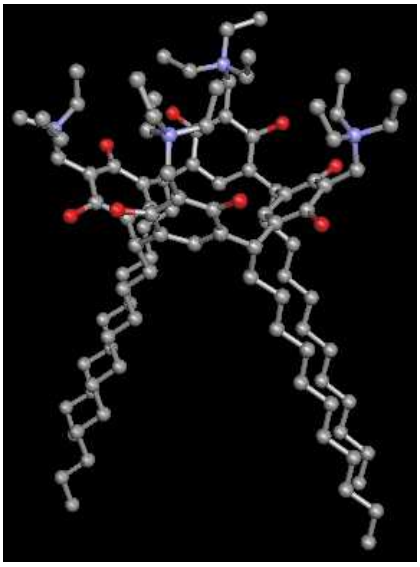

Figure 4.3 *- The 3D structure of o-triethylammoniummethyl calix[4]dodecylresorcinarene showing the deeper cavitand caused by the lack of π-π interactions.*

Both calix[4]dodecylresorcinarene derivatives show a similar pattern, with guanine, cytosine, and uracil binding more strongly to the host molecule than adenine and thymine. The sulfonic acid derivative shows some specificity between the amino acids, whereas the quaternary amine derivative bound all three molecules with approximately the same binding strength. The structures of the analytes that were modelled are given in Figure 4.4.

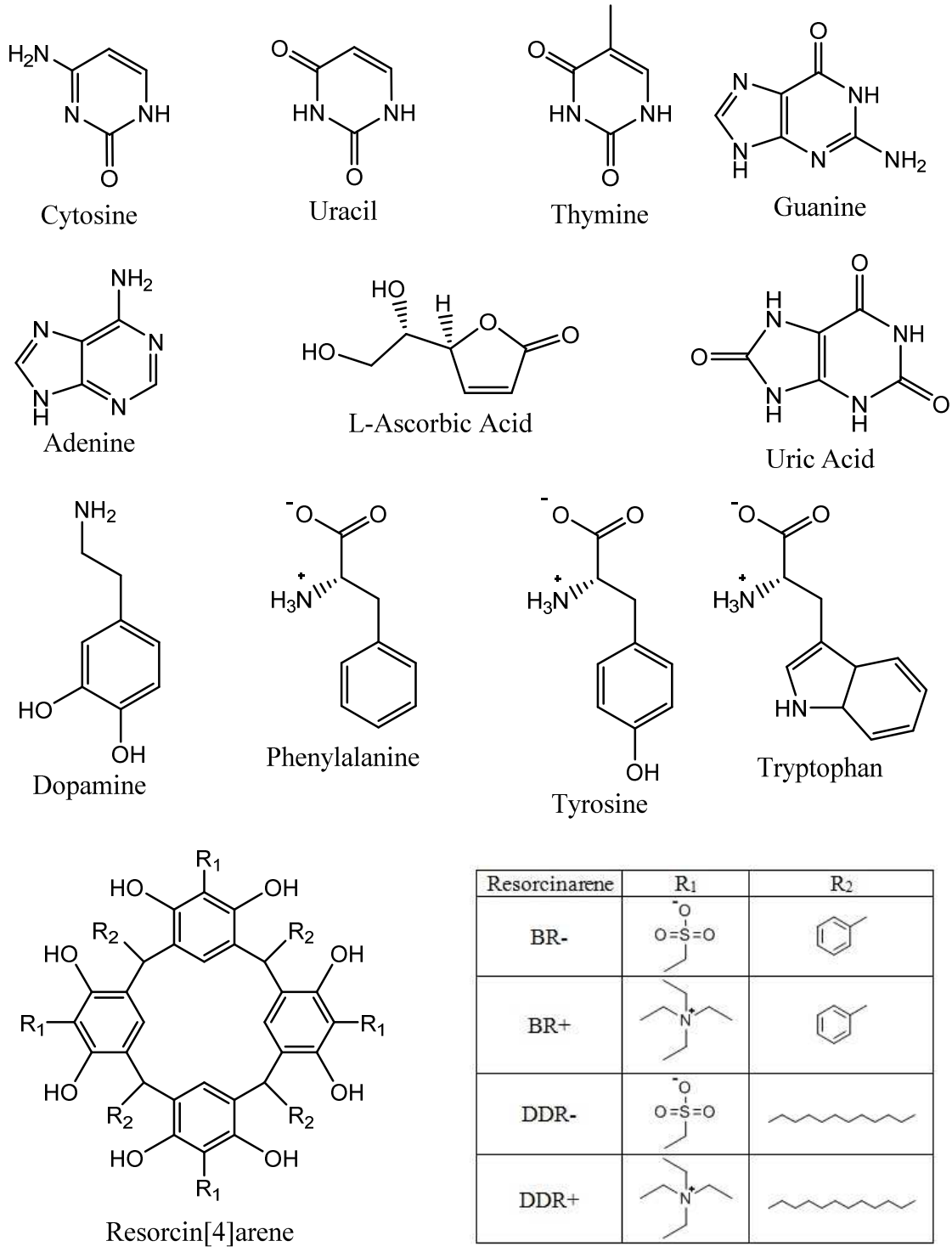

Resorcinarene	R_1	R_2
BR-		
BR+		
DDR-		
DDR+		

Figure 4.4 *– The guest molecules and the host resorcinarene derivatives used for the in-silico modelling experiments.*

The NMR and IR data given in Section 4.4.1 showed a different structure to what was intended and because of this, another molecular modelling experiment was performed using the new structure.

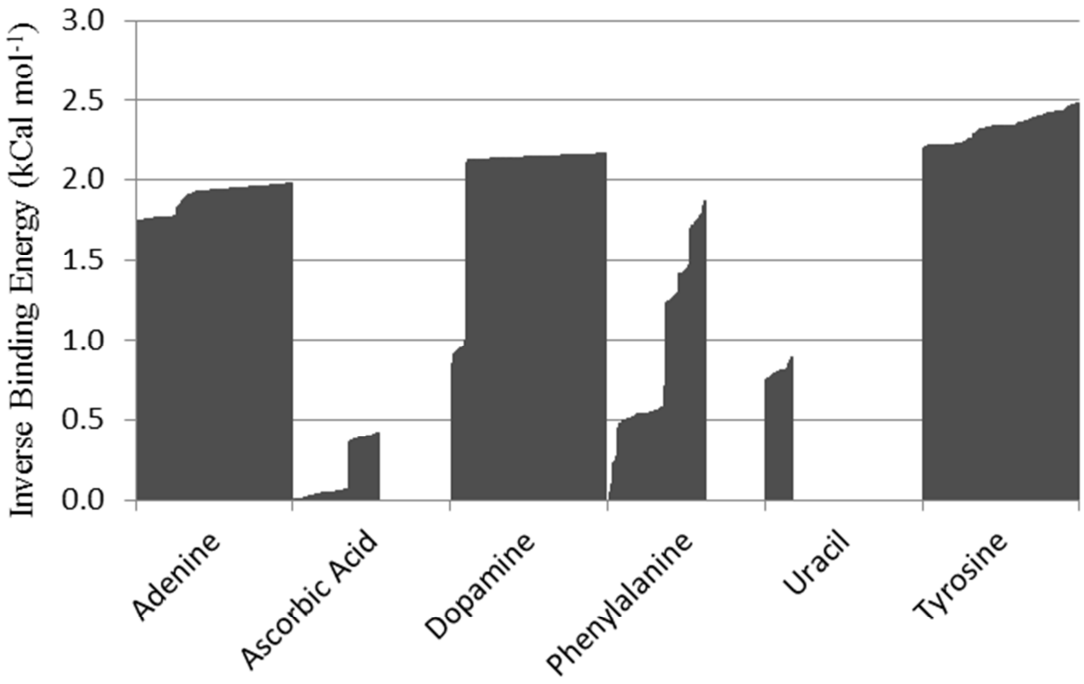

Figure 4.5 – *Binding energy from 100 simulated anneals for 6 different guest-host complexes showing successful complex formation. The gaps show analytes that did not form a guest-host complex in all 100 simulations.*

The data in Figure 4.5 shows the binding energy obtained from 100 simulated anneals on each of the six analytes. The binding energy was put in ascending order to show the range of energies given by the software. In some cases the software was unable to generate a binding energy, these data runs are emitted and show as gaps. This shows that some of the simulated guest-host complexes formed with higher binding energies than others and some complexes were not stable enough to form with each simulated anneal. The average complex energy and standard deviations are shown in Figure 4.6.

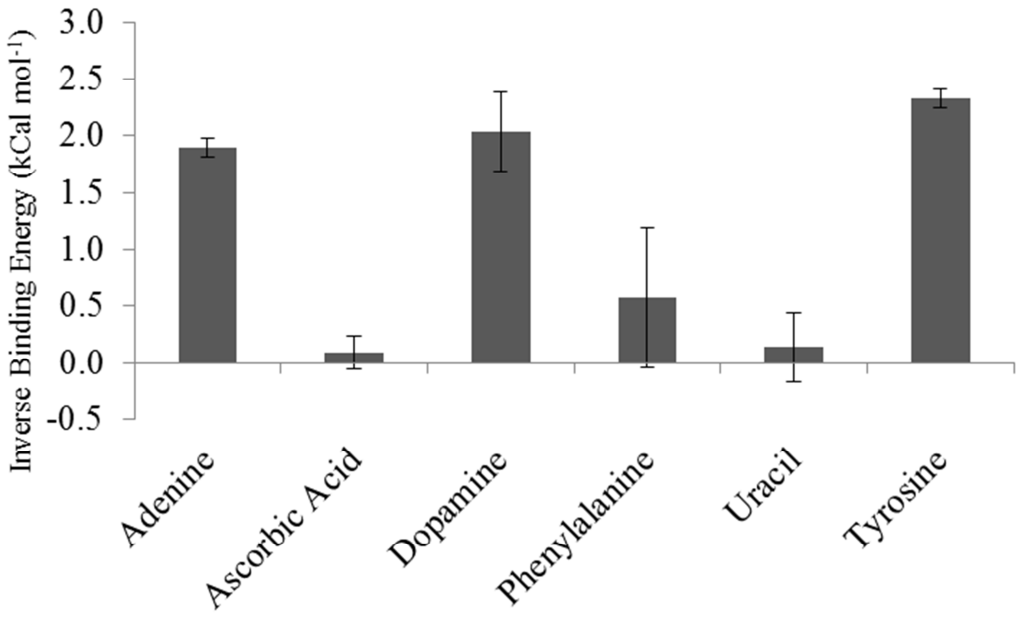

Figure 4.6 – *Average simulated binding energies and standard deviation for 6 guest-host complexes.*

It is clear from Figure 4.5 & Figure 4.6 that only adenine, dopamine, and tyrosine reliably form stable complexes. The comparatively lower binding energy for ascorbic acid, phenylalanine, and uracil coupled with the fact that the standard deviation for these complexes goes below zero suggest that these complexes (if formed at all) would not be sufficiently stable.

Assuming an equilibrium between the bound and unbound states; adenine, dopamine, and tyrosine would lie towards the bound state, and ascorbic acid, phenylalanine, and uracil towards the unbound state.

4.4.2 Validation of Computer Model

It was clear after synthesis of all four compounds was complete that not all of them offered sufficient solubility in water to be of any use in further work. Because of this, it was decided that only the o-sulfonato calix[4]benzylresorcinarene would be validated according to the *in-silico* data that was generated by the molecular modelling experiments. Since these novel resorcinarene molecules are designed to be adsorbed onto a graphene surface as selective

receptors, the specific binding constants for each guest-host interaction was not calculated empirically. Only a simple binding experiment to determine whether or not binding would occur was needed. Additionally the orientation of the guest molecule in the host molecule cavitand can be seen from the NMR data by looking at the displaced peaks for each binding interaction.

4.4.3 Spectroscopic Analysis

The results of the various spectroscopic techniques used to analyse the novel resorcinarene compound will be discussed.

4.4.3.1 Solubility and Surface Activity

The solubility of all but one of the compounds in water made them unsuitable to make graphene since they did not reach the required surface tension of 41 mJ m^{-2}. Only the o-sulfonato calix[4]benzylresorcinarene was soluble enough and surface active enough to lower the surface tension by the required amount. This is why only this compound was analysed further.

4.4.3.2 NMR Spectroscopy

NMR spectroscopy, including ^{13}C-NMR, ^{1}H-NMR, distortionless enhancement by polarisation transfer (DEPT) and heteronuclear single quantum coherence (HSQC) NMR, was performed on the sample using a Bruker Ascend 400 MHz spectrometer. To aid in interpretation, NMR predictions were created using Marvin Sketch (ChemAxon Software). Figure 4.7 shows the predicted carbon and proton NMR for the expected product o-sulfonato calix[4]benzylresorcinarene. This prediction differs considerably from the actual spectra acquired for this product (Figure 4.8). The main difference in the ^{1}H-NMR spectrum is the absence of the multiplet at around 7.25 ppm corresponding to the protons on the benzene ring of the resorcinol and benzaldehyde residues. In its place is a singlet, suggesting that only one

of these protons is present in the molecule. Additionally, the two singlets at around 4.50 ppm are showing as a single singlet, suggesting that these two protons have now become equivalent and therefore no longer split on each other. The carbon NMR gives more evidence that the product did not have the anticipated structure. There are only four peaks in the benzene region of the product spectrum, compared with eight in the predicted spectrum. This suggests that the benzene on the lower rim is not present in the molecule.

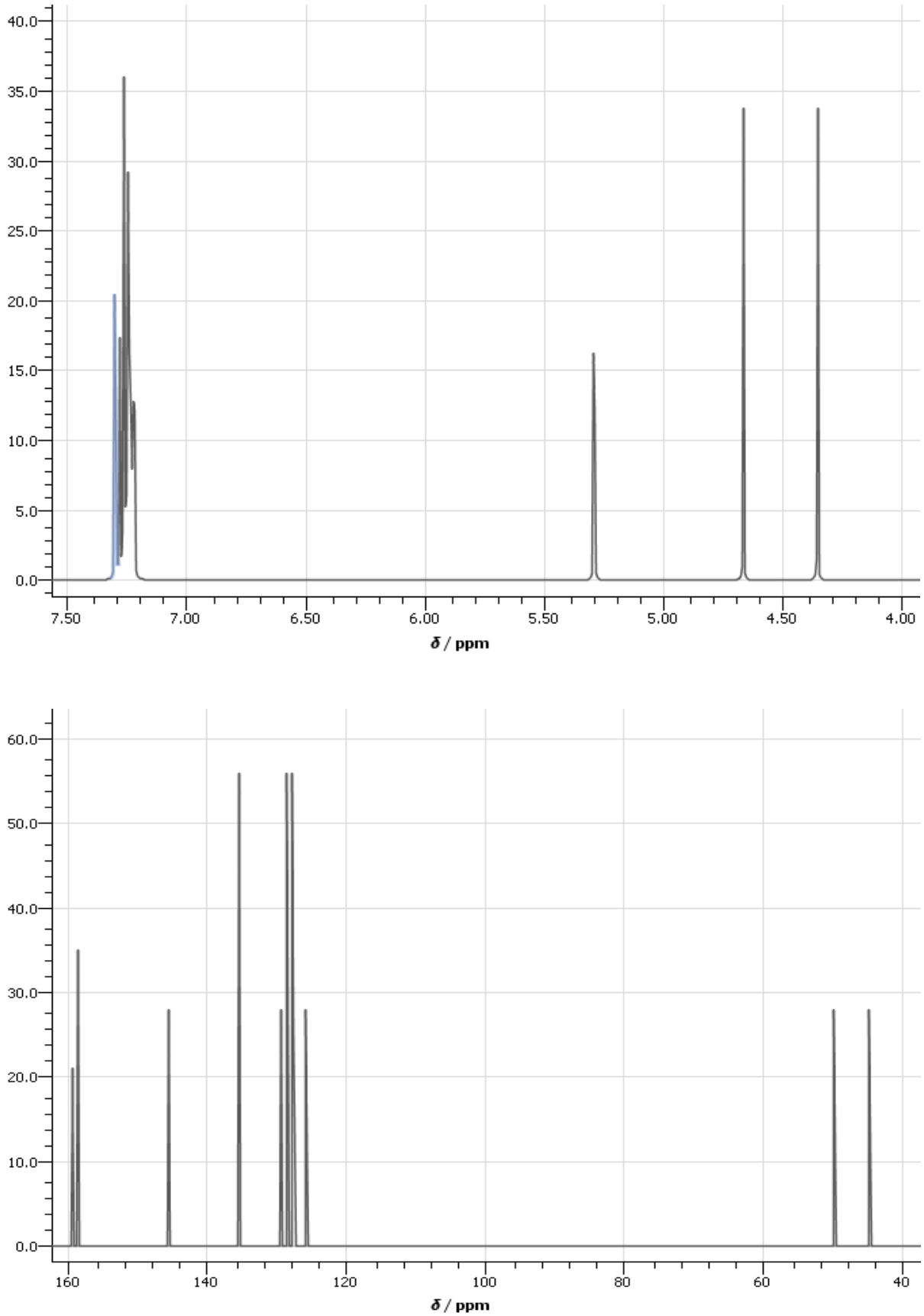

Figure 4.7 *– The predicted ^{1}H-NMR (top) and ^{13}C-NMR (bottom) for o-sulfonato calix[4]benzylresorcinarene. Predictions were made using Marvin Sketch (ChemAxon).*

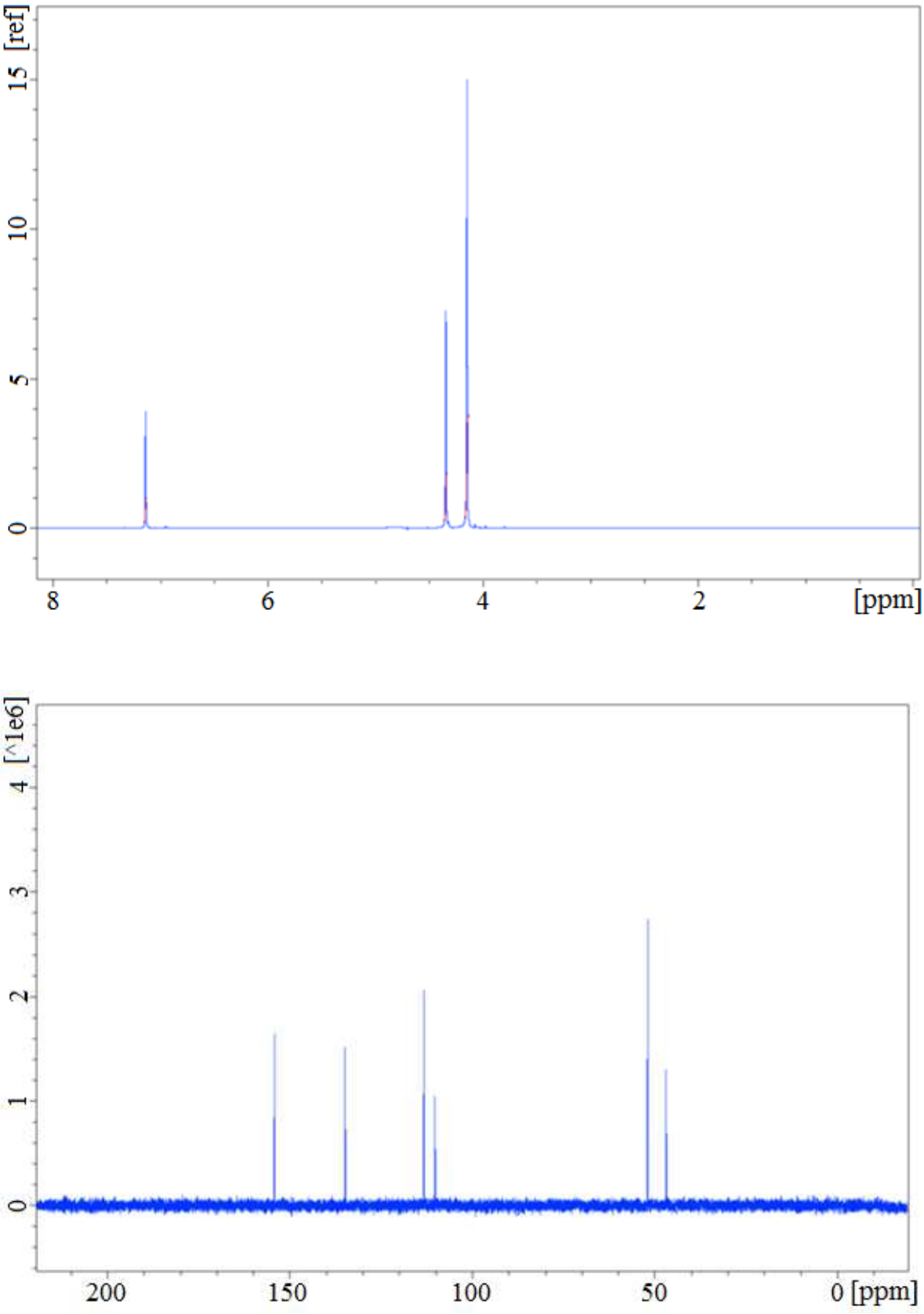

Figure 4.8 *– The proton (top) and carbon (bottom) NMR spectra of the obtained product.*

Further investigations (by DEPT NMR spectroscopy) were performed to confirm that the lower rim benzene was missing from the molecule. Figure 4.9 shows the DEPT45 spectrum of the product. In DEPT45 all carbon atoms within the molecule that have at least one proton on it is shown.

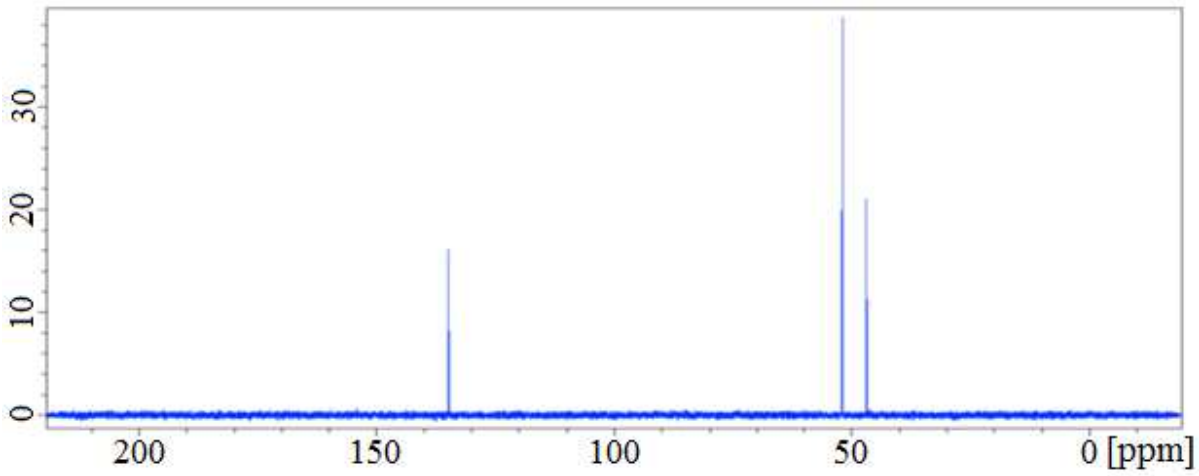

Figure 4.9 *– The DEPT45 spectrum of the resorcinarene showing all protonated carbons.*

This spectrum shows only a single protonated carbon in the benzene region. If the lower rim benzene was still attached to the molecule then there would be six carbons in this region. Figure 4.10 shows the DEPT135 spectrum of the product. In DEPT135 all CH and CH_3 groups are shown in the opposite phase to CH_2 groups.

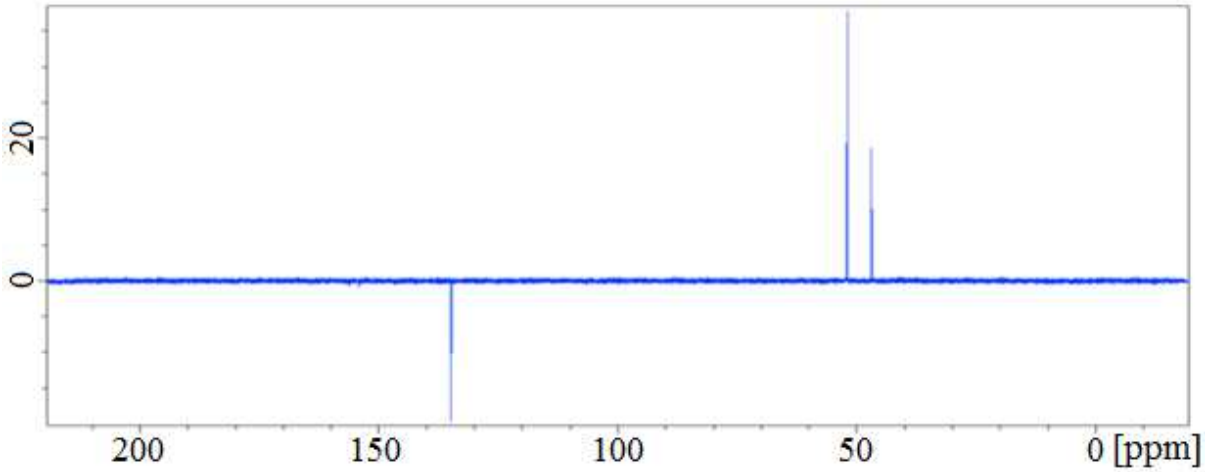

Figure 4.10 *– The DEPT135 spectrum of the resorcinarene showing CH and CH_2 groups in opposite phases.*

The two peaks at around 50 ppm are both above the line, meaning that they both represent CH_2 groups. This would not be the case if the lower rim benzene were present, there would be a CH_2 peak (representing the bridging carbon group connecting the sulfate group to the benzene ring) above the line, and a CH peak (representing the methyne group between the resorcinol residues) below the line. The HSQC spectrum for the product shows which peaks in the ^{1}H-NMR represent protons bonded to specific carbons in the ^{13}C-NMR. The HSQC spectrum is shown in Figure 4.11.

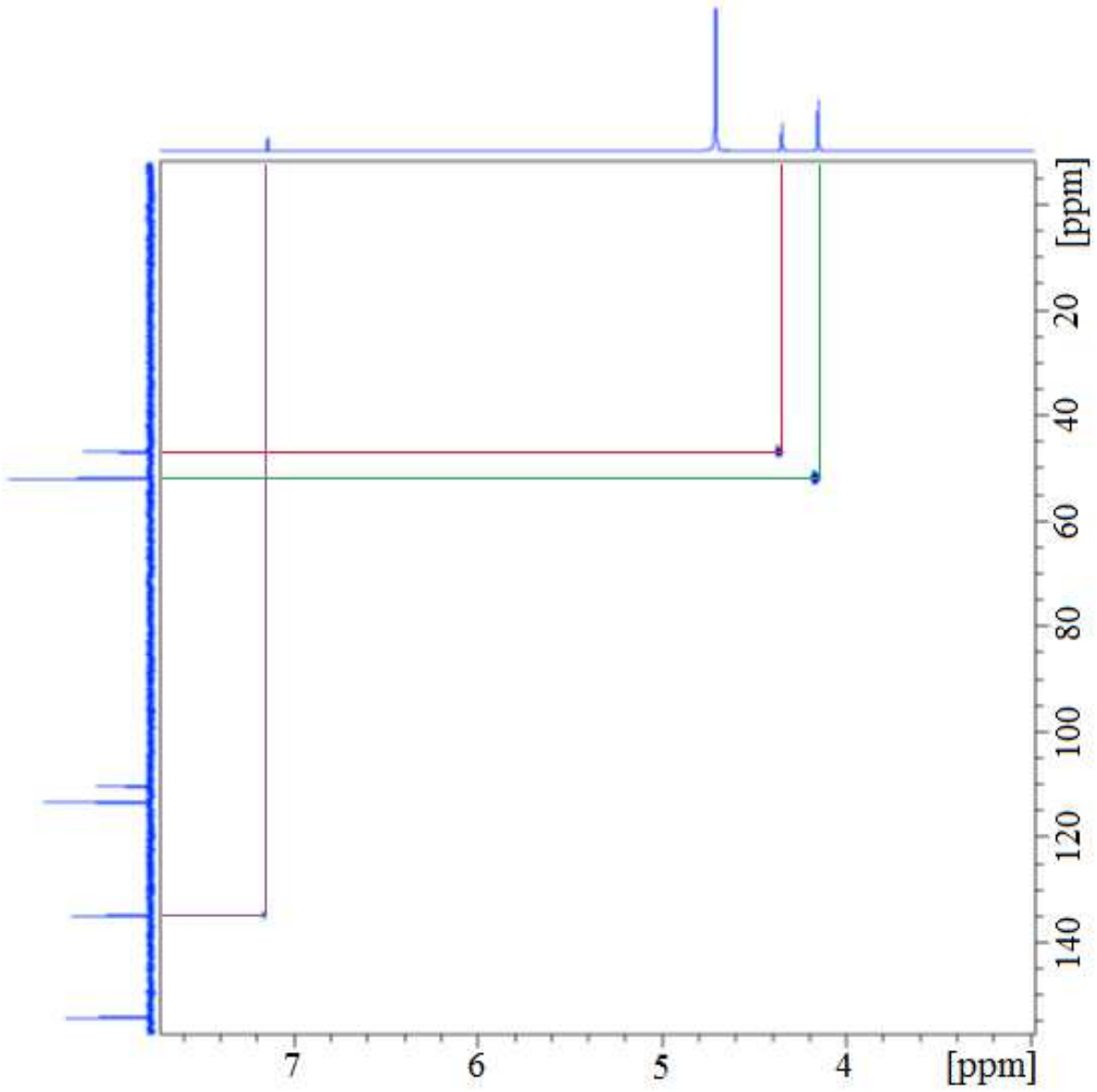

Figure 4.11 *– The HSQC spectrum for the resorcinarene product showing correlation between the ^{13}C-NMR and ^{1}H-NMR.*

The HSQC spectrum confirms that only one peak in the benzene region of the ^{13}C-NMR correlates with a peak on the ^{1}H-NMR, meaning that this is the only carbon that is both aromatic and protonated.

There is sufficient evidence from the NMR to suggest a new structure for the resorcinarene product. The suggested structure is shown in Figure 4.12.

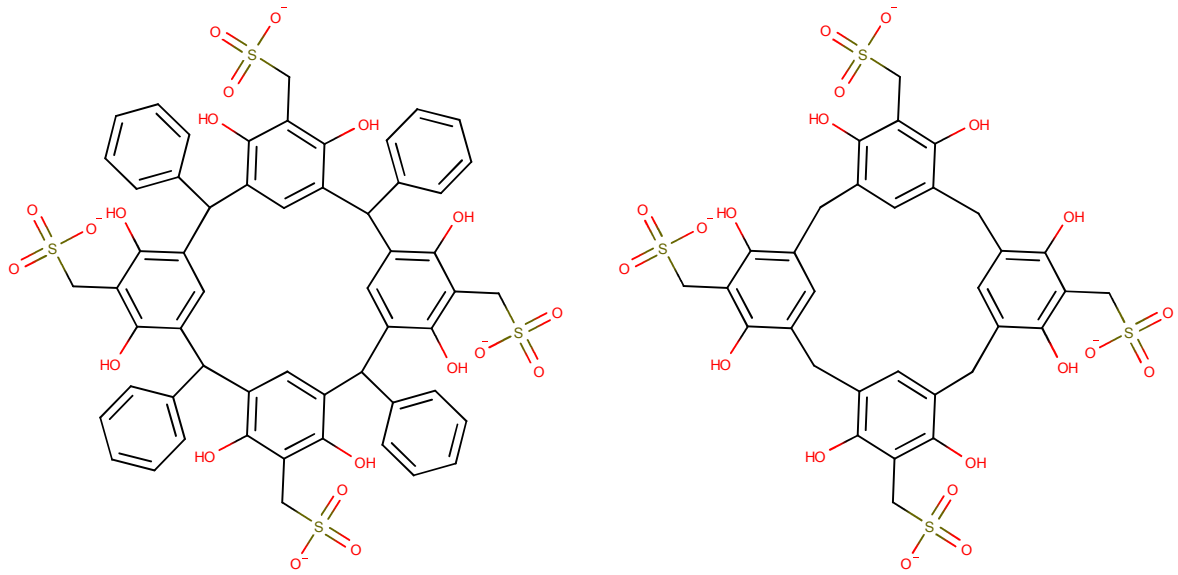

Figure 4.12 *– The expected structure of the resorcinarene (left) and the actual structure obtained (right).*

This structure fits with the spectra obtained from the NMR experiments. The interpreted spectra with structures are shown in Figure 4.13.

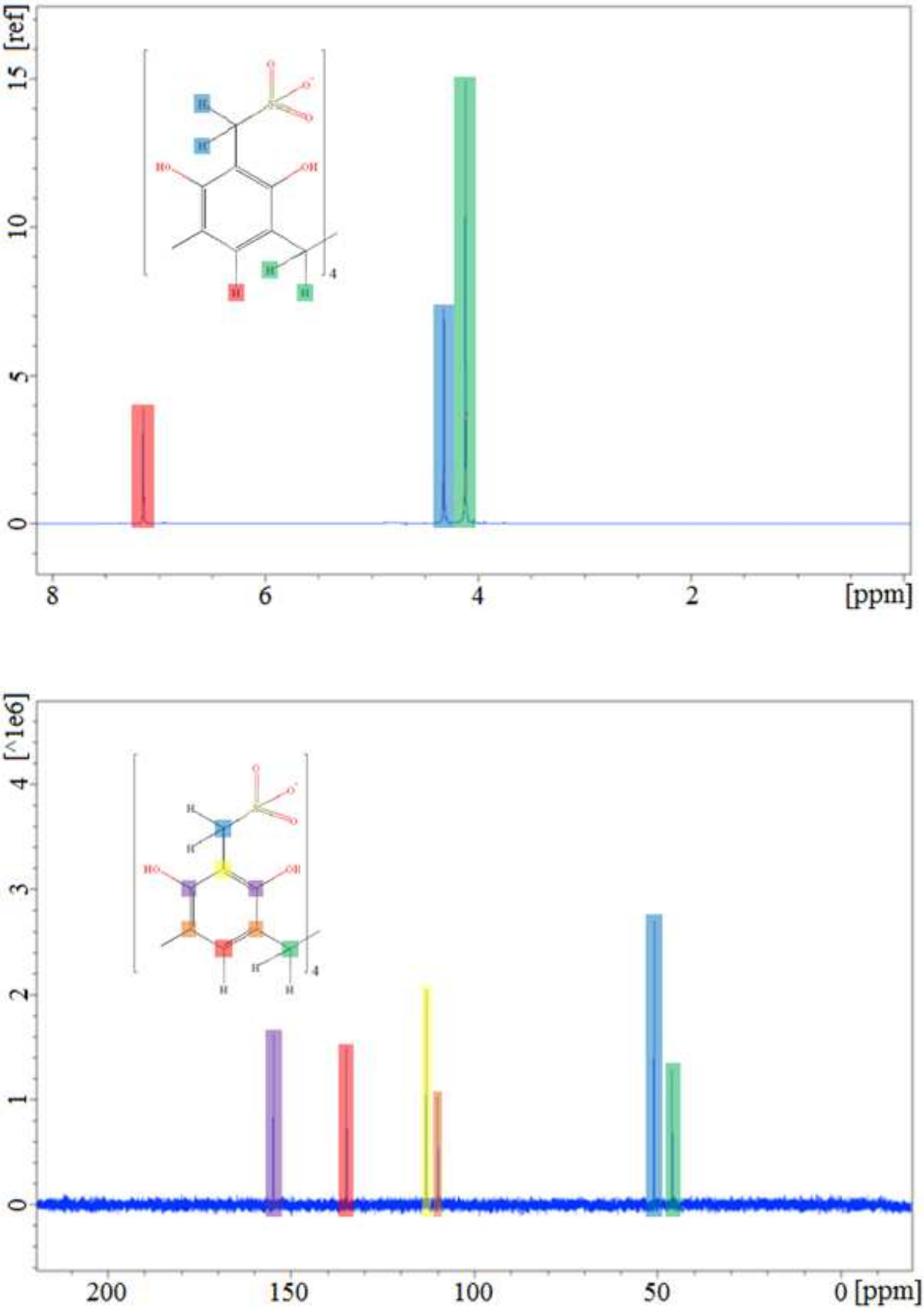

Figure 4.13 *– The interpreted ^{1}H-NMR (top) and ^{13}C-NMR (bottom) spectra for the novel resorcinarene that was produced. The colour coding shows which peak represents which part of the molecule.*

It is unclear as to how the lower rim benzene could have detached during synthesis, and future work will see this structure verified using techniques such as x-ray crystallography, surface ellipsometry, or neutron scattering. Furthermore the molecular weight and elemental composition of the resorcinarene should also be determined.

There is evidence from the NMR that a small amount of the intended product was present as a minor product. Figure 4.14 shows the benzene region from the ^{1}H-NMR containing several small peaks. Further analysis, including a chromatographic separation, is required to ascertain whether or not this is the intended product of an impurity. As discussed earlier, the bridging methylene groups in calix[4]arenes are often asymmetric and therefore in the NMR spectra a double-doublet is obtained. Since the methylene group in the sulfonated resorcinarene gives a singlet, this indicates that the molecule is conformationally mobile.

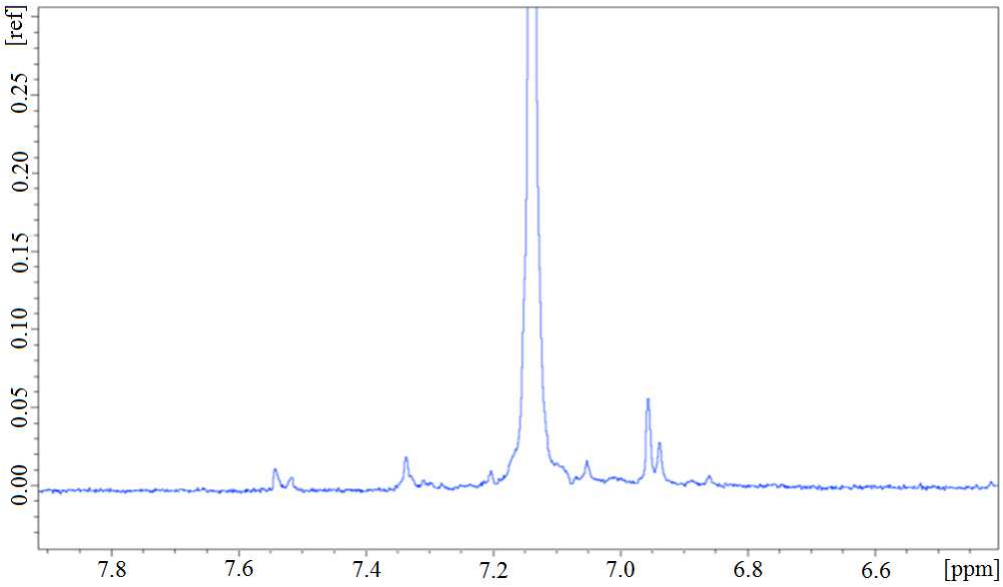

***Figure 4.14** – The ^{1}H-NMR of the resorcinarene with the benzene region expanded to show the presence of a minority product.*

4.4.3.3 Complex Visualisation by NMR

The guest-host complexes were prepared in D_2O at a ratio of 10:1 (guest : host) and analysed by ^{1}H-NMR. The spectrum of the mixture was then overlaid with both spectra taken of both the guest and the host in isolation to compare the position of the peaks.

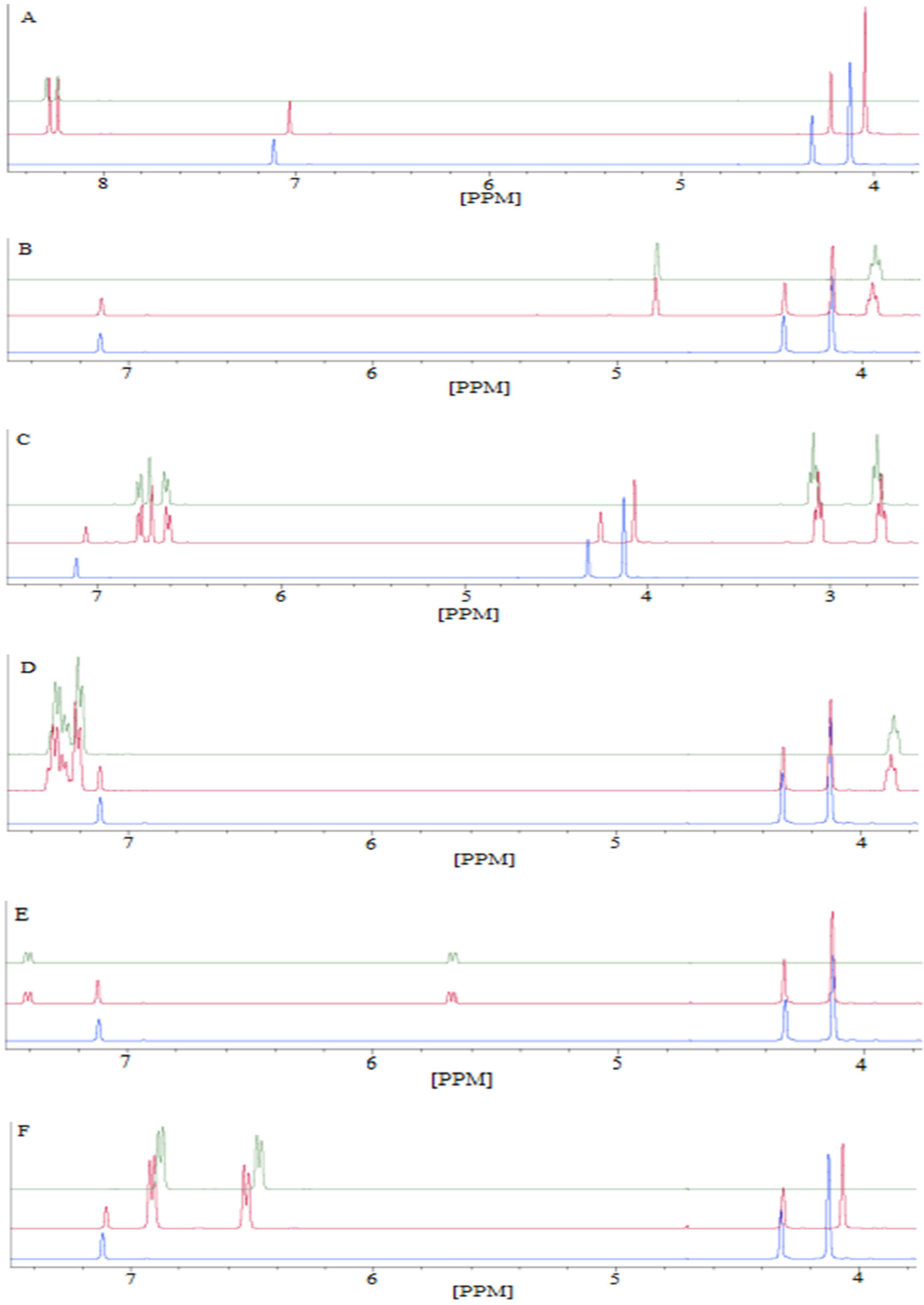

Figure 4.15 *– Guest-host complex NMR spectra for; adenine (A), ascorbic acid (B), dopamine (C), phenylalanine (D), uracil (E), and tyrosine (F). All spectra show the guest (green), the host (blue), and the complex (red).*

The spectra for the complexes of adenine, dopamine, and tyrosine show peak displacement when compared with the spectra of the host with no guest included. This is because the complexation causes shielding or deshielding of the protons which are involved, which in turn changes the position of the peak. If a peak shows increased shielding then this is likely caused by hydrogen bonding. If the peak is deshielded then this is a sign that Van-der-Waals forces are involved. In the case of these guest-host complexes only deshielding is observed. This is consistent with the type of π-interactions that are generally involved in guest-host complexes of calixarenes and resorcinarenes. The degree to which each peak is displaced is shown in Table 4.1.

Table 4.1 *– The shift in peak position for some guest-host complexes.*

Guest Molecule	Shift in Peak 1 (7.1151 ppm)	Shift in Peak 2 (4.3219 ppm)	Shift in Peak 3 (4.1248 ppm)
Adenine	0.0822	0.0972	0.0786
Dopamine	0.0521	0.0691	0.0575
Tyrosine	0.0156	0.0090	0.0583

Furthermore, since the shifting of the three peaks involved is not uniform it is possible to determine binding orientation from the degree to which each peak is shifting within a complex. For instance, the tyrosine complex shows the highest displacement for peak 3, which represents the bridging carbon between the resorcinol residues. The displacement of peak 2, which represents the bridging carbon connecting the sulfate group to the benzene ring, is lower and therefore indicates that tyrosine likely penetrates deep into the cavitand.

Adenine and dopamine, being larger molecules, not only form interactions with the protons deep in the cavitand, but also with the upper rim protons. This is shown by the fact that all three peaks are displaced to a similar degree. Adenine displays the greatest peak displacement of all three successful complexes. Since the degree to which a peak is displaced depends on proximity (via the Nuclear Overhauser Effect) it can be assumed that the adenine complex

will display the highest binding constant. However the current data is not sufficient to determine binding constants, this can only be done by a full NMR titration.

4.4.3.4 Infra-Red Spectroscopy

Infra-red spectroscopy was performed on the sample to assess whether or not the reaction had occurred correctly the IR spectrum of the product is shown in Figure 4.16.

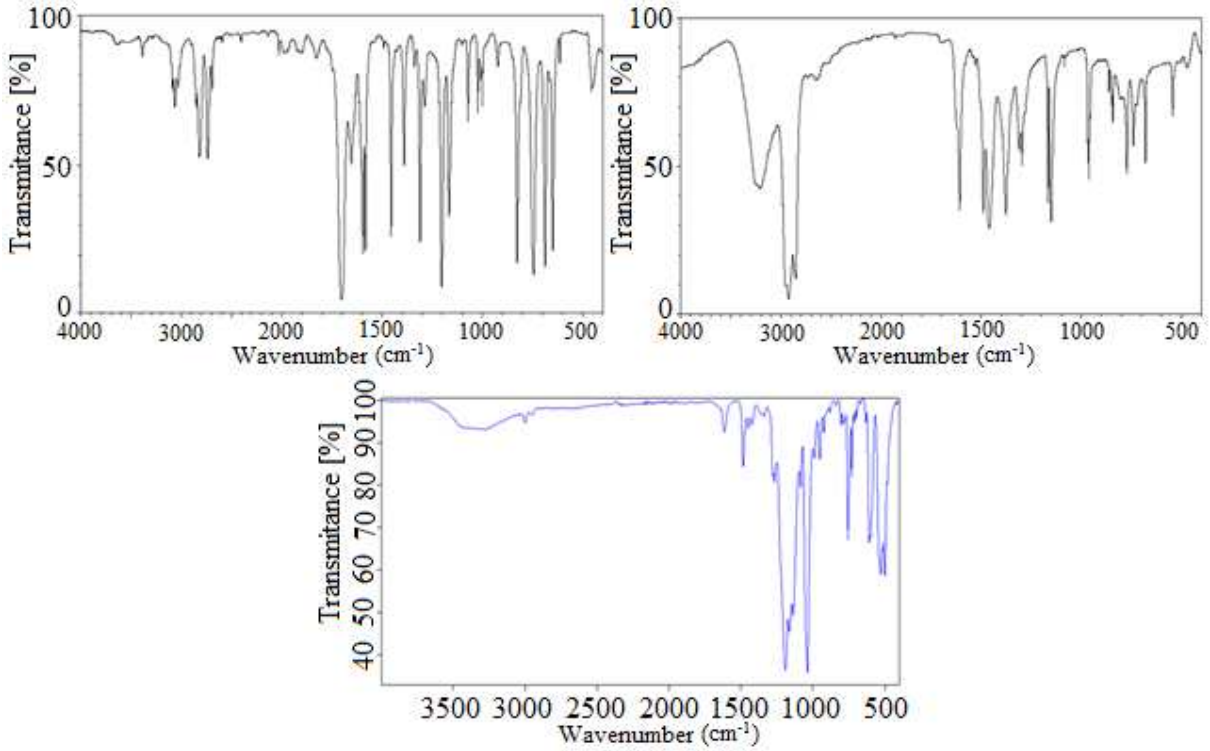

Figure 4.16 *– The IR spectrum of the resorcinarene product (bottom) compared with that of benzaldehyde (top left) and resorcinol (top right).*

The absorbance showing the carbonyl in the aldehyde (~1650 cm^{-1}) is absent in the product spectrum. This shows that the aldehyde has reacted to cyclise the resorcinol, losing the carbonyl group in the process. Additionally the aromatic C-H stretch (~3000 cm^{-1}) in both spectra are significantly diminished in the product. This shows that the majority of the hydrogens have been removed from the resorcinol during the reaction.

The O-H stretch absorbance caused by the OH groups in the resorcinol has been significantly diminished. This indicates that those groups are involved in hydrogen bonding, as this causes

broadening and shallowing of this peak. Hydrogen bonding of this type suggests that the molecule is in the cone conformation, with hydrogen bonding occurring between the OH groups on the upper rim. Crucially, this shallow absorbance in this region confirms that the product is dry. Resorcinarenes, being specifically designed for form guest-host complexes, are notoriously difficult to dehydrate once water molecules have been introduced to the cavitand. If water was still present then this absorbance would be far deeper.

4.4.3.5 Langmuir-Blodgett Isotherms

The Langmuir-Blodgett isotherm data was used to determine the surface area per molecule and stability of the resorcinarene as a thin film. The resorcinarene isotherms are shown in Figure 4.17. The compounds analysed were calix[4]dodecylresorcinarene (DDR) and calix[4]benzylresorcinarene (BR) derivatised in the *ortho* position with either a sulfate group (-), trimethylamine (+), or diethylamine (DEA).

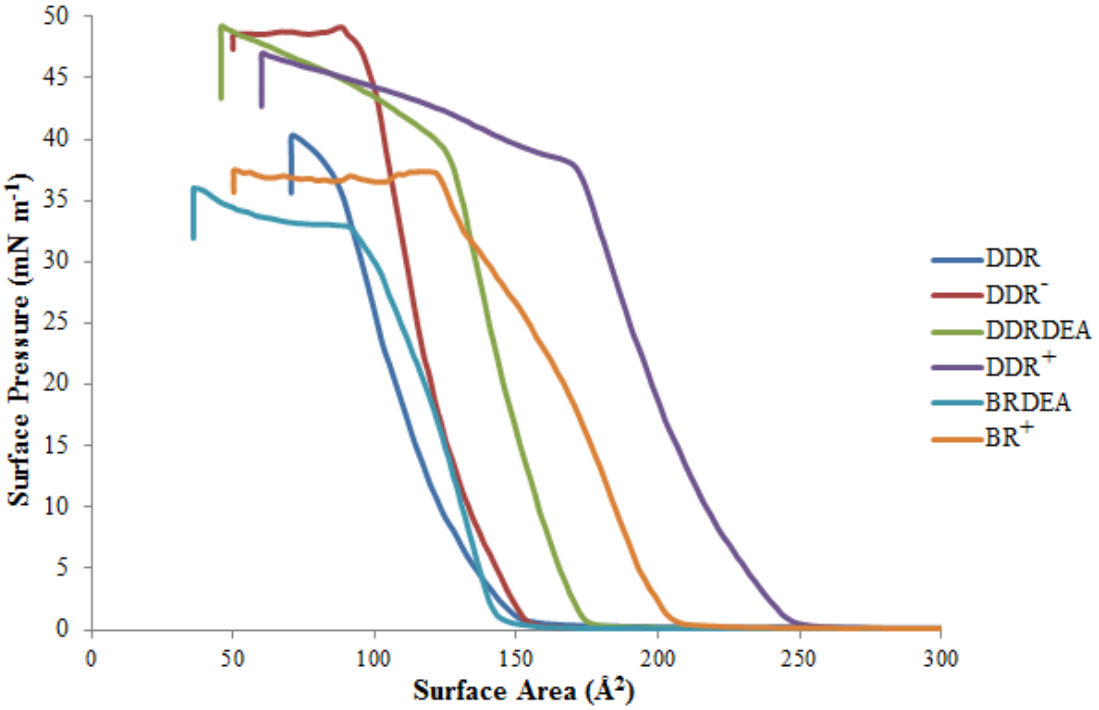

***Figure 4.17** –Isotherm thin film compression traces for some novel resorcinarene compounds obtained using Langmuir-Blodgett.*

The surface area per molecule was calculated by the NIMA software that was used to operate the trough. This was done by inputting the concentration and spreading volume for each sample. The area is then determined by tracing the steepest gradient of the isotherm trace back the X axis. The maximum surface pressure before which the film begins to collapse was calculated by finding the point at which the isotherm trace begins to plateau after the steepest gradient and reading the pressure from the Y axis. This reading is an indication of the stability of a thin film of each resorcinarene molecule, assuming a monolayer is formed. The data concerning the surface area and maximum pressure for each resorcinarene compound is shown in Table 4.2.

Table 4.2 *– Surface area and maximum surface pressure of resorcinarenes.*

Resorcinarene	Area ($Å^2$ $molecule^{-1}$)	Surface Pressure ($mN\ m^{-1}$)
Calix[4]dodecylresorcinarene (DDR)	130	36.8
o-sulfonato calix[4]dodecylresorcinarene (DDR^-)	133	45.4
o-diethylaminomethyl calix[4]dodecylresorcinarene (DDRDEA)	166	38.6
o-triethylammoniummethyl calix[4]dodecylresorcinarene (DDR^+)	227	37.4
o-diethylaminomethyl calix[4]benzylresorcinarene (BRDEA)	143	32.8
o-triethylammoniummethyl calix[4]benzylresorcinarene (BR^+)	191	37.2

The o-sulfonato calix[4]benzylresorcinarene was not sufficiently soluble in chloroform or toluene, and therefore it was not possible to obtain an isotherm for this molecule. The same was also true of the calix[4]benzylresorcinarene without any other modifications. However, assuming that similar intermolecular forces are acting between molecules of this compound as with the other resorcinarenes, a rough estimate can be made for the surface area per molecule o-sulfonato calix[4]benzylresorcinarene. The increase in surface area when the trimethylamine group was added to calix[4]dodecylresorcinarene was 97 $Å^2$ $molecule^{-1}$. Therefore the surface area of calix[4]benzylresorcinarene alone (without the trimethylamine group) can be calculated at 94 $Å^2$ $molecule^{-1}$. This would appear to be consistent with the smaller side chains on the calix[4]benzylresorcinarene compared with the calix[4]dodecylresorcinarene. The increase in surface area when the sulfate group was added

to calix[4]dodecylresorcinarene was 3 $Å^2$ $molecule^{-1}$. Therefore the surface area of o-sulfonato calix[4]benzylresorcinarene can be roughly calculated at 97 $Å^2$ $molecule^{-1}$. This calculation is only theoretical, however, and does not take into account the orientation of the molecules on the water surface. This could be determined using surface sensitive techniques such as neutron scattering spectrometry. The NMR also shows that the structure of this molecule is not as expected.

4.5 Conclusions

The resorcinarene synthesised, although not the intended product, does appear to show some specificity towards different analytes. Some guest molecules (adenine, dopamine, and tyrosine) were able to form complexes with the resorcinarene whereas others (ascorbic acid, phenylalanine, and uracil) were not. Furthermore, the *in-silico* model was able to predict with a high degree of accuracy which guest molecules would form stable guest-host complexes and which would not. The model can therefore be relied upon to predict when these complexes will form.

The surface area of the new resorcinarene molecules was also determined. This information will allow for the calculation of a theoretical maximum number of binding sites per m^2 of graphene in the final graphene-resorcinarene product, and hence the surface capacity in terms of analyte concentration.

Final Conclusions

A simple semi-automated method for the sonochemical production of surfactant-stabilised graphene was used to produce graphene functionalised with two different surfactants; sodium dodecyl sulfate (SDS) and cetyl trimethylammonium bromide (CTAB). Monolayer films of these graphene-surfactant complexes were produced using Langmuir-Blodgett and layer-by-layer deposition techniques. These monolayers were then analysed using spectroscopic ellipsometry and atomic force microscopy to determine their thickness. The layer thickness was observed to be between 2 – 2.5 nm. The graphene samples were also analysed by NMR spectroscopy to determine the extent of the interaction between the surfactant and the graphene surface.

The graphene was used to modify commercially available screen-printed carbon electrodes to determine the effect on the electrode's electrochemical activity. It was observed that the graphene coating provided a superior electrode surface with a lower resistance to electron transfer compared with screen printed carbon alone. This resulted in a lower limit of detection against the chosen analytes as well as a change in peak position during analysis by cyclic voltammetry. The shift in peak position differs between different analytes, which allows for quantification of multiple analytes in a mixture simultaneously, which is not always possible with screen printed carbon alone.

The resorcinarene that was synthesised, although not the originally intended product, was shown to demonstrate selectivity between analytes. This was successfully predicted by *in-silico* experiments and then verified using NMR spectroscopy. This could indicate that it will be a suitable binding ligand for future functionalisation of graphene flakes for specific detection of the analytes in question.

Future Work

The structure of the resorcinarene will be verified using LC-NMR and x-ray crystallography and the chemical composition and molecular mass will be determined by combustion analysis and MALDI MS respectively. Once the structure has been verified the binding constants of the three successful guest-host complexes should be determined using NMR or UV/vis titration, or by differential scanning calorimetry.

Once the binding behaviour of the resorcinarene has been studied fully, a graphene-resorcinarene composite will be produced that may allow for selective electrochemical detection of the analytes mentioned in this chapter. There are several potential medical applications of this type of sensor, for instance the detection of genetic mutations and the quantification of dopamine. The partially selective nature of resorcinarenes as binding ligands coupled with the fact that not all analytes are electrochemically active should minimise interference from other analytes in a sample.

Further study will yield other molecules such as calixarenes, resorcinarenes, porphyrins, and phthalocyanines that can also be used to create graphene complexes and will utilise the guest-host complex forming nature of these molecules to allow for the specific and simultaneous detection of a wide array of analytes by electrochemical methods. Such methods are far less expensive than many alternatives and generally do not require costly pieces of equipment to perform.

References

Akita, T., Matsui, Y., & Yamamoto, T. (2014). *A 1H NMR titration study on the binding constants for D- and l-tryptophan inclusion complexes with 6-O-α-D-glucosyl-β-cyclodextrin. Formation of 1:1 and 2:1 (host:guest) complexes*. Journal of Molecular Structure, *1060*(**1**), 138–141.

Alzari, V., Nuvoli, D., Scognamillo, S., Piccinini, M., Gioffredi, E., Malucelli, G., Marceddu, S., Sechi, M., Sanna, V., & Mariani, A. (2011). *Graphene-containing thermoresponsive nanocomposite hydrogels of poly(N-isopropylacrylamide) prepared by frontal polymerization*. Journal of Materials Chemistry, *21*(**24**), 8727–8733.

Andersson, M. R., Selse, D., Berggren, M., Järvinen, H., Hjertberg, T., Inganäs, O., Wennerström, O., & Österholm, J.-E. (1994). *Regioselective polymerization of 3-(4-octylphenyl)thiophene with FeCl3*. Macromolecules®, *27*(**22**), 6503–6506.

Andreetti, G. D., Ungaro, R., & Pochini, A. (1979). *Crystal and molecular structure of cyclo{quater[(5-t-butyl-2-hydroxy-1,3- phenylene)methylene]} toluene (1 : 1) clathrate*. Journal of the Chemical Society, Chemical Communications, (**22**), 1005–1007.

Aoyama, Y., Tanaka, Y., & Sugahara, S. (1989). *Molecular recognition. 5. Molecular recognition of sugars via hydrogen-bonding interaction with a synthetic polyhydroxy macrocycle*. Journal of the American Chemical Society, *111*(**14**), 5397–5404.

Arena, G., Casnati, A., Contino, A., Magrì, A., Sansone, F., Sciotto, D., & Ungaro, R. (2006). *Inclusion of naturally occurring amino acids in water soluble calix[4]arenes: A microcalorimetric and 1H NMR investigation supported by molecular modeling*. Organic and Biomolecular Chemistry, *4*(**2**), 243–249.

Ates, M. (2013). *A review study of (bio)sensor systems based on conducting polymers*. Materials Science and Engineering C, *33*(**4**), 1853–1859.

Azzam, R. M. A., & Bashara, N. M. (2003). *Ellipsometry and Polarized Light*. London: Elsevier.

Bada, J. L., Glavin, D. P., McDonald, G. D., & Becker, L. (1998). *A search for endogenous amino acids in martian meteorite ALH84001*. Science, *279*(**5349**), 362–365.

Bada, J. L., & McDonald, G. D. (1996). *Detecting amino acids on Mars*. Analytical Chemistry, *68*(**21**), 668A–673A.

Bae, S., Kim, H., Lee, Y., Xu, X., Park, J.-S., Zheng, Y., Balakrishnan, J., Lei, T., Ri Kim, H., Song, Y. I., Kim, Y.-J., Kim, K. S., Özyilmaz, B., Ahn, J.-H., Hong, B. H., & Iijima, S. (2010). *Roll-to-roll production of 30-inch graphene films for transparent electrodes*. Nature Nanotechnology, *5*(**8**), 574–578.

Baeyer, A. (1872). *Uber die Verbindungen der Aldehyde mit den Phenolen und aromatischen Kohlenwasserstoffen*. Berichte Der Deutschen Chemischen Gesellschaft, *5*(**2**), 1094–1100.

Bandarenka, A. S. (2013). *Exploring the interfaces between metal electrodes and aqueous electrolytes with electrochemical impedance spectroscopy*. Analyst, *138*(**19**), 5540–5554.

Batch, B. C., Hyland, K., & Svetkey, L. P. (2014). *Branch chain amino acids: Biomarkers of health and disease*. Current Opinion in Clinical Nutrition and Metabolic Care, *17*(**1**), 86–89.

Bayes, M., & Gut, I. G. (2012). *Overview of Genotyping*. In R. Rapley & S. Harbron (Eds.), *Molecular Analysis and Genome Discovery* (Vol. 2). Chichester: Wiley.

Belanger, D., Laperriere, G., & Gravel, L. (1990). *Polypyrrole films doped with tetrathiomolybdate anions. The first step toward a polypyrrole-amorphous molybdenum sulfide electrode*. Journal of the Electrochemical Society, *137*(**1**), 365–366.

Bernstein, M. P., Dworkin, J. P., Sandford, S. A., Cooper, G. W., & Allamandola, L. J. (2002). *Racemic amino acids from the ultraviolet photolysis of interstellar ice analogues*. Nature, *416*(**6879**), 401–403.

Böhmer, V., Marschollek, F., & Zetta, L. (1987). *Calix[4]arenes with four differently substituted phenolic units*. Journal of Organic Chemistry, *52*(**15**), 3200–3205.

Böhmer, V., Merkel, L., & Kunz, U. (1987). *Asymmetrically-substituted calix(4)arenes*. Journal of the Chemical Society, Chemical Communications, (**12**), 896–897.

Bruch, M. (1996). *NMR Spectroscopy Techniques* (Vol. 2). New York: Marcel Dekker.

Cambridge, U. of. (2013). *Linear Sweep and Cyclic Voltametry: The Principles*. Retrieved from http://www.ceb.cam.ac.uk/pages/linear-sweep-and-cyclic-voltametry-the-principles.html

Carvalho, A. A., & Radwin, R. G. (1996). *A new method for extending the range of conductive polymer sensors for contact force*. International Journal of Industrial Ergonomics, *17*(**3**), 285–290.

Castano, L. M., Winkelmann, A. E., & Flatau, A. B. (2010). *Foot angle determination using conductive polymer sensors*. In *Sensors and Smart Structures Technologies for Civil, Mechanical, and Aerospace Systems 2010* (Vol. 7647, pp. 76470Z–1 – 76470Z–12).

Celej, M. S., Dassie, S. A., González, M., Bianconi, M. L., & Fidelio, G. D. (2006). *Differential scanning calorimetry as a tool to estimate binding parameters in multiligand binding proteins*. Analytical Biochemistry, *350*(**2**), 277–284.

Chen, J.-H., Jang, C., Adam, S., Fuhrer, M. S., Williams, E. D., & Ishigami, M. (2008). *Charged-impurity scattering in graphene*. Nature Physics, *4*(**5**), 377–381.

Cheng, Z., Li, Q., Li, Z., Zhou, Q., & Fang, Y. (2010). *Suspended graphene sensors with improved signal and reduced noise*. Nano Letters, *10*(**5**), 1864–1868.

Chiang, J.-C., & MacDiarmid, A. G. (1986). *"Polyaniline": Protonic acid doping of the emeraldine form to the metallic regime*. Synthetic Metals, *13*(**1-3**), 193–205.

Choong, C.-L., Shim, M.-B., Lee, B.-S., Jeon, S., Ko, D.-S., Kang, T.-H., Bae, J., Lee, S. H., Byun, K.-E., Im, J., Jeong, Y. J., Park, C. E., Park, J.-J., & Chung, U.-I. (2014). *Highly stretchable resistive pressure sensors using a conductive elastomeric composite on a micropyramid array*. Advanced Materials, *26*(**21**), 3451–3458.

Clark Jr., L. C., & Lyons, C. (1962). *Electrode systems for continuous monitoring in cardiovascular surgery.* Annals of the New York Academy of Sciences, *102*, 29–45.

Collyer, S. D., Davis, F., & Higson, S. P. J. (2010). *Sonochemically fabricated microelectrode arrays for use as sensing platforms*. Sensors, *10*(**5**), 5090–5132.

Cornforth, J. W., Hart, P. D., Rees, R. J. W., & Stock, J. A. (1955). *Antituberculous effect of certain surface-active polyoxyethylene ethers*. British Journal of Pharmacology, *10*(**1**), 73–86.

Cronin, J. R., & Pizzarello, S. (1999). *Amino acid enantiomer excesses in meteorites: Origin and significance*. Advances in Space Research, *23*(**2**), 293–299.

Czugler, M., Tisza, S., & Speier, G. (1991). *Versatility in inclusion hosts. Unusual conformation in the crystal structure of the p-t-butylcalix[8]arene: Pyridine (1:8) clathrate*. Journal of Inclusion Phenomena and Molecular Recognition in Chemistry, *11*(**4**), 323–331.

Das, M., Borah, N. C., Ghose, M., & Choudhury, N. (2014). *Reference ranges for serum uric acid among healthy Assamese people*. Biochemistry Research International, *2014*, 1 – 7.

De, S., & Coleman, J. N. (2010). *Are there fundamental limitations on the sheet resistance and transmittance of thin graphene films?* ACS Nano, *4*(**5**), 2713–2720.

Dickert, F. L., Bäumler, U. P. A., & Stathopulos, H. (1997). *Mass-Sensitive Solvent Vapor Detection with Calix[4]resorcinarenes: Tuning Sensitivity and Predicting Sensor Effects*. Analytical Chemistry, *69*(**6**), 1000–1005.

Dong, S., & Ding, J. (1987). *Study on polypyrrole film by electrochemical polymerization in aqueous solution*. Synthetic Metals, *20*(**1**), 119–124.

Dumazet, I., Ehlinger, N., Vocanson, F., Lecocq, S., Lamartine, R., & Perrin, M. (1997). *p-tert-Butylcalix[5]arene: A new synthetic pathway and crystal structure of the N ,N-Dimethylformamide complex*. Journal of Inclusion Phenomena and Molecular Recognition in Chemistry, *29*(**2**), 175–185.

Durairaj, R. B. (2005). *Resorcinol: Chemistry, Technology and Applications*. Heidelberg: Springer.

Durmaz, F., Memon, F. N., Memon, N. A., Memon, S., Memon, S., & Kara, H. (2013). *Preconcentration and determination of toxic metals by a new calix[4]arene bonded HPLC column*. Chromatographia, *76*(**15-16**), 909–919.

Ekabutr, P., Chailapakul, O., & Supaphol, P. (2013). *Modification of disposable screen-printed carbon electrode surfaces with conductive electrospun nanofibers for biosensor applications*. Journal of Applied Polymer Science, *130*(**6**), 3885–3893.

El-Kosasy, A. M., Nebsen, M., Abd El-Rahman, M. K., Salem, M. Y., & El-Bardicy, M. G. (2011). *Comparative study of 2-hydroxy propyl beta cyclodextrin and calixarene as ionophores in potentiometric ion-selective electrodes for neostigmine bromide*. Talanta, *85*(**2**), 913–918.

El-Sayed, M. A. (2014). *Advantages of the incorporation of 2-hydroxyl propyl beta cyclodextrin and calixarene as ionophores in potentiometric ion-selective electrodes for rivastigmine with a kinetic study of its alkaline degradation*. Sensors and Actuators, B: Chemical, *190*, 101–110.

Farokhcheh, A., & Alizadeh, N. (2014). *Amino acid detection using fluoroquinolone-Cu2+ complex as a switch-on fluorescent probe by competitive complexation without derivatization*. Journal of Luminescence, *145*, 708–712.

Feast, W. J., Tsibouklis, J., Pouwer, K. L., Groenendaal, L., & Meijer, E. W. (1996). *Synthesis, processing and material properties of conjugated polymers*. Polymer, *37*(**22**), 5017–5047.

Firdaus, M., Jumina., & Anwar, C. (2008). *Green Synthesis of C-4-Hydroxy-3-methoxyphenylcalix[4]resorcinarene, and C-4-Methoxyphenylcalix[4]resorcinarene*. Proceedings of the International Seminar on Chemistry, *30-31*, 346–350.

Gao, J., Yang, H., Chen, J., Fang, J., Chen, C., Liang, R., Yang, G., Wu, H., Wu, C., & Li, S. (2013). *Analysis of serum metabolites for the discovery of amino acid biomarkers and the effect of galangin on cerebral ischemia*. Molecular BioSystems, *9*(**9**), 2311–2321.

Georghiou, P. E., Rahman, S., Valluru, G., Dawe, L. N., Rahman, S. M. S., Alodhayb, A. N., & Beaulieu, L. Y. (2013). *Synthesis of an upper- and lower-rim functionalized calix[4]arene for detecting calcium ions using a microcantilever sensor*. New Journal of Chemistry, *37*(**5**), 1298–1301.

Ghoufi, A., Morel, J. P., Morel-Desrosiers, N., & Malfreyt, P. (2005). *MD simulations of the binding of alcohols and diols by a calixarene in water: Connections between microscopic and macroscopic properties*. Journal of Physical Chemistry B, *109*(**49**), 23579–23587.

Goldburg, W. I. (1999). *Dynamic light scattering*. American Journal of Physics, *67*(**12**), 1152–1160.

Groenendaal, L., Jonas, F., Freitag, D., Pielartzik, H., & Reynolds, J. R. (2000). *Poly(3,4-ethylenedioxythiophene) and its derivatives: past, present, and future*. Advanced Materials, *12*(**7**), 481–494.

Grootenhuis, P. D. J., Kollman, P. A., Groenen, L. C., Reinhoudt, D. N., Van Hummel, G. J., Ugozzoli, F., & Andreetti, G. D. (1990). *Computational study of the structural, energetical, and acid-base properties of calix[4]arenes*. Journal of the American Chemical Society, *112*(**11**), 4165–4176.

Guo, X., Jian, J., Lin, L., Zhu, H., & Zhu, S. (2013). *O2 plasma-functionalized SWCNTs and PEDOT/PSS composite film assembled by dielectrophoresis for ultrasensitive trimethylamine gas sensor*. Analyst, *138*(**18**), 5265–5273.

Gutsche, C. D. (2008). *Calixarenes: an introduction*. *Monographs in supramolecular chemistry* (Vol. 2). Cambridge: RSC Pub.

Gutsche, C. D., Dhawan, B., Leonis, M., & Stewart, D. (1990). *p-tert-butylcalix[6]arene*. Organic Syntheses, *68*, 238.

Gutsche, C. D., Dhawan, B., No, K. H., & Muthukrishnan, R. (1981). *Calixarenes. 4. The synthesis, characterization, and properties of the calixarenes from p-tert-butylphenol*. Journal of the American Chemical Society, *103*(**13**), 3782–3792.

Gutsche, C. D., Gutsche, A. E., & Karaulov, A. I. (1985). *Calixarenes 11. Crystal and molecular structure of p-tert-butylcalix[8]arene*. Journal of Inclusion Phenomena, *3*(**4**), 447–451.

Gutsche, C. D., & Munch, J. H. (1990). *p-tert-butylcalix[8]arene*. Organic Syntheses, *68*, 243.

Guziński, M., Lisak, G., Kupis, J., Jasiński, A., & Bocheńska, M. (2013). *Lead(II)-selective ionophores for ion-selective electrodes: A review*. Analytica Chimica Acta, *791*, 1–12.

Hahn, S. J., Stanchina, W. E., Gajda, W. J., & Vogelhut, P. (1986). *The effect of growth rate variation on the conductivity and morphology of polypyrrole thin films*. Journal of Electronic Materials, *15*(**3**), 145–149.

Hajipour, A. R., Habibi, S., & Ruoho, A. E. (2010). *Modification of poly acrylic acid using calix[4]arene derivative for the adsorption of toxic heavy metals*. Journal of Applied Polymer Science, *118*(**2**), 818–826.

Harrowfield, J. M., Ogden, M. I., Richmond, W. R., & White, A. H. (1991). *Lanthanide ions as calcium substitutes: A structural comparison of europium and calcium complexes of a ditopic calixarene*. Journal of the Chemical Society, Dalton Transactions, (**8**), 2153–2160.

Harrowfield, J. M., Ogden, M. I., & White, A. H. (1991). *Actinide complexes of the calixarenes. Part 2. Synthesis and crystal structure of a novel thorium(IV) complex of p-tert-butylcalix[8]arene*. Journal of the Chemical Society, Dalton Transactions, (**10**), 2625–2632.

Hassen, W. M., Martelet, C., Davis, F., Higson, S. P. J., Abdelghani, A., Helali, S., & Jaffrezic-Renault, N. (2007). *Calix[4]arene based molecules for amino-acid detection*. Sensors and Actuators, B: Chemical, *124*(**1**), 38–45.

Haupt, R. L., & Haupt, S. E. (2004). *Practical Genetic Algorithms* (Vol. 2). Hoboken: Wiley.

Hayashi, N., Ujihara, T., & Kohata, K. (2004). *Binding energy of tea catechin/caffeine complexes in water evaluated by titration experiments with 1H-NMR*. Bioscience, Biotechnology and Biochemistry, *68*(**12**), 2512–2518.

Hayes, B. T., & Hunter, R. F. (1958). *Phenol-formaldehyde and allied resins VI: Rational synthesis of a "cyclic" tetranuclear p-cresol novolak*. Journal of Applied Chemistry, *8*(**11**), 743–748.

He, M., Johnson, R. J., Escobedo, J. O., Beck, P. A., Melancon, B. J., Treleaven, W. D., Strongin, R. M., Lewis, P. T., Kim, K. K., St. Luce, N. N., Mrse, A. A., Davis, C. J., & Fronczek, F. R. (2002). *Chromophore formation in resorcinarene solutions and the visual detection of mono- and oligosaccharides*. Journal of the American Chemical Society, *124*(**18**), 5000–5009.

Hehre, W. J. (2003). *A Guide to Molecular Mechanics and Quantum Chemical Calculations*. Irvine: Wavefunction Inc.

Heinig, M., & Johnson, R. J. (2006). *Role of uric acid in hypertension, renal disease, and metabolic syndrome*. Cleveland Clinic Journal of Medicine, *73*(**12**), 1059–1064.

Hernandez, Y., Nicolosi, V., Lotya, M., Blighe, F. M., Sun, Z., De, S., McGovern, I. T., Holland, B., Byrne, M., Gun'ko, Y. K., Boland, J. J., Niraj, P., Duesberg, G., Krishnamurthy, S., Goodhue, R., Hutchison, J., Scardaci, V., Ferrari, A. C., & Coleman, J. N. (2008). *High-yield production of graphene by liquid-phase exfoliation of graphite*. Nature Nanotechnology, *3*(**9**), 563–568.

Heurich, M., Altintas, Z., & Tothill, I. E. (2013). *Computational design of peptide ligands for ochratoxin A*. Toxins, *5*(**6**), 1202–1212.

Hobza, P., Selzle, H. L., & Schlag, E. W. (1994). *Potential energy surface of the benzene dimer: Ab initio theoretical study*. Journal of the American Chemical Society, *116*(**8**), 3500–3506.

Hobza, P., Selzle, H. L., & Schlag, E. W. (1996). *Potential energy surface for the benzene dimer. Results of ab Initia CCSD(T) calculations show two nearly isoenergetic structures: T-shaped and parallel-displaced*. The Journal of Physical Chemistry®, *100*(**48**), 18790–18794.

Hu, Z., Zhang, J., & Zhu, Y. (2014). *Effects of solvent-treated PEDOT: PSS on organic photovoltaic devices*. Renewable Energy, *62*, 100–105.

Huang, C. H., Su, C. Y., Okada, T., Li, L. J., Ho, K. I., Li, P. W., Chen, I. H., Chou, C., Lai, C. S., & Samukawa, S. (2013). *Ultra-low-edge-defect graphene nanoribbons patterned by neutral beam*. Carbon, *61*, 229–235.

Huang, L.-M., Chen, C.-H., & Wen, T.-C. (2006). *Development and characterization of flexible electrochromic devices based on polyaniline and poly(3,4-ethylenedioxythiophene)-poly(styrene sulfonic acid)*. Electrochimica Acta, *51*(**26**), 5858–5863.

Hummers Jr., W. S., & Offeman, R. E. (1958). *Preparation of graphitic oxide*. Journal of the American Chemical Society, *80*(**6**), 1339.

Inzelt, G. (2012). *Conducting Polymers: A New Era in Electrochemistry* (Vol. 2). Heidelberg: Springer.

Jaffe, R. L., & Smith, G. D. (1996). *A quantum chemistry study of benzene dimer*. Journal of Chemical Physics, *105*(**7**), 2780–2788.

Jayakannan, M., Babourina, O., & Rengel, Z. (2011). *Improved measurements of Na + fluxes in plants using calixarene-based microelectrodes*. Journal of Plant Physiology, *168*(**10**), 1045–1051.

Jerew, B. (2013). *Graphene Oxide Offers New Hope for Water Decontamination*. Retrieved from http://www.greenoptimistic.com/2013/01/09/graphene-oxide-offers-new-hope-for-water-decontamination/#.Unj8i_nIbi0

Johnson, R. E., Washington, M. T., Prakash, S., & Prakash, L. (2000). *Fidelity of human DNA polymerase η*. Journal of Biological Chemistry, *275*(**11**), 7447–7450.

Kämmerer, H., Happel, G., Böhmer, V., & Rathay, D. (1978). *Stepwise synthesis of 4,11,18,25-tetra-t-butyl-[1.1.1.1]metacyclophane-7,14,21,28-tetraol and 4,11-dimethyl-[1.1.1.1]metacyclophane-7,14,21,28-tetraol*. Monatshefte Für Chemie, *109*(**4**), 767–773.

Kane, P., Fayne, D., Diamond, D., Bell, S. E. J., & McKervey, M. A. (1998). *Modelling of the sodium complex of a calixarene tetraester in the 1,3-alternate conformation*. Journal of Molecular Modeling, *4*(**8**), 259–267.

Kane, P., Kincaid, K., Fayne, D., Diamond, D., & McKervey, M. A. (2000). *Modelling metal complexes of calixarene esters and phosphine oxides using molecular mechanics*. Journal of Molecular Modeling, *6*(**2**), 272–281.

Karami, B., Khodabakhshi, S., Safikhani, N., & Arami, A. (2012). *A green and highly efficient solvent-free synthesis of novel calicx[4]resorcinarene derivatives using tungstate sulfuric acid*. Bulletin of the Korean Chemical Society, *33*(**1**), 123–127.

Katz, E., & Willner, I. (2003). *Probing biomolecular interactions at conductive and semiconductive surfaces by impedance spectroscopy: Routes to impedimetric immunosensors, DNA-sensors, and enzyme biosensors*. Electroanalysis, *15*(**11**), 913–947.

Keeler, J. (2010). *Understanding NMR Spectroscopy* (Vol. 2). Chichester: Wiley.

Khersonsky, O., Röthlisberger, D., Wollacott, A. M., Murphy, P., Dym, O., Albeck, S., Kiss, G., Houk, K. N., Baker, D., & Tawfik, D. S. (2011). *Optimization of the in-silico-designed Kemp eliminase KE70 by computational design and directed evolution*. Journal of Molecular Biology, *407*(**3**), 391–412.

Kim, J. Y., Jung, J. H., Lee, D. E., & Joo, J. (2002). *Enhancement of electrical conductivity of poly(3,4-ethylenedioxythiophene)/poly(4-styrenesulfonate) by a change of solvents*. Synthetic Metals, *126*(**2-3**), 311–316.

Kim, T., & Kwak, D. (2012). *Flexible VOC sensors using conductive polymers and porous membranes for application to textiles*. Fibers and Polymers, *13*(**4**), 471–474.

Kim, Y.-R., Bong, S., Kang, Y.-J., Yang, Y., Mahajan, R. K., Kim, J. S., & Kim, H. (2010). *Electrochemical detection of dopamine in the presence of ascorbic acid using graphene modified electrodes*. Biosensors and Bioelectronics, *25*(**10**), 2366–2369.

Kunsági-Máté, S., Szabó, K., Lemli, B., Bitter, I., Nagy, G., & Kollár, L. (2005). *Host-guest interaction between water-soluble calix[6]arene hexasulfonate and p-nitrophenol*. Thermochimica Acta, *425*(**1-2**), 121–126.

Langford, N. (2013). *Graphene Modified Electrodes*. Masters Thesis. Cranfield University.

Lawal, O., Iqbal, K. S. J., Mohamadi, A., Razavi, P., Dodd, H. T., Allen, M. C., Siddiqui, S., Fucassi, F., & Cragg, P. J. (2009). *An artificial sodium ion channel from calix[4]arene in the 1,3-alternate conformation*. Supramolecular Chemistry, *21*(**1-2**), 55–60.

Lee, B. M., Lee, S. K., & Kim, H. S. (1998). *Inhibition of oxidative DNA damage, 8-OHdG, and carbonyl contents in smokers treated with antioxidants (vitamin E, vitamin C, ß-carotene and red ginseng)*. Cancer Letters, *132*(**1-2**), 219–227.

Lee, S., Han, J., & Paik, W.-K. (1993). *Conducting polypyrrole doped with hexacyanoferrate and perchlorate ions: Effects of temperature on the structure and polymerization rate*. Synthetic Metals, *55*(**2-3**), 1129–1134.

Lee, W., Roberts, S. M., & Labbe, R. F. (1997). *Ascorbic acid determination with an automated enzymatic procedure*. Clinical Chemistry, *43*(**1**), 154–157.

Liu, F., Choi, K. S., Park, T. J., Lee, S. Y., & Seo, T. S. (2011). *Graphene-based electrochemical biosensor for pathogenic virus detection*. Biochip Journal, *5*(**2**), 123–128.

Liu, J., Wang, R., Cui, L., Tang, J., Liu, Z., Kong, Q., Yang, W., & Gooding, J. (2012). *Using molecular level modification to tune the conductivity of graphene papers*. Journal of Physical Chemistry C, *116*(**33**), 17939–17946.

MacDiarmid, A. G. (2001). *"Synthetic metals": A novel role for organic polymers (Nobel lecture)*. Angewandte Chemie - International Edition, *40*(**14**), 2581–2590.

MacDiarmid, A. G., Mammone, R. J., Kaner, R. B., & Porter, S. J. (1985). *The Concept of "Doping" of Conducting Polymers: The Role of Reduction Potentials*. Philosophical Transactions of the Royal Society, *314*(**3-15**), 3–15.

Malvern. (2012). *Dynamic Light Scattering: An introduction in 30 minutes, DLS technical note, MRK656-01*. Retrieved from www3.nd.edu/~rroeder/ame60647/slides/dls.pdf

Manecke, G. (1974). *Oxidation-Reduction Polymers*. Pure and Applied Chemistry, *38*(**1-2**), 181–199.

Matthews, R. P., Welton, T., & Hunt, P. A. (2014). *Competitive pi interactions and hydrogen bonding within imidazolium ionic liquids*. Physical Chemistry Chemical Physics, *16*(**7**), 3238–3253.

McDonald, G. D., & Bada, J. L. (1995). *A search for endogenous amino acids in the Martian meteorite EETA79001*. Geochimica et Cosmochimica Acta, *59*(**6**), 1179–1184.

Md Yasin, F., Iyer, K. S., & Raston, C. L. (2013). *Palladium nano-carbon-calixarene based devices for hydrogen sensing*. New Journal of Chemistry, *37*(**10**), 3289–3293.

Mel'nikova, N. B., Kazakova, E. K., Guljaev, I. V., Volkov, a. a., Gusikhina, M. S., Zakharova, L. Y., Voronin, M. a., Makarova, N. a., Muslinkina, L. a., & Konovalov, a. I. (2009). *Monolayers and Langmuir–Blodgett films of amphiphilic tetramethylsulphonatocalix[4]resorcinarene and their interactions with polyethyleneimine and caeruloplasmin*. Supramolecular Chemistry, *21*(**6**), 532–538.

Menon, S. K., Modi, N. R., Pandya, A., & Lodha, A. (2013). *Ultrasensitive and specific detection of dimethoate using a p-sulphonato-calix[4]resorcinarene functionalized silver nanoprobe in aqueous solution*. RSC Advances, *3*(**27**), 10623–10627.

Meyer, E. F., Swanson, S. M., & Williams, J. A. (2000). *Molecular modelling and drug design*. Pharmacology and Therapuetics, *85*(**3**), 113–121.

Mohamoud, M. A. (2008). *Conducting polymers: Smart materials with nanotechnology applications*. Plastics Engineering, *64*(**10**), 32–38.

Mokhtari, B., & Pourabdollah, K. (2012). *Preparation and characterization of bonded-phases of calixarene-sulfonyl- carboxamides in partial-cone conformation for determination of salbutamol in livestock by nano-mediated bonded-phases: Nano-baskets of calixarene in partial-cone conformation*. Journal of the Chilean Chemical Society, *57*(**2**), 1150–1154.

Mustafa, A., Gupta, S., Hudes, G. R., Egleston, B. L., Uzzo, R. G., & Kruger, W. D. (2011). *Serum amino acid levels as a biomarker for renal cell carcinoma*. Journal of Urology, *186*(**4**), 1206–1212.

Muthu Mareeswaran, P., Prakash, M., Subramanian, V., & Rajagopal, S. (2012). *Recognition of aromatic amino acids and proteins with p-sulfonatocalix[4] arene - A luminescence and theoretical approach*. Journal of Physical Organic Chemistry, *25*(**12**), 1217–1227.

Newman, J. D., & Turner, A. P. F. (2005). *Home blood glucose biosensors: A commercial perspective*. Biosensors and Bioelectronics, *20*(**12**), 2435–2453.

Nie, T., Xu, J.-K., Lu, L.-M., Zhang, K.-X., Bai, L., & Wen, Y.-P. (2013). *Electroactive species-doped poly(3,4-ethylenedioxythiophene) films: Enhanced sensitivity for electrochemical simultaneous determination of vitamins B2, B6 and C*. Biosensors and Bioelectronics, *50*, 244–250.

Nikiforovich, G. V. (1994). *Computational molecular modeling in peptide drug design*. International Journal of Peptide and Protein Research, *44*(**6**), 513–531.

No, K. H., & Gutsche, C. D. (1982). *Calixarenes. 8. Short, stepwise synthesis of p-phenylcalix[4]arene, p-phenyl-p-tert-butylcalix[4]arene, and derived products*. Journal of Organic Chemistry, *47*(**14**), 2713–2719.

Notley, S. M. (2012). *Highly concentrated aqueous suspensions of graphene through ultrasonic exfoliation with continuous surfactant addition*. Langmuir, *28*(**40**), 14110–14113.

Novoselov, K. S., Geim, A. K., Morozov, S. V, Jiang, D., Zhang, Y., Dubonos, S. V, Grigorieva, I. V, & Firsov, A. A. (2004). *Electric field in atomically thin carbon films*. Science, *306*(**5696**), 666–669.

Nuvoli, D., Valentini, L., Alzari, V., Scognamillo, S., Bon, S. B., Piccinini, M., Illescas, J., & Mariani, A. (2011). *High concentration few-layer graphene sheets obtained by liquid phase exfoliation of graphite in ionic liquid*. Journal of Materials Chemistry, *21*(**10**), 3428–3431.

Ouyang, J. (2013). *"Secondary doping" methods to significantly enhance the conductivity of PEDOT:PSS for its application as transparent electrode of optoelectronic devices*. Displays.

Ouyang, J., Guo, T.-F., Yang, Y., Higuchi, H., Yoshioka, M., & Nagatsuka, T. (2002). *High-performance, flexible polymer light-emitting diodes fabricated by a continuous polymer coating process*. Advanced Materials, *14*(**12**), 915–918.

Park, S. J., Kwon, O. S., Lee, J. E., Jang, J., & Yoon, H. (2014). *Conducting polymer-based nanohybrid transducers: A potential route to high sensitivity and selectivity sensors*. Sensors (Switzerland), *14*(**2**), 3604–3630.

Patra, S., Lo, R., Chakraborty, A., Gunupuru, R., Maity, D., Ganguly, B., & Paul, P. (2013). *Calix[4]arene based fluorescent chemosensor bearing coumarin as fluorogenic unit: Synthesis, characterization, ion-binding property and molecular modeling*. Polyhedron, *50*(**1**), 592–601.

Peng, J. B., Ketterson, J. B., & Dutta, P. (1988). *A study of the transition from Y- to X-type transfer during deposition of lead stearate and cadmium stearate Langmuir-Blodgett films*. Langmuir, *4*(**5**), 1198–1202.

Perret, F., Bonnard, V., Danylyuk, O., Suwinska, K., & Coleman, A. W. (2006). *Conformational extremes in the supramolecular assemblies of para-sulfonato-calix[8]arene*. New Journal of Chemistry, *30*(**7**), 987–990.

Pesavento, M., D'Agostino, G., Profumo, A., Biesuz, R., & Alberti, G. (2014). *Potentiometric sensors based on molecular imprinted polymers*. 1st National Conference on Sensors, *162 LNEE*, 141–144.

Phillips, C. L., & Yeowell, H. N. (1997). *Vitamin C, Collagen Biosynthesis, and Aging*. In L. Packer & J. Fuchs (Eds.), *Vitamin C in Health and Disease* (p. 205). New York: Marcel Dekker.

Premstaller, A., & Oefner, P. J. (2003). *Denaturing High-Performance Liquid Chromatography*. In P. Y. Kwok (Ed.), *Single Nucleotide Polymorphisms: Methods and Protocols* (p. 15). Totowa: Humana Press.

Pungor, E. (1995). *A Practical Guide to Instrumental Analysis*. Boca Raton: CRC Press.

Purse, B. W., Gissot, A., & Rebek Jr., J. (2005). *A deep cavitand provides a structured environment for the Menschutkin reaction*. Journal of the American Chemical Society, *127*(**32**), 11222–11223.

Qazi, M. A., Ocak, Ü., Ocak, M., & Memon, S. (2013). *An excellent copper selective chemosensor based on calix[4]arene framework.* Analytica Chimica Acta, *761*, 157–168.

Qin, X., Liu, X., Hong-Bo, L., Li-Na, Y., & Xiaoya, H. (2013). *Electrochemical determination of purine and pyrimidine DNA bases based on the recognition properties of azocalix[4]arene*. Biosensors and Bioelectronics, *42*(**1**), 355–361.

Ray, A., Asturias, G. E., Kershner, D. L., Richter, A. F., MacDiarmid, A. G., & Epstein, A. J. (1989). *Polyaniline: Doping, structure and derivatives*. Synthetic Metals, *29*(**1**), 141–150.

Regnouf-De-Vains, J.-B., Cartier, A., Fenet, B., & Pellet-Rostaing, S. (2005). *A macrobicyclic calix[6]arene phosphocine: Conformational studies involving high-resolution NMR analysis and molecular modeling*. Helvetica Chimica Acta, *88*(**5**), 1110–1125.

Rentzos, M., Nikolaou, C., Anagnostouli, M., Rombos, A., Tsakanikas, K., Economou, M., Dimitrakopoulos, A., Karouli, M., & Vassilopoulos, D. (2006). *Serum uric acid and multiple sclerosis*. Clinical Neurology and Neurosurgery, *108*(**6**), 527–531.

Reynolds, J. R., Pyo, M., & Qiu, Y.-J. (1994). *Charge and ion transport in poly(pyrrole copper phthalocyanine tetrasulfonate) during redox switching*. Journal of the Electrochemical Society, *141*(**1**), 35–40.

Roberts, B. A., Cave, G. W. V, Raston, C. L., & Scott, J. L. (2001). *Solvent-free synthesis of calix[4]resorcinarenes*. Green Chemistry, *3*(**6**), 280–284.

Rost, H. (2005). *From polymer transistor to printed electronics*. Kunststoffe Plast Europe, *95*(**10**), 209–214.

Safina, G. D., Ziganshin, M. A., Gubaidullin, A. T., & Gorbatchuk, V. V. (2013). *Analysis of guest binary mixtures by tert-butylcalix[6]arene using host memory of previously bound guests*. Organic and Biomolecular Chemistry, *11*(**8**), 1318–1325.

Samy, S., Robinson, J., & Hays, M. D. (2011). *An advanced LC-MS (Q-TOF) technique for the detection of amino acids in atmospheric aerosols*. Analytical and Bioanalytical Chemistry, *401*(**10**), 3103–3113.

Schazmann, B., Alhashimy, N., & Diamond, D. (2006). *Chloride selective calix[4]arene optical sensor combining urea functionality with pyrene excimer transduction*. Journal of the American Chemical Society, *128*(**26**), 8607–8614.

Schedin, F., Geim, A. K., Morozov, S. V, Hill, E. W., Blake, P., Katsnelson, M. I., & Novoselov, K. S. (2007). *Detection of individual gas molecules adsorbed on graphene*. Nature Materials, *6*(**9**), 652–655.

Schelstraete, S., Schepens, W., & Verschelde, H. (1999). *Energy minimization by smoothing techniques: a survey*. In P. B. Balbuena & J. M. Seminario (Eds.), *Molecular Dynamics: From Classical for Quantum Methods* (p. 129). Amsterdam: Elsevier.

Schmidt, W., & Reith, M. (2005). *Dopamine and Glutamate in Psychiatric Disorders*. Totowa: Humana Press.

Shan, C., Yang, H., Song, J., Han, D., Ivaska, A., & Niu, L. (2009). *Direct electrochemistry of glucose oxidase and biosensing for glucose based on graphene*. Analytical Chemistry, *81*(**6**), 2378–2382.

Sheff, J. T., Lucius, A. L., Owens, S. B., & Gray, G. M. (2011). *Generally applicable NMR titration methods for the determination of equilibrium constants for coordination complexes: Syntheses and characterizations of metallacrown ethers with α,ω-bis(phosphite)- Polyether ligands and determination of equilibrium bindin*. Organometallics, *30*(**21**), 5695–5709.

Shirakawa, H., Louis, E. J., MacDiarmid, A. G., Chiang, C. K., & Heeger, A. J. (1977). *Synthesis of electrically conducting organic polymers: Halogen derivatives of polyacetylene, (CH)x*. Journal of the Chemical Society, Chemical Communications, (**16**), 578–580.

Singh, S., & Rani, G. (2012). *Comparative study of holmium (III) selective sensors based on thiacalixarene and calixarene derivatives as an ionophore*. Bulletin of the Korean Chemical Society, *33*(**7**), 2229–2237.

Sinnokrot, M. O., Valeev, E. F., & Sherrill, C. D. (2002). *Estimates of the ab initio limit for p-p interactions: The benzene dimer*. Journal of the American Chemical Society, *124*(**36**), 10887–10893.

Soldano, C., Mahmood, A., & Dujardin, E. (2010). *Production, properties and potential of graphene*. Carbon, *48*(**8**), 2127–2150.

Stankovich, S., Dikin, D. A., Piner, R. D., Kohlhaas, K. A., Kleinhammes, A., Jia, Y., Wu, Y., Nguyen, S. T., & Ruoff, R. S. (2007). *Synthesis of graphene-based nanosheets via chemical reduction of exfoliated graphite oxide*. Carbon, *45*(**7**), 1558–1565.

Sunner, J., Nishizawa, K., & Kebarle, P. (1981). *Ion-solvent molecule interactions in the gas phase. The potassium ion and benzene*. Journal of Physical Chemistry, *85*(**13**), 1814–1820.

Sutter, P. (2009). *Epitaxial graphene: How silicon leaves the scene*. Nature Materials, *8*(**3**), 171–172.

Taft, R. W., Anvia, F., Gal, J. F., Walsh, S., Capon, M., Holmes, M. C., Hosn, K., Oloumi, G., Vasanwala, R., & Yazdani, S. (1990). *Free energies of cation-molecule complex formation and of cation-solvent transfers*. Pure and Applied Chemistry, *62*(**1**), 17–23.

Taryba, M. G., & Lamaka, S. V. (2014). *Plasticizer-free solid-contact pH-selective microelectrode for visualization of local corrosion*. Journal of Electroanalytical Chemistry, *725*, 32–38.

Tewari, V. C., Paliwal, B. S., & Venkatakrishna, K. (2002). *Discovery of amino acids from Didwana-Rajod meteorite and its implication on origin of life*. Journal of the Geological Society of India, *60*(**1**), 107–110.

Tompkins, H. A. (2005). *Handbook of Ellipsometry*. Heidelberg: Springer-Verlag.

Topliss, S. M., James, S. W., Davis, F., Higson, S. P. J., & Tatam, R. P. (2010). *Optical fibre long period grating based selective vapour sensing of volatile organic compounds*. Sensors and Actuators, B: Chemical, *143*(**2**), 629–634.

Tsue, H., Matsui, K., Ishibashi, K., Takahashi, H., Tokita, S., Ono, K., & Tamura, R. (2008). *Azacalix[7]arene heptamethyl ether: Preparation, nanochannel crystal structure, and selective adsorption of carbon dioxide*. Journal of Organic Chemistry, *73*(**19**), 7748–7755.

Vernitskaya, T. V. (1997). *Polypyrrole: A conducting polymer; its synthesis, properties and applications*. Russian Chemical Reviews, *66*(**5**), 443–457.

Walch, N. J., Davis, F., Langford, N., Holmes, J. L., Collyer, S. D., & Higson, S. P. J. (2015). *Enhancement of Electrode Performance by a Simple Casting Method Using Sonochemically Exfoliated Graphene*. Analytical Chemistry, *87*(**18**), 9273–9279.

Wang, J.-Y., Chen, L.-C., & Ho, K.-C. (2013). *Synthesis of redox polymer nanobeads and nanocomposites for glucose biosensors*. ACS Applied Materials and Interfaces, *5*(**16**), 7852–7861.

Wang, L., Yang, C., Zhang, Q., Wang, S., Lang, H., Zhang, S., Zhao, W., & Zhang, J. (2013). *SPE-HPLC-MS/MS method for the trace analysis of tobacco-specific N-nitrosamines and 4-(methylnitrosamino)-1-(3-pyridyl)-1-butanol in rabbit plasma using tetraazacalix[2]arene[2]triazine-modified silica as a sorbent*. Journal of Separation Science, *36*(**16**), 2664–2671.

Wang, W., Zhu, X., & Yan, C. (2013). *Determination of safranine T in food samples by CTAB sensitised fluorescence quenching method of the derivatives of calix[4]arene*. Food Chemistry, *141*(**3**), 2207–2212.

Wasylewski, M. (2004). *Evaluation of riboflavin binding protein domain interaction using differential scanning calorimetry*. Biochimica et Biophysica Acta - Proteins and Proteomics, *1702*(**2**), 137–143.

Winther-Jensen, O., Kerr, R., & Winther-Jensen, B. (2014). *Alcohol vapour detection at the three phase interface using enzyme-conducting polymer composites*. Biosensors and Bioelectronics, *52*, 143–146.

Wolfgong, W. J., Talafuse, L. K., Smith, J. M., Adams, M. J., Adeogba, F., Valenzuela, M., Rodriguez, E., Contreras, K., Carter, D. M., Bacchus, A., Mcguffey, A. R., & Bott, S. G. (1996). *The influence of solvent of crystallization upon the solid-state conformation of calix[6]arenes'*. Supramolecular Chemistry, *7*(**1**), 67–78.

Wu, X., Li, F., Wu, W., & Guo, T. (2014). *Flexible organic light emitting diodes based on double-layered graphene/PEDOT:PSS conductive film formed by spray-coating*. Vacuum, *101*, 53–56.

Wujcik, E. K., Blasdel, N. J., Trowbridge, D., & Monty, C. N. (2013). *Ion sensor for the quantification of sodium in sweat samples*. IEEE Sensors Journal, *13*(**9**), 3430–3436.

Yu, E. H., & Sundmacher, K. (2007). *Enzyme electrodes for glucose oxidation prepared by electropolymerization of pyrrole*. Process Safety and Environmental Protection, *85*(**5 B**), 489–493.

Yu, S. H., Lee, J. H., Choi, M. S., Park, J. H., Yoo, P. J., & Lee, J. Y. (2013). *Improvement of electrical conductivity of poly(3,4-ethylenedioxythiophene) (PEDOT) thin film*. Molecular Crystals and Liquid Crystals, *580*(**1**), 76–82.

Zhang, B., Li, Q., & Cui, T. (2012). *Ultra-sensitive suspended graphene nanocomposite cancer sensors with strong suppression of electrical noise*. Biosensors and Bioelectronics, *31*(**1**), 105–109.

Zhang, F., Luo, L., Sun, Y., Miao, F., Bi, J., Tan, S., Tian, D., & Li, H. (2013). *Synthesis of a novel fluorescent anthryl calix[4]arene as picric acid sensor*. Tetrahedron.

Zhou, M., Zhai, Y., & Dong, S. (2009). *Electrochemical sensing and biosensing platform based on chemically reduced graphene oxide*. Analytical Chemistry, *81*(**14**), 5603–5613.

Zielenkiewicz, W., Marcinowicz, A., Poznanski, J., Cherenok, S., & Kalchenko, V. (2005). *Complexation of isoleucine by phosphorylated calix[4]arene in methanol followed by calorimetry, NMR and UV-VIS spectroscopies, and molecular modeling methods*. Selected Papers of the 2nd International Symposium on the Thermodynamics and Structure of Liquids, *121*(**1**), 8–14.

Zinger, B. (1989). *Electrochemistry of quinoid dopants in conducting polymers*. Synthetic Metals, *30*(**2**), 209–225.

Zinke, A., & Zeigler, E. (1941). *Zur Kenntnis des Härtungsprozesses von Phenol-Formaldehyd-Harzen, VII. Mitteilung*. Berichte Der Deutschen Chemischen Gesellschaft (A and B Series), *74*(**11**), 1729–1736.

Zinke, A., & Zeigler, E. (1944). *Zur Kenntnis des Härtungsprozesses von Phenol-Formaldehyd-Harzen, X. Mitteilung*. Berichte Der Deutschen Chemischen Gesellschaft (A and B Series), *77*(**3-4**), 264–272.

Appendix 1: Enhancement of Electrode Performance by a Simple Casting Method Using Sonochemically Exfoliated Graphene

Walch, N.J., Davis, F., Langford, N., Holmes, J.L., Collyer, S.D. & Higson, S.P.J. (2015) "Enhancement of Electrode Performance by a Simple Casting Method Using Sonochemically Exfoliated Graphene", *Analytical Chemistry*, 87(18), pp. 9273–9279.

Enhancement of electrode performance by a simple casting method using sonochemically exfoliated graphene.

Nathan Langford[1], Frank Davis[2], Nik J. Walch[2], Joanne L. Holmes[3], Stuart D. Collyer[4], and [*]Séamus P. J. Higson[5]

[1]*School of Geography, Earth and Environmental Sciences, University of Birmingham, Birmingham, B15 2TT, UK.*

[2]*Cranfield Biotechnology Centre, Cranfield University, Bedfordshire, MK43 0AL, UK.*
[3]*Metrohm UK Ltd, Runcorn, Cheshire, WA7 1LZ UK.*

[4]*Microarray Ltd, Colworth Science Park, Sharnbrook, Bedford, MK44 1LQ, UK.*

[5]*The University of Chichester, College Lane, Chichester, West Sussex, PO19 6PE, UK*

[*] Corresponding author. Tel: +44(0)-1234-758546. Fax: +44(0)-1234-758380. Email address: s.p.j.higson@cranfield.ac.uk

Abstract
We demonstrate within this paper a method for modifying commercial screen-printed electrodes with aqueous graphene suspensions to enhance their electrochemical activity. The graphene suspensions are synthesised by a simple ultrasonic exfoliation method from graphite, where re-aggregation is prevented by the addition of common cationic or anionic surfactants, thereby avoiding the use of organic solvents or harsh chemical procedures. These suspensions can then be simply cast onto the screen-printed electrodes. Cyclic voltammetry with a number of redox active species such as phenols, as well as impedance measurements, were made to characterise these systems. The modified electrodes are shown to demonstrate significantly enhanced electrochemical activity and greatly lowered electron transfer resistances compared to the unmodified electrodes. Initial proof of concept applications of these electrodes, including the detection of heavy metals by absorptive stripping voltammetry, are also shown.

Keywords:
Graphene; screen-printed electrodes; heavy metals; dopamine; phenols

Introduction

Over the last few decades, there has been a dramatic increase in the utilisation of novel forms of carbon within the field of chemical and biochemical sensing. A host of new materials such as fullerenes, carbon nanotubes, carbon dots and graphene have made their appearance in sensors. Currently there is intensive study focussed towards the properties and uses of graphene i.e. carbon in the form of two-dimensional carbon sheets - just one or a few atoms in thickness. Graphene displays a range of interesting properties such as high stiffness and optical transparency as well as high surface area and good electrical conductivity. It is the high surface area and its electrical properties that make graphene a candidate material for enhancing the performance of chemical and biosensors[1].

Graphene was initially produced in small quantities by mechanical exfoliation using adhesive tape[2], however this method only produces small amounts of graphene. Thin layers of graphene can be deposited using such techniques as chemical vapour deposition onto copper[3], allowing the construction of high quality films as large as 30 inches using a roll to roll production system. These types of techniques are however unsuitable for producing gram or kilogram quantities of graphene.

Many methods of producing graphene involve the exfoliation of graphite. Graphite can be oxidised using strong oxidising mixtures such as solutions of nitrate and permanganate in sulphuric acid[4] and the resultant dispersed graphite oxide can then be assembled onto thin films and reduced to graphene by chemical reagents such as hydrazine[5,6], by thermal methods or electrochemical approaches[7,8]. The electrical properties of reduced graphene oxide can however be very different to those of pristine graphene[1].

Ultrasonication has been utilised as a method for exfoliating graphite to give graphene flakes, with for example the ultrasonication of graphite in N-methyl pyrrolidinone giving dilute graphene suspensions[9]. This technique may also be applied to other layered materials such as molybdenum disulphide or boron nitride, however the strong Van der Waals interactions between graphene sheets generally mean only dilute solutions can be obtained. Aqueous dispersions can also be made providing a stabilising agent can be used and these may include common surfactants such as sodium dodecyl sulphate and cetyltrimethylammonium bromide, as well as polymeric materials such as the Pluronic series of surfactants[10], polyethyleneimine[11] and polyvinyl pyrrolidinone[12]. Using these methods it has proved possible to make dispersions containing up to 10 mg ml^{-1} of graphene, which have been shown to be mainly single layer graphene[10]. Recently mechanical exfoliation of graphite has been reported to produce high yields of graphene in aqueous or organic solvent systems[13].

To take advantage of the many distinct properties of graphene, various biosensors based on this material have been recently fabricated[1,14]. It has been demonstrated that modification of glassy carbon electrodes with graphene leads to an increase in oxidation peak currents and the lowering of oxidation overpotentials[15]. The dominance of glucose detection in the biosensors market means that much work has been undertaken on utilising graphene in glucose biosensors. For the detection of glucose, graphene based sensors are usually modified with glucose oxidase (GOD) and this review compares a number of these systems[14]. Comparisons between similar sensors fabricated with graphene oxide and reduced graphene oxide demonstrated much higher sensitivities for the reduced graphene. Electrochemical impedance measurements showed a much higher charge transfer resistance for graphene oxide than its reduced form[16]. Other enzymes that have been immobilised onto graphene electrodes to give electrochemical biosensors include catalase[17], urease[18], horseradish

peroxidase[19] and alcohol dehydrogenase[20]. Much of the work on the fundamental electrochemistry of graphene, and its possibilities for sensing, have been recently reviewed[21, 22].

Another important area under investigation is the development of sensors for the direct detection of small biomolecules without the use of enzymes. Graphene makes an ideal candidate for these electrochemical sensors because of its enhanced electro-catalytic effects and fast electron transfer kinetics, over that of traditional sensor materials. Dopamine is most widely investigated, because its concentration can be directly linked to a number of clinical conditions. Of particular interest is the development of a dopamine electrochemical sensor that can selectively distinguish dopamine even in the presence of uric acid and ascorbic acid, which have overlapping voltammetric responses[23]. Use of a 3D graphene foam combined with cobalt oxide nanowires gave a sensor which could determine glucose at level <25 nM[24]. A number of transition or noble metals combined with graphene have been utilised in similar schemes as reviewed here[1]. Serotonin can also be determined in the presence of dopamine and ascorbate by using reduced graphene oxide modified glassy carbon electrodes and differential pulse voltammetry[25]. Graphene/gold nanoparticle composites could be used to detect the neurotransmitter epinephrine with a limit of detection of 7 nM in the presence of ascorbate[26]. Direct oxidation of the four bases in DNA can also be detected with separate peaks being obtained for each base in both single and double-stranded DNA[15]. More recently, a series of commercial graphene inks suitable for screen-printing have been released and their structure and electrochemical behaviour when deposited as electrodes has been extensively examined, along with their suitability in detecting species such as dopamine, ascorbate and uric acid[27].

Sonochemically exfoliated graphene has been utilised previously for the modification of electrodes with mixed results. Commercial graphene is often mechanically or sonochemically exfoliated and stabilised using surfactants. Some studies have shown that the presence of surfactants can actually be detrimental to electrode performance: for example when using graphene stabilised with sodium cholate, the surfactant has been shown to be detrimental to the oxidation of species such as acetaminophen and NADH[28]. Similar effects have been noted in the construction of graphene based supercapacitors[29], where the presence of sodium cholate can increase the capacitance of these systems compared to unmodified electrodes and mask any changes due to the graphene itself. Other work has shown that graphene can in some cases hinder electron transfer at pyrolytic graphite electrodes, depending on the level of surface coverage[30].

Immunosensors made by coupling antibodies to graphene-modified electrodes have been constructed for immunoglobulins and while a detailed review is beyond the scope of this article, many of these have been previously described[1]. Graphene modified electrodes have also be used in the field of impedimetric immunosensors, and genosensors as previously reviewed here[31]. Immunosensors made by coupling antibodies to graphene-modified electrodes have been constructed for immunoglobulins[1]. Antibodies have been coupled to a graphene sheet/methylene blue composite for the detection of prostate specific antigen. Methylene blue has an efficient absorption profile for antigens and shows improved electrical activity in the presence of graphene; sensors built using this methods show a detection limit of 13 $pgml^{-1}$[32]. Sensors fabricated using graphene/silver nanoparticles/carbon nanotubes composites could be used for the detection of chorionicgonadotropin[33]. Graphite could be sonochemically exfoliated in the organic solvent N-methyl pyrrolidinone to give suspensions which when deposited onto glassy carbon electrodes demonstrated enhanced detection of a

variety of analytes[34]. Other workers exfoliated graphite in water-ethanol mixtures to give graphenes of various thicknesses which could be applied to screen-printed carbon electrodes and used to measure the concentration of hydrogen peroxide[35].

The rationale behind this research was the challenge that biosensors can be very difficult to regenerate and also if used for analysis of physiological samples, can be subject to biofouling. One solution is of course the use of inexpensive, single-shot biosensors such as used in glucose monitoring. We therefore have attempted to combine the use of a simple ultrasonic method for generating graphene coatings with uncharged, anionic or cationic surfactants without the need for harsh chemicals or organic solvents[10], with the use of inexpensive screen-printed electrodes and simple casting methods.

Materials and methods

Chemicals, equipment and electrodes

Sodium dodecyl sulphate (SDS) and graphite powder (general purpose grade) were supplied by Fisher (UK). Cetyltrimethylammonium bromide (CTAB) dopamine, catechol, hydroquinone, potassium ferrocyanide, potassium ferricyanide, ferrocene carboxylic acid (FCA), cupric chloride, lead acetate and mercury chloride were obtained from Sigma-Aldrich Chemical Company (Gillingham, UK). The phosphate buffer solution (PBS) consisted of 18.9 g of $Na_2HPO_4.12H_2O$, 1.79 g H_2NaPO_4, and 0.29 g NaCl, supplied by Fisher (UK) and dissolved in 1 L of deionised water from a Milli-Q water purifier (Millipore).

All screen printed electrodes were supplied by Microarray Ltd. The electrodes consisted of 2 identical DuPont 7102 carbon working electrodes (which meant it was possible to have a modified and control electrode on the same platform), a carbon counter electrode, and a silver/silver chloride reference electrode (DuPont Ink 5874) together with DuPont 5108 dielectric. Electrodes are printed on a polycarbonate substrate (0.5 mm thick) and the area of each working electrode is 21.78 mm^2.Figures 2 and S1 (supplementary information) show the layout of the electrodes and their formulation. The use of the four electrode system allows one working electrode to be treated with graphene whilst the other remains as an internal unmodified control. A Thermo Scientific Megafuge 160 was used for centrifugation of samples. UV/Vis spectra were obtained using a Shimadzhu UV-2101PC spectrometer, particle sizing was undertaken with a Zetasizer 3000 (Malvern Instruments, UK) which measures particle sizes from below a nm to several µm using dynamic light scattering. Atomic force microscopy was carried out with a Bruker Dimension 3100 AFM and scanning electron microscopy (SEM) with a FEI XL30 ESEM and FEI XL30 SFEG. Freeze-drying was carried out using a Scanvac Coolsafe system (LaboGene ApS Industrivej, Lynge, Denmark).Raman studies were carried out using a Renishaw-InVia Raman microscope (laser wavelength: 532 nm) on freeze-dried graphene samples.

Sonochemical production of graphene and characterisation.

Sonochemical formation of graphene has been previously reported[9, 10, 34, 35]. Our procedure was based on a batch production method using surfactants previously described[10]. For graphene production, an ultrasonic horn operating at 20 kHz with a power output of 100 W (Branson Digital Cell Disruptor, 250 series) was used. In a typical synthesis 200 ml of water, 2 g of graphite powder, and 43.5 mg of CTAB were combined. The concentration of CTAB (0.6 mM) is such to reduce the surface tension of the water to 41 mJ m^{-2}, which is the surface free energy of graphene, previous reports[10] have shown this to be the optimal surface tension. The concentration of SDS, (to produce negatively charged graphene), needed to achieve this tension is 7 mM. The mixture of graphite and surfactant in water was then placed

under a sonicating horn with the probe depth being 1.5-2 times the diameter of the probe tip for optimal sonication efficiency. The mixture was then left under sonication (100 W) for 5 minutes. During sonication, the surface area of the graphite/graphene will greatly increase, due to the ablation of graphene sheets from the graphite. This causes the surfactant to be adsorbed from the solution onto the surface of the graphene, raising the surface tension. After 5 minutes, the majority of the surfactant had been adsorbed onto the ablated sheets, and the sonication probe was turned off. Another batch of surfactant, equal to the first is then added to the mixture to lower the surface tension to the desired value again, and the sonication repeated. This process is repeated a total of 30 times.

After sonication, the resulting solution is then centrifuged at 3500RPM for 15 minutes, to remove any large or aggregated particles and the supernatant containing the graphene was syphoned off. The resultant suspensions were stable for at least several months at room temperature. It also proved possible to increase the concentration of the graphene by freeze drying the suspensions with the resultant solid material being able to be easily re-dispersed in water by sonication for a few minutes.

Modification and characterisation of electrodes

The graphene coated electrodes were prepared by pipetting 10 µL of graphene solution onto one of the two working electrodes (the untreated working electrode was used as a control). The solution was then left to air dry for several hours. After the drying period, the electrodes were immersed in deionised water to wash away any remaining surfactant. A similar casting method onto a silicon wafer was used to formulate samples for AFM and SEM.

Cyclic voltammetry was carried out using a Sycopel AEW-2 Potentiostat (Sycopel Ltd, Newcastle-Upon-Tyne) for all electrochemical studies: current/charge transients were recorded using a PC with dedicated software.CV measurements were performed between -800 and +800 mV at a scan rate of 50 mVs^{-1} unless otherwise stated. Adsorptive stripping voltammetry (ASV) was performed by firstly removing any oxidisable material from the electrode by polarising at +1 V for one minute, then depositing trace metal species by polarising the electrode at -1 V for five minutes and finally sweeping at 50 mV s^{-1}back to +1 V (vs. Ag/AgCl) to strip the metal. AC impedance measurements were performed using a Gill ACM Auto AC DSP frequency response analyser and potentiostat (Cark, UK) linked to a PC. For AC measurements a mixed solution of 5 mM each of $K_3Fe(CN)_6$ and $K_4Fe(CN)_6$ in PBS was used. The AC signal amplitude was 10 mV, the frequency range 1 Hz-10 kHz and a DC offset of 120 mV vs. Ag/AgCl was applied. A small AC perturbation, 10 mV or less is used since current-voltage relationship is often linear only for such amplitudes and also will not disrupt the probe layer. The DC bias is applied since the impedance of the system as a whole is lowest at the formal potential of the ferri/ferrocyanide couple (120 mV).

Results and discussion

Characterisation of graphene

UV-visible spectra of graphene solutions exhibited the expected peak at approximately 265 nm, indicating that for both CTAB and SDS treated graphite, exfoliation produced graphene[9] solutions as concentrated as 0.2 mg ml^{-1} were obtained using our modified protocol[10]. Analysis of Zetasizer results indicated an average particle size of 117 nm for the SDS dispersed samples (G-) and 278 nm for the CTAB samples (G+). Raman studies (Figure S2, supplementary information) clearly demonstrated the formation of graphene as was also shown by the original developers of our experimental protocol[10]. The Raman spectra indicate the formation of single or few layer graphene with the presence of some defects[36].

The Zetasizer models assumes that the particles are spherical, however a more accurate measurement of particle size was obtained using AFM and SEM. Figure 1 shows SEM and AFM images of G- cast onto a silicon wafer. As can be seen, the particle sizes are approximately as predicted by the Zetasizer measurements. Using the AFM it is possible to measure the thickness of the graphene flakes (Figure 1c). Most of the flakes are under 5 nm in thickness and some under 1 nm indicating that we have single or few layer graphene; unfortunately it is not possible calculate how much of the thickness is due to the adsorbed surfactants.

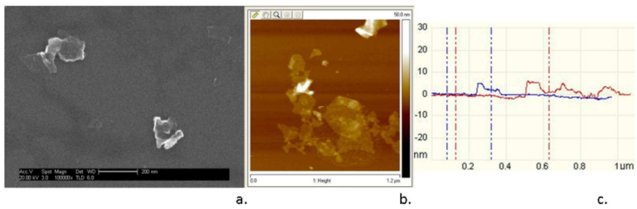

Figure 1. (a) SEM and (b) AFM measurements of sonicated graphene on silicon (c) height measurements across the silicon wafer.

Impedance of graphene modified electrodes

AC impedance measurements were made of both graphene-modified and unmodified working electrodes and the Nyquist plots are displayed in Figure 2. There is a large and obvious difference between the electrodes when studied under AC impedance, showing that the graphene enhanced electrodes demonstrate a much higher conductance than the unmodified electrodes. The electron transfer resistance can be calculated from the semi-circle width of the Nyquist plots and demonstrates that the electron transfer resistance of the graphene-modified electrodes is over 50 times less than that of the unmodified carbon.

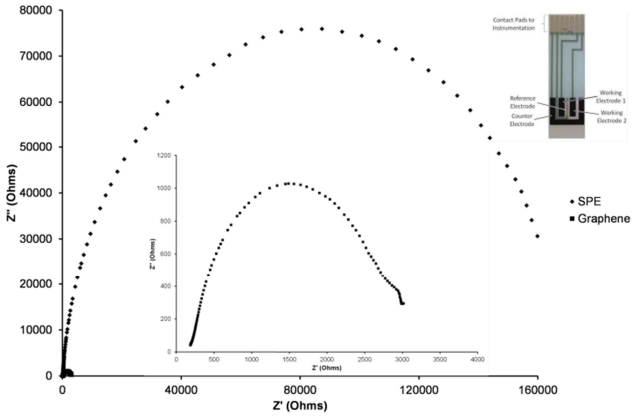

Figure 2.Nyquist plots of screen-printed carbon electrodes, with and without graphene, in ferri/ferrocyanide solution (PBS). Insets show the Nyquist plot of the graphene electrode and the format of the screen-printed electrodes. Inset: Nyquist plots of the graphene electrode on an expanded scale.

Cyclic voltammetry of graphene modified electrodes in different redox couples

Figure 3 shows cyclic voltammograms of both electrode systems in 1 mM solutions of FCA and three phenolic redox couples. As shown, in all cases the graphene modified electrodes display an enhanced sensitivity as exhibited by the increased peak current values compared to those obtained for the same solution using the unmodified screen-printed electrodes. There are also noticeable shifts in the position of the peak (ΔE_p), with the oxidation peaks showing lower over-potentials on the graphene modified electrodes. Also ΔE_p is lowered for the

modified electrodes and the peaks are noticeably sharper. This is consistent with results obtained by other workers[15] and indicates that graphene modified electrodes are more electroactive than their unmodified counterparts. Obvious explanations for this include the enhanced conductivity of the graphene and also its larger surface area to volume ratio compared to graphite since it has been exfoliated into thin sheets. Table 1 shows the enhanced currents and narrower peak separations obtained by modifying screen-printed carbon electrodes with graphene.

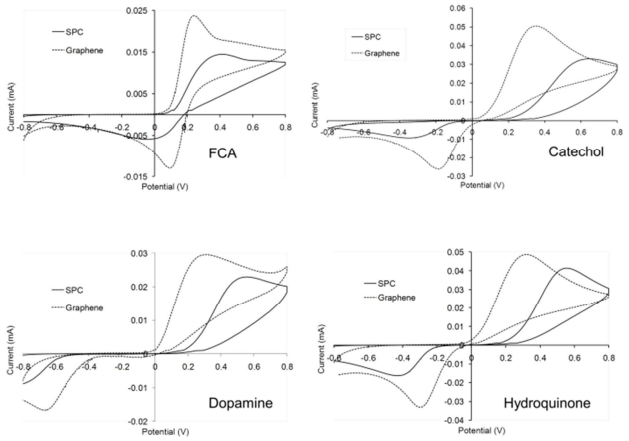

Figure 3.Cyclic voltammograms of 1 mM solutions in PBS of FCA, catechol, dopamine and hydroquinone.

Analyte & Electrode	Oxidative Peak Position	Reductive Peak Position	Peak Separation
Screen Printed Carbon			
FCA	417 mV, 0.0145 mA	-47 mV, -0.00594 mA	464 mV
Dopamine	537 mV, 0.0229 mA	-910mV, -0.00890 mA	1447 mV
Hydroquinone	547 mV, 0.0414 mA	-412 mV, -0.0162 mA	959 mV
Catechol	653 mV, 0.0239 mA	-335 mV, -0.00919 mA	988 mV
Graphene Coated Carbon			
FCA	241 mV, 0.0237 mA	91 mV, -0.0129 mA	150 mV
Dopamine	281 mV, 0.0294 mA	-645 mV, -0.0159 mA	926 mV
Hydroquinone	312 mV, 0.0485 mA	-282 mV, -0.0329 mA	594 mV
Catechol	333 mV, 0.0502 mA	-178 mV, -0.0261 mA	511 mV

Table 1: Peak positions and separation of carbon and graphene CV peaks in 1 mM phenolic or FCA solutions. Experiments were run in triplicate and in all cases SDs of <5% were observed.

Attempts were made to optimise the amounts of graphene used for electrode modification. Freeze dried graphene was re-dispersed in water and diluted to give a range of concentrations and 10 µL of each solution cast onto screen-printed carbon electrodes as previously described. CVs were then run for all the electrodes in 1 mM dopamine solution. A slower scan rate (10 mV s^{-1}) was employed to permit enhanced signal differentiation. Figure 4 shows the obtained CVs and also the changes of oxidation peak current and ΔE_p for differing graphene concentrations. As can be seen there appears to be a steady increase of peak current and decrease in peak separation up to a concentration of 0.2 mg ml^{-1}, with the effect of higher concentrations tending towards a plateau after that and 0.2 mg ml^{-1} was therefore used as the optimum graphene concentration. At this concentration and using just 10 µL of solution, this corresponds to 2 µg per electrode. Taking the weight of single layer graphene to be 0.77 mg m^{-2} as commonly reported[37], if we assume that our graphene is of this type, this would correspond to an area of 2600 mm^2, much greater than the surface area of the electrode (21.78 mm^2). Previous workers[30] have described graphene coverage and effects on electrochemical activity as being either zone 1 (incomplete coverage of the substrate) or zone 2 (complete coverage with build-up of multilayers); our system is clearly in zone 2.

The graphene could form a number of structures on the electrode surface, from a compact layered structure to a much more porous open structure. Unfortunately there is insufficient contrast between graphene and the underlying screen-printed electrode to clearly distinguish the graphene rescheduling SEM. Further work is investigating different electrodes and deposition methods in an attempt to determine and control the graphene structure.

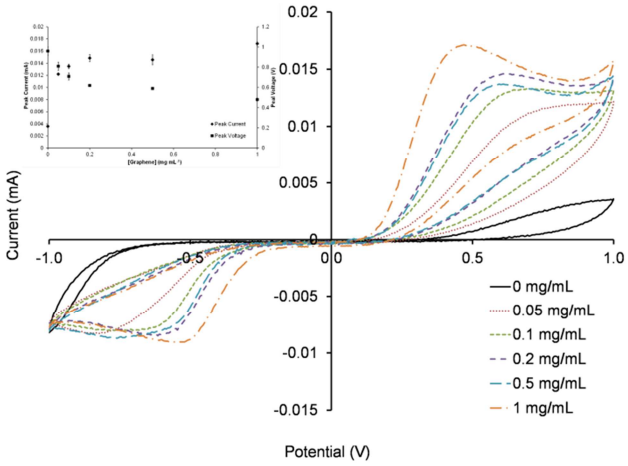

Figure 4.Cyclic voltammograms of 1 mM dopamine solutions in PBS utilising electrodes constructed using different graphene concentrations. Inset: effect of graphene concentration on oxidative peak current and peak potential.

Since previous workers have reported surfactants to have a major effect, in some cases being the source for perceived enhancements in graphene-treated electrodes, controls were run by treating the electrodes with 5µL concentrated CTAB solution (50 mg ml^{-1}). As can be seen in Figure 4 this led to some increase in peak current but much smaller than observed for graphene/CTAB composites and no shift in peak potential. A lower concentration (6.5 mg ml^{-1}) showed minimal differences between a treated and an untreated electrode. This demonstrates that in our systems, the surfactant only has a small effect. Addition of a freshly shaken graphite solution to the electrode and drying was attempted as a control but on placing in test solutions the graphite could visually be seen to detach from the electrode and had minimal effects on electrochemical performance.

Cyclic voltammograms obtained for graphene modified electrodes in 1 mM dopamine taken immediately after and one hour after continuous immersion in the solution showed only minimal differences, indicating that the graphene modification was stable over this time period, well in excess of that required for any measurements to be made.

A series of voltammograms for FCA at different scans rates were also made (Figure 5 shows the results for graphene modified electrodes) and clearly demonstrate good electro-chemical behaviour with the peak current being proportional to the square root of the scan rate, with a similar trend also being found for unmodified electrodes. The inset (Figure 5) shows good linear correlation of peak current with the square root of scan rate for both electrodes (R^2>0.995). This suggests that a possible limiting factor of the electro-chemical response of the graphene modified systems is the underlying carbon system itself and not the graphene layers per se.

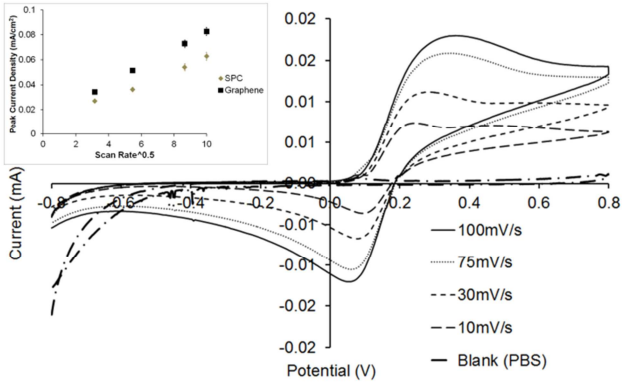

Figure 5.Cyclic voltammograms of 1 mM solutions of FCA in PBS at differing scan rates.

Absorptive stripping voltammetry of graphene modified electrodes

Heavy metals are a major environmental threat, especially when waterborne and are commonly produced by mining areas as well as being naturally present in some parts of the world, such as mercury contamination of the environment in small gold mining communities[38]. The use of graphene modified electrodes for the detection of a range of heavy metals has been recently reviewed[39]. For example graphene-Nafion composites could be used for the anodic stripping voltammetric detection of lead and cadmium[40] and in further work was extended to the detection of copper and zinc[41]. However other workers have again reported that the use of surfactant (sodium cholate) stabilised graphene, inhibited the stripping transition of cadmium metal to the ion and greatly reduced any peaks corresponding to this step[42]. We therefore report preliminary studies on the use of graphene-modified electrodes for the detection of three potential contaminants, namely copper, lead and mercury. It was suggested that graphene stabilised with an anionic surfactant would be more effective at binding metal ions and therefore graphene stabilised with SDS was produced. However SDS proved to be less effective as an exfoliating agent using our methodology and a solution containing 0.05 mg ml^{-1} graphene was obtained.

In ASV, the electrode is initially cleaned by polarising at 1V to remove oxidisable material and then polarised at -1V. This causes metal ions in solution to be reduced to the metal at the electrode surface. The polarisation is then increased at a controlled rate and each individual metal is oxidised at a specific potential, the resultant current giving a measure of the concentration of the individual metal species[43]. A range of individual metal ion solutions were produced and analysed by ASV. It is worth noting that as of yet we have not performed a conclusive study of the concentration / electrochemistry or optimised the metal deposition and stripping procedure - and we intend this work to follow on in subsequent publications. However by comparing measurements obtained by the differing systems described herein, with the same concentrations of metal ions, it was once again obvious that the presence of graphene greatly enhanced the electrochemical detection of these species. An example of this is demonstrated in Figure 6 which shows the ASV of a solution containing 1 ppm each of the three metal ion species. As can be seen, both the anionic and cationic graphene modified electrodes display enhanced stripping currents for each of the metallic ions when compared to the unmodified electrodes. This demonstrates the potential for this simple treatment protocol to enhance the sensitivity of electrochemical detection of heavy metal pollutants.

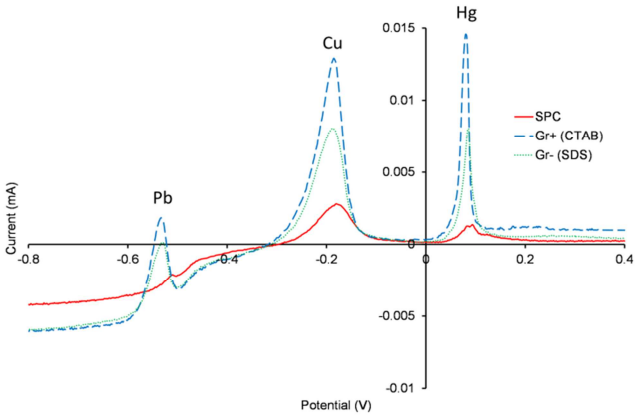

Figure 6. Absorptive stripping voltammograms on control, G- and G+ modified screen printed carbon in 1 ppm solutions of Cu^{2+}, $Hg^{2+}$and Pb^{2+} in 0.1 M HCl.

Conclusions

We have developed a relatively simple protocol for sonochemical fabrication of graphene and its application by casting onto screen-printed electrodes. The resultant electrodes displayed lower electron transfer resistance and higher electrochemical activity when compared to the unmodified base screen printed electrodes. When used with ferrocene or phenolic redox active species, enhanced currents, reduced peak separation and lower oxidation potentials were apparent and no depreciation in electro-chemical behaviour was noted even after 1 hour continuous immersion. The graphene modified electrodes also displayed enhanced performance assessed for simultaneous detection of three toxic heavy metal species. The simplicity of the procedure, use of inexpensive screen-printed electrodes and modification techniques, as well as no requirement for harsh chemicals or organic solvents, suggest these systems have scope for use in single-shot ‘point of care’ or environmental monitoring applications.

Acknowledgement

The authors would like to acknowledge Dr Alex Skordos and Dr Christine Kimpton for AFM/SEM studies and Dr Isaac Chang and Dr Shei Su of the University of Birmingham for Raman measurements.

Supporting Information Available. This information is available free of charge via the Internet at http://pubs.acs.org/.

References

(1) Fang, Y.; Wang, E. *Chem. Commun.***2013,** *49*, 9526-9539.
(2) Novoselov, K. S.; Geim, A. K.; Morozov, S. V.; Jiang, D.; Zhang, Y.; Dubonos, S. V.; Grigorieva, I. V.; Firsov, A. A. *Science*,**2004**, *306*, 666-669.
(3) Bae, S.; Kim, H.; Lee, Y.; Xu, X. *et al*, *Nature Nanotech.* **2010,** *5*, 574-578.
(4) Hummers, W. S.; Offeman, R. E. *J. Am. Chem. Soc.***1958**, *80*, 1339.
(5) Fowler, J. D.; Allen, M. J.; Tung, V. C.; Yang, Y.; Kaner, R. B.; Weiller, B. H. *ACS Nano*, **2008,** *3*, 301-306.
(6) Tung, V. C.; Allen, M. J.; Yang, Y.; Kaner, R. B.*Nat. Nanotechnol.***2009,** *4*, 25-29.
(7) Kauppila, J.; Kunnas, P.; Damlin, P.; Viinikanoja, A.; Kvarnström, C. *Electrochim. Acta*,**2013,** *89*, 84-89.
(8) Huang, D.; Zhang, B.; Zhang, Y.; Zhan, F.; Xu, X.; Shen, Y.; Wang, M. *J. Mater. Chem. A*, **2013,** *1*, 1415-1420.
(9) Coleman, J. N.; Lotya, L.; O'Neill, A.; Bergin S. D. *Science*,**2001,** *331*, 568-571.
(10) Notley, S. M. *Langmuir*,**2012**, *28*, 14110-14113.
(11) Sham, A. Y. W.; Notley, S. M. *Langmuir*,**2014,** *30*, 2410-2418.
(12) Bourlinos, A. B.; Georgakilas, V.; Zboril, R.; Steriotis, T.A.; Stubos, A.K.; Trapalis, C. *Solid State Comm.***2009,** *149*, 2172-2176.
(13) Paton, K. R.; Varrla, E.; Backes, C.; Smith, R. J.; Khan, U.; O'Neill, A. *et al*. *Nature Mat.***2014,** *13*, 624–630.
(14) Wu, S.; He, Q.; Tan, C.; Wang, Y.; Zhang, H. *Small*, **2013**, *9*, 1160 -1172.
(15) Zhou, M.; Zhai, Y.; Dong, S. *Anal. Chem.***2009**, *81*, 5603-5613.
(16) Casero, E.; Parra-Alfambra, A. M.; Petit-Domínguez, M. D.; Pariente, F.; Lorenzo, E.; Alonso, C. *Electrochem. Comm.***2012,** *20*, 63-66.
(17) Huang, K. J.; Niu, D. J.; Liu, X.; Wu, Z. W.; Fan, Y.; Chang, Y. F.; Wu,Y. Y. *Electrochim.Acta*, **2011,** *56*, 2947-2953.
(18) Srivastava, R. K.; Srivastava, S.; Narayanan, T. N.; Mahlotra, B. D.; Vajtai, R.; Ajayan, P. M.; Srivastava, A. *ACS Nano*, **2011,** *6*, 168-175.
(19) Zhang, Q.; Yang, S.; Zhang, J.; Zhang, L.; Kang, P.; Li, J. *et al*.*Nanotechnology*, **2011,** *22*, 494010.
(20) Prasannakumar, S.; Manjunatha, R.; Nethravathi, C.; Suresh, G. S.; Rajamathi, M.; Venkatesha, T. V.; *J. Solid State Electrochem*. **2012,** *16*, 3189-3199.
(21) Brownson, D. A. C.; Kampouris. D. K.; Banks, C. E. *Chem. Soc. Rev.* **2012**, *41*, 6944–6976.
(22) Pumera, M. *The Chemical Record*, **2009**, *9*, 211–223.
(23) Kim, Y. R.; Bong, S.; Kang, Y. J.; Yang, Y.; Mahajan, R. K. J. S.; Kim, H. *Biosens. Bioelec.* **2010**, *25*, 2366-2369.
(24) Dong, X.-C.; Xu, H.; Wang, X.-W.; Huang, Y.-X.; Chan-Park, M. B.; Zhang, H.; Wang, L.-H.; Huang,W.; Chen, P. *ACS Nano*, **2012,** *6*, 3206-3213.
(25) Kim, S. K.; Kim D.; Jeon, S. *Sens. Actuators, B*, **2012**, *174*, 285-291.
(26) Cui, F.; Zhang, X. *J. Electroanal. Chem.* **2012**, *669*, 35-41.
(27) Randviir, E. P.; Brownson, D. A. C.; Metters, J. P.; Kadara, R. O.; Banks,C. E. *Phys. Chem. Chem. Phys.* **2014,** *16*, 4598-4611.
(28) Brownson, D. A. C.; Metters, J. P.; Kampouris, D. K.; Banks, C. E. *Electroanalysis*, **2011**, *23*, 894-899.
(29) Brownson, D. A. C.; Banks, C. E. *Chem. Commun.* **2012**, *48*, 1425-1427.
(30) Brownson, D. A. C.; Munro, L. J.; Kampouris, D. K.; Banks, C. E.*RSC Advances*, **2011**, *1*, 978–988.
(31) Bonanni, A.; Loo, A. H.; Pumera, M. *Trends Anal. Chem.***2012**, *37*, 12-21.
(32) Mao, K.; Wu, D.; Li, Y.; Ma, H. *et al*, *Anal. Biochem.* **2012**, *422*, 22-27.

(33) Lu, J.; Liu, S.; Ge, S.; Yan, M.; Yu, J.; Hu, X. *Biosens. Bioelec.* **2012**, *33*, 29-35.
(34) Wu, C.; Cheng, Q.; Wu, K.; Wu, G.; Li. Q. *Anal.Chim.Acta*, **2014**, *825*, 26-33.
(35)Chia, J. S. Y.; Tan, M. T. T.; Khiew, P. S.; Chin, J. K.; Lee, H.; Bien, D.C.S.; Siong, C. W.*Chem. Eng. J.* **2014**, *249*, 270-278.
(36) Ferrari, A. C.; Basko, D. M. *Nat. Nanotech.* **2013**, *8*, 235-246.
(37) Kong, E. S. W.; Nanomaterials, Polymers and Devices: Materials Functionalization and Device Fabrication: Industrial Applications of Smart Materials, Wiley-Blackwell: New York, 2015.
(38) Gibb, H.; O'Leary.K. G. *Environ. HealthPersp.* **2014**, *122*, 667-672.
(39) Chang, J.; Zhou, G.; Christensen, E. R.; Heideman, R.; Chen, J. *Anal.Bioanal. Chem.***2014**, *406*, 3957-3975.
(40) Li, J.; Guo, S. J.; Zhai, Y. M.; Wang, E. K. *Anal.Chim.Acta*, **2009**, *649*, 196-201.
(41) Willemse, C. M.; Tlhomelang, K.; Jahed, N.; Baker, P. G.; Iwuoha, E. I. *Sensors*, **2011,** *11*, 3970-3987.
(42) Brownson, D. A. C.; Banks, C. E. *Electrochem. Comm.***2011**, *13*, 111-113.
(43) Baron-Haines, J.; Joya, M.R.; Barba-Ortega, J.; Anodic stripping voltammetry (ASV) for the determination of heavy metals, J. Phys. Conf. Ser., 2013, *466*, 012023.

Appendix 2: Characterisation of thin films of graphene-surfactant composites produced via a novel semi-automated method.

Walch, N.J., Nabok, A., Davis, F. and Higson, S.P.J. (2016) “Characterisation of thin films of graphene–surfactant composites produced through a novel semi-automated method”, *Beilstein Journal of Nanotechnology,* 7, pp. 209–219.

Characterisation of thin films of graphene-surfactant composites produced via a novel semi-automated method.

Nik J. Walch[1*], Alexei Nabok[2], Frank Davis[1], & Séamus P. J. Higson[1, 3]

[1]Cranfield Biotechnology Centre, Cranfield University, College Road, Cranfield, MK43 0AL, UK

[2]Sheffield Hallam University, Materials & Engineering Research Institute, Howard Street, S1 1WB, UK

[3]The University of Chichester, College Lane, Chichester, West Sussex, PO19 6PE, UK

[*] corresponding author, e-mail: N.J.Walch@Cranfield.ac.uk

Abstract

In this paper we detail a novel semi-automated method for the production of graphene by sonochemical exfoliation of graphite in the presence of ionic surfactants, e.g. sodium dodecyl sulfate (SDS) and cetyl trimethylammonium bromide (CTAB). The formation of individual graphene flakes was confirmed by Raman spectroscopy, while the interaction of graphene with surfactants was proven by NMR spectroscopy. The resulting graphene-surfactant composite material formed a stable suspension in water and some organic solvents, such as chloroform; graphene thin films were then produced using Langmuir-Blodgett (LB) or electrostatic layer-by-layer (LbL) deposition techniques. The composition and morphology of the films produced was studied with SEM-EDX and AFM; the best results in terms of adhesion and surface coverage were achieved using LbL deposition of graphene(-)SDS alternated with poly-ethyleneimine (PEI). The optical study of graphene thin films deposited on different substrates was carried out using UV-vis absorption spectroscopy and spectroscopic ellipsometry. A particular focus was on studying graphene layers deposited on gold-coated glass using a method of total internal reflection ellipsometry (TIRE) which revealed the enhancement of the surface plasmon resonance in thin gold films by depositing graphene layers.

Keywords: characterization; ellipsometry; graphene; ^{1}H-NMR; surfactant.

1. Introduction

Since its initial discovery and development by Novoselov *et al*. [1] graphene has been of great interest to the scientific community due to its interesting optical and electrical properties. Graphene is defined as a single layer of sp^2 hybridised carbon with no 3rd dimension. The double bonded structure of graphene is responsible for the electrical properties of the material as the movement of π-bonds between adjacent carbon atoms can be used to transmit an electrical current. Because of this electrical activity in particular, graphene is being examined as a base material in a number of different applications including sensor applications, for use in flexible electronics [2] and graphene based printable inks for printed electrical circuits [3].

Graphene has reportedly been produced in a number of different ways. The method chosen for this research is by sonochemical exfoliation in water in the presence of a surfactant, as first reported by Notley *et al.* [4]. This method was chosen for a number of reasons; firstly, it does not require the use of hazardous chemicals such as sodium nitrate, sulfuric acid,

potassium permanganate and hydrazine hydrate, which are used in the oxidation of graphite to graphite oxide and then reduction to graphene [5], and secondly it guarantees single-layer or few-layer graphene, rather than the potential for larger products or graphene sheets with an uneven size distribution that might be produced in other techniques such as mechanical exfoliation (the "scotch tape" method). The sonochemical method was carried out using a semi-automated apparatus designed specifically for the purposes of this research.

In previous work [6] we manufactured graphene surfactant complexes using the Notley method and applied them to carbon electrodes, thereby enhancing their electrochemical activity. Further work was then carried out on optimising graphene production, characterising the products and also depositing graphene layers by more controlled techniques than simple casting.

In this work a semi-automated technology of graphene production by sonochemical exfoliation of graphite in the presence of ionic surfactants is described in detail. The composite graphene-surfactant materials produced were characterised with NMR and Raman spectroscopy to confirm the formation of graphene. Thin films of graphene composites were deposited using the techniques of Langmuir-Blodgett (LB) and electrostatic layer-by-layer (LbL) deposition. Films composed of these new graphene composite materials were then characterised using SEM, AFM, and spectroscopic ellipsometry. The study of SPR in gold films coated with graphene using total internal reflection ellipsometry was carried out for the first time.

2. Methods

2.1 Semi-automated sonochemical exfoliation of graphene.

Two different surfactants were used to synthesise graphene-surfactant complexes; sodium dodecyl sulphate (SDS) and cetyl trimethylammonium bromide (CTAB). Firstly the surfactant solutions were prepared by dissolving in water. The SDS solution was made to a concentration of 462.9 mg ml^{-1} while the CTAB solution concentration was made up to 49.7 mg ml^{-1}. These solutions were prepared and then placed into a water bath heated to 50^{o}C to aid dissolution.

Once dissolved, the surfactant solution was placed into the surfactant reservoir of the synthesiser. This solution was then pumped into the reactor during synthesis at a rate of 35 μL min^{-1} giving an addition rate of 16.2 mg min^{-1} for the SDS and 1.74 mg min^{-1} for the CTAB. The addition rate was crucial to maintain a surface tension of 41 mJ m^{-2}, which is both the optimum surface tension for graphene production and also the surface free energy of graphene. The graphite suspension (10 - 50 %) was then placed into the reactor, and sonicated continuously for 120 minutes at a power of 50 W. A total of 3.15 ml of surfactant solution was added in each case over the course of the synthesis. The sonication step was carried out in a fume cabinet, as an aerosol containing potentially harmful graphene nanoparticles is produced at this stage. A schematic diagram of this apparatus is shown below (Figure 1).

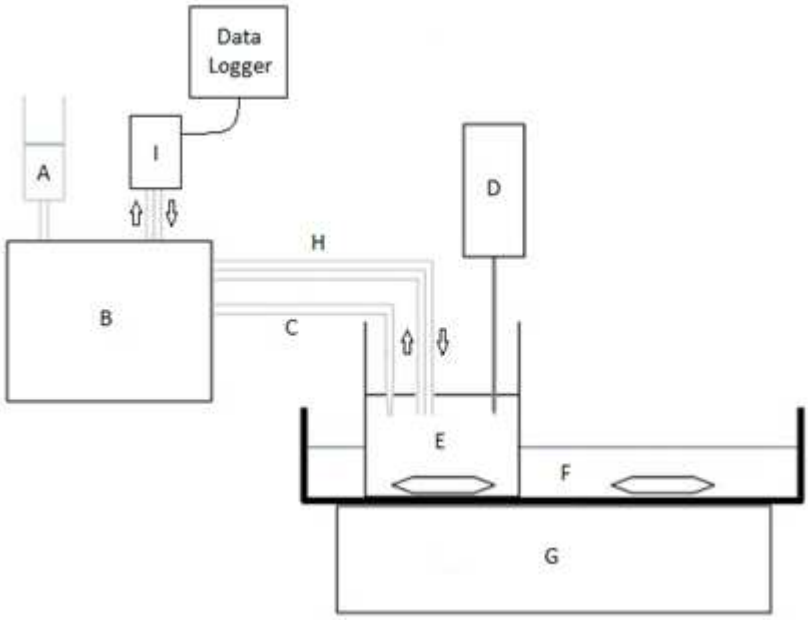

Figure 1. A schematic diagram of the apparatus used to synthesis graphene. (A) surfactant solution, (B) peristaltic pump, (C) heat, (D) ultrasonic probe, (E) reactor, (F) water, (G) magnetic stirring unit, (H) sampling loop, and (I) photometric flow cell.

The apparatus was designed to alleviate the time constraints of the Notley method. In that method, solid surfactant must be added every 5 minutes whilst continuous sonication is carried out. This method with its continuous addition of aqueous surfactant eliminates the need for constant supervision of the process as well as providing the reproducibility of automation. This is only semi-automated, however, as full automation would require the monitoring of surface tension throughout the synthesis as well as automatic adjustments to the surfactant flow rate to maintain this at the required level of 41 mJ m^{-2}.

Figure 1 depicts the assembled apparatus, the function of which is explained here. The aqueous suspension of graphite is placed into the reactor (E). The graphite is kept in suspension throughout the procedure using a magnetic stirrer (G). The ultrasonic probe (D) operating at a power of 50 W, penetrates approximately 1 cm into the graphite suspension. The surfactant solution (A) is pumped into the reactor via a peristaltic pump (B). The reservoir containing the surfactant and the tubing carrying it to the reactor are heated to 50^{o}C in a water bath (C) to prevent precipitation of the surfactant from solution in the tubing. A water trough (F) is used as a heat sink to dissipate any heat produced in the reactor during synthesis, as the tip of the ultrasonic probe can reach temperatures of up to 100^{o}C during continuous operation. The heat sink is stirred continuously, also using the magnetic stirrer (G), to maximise cooling efficiency.

A sampling loop (H) continuously cycles the liquid contents of the reactor through a photometric flow cell (I) which determines the concentration of graphene by measured absorbance at 650 nm. The concentration data is then recorded using a data logger.

Upon completion of the 120 minute cycle, the contents of the reactor were removed and placed into a 50 ml centrifuge tube and spun at 3500 RPM for 20 minutes. The supernatant was then removed and the pellet (containing mostly unreacted graphite as well as some precipitated graphene) was re-suspended in 40 ml of deionised water. This was then

centrifuged at 3500 RPM for 20 minutes. This process was repeated until no more graphene was contained in the supernatant. If a dry sample was required, then the graphene suspension was frozen and then placed into a freeze dryer (Labogene) for 3 – 4 days (depending on the sample size) and then subsequently into a vacuum oven at 70^{o}C overnight to remove all traces of water.

2.2 Characterisation of graphene-surfactant composite material

Graphene-surfactant complexes were characterised by a range of different techniques. The presence of graphene was determined by Raman microscopy.

The concentration of graphene in solution was obtained by spectrophotometry. The absorbance of a graphene solution at 650 nm wavelength was determined and the Beer-Lambert law applied, using an extinction coefficient of 13.9 mg ml^{-1} cm^{-1} [7].

The interaction of the surfactant with the graphene surface was also analysed using NMR spectroscopy. Dried graphene-surfactant complex was dissolved in D_2O and placed into an NMR tube. Another tube containing the surfactant alone was also prepared. Both were scanned individually and then the spectra were compared to show shift in peak position corresponding to interaction between the surfactant and the graphene. NMR experiments were performed on a Bruker 400 MHz spectrometer running topspin analysis software. This analysis works according to the Nuclear Overhauser Effect (NOE). The NOE, which is present in nuclear magnetic resonance (NMR) spectroscopy, can be used to determine the amount of contact between the surfactant and the graphene sheet. This is achieved by observing peak shifting which occurs when two nuclei are within 5 Å of each other.

The dried graphene sample was deposited onto a glass microscope slide and then scanned using a Renishaw In-Via Raman microscope at an excitation wavelength of 532 nm. Data were recorded between 100 – 3200 cm^{-1}.

2.3 Deposition of thin films of graphene-surfactant composites.

2.3.1 Langmuir-Blodgett and Langmuir-Schaefer deposition

Both composite materials obtained, e.g. Graphene(+)CTAB and Graphene(-)SDS, appeared to be soluble in water due to the presence of ionic groups, NH_3^+ and SO_2^- respectively. Yet, the presence of alkyl chains and π-systems facilitated their solubility in chloroform, hence the use of Langmuir-Blodgett (LB) technology (Nima 610 trough) was an obvious choice for thin films deposition. The standard LB procedure was applied [8]: 1 mg ml^{-1} solution of graphene(+)CTAB in chloroform was spread onto the surface of deionised water (Millipore). Surface pressure was then recorded using a Wilhelmy plate based sensor. Because of the unknown ratio of graphene / surfactant within the complex the area per molecule (or repeated unit) was difficult to calculate, so the area was presented in actual units of cm^2.

Another method known as Langmuir-Shaefer (LS) deposition [9]; where the hydrophilic substrate is held horizontally to the assembled monolayer and then lowered slowly to gently touch water surface; the monolayer is then transferred onto the substrate surface was also used to prepare monolayer films.

Organised monolayer films obtained in this fashion were then characterised by AFM (Nanoscope III) operating in tapping mode using Veeco cantilevers with silicon nitride tips having a radius of less than 10 nm.

2.3.2 Electrostatic LbL deposition

Much better results (in terms of adhesion and surface coverage) were obtained by using a simple technique of electrostatic layer-by-layer (LbL) deposition, a well-established technique developed first for poly-electrolytes [10] and later adapted for deposition of other objects, i.e. nanoparticles, biomolecules (proteins, antibodies, enzymes, DNA, etc.) [9, 11]. Multi layered films of graphene were deposited onto gold coated glass microscope slides by alternating layers of a graphene-surfactant with oppositely charged polyelectrolytes, e.g. graphene(+)CTAB layers alternated with polyanionic layers of polystyrene sulfonate sodium salt (PSS), while graphene(-)SDS was alternated with layers of polycationic species such as polyallylamine hydrochloride (PAH) or polyethyleneimine (PEI). Alternating layers of graphene(-)SDS and graphene(+)CTAB was also attempted. The films were deposited by consecutive dipping of gold coated glass or silicon wafers into 1 mg ml^{-1} solutions of the above chemicals in deionised water. The mutlilayered films obtained were then characterised with scanning SEM combined with EDX (energy dispersing X-ray) elemental analysis (SEM NOVA) and AFM.

2.4 Optical characterisation of thin graphene-surfactant films

2.4.1 Spectroscopic ellipsometry study

UV-vis spectra of graphene-surfactant samples are featureless showing almost constant absorbance over the spectral range of 350 - 800 nm, while the main absorption band of graphene lies in UV at about 280 nm. Therefore, optical properties of novel graphene-surfactant composites were studied via spectroscopic ellipsometry using a J. A. Woollam M2000 instrument operating in the 370 - 1000 nm spectral range. The measurements were performed on graphene-surfactant films deposited on different substrates, i.e. glass, silicon, and gold-coated glass. Experimental parameters were found by fitting data, the procedure for which is explained in the results and discussion section below.

For the LbL deposition of alternating layers of graphene(-)SDS and graphene(+)CTAB on gold-coated glass slides, a gold film of approximately 25 nm thickness was thermally evaporated onto a 3 nm under layer of chromium (which was used to improve adhesion between the gold and the glass). Metal evaporation was carried out in a vacuum of 10^{-6} Torr using an Edwards 360 unit. Prior to LbL deposition, gold coated slides were treated overnight in cystamine hydrochloride solution in order to make the gold surface positively charged. Then LbL deposition started with the layer of graphene(-)SDS (negatively charged) followed by deposition of graphene(+)CTAB (positively charged). This procedure was repeated four times, so that four graphene bilayers were deposited. Layer by layer deposition onto other substrates was performed in a similar manner.

2.4.2 TIRE study

The surface plasmon resonance (SPR) phenomenon in graphene films deposited on thin films of gold was studied in more detail using the method of total internal reflection ellipsometry (TIRE) which was developed in the last decade [12-14]. TIRE experimental set-up (shown

schematically as inset in Fig. 12) was built on the basis of J.A. Woollam M2000 spectroscopic instrument in which the light is coupled into a thin gold film deposited on glass through a 68^{o} prism providing total internal reflection conditions. The cell attached underneath allows measurements in different media. The advantage of using TIRE is in 10-fold sensitivity enhancement as compared to traditional SPR [15]. The samples were constructed by electrostatic LbL deposition of PEI and graphene(-)SDS on chromium/gold coated glass slides, as described above.

3. Results and Discussion

3.1 Characterisation of graphene-surfactant composite material

Graphene was synthesised using graphite suspensions of 10 - 50 % using either SDS or CTAB as the surfactants. The concentration of the final graphene solution obtained from each synthesis was determined by spectrophotometry (Figure 2).

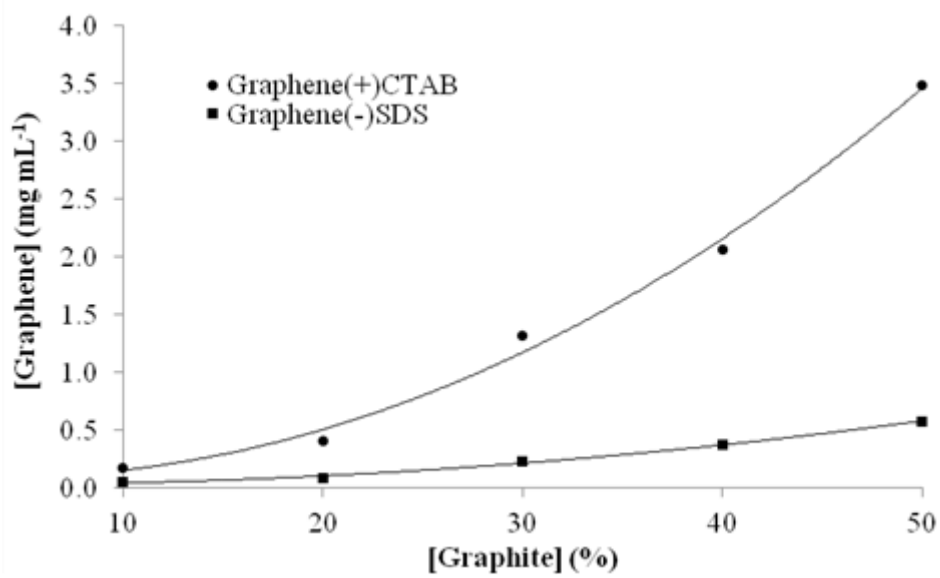

Figure 2. Effect of initial graphite suspension concentration in water on final graphene concentration after sonication for 120 minutes in the presence of different surfactants.

The ^{1}H-NMR of the graphene-surfactant complex, when compared to the ^{1}H-NMR of the surfactant alone, shows shifting of peaks representing hydrogens involved in the complexation interaction (Figure 3). The data shows a peak shift towards the left for almost every peak. This is a shielding effect caused by the delocalised electrons in the graphene sheet which only occurs when the proton is in close proximity (less than 5 Å) and involved in Van-der-Waals interactions. This suggests that the hydrophobic chains of each surfactant lie flat against the graphene sheet with the exception of carbon-1 (the carbon attached directly to the polar head group), which is pulled away from it by the polar head group and therefore does not undergo as much of a shielding effect in the SDS-graphene complex.

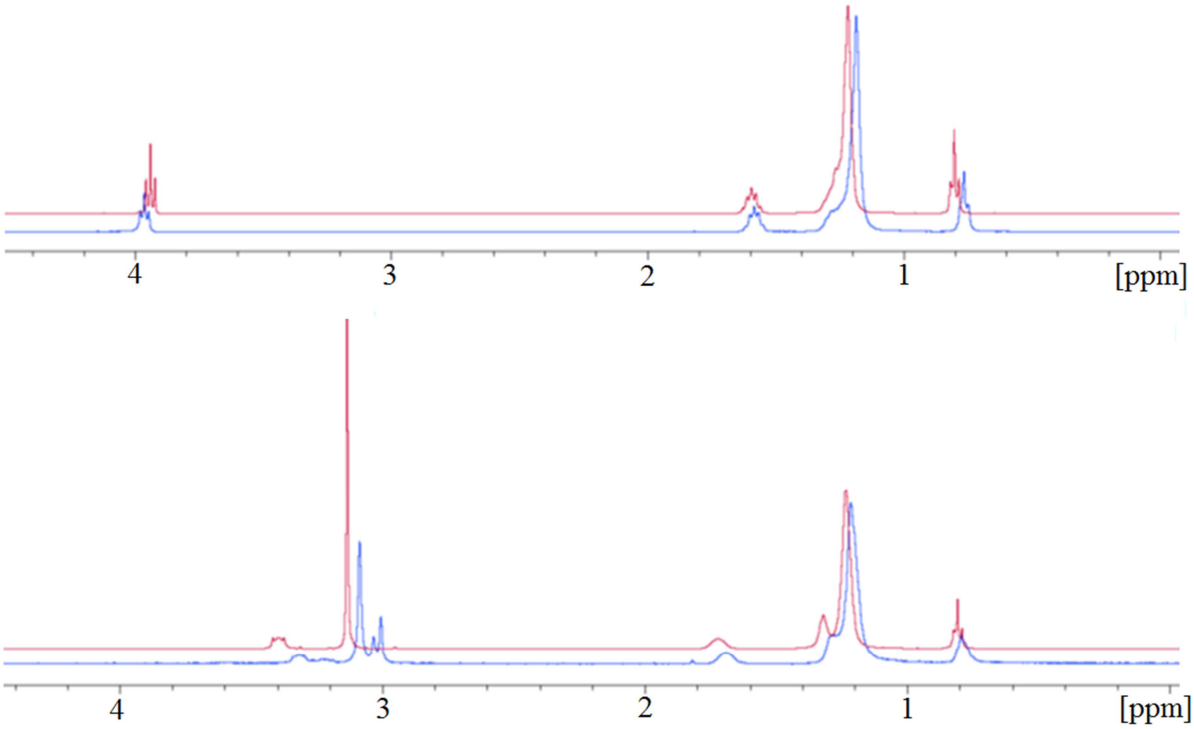

Figure 3. The ^{1}H-NMR of the graphene-surfactant complexes (blue) for SDS (top) and CTAB (bottom) stabilized graphene compared with the surfactant alone (red).

Additionally, for the CTAB-graphene complex, two of the methyl groups on the quaternary amine are interacting with the graphene sheet. This is shown by the splitting of the peak representing them into three peaks. This interaction causes the CTAB to lie much flatter against the graphene than SDS, resulting in the polar head being pulled closer to the sheet. This is why the peak for carbon-1 in the CTAB-graphene complex is displaced further towards the left than its equivalent in the SDS stabilised graphene.

The peak representing carbon-1 in SDS (at around 4 ppm) is shifted downfield by complexation with the graphene. This means that the protons are deshielded by the presence of the graphene. Since the carbon-sulfur bond is polar the electron density around the carbon atom is already lower than it would normally be in a carbon-carbon bond. Repulsion between the graphene and the sulfate group could cause lengthening of the carbon-sulfur bond. This could in turn lead to a lower electron density around the nuclei responsible for this peak [16].

The sample was also analysed using Raman spectroscopy (Figure 4) which, when compared to the spectrum for graphite, was used to verify the presence of graphene. The spectrum shows intense peaks at 1350 cm^{-1} (D) and 1620 cm^{-1} (G & D`). Additionally the peak labelled 2D is slightly broader, between 2650 – 2700 cm^{-1}. This is indicative of graphene flakes with a high number of edge defects [17].

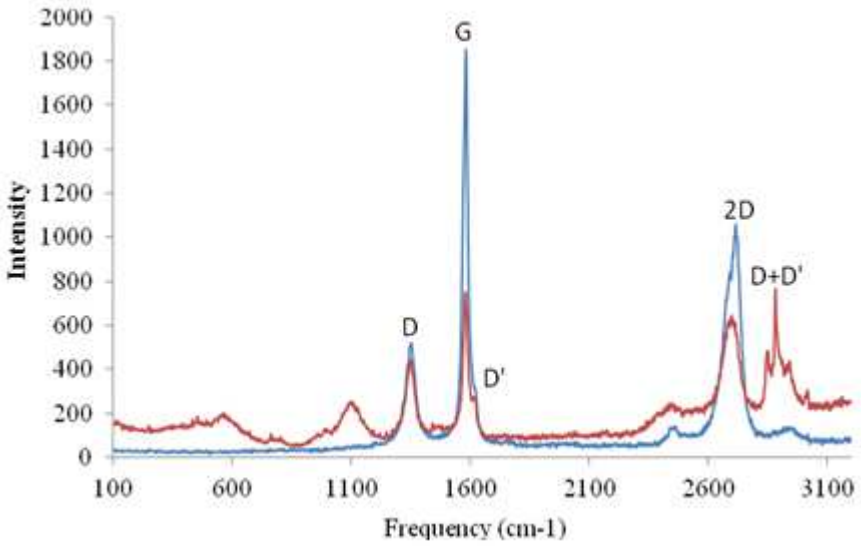

Figure 4. The Raman structure spectrum of surfactant stabilised graphene (red) compared with the spectrum of graphite (blue).

The G band is present in all sp^2 hybridised carbon materials, and is caused by stretching of the C-C bond. The reduction in intensity in the graphene spectrum compared with the graphite spectrum is caused by the reduced number of layers. The D and D' bands are caused by disorder in the graphene flakes. The D' band is present when there are surface defects; such as charging or other impurities adsorbed onto the surface. The D band is caused by edge defects such as a "zig-zag" or "chair" shape on the edge. Edge defects provide an enhancement to electrochemical systems by increasing the total capacitance of the electrode surface. Both the D & D' are not present in pristine graphene with straight edges [17].

The 2D band is also present in many sp^2 hybridized systems and can be used to estimate the number of layers [18]. However the intensity is also dependant on the excitation laser frequency and so cannot be solely relied upon. Further details on the electrochemistry and usage of graphene produced by this method are detailed in another paper [6].

3.2 Deposition of thin films of graphene-surfactant composites.

3.2.1 LB (LS) deposition

Typical surface pressure vs. area diagrams of graphene(+)CTAB in Figure 5 showed formation of a stable monolayer on the water surface, similar to that found for classical amphiphilic compounds. The consecutive compressions of the monolayer did not yield substantial losses of material caused either by the monolayer collapse or dissolving the material in water. Graphene(-)SDS composite showed a similar behaviour.

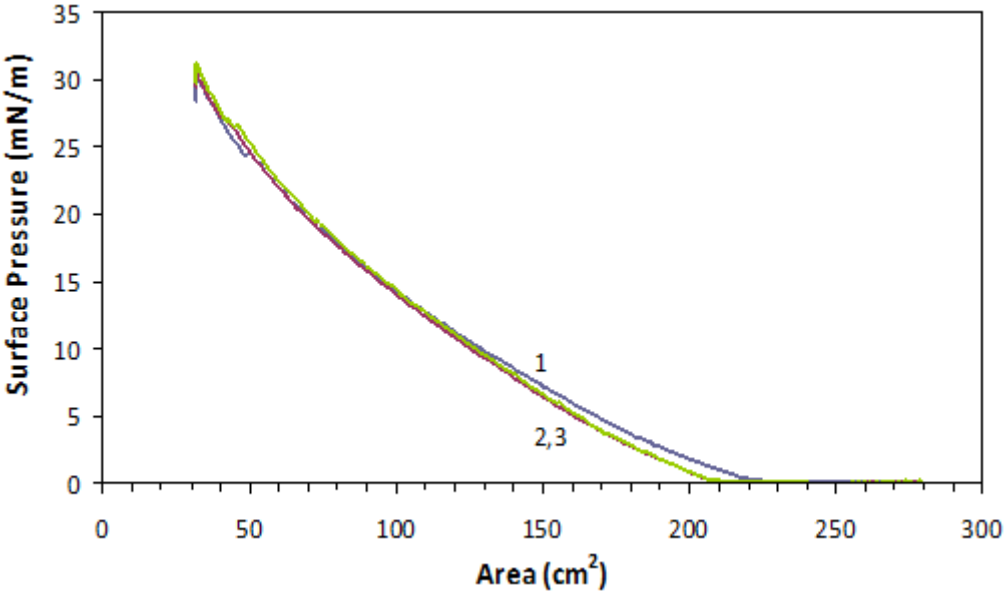

Figure 5. Surface pressure / area isotherms of graphene(+)CTAB monolayers on the water surface; numbers 1, 2, and 3 indicate consecutive compressions of the monolayer.

However, for LB deposition onto hydrophilic substrates such as glass or oxidised silicon, which are slightly negatively charged due the presence of OH^- groups, positively charged graphene(+)CTAB was chosen; as this provided good adhesion between the substrate and monolayer.

Attempts at depositing thin films of graphene(+)CTAB using a traditional LB process, e.g. vertical dipping and withdrawing the substrate through the monolayer, were not successful since the transfer ratio was poor. The first withdrawal yielded about 60%; then the layer was shown to peel off during subsequent dipping cycles. The overall transfer ratio by area (when substrate surface area was compared with graphene LB isotherm) was 10 – 20 %. The most significant cause of this was poor adhesion of the first graphene layer to hydrophilic substrates. This could be improved in future work via the use of substrates with surface modifications which either enhance the surface charge or make the surface more hydrophobic. Much better results were obtained using the horizontal lifting method known as Langmuir-Shaefer (LS) deposition [8]; where the hydrophilic substrate is held horizontally to the assembled monolayer and then lowered slowly to gently touch water surface; the monolayer is then transferred onto the substrate surface. Only a single layer of graphene(+)CTAB could be deposited by LS deposition. Attempts to deposit multilayers by the LS technique failed, as the deposited layers began to peel off upon consecutive depositions.

Organised monolayer films obtained in this fashion were then characterised by AFM (Nanoscope III) operating in tapping mode using Veeco cantilevers with silicon nitride tips having a radius of less than 10 nm. A typical AFM image of graphene(+)CTAB flakes deposited onto a piece of silicon wafer using LS method is shown in Figure 6. The larger scale image (a) shows a number of irregularly shaped graphene(+)CTAB flakes with gaps between; the flakes were sometimes shown to overlap, forming double and sometimes triple layers. Image (b) shows, a pseudo 3D image of a flat individual flake of about 500 nm in size with another smaller flake lying on top.

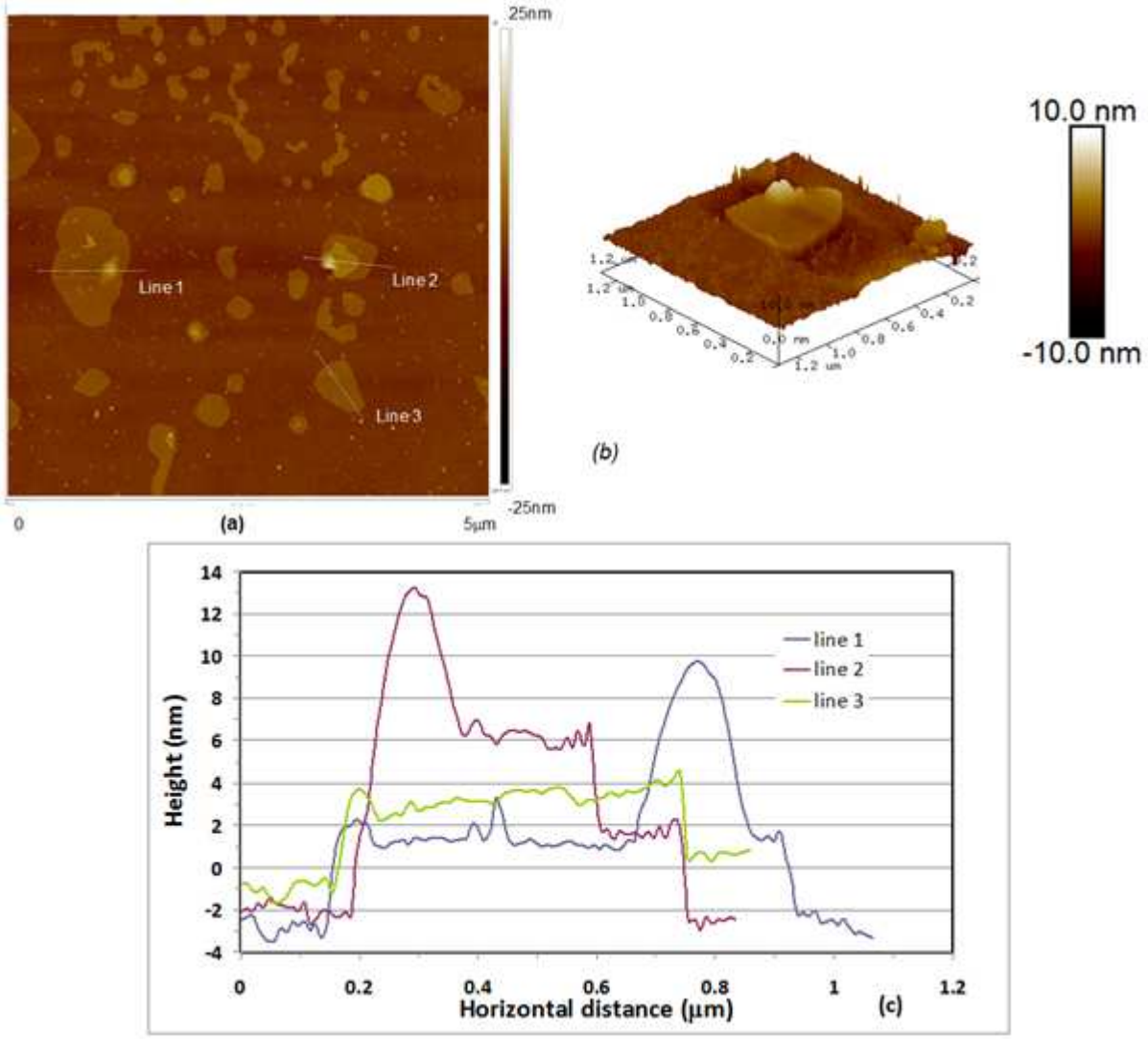

Figure 6. AFM images of the same sample of a graphene(+)CTAB layer deposited onto a silicon substrate using the LS method: (a) 2D image 5 μm; (b) pseudo-3D image of individual graphene flake. (c) Sectional analysis of the image in (a).

Sectional analysis of AFM image along the lines shown, allows for an estimation of the graphene(+)CTAB flake thickness at 2 nm, which is significantly higher than the reported thickness of pristine graphene of 0.355 nm [19]. The obtained value of 2 nm for an individual graphene(+)CTAB is likely due to the presence of surfactant molecules, CTAB in this case.

It is clear from these images that the surface coverage is not optimal. Additionally the graphene flakes were seen to change position and shape during scanning, suggesting poor adhesion to the silicon surface. This could potentially be overcome in future work by using surface modified silicon wafers for sample deposition.

3.2.2 Electrostatic LbL deposition

The multi layered films obtained from layer-by-layer deposition method were characterised with scanning SEM combined with EDX (energy dispersing X-ray) elemental analysis (SEM NOVA) and AFM.

Not all alternating combinations worked well, however. For example, the most promising combination of graphene(+)CTAB with graphene(-)SDS was not successful, while the alternation of graphene(+)CTAB with PAH (or with PEI) proved to be the most optimal. Deposition on glass or silicon samples was performed by electrostatic adsorption of PAH (or PEI) for 20 - 30 min followed by dipping into a solution of graphene(-)SDS for 10 - 15 min. This sequence was repeated several times with a typical incubation time of 10 - 15 min.

Figure 7 shows an SEM image of alternating layers of PAH and graphene(-)SDS deposited onto a silicon substrate. Separate flakes are clearly visible, the largest of which is approximately 30 μm. EDX spectral analysis (b) performed on a flake show a dominating peak of carbon while on the empty space (c) silicon is the dominant peak. This shows, that the graphene flakes consist predominantly of carbon, with a few trace elements. Deposition of the first few layers gives a less than optimal coverage. The reason for this is likely poor adhesion between layers of graphene(-)SDS and PAH. Deposition of subsequent layers greatly improves the coverage by overlapping adjacent graphene flakes.

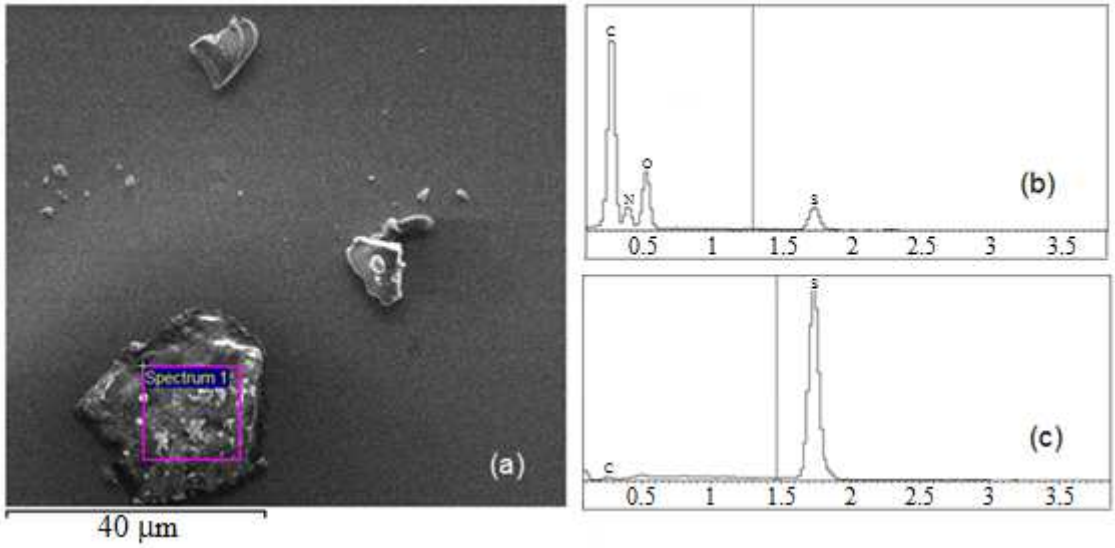

Figure 7. (a) SEM image of PAH/graphene(-)SDS layer on a silicon surface; (b) EDX spectra recorded on a graphene flake, and (c) an empty space.

Adhesion between graphene and substrate was greatly improved when using a stronger polycation such as PEI. The AFM image of graphene(-)SDS deposited onto a layer of PEI in Figure 8 shows far better surface coverage. However it can be seen that graphene flakes overlap and form double and, in some cases, triple layers.

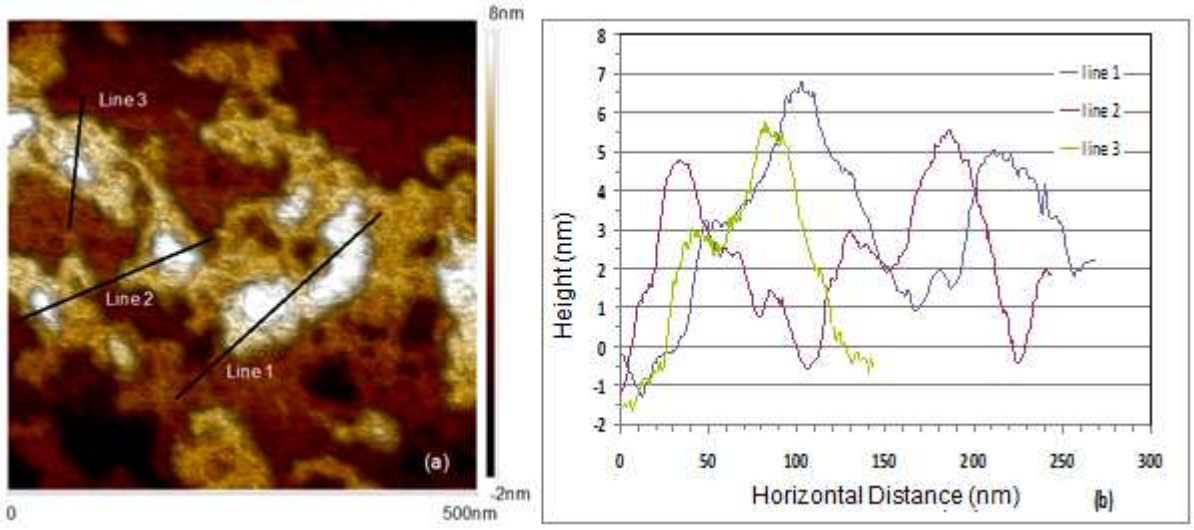

Figure 8. (a) AFM image (tapping mode) of a PEI/graphene(-)SDS film, and (b) a corresponding sectional analysis.

Sectional analysis performed on the sample shows the double and triple layers, and shows the thickness of a single flake at approximately 2.5 nm. This is a somewhat higher than that for LS films in Fig. 6; the difference could potentially be caused by the presence of PEI layer.

3.3 Optical characterisation of thin graphene-surfactant films

3.3.1 Spectroscopic ellipsometry study

The analysis of graphene films by spectroscopic ellipsometry has already been carried out by other groups, and so is fairly well described [20, 21].

Typical set of spectra of spectra of Ψ and Δ of graphene(-)SDS deposited on Si by alternation with PAH are shown in Figure 9a. Numbers 1, 2, and 3 indicate the number of PAH/graphene bilayers deposited. It can be seen from the data that all Ψ spectra almost coincide with each other, while Δ spectra shift downwards upon deposition of bilayers of PAH/graphene(-)SDS.

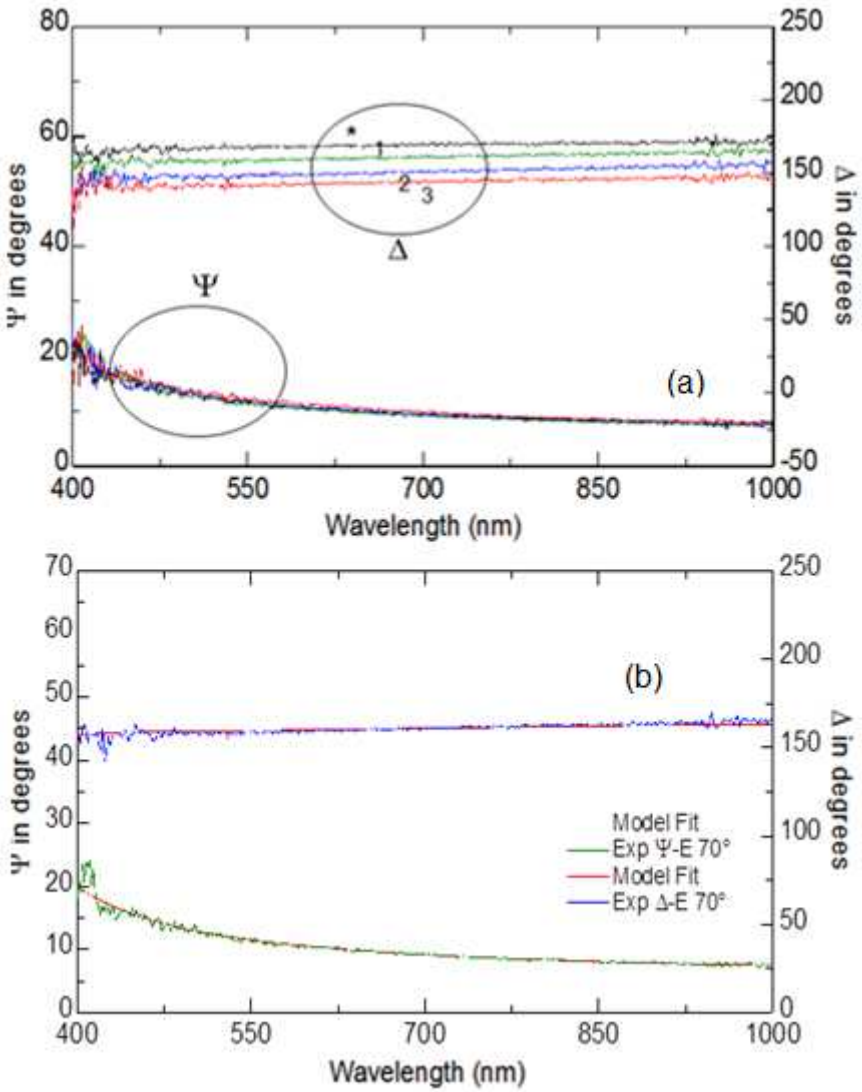

Figure 9. (a) Spectra of ellipsometric parameters Ψ and Δ recorded on a bare silicon surface (*) and on PAH/graphene(-)SDS films deposited on it (the numbers 1, 2, 3 correspond to the number of PAH/graphene bilayers); (b) The example of data fitting for one bilayer of PAH/Graphene deposited on silicon using three-layer model .

The thickness values (*d*) and dispersions, e.g. spectra, of refractive index and (*n*) and extinction coefficient (*k*) of graphene films can be found by fitting the above spectra to the model using dedicated J.A. Woollam software. In this particular case, the model of the reflecting system consists of the following three layers: (1) Si substrate; (2) the layer of native oxide (SiO_2) which is typically present on the surface of Si; (3) the deposited layer of PAH/graphene(-)SDS; the ambient was air. Optical parameters for Si and SiO_2 were taken from J.A. Woollam database). The fitting was first performed for ellipsometric spectra of Si-SiO2 substrate. For the set of data in Figure 9a, the fitting for the thickness of the native SiO_2 layer was performed first using the data for the bare Si substrate. The thickness of SiO_2 layer obtained (d=3.2nm) were then fixed for consecutive fittings. The PAH/graphene(-)SDS film was considered as one layer in the following fittings which is justified by the fact that aliphatic chains of SDS interlock with PAH and form a mixed composite layer of PAH/graphene(-)SDS. Several possible models were tried for fitting PAH/graphene(-)SDS layers, and the best results were achieved using a Lorentz oscillator model from J.A.

Woollam data analysis software which is given below as a dispersion function of a complex dielectric permittivity $\varepsilon(h\nu)$:

$$\varepsilon(h\nu) = \varepsilon_{1\infty} + \sum_k \frac{A_k}{E_k^2 - (h\nu)^2 - jB_k h\nu}$$

where $\varepsilon_{1\infty}$ is the dielectric permittivity at infinitive frequency, E_k, A_k, and B_k are, respectively, the position, amplitude, and half-width of *k*-Lorenzian peak; there could be a number of peaks from 1 to *k*. The best fit was obtained with the use of a single Lorenzian the following parameters: $\varepsilon_{1\infty} = 1.31$; $E_k = 0.625\,eV$; $A_k = 1.759\,(eV)^2$; $B_k = 3.86\,eV$. The presence of Lorenz peak in IR region gives a featureless dispersion of k for graphene-surfactant composite films in visible spectral range similar to that reported in [22, 23]. The absorption peak of graphene reported earlier [22, 23] at about 260 nm is outside the spectral range of our ellipsometric instrument (370 – 1000 nm). The example of ellipsometry data fitting for one PAH/graphene bilayer deposited on Si is shown in Figure 9b with the dotted (fitting) lines almost coinciding with the experimental spectra (solid lines). The thickness was found to be of 6.65 nm, 9.3 nm, and 10.88 nm for 1st, 2nd, and 3rd PAH/graphene bilayer, respectively. Although the *d* value of the first bilayer appeared to be too high, the average thickness increment $\Delta d = 3.63 \pm 2$ nm is reasonable and close to that observed with AFM.

Spectroscopic ellipsometry measurements were carried out on samples after each layer was deposited and similarly to the previous experiments Ψ spectra were not changed much while Δ spectra were shifted downwards upon layers deposition. The ellipsometry data fitting was performed in a similar way as described above using a three layer model containing the substrate glass, chromium/gold layer, and graphene layer, the ambient was air. Parameters *d*, *n(λ)*, and *k(λ)* of chromium/gold layer were found by fitting the data for uncoated samples, and then used as fixed parameters for subsequent fittings. Graphene layers were modeled by Lorenz oscillator as before; the values for thickness obtained are plotted against the graphene layers deposited in Figure 10. As one can see the deposition is not consistent, the graphene layers started to peel off after 3rd deposition most-likely because of poor adhesion between graphene layers. However, the thickness increment of 0.87±0.03 nm in the middle of the graph is much smaller and corresponds to graphene-surfactant layers without the input of intermediate polycation layers.

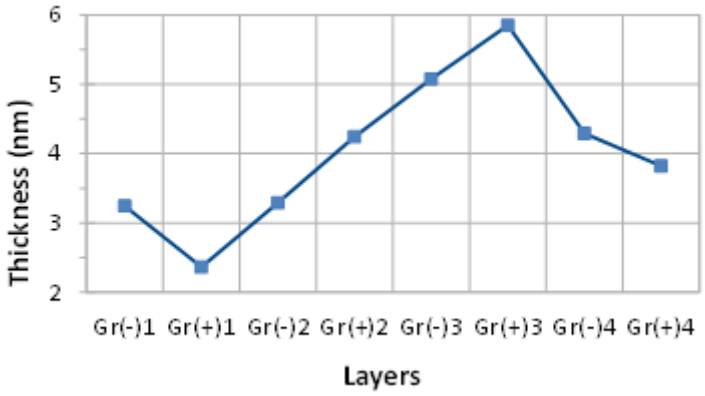

Figure 10. The variation of the film thickness upon deposition of alternating graphene(-)SDS and graphene(+)CTAB graphene layers on Au-gold coated glass slides.

As mentioned above, the use of PEI as a binding layer alternating with graphene(-)SDS improves graphene deposition. The ellipsometry spectra recorded on samples of PEI/graphene(-)SDS deposited on gold-coated glass are shown in Figure 11a. Both Ψ and Δ spectra show the characteristic features at around 450 nm associated with surface plasmon oscillations in thin gold films. Also, the spectra shift upwards and downwards, respectively, upon deposition of PEI/graphene layers which is consistent with the thickness increment of 2.5 nm obtained by fitting of the data in Figure 11a. Following the approach developed in [24], in Figure 11b we attempted to present these data as differential spectra of $\delta\Psi = \Psi - \Psi*$, and $\delta\Delta = \Delta - \Delta*$ ($\Psi*$ and $\Delta*$ correspond to spectra of uncoated gold samples) which allows to clearly distinguish a contribution of deposited layers.

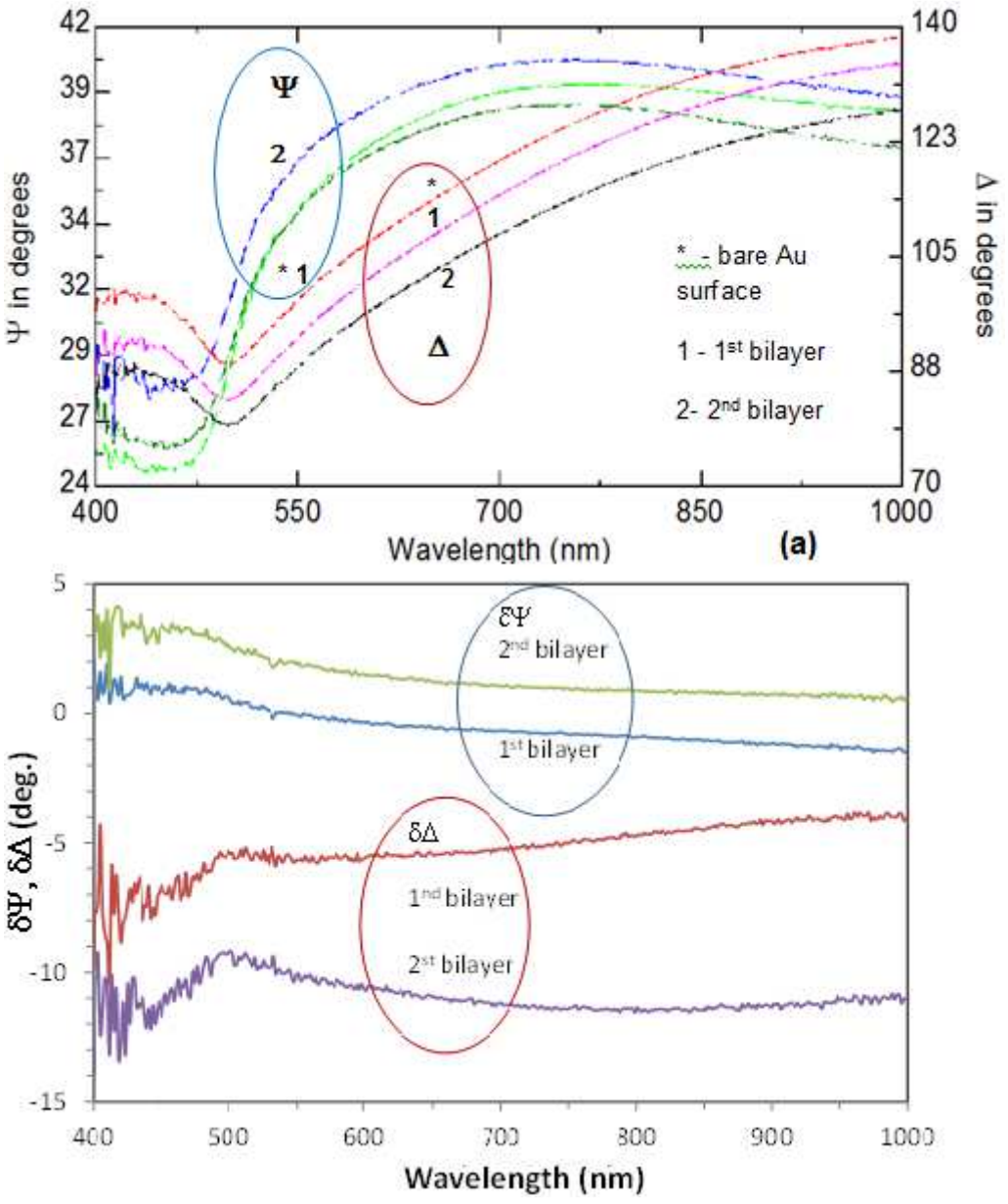

Figure 11. Ψ, Δ (a) and δΨ, δΔ (b) spectra of PEI/graphene(-)SDS films deposited on gold coated glass slides.

It is quite remarkable to observe spectral features around plasmon resonance frequency of gold substrate which are not related to graphene itself [22, 23] but rather appeared as a result of interaction of π-electrons in graphene with free electrons in gold film.

3.3.2 TIRE study

The samples were constructed by electrostatic LbL deposition of PEI and graphene(-)SDS on chromium/gold coated glass slides, as described above. The results obtained are shown in Figure 12 as TIRE spectra of Ψ and Δ. Spectra of Ψ resemble a traditional SPR curve with the maximum corresponding to conditions of total internal reflection of light, while the minimum is the actual plasmon resonance. The spectra of Δ, which do not exist in traditional SPR, represent a new phase related characteristic, show a sharp drop near the resonance wavelength.

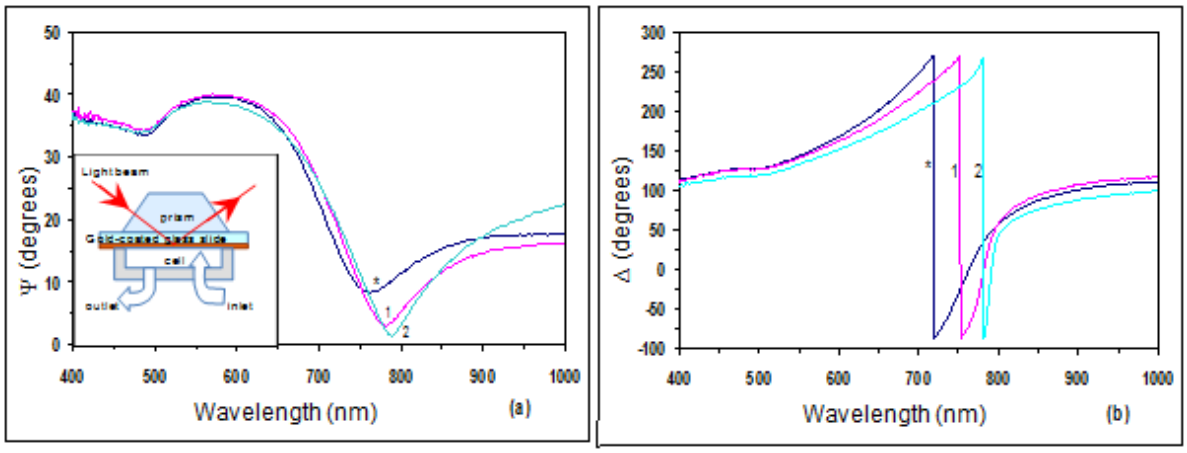

Figure 12. TIRE spectra of (a) Ψ, and (b) Δ recorded on a bare gold-coated glass slide (*) and after deposition of bilayers of PEI/graphene(-)SDS. Numbers 1, 2, and 3 indicate the number of bilayers deposited. The inset shows the geometry of TIRE set-up.

Deposition of graphene layers made the SPR minimum even lower on the Ψ spectra while causing an additional phase shift on Δ spectra. The enhancement of the SPR peak due to the deposition of graphene layers is observed for the first time. It is interesting to note that graphene itself does not show plasmonic behavior in the visible spectral range as was proven by ellipsometry measurements shown before (Fig. 9). At the same time the interaction of π-electrons in graphene and free electrons in gold (which we suspected earlier) may lead to the enhancement of SPR in gold layers. The TIRE data fitting revealed a similar thickness increment of 2.5 nm per PEI/graphene bilayer which was reported earlier.

4. Conclusions

A simple semi-automated technique for graphene production by aqueous sonochemical exfoliation of graphite in the presence of ionic surfactants, e.g. CTAB or SDS, was developed. Full automation could be potentially achieved by adding surface tension sensors to control the amount of surfactant being added to the reactor, thus maintaining a constant and optimum surface tension. The formation of individual graphene flakes and the interaction of alkyl chains of the surfactants with graphene were, respectively, confirmed with Raman spectroscopy and NMR measurements.

The two different graphene-surfactant complexes produced (graphene(+)CTAB and graphene(-)SDS) appeared to be soluble in water and thus suitable for electrostatic LbL deposition. Both compounds were also found to be amphiphilic and soluble in chloroform, hence it was possible to form stable monolayers on the water surface. Thin films of the above graphene composites were deposited onto different solid substrates, i.e. silicon, glass and gold-coated glass, using either electrostatic LbL or LB (LS) deposition techniques. SEM and AFM study showed that LB (or LS) films of graphene(+)CTAB had poor surface coverage and adhesion to the substrate. Electrostatic LbL deposition of graphene by alternation of graphene with oppositely charged polyelectrolytes was much more promising in these aspects. Several combinations of materials were tried including the alternation of graphene(+)CTAB and graphene(-)SDS. The best results were achieved by alternation of graphene(-)SDS with PEI. AFM study allowed the estimation the thickness of an individual graphene-surfactant flakes of about 2 - 2.5 nm.

The spectroscopic ellipsometry study of graphene thin films gave similar values for the thickness of the graphene-surfactant composite layer. While the dispersions of refractive index and extinction coefficient were modelled by a single Lorenzian peak lying in IR region, the absorption peak of graphene at approximately 260 nm was outside the spectral range (370 – 1000 nm) of the ellipsometric instrument. Interesting results were obtained when studying the SPR effect in gold films coated with a few layers of graphene using both external and internal (TIRE) reflection ellipsometry. Although graphene itself shows no spectral features associated with plasmon oscillations in the above spectral range, the deposition of graphene layers on gold progressively enhances the plasmon resonance on TIRE Ψ-spectra and caused an extra phase shift on TIRE Δ-spectra. This phenomenon can be explored in future for enhancing the performance of SPR-based bio-sensors.

Acknowledgements
The authors would like to acknowledge Dr Isaac Chang and Dr Shei Su of the University of Birmingham for Raman measurements.

References
[1] Novoselov, K. S.; Geim, A. K.; Morozov, S. V.; Jiang, D.; Zhang, Y.; Dubonos, S. V.; Grigorieva, I. V.; Firsov, A. A., *Science*, **2004**, 306, 666 - 669.
[2] Sharma, B. K.; Ahn, J., *Solid-State Electronics*, **2013**, 89, 177 - 188.
[3] Torrisi, F.; Hasan, T.; Wu, W.; Sun, Z.; Lombardo, A.; Kulmala, T. S.; Hsieh, G.; Jung, S.; Bonaccorso, F.; Paul, P. J.; Chu, D.; Ferrari, A. C., *ACS Nano*, **2012**, 6, 2992 – 3006.
[4] Notley, S. M.*; Langmuir*, **2012**, 28**,** 40, 14110 - 14113.
[5] Hummers Jr. W. S.; Offeman, R. E., *Journal of the American Chemical Society*, **1958**, 80, 1339.
[6] Walch, N. J.; Davis, F.; Langford, N.; Holmes, J. L.; Collyer, S. D.; Higson, S. P. J.; *Analytical Chemistry*, **2015,** 87, 9273 – 9279.
[7] Fan, J.; Shi, Z.; Ge, Y.; Wang, J.; Wang, Y.; Yin, J., *Journal of Materials Chemistry*, **2012**, 22, 13764 - 13772.
[8] Petty M. C., Langmuir-Blodgett Films. An introduction, Cambridge University Press: Cambridge, 1996.
[9] Nabok, A., Organic and Inorganic Nanostructures, Artech House: London, 2005.
[10] Lvov, Y.; Decher, G.; Möhwald, H., *Langmuir*, **1993**, 9, 481 - 486.
[11] Lvov, Y.; Decher, G.; *Crystallography Reports*, **1994**, 39, 696 - 616.

[12] Westphal, P.; Bornmann, A.; *Sensors and Actuators B*, **2002**, 84, 278 - 282.
[13] Poksinski, M.; Arwin, H.; *Sensors and Actuators B*, **2003**, 94, 247 – 252.
[14] Nabok, A.; Tsargorodskaya, A.; Hassan, A. K.; Starodub, N. F.; *Applied Surface Science*, **2005**, 246, 381 – 386.
[15] Nabok, A.; Tsargorodskaya, A.; *Thin Solid Films*, **2008**, 516, 8993 - 9001.
[16] Webb, G. A.; Modern Magnetic Resonance: Applications in Chemistry, Biological and Marine Sciences, Springer: Dordrecht, 2008.
[17] Huang, C. H.; Su, C. Y.; Okada, T.; Li, L. J.; Ho, K. I.; Li, P. W.; Chen, I. H.; Chou, C.; Lai, C. S.; Samukawa, S.; *Carbon N. Y.* **2013**, 61, 229 – 235.
[18] Matthews, M. J.; Pimenta, M. A.; Dresselhaus, G.; Dresselhaus, M. S.; Endo, M.; *Phys. Rev. B - Condens. Matter Mater. Phys.* **1999**, 59, R6585 - R6588.
[19] Gupta, A.; Chen, G.; Joshi, P.; Tadigadapa, S.; Eklund. P. C., *Nano Letters*, **2006**, 6, 2667 - 2673.
[20] Isić, G.; *J. Nanophotonics* **2011**, 5, 051809.
[21] Losurdo, M.; Giangregorio, M. M.; Bianco, G. V.; Capezzuto, P.; Bruno, G.; *Thin Solid Films* **2014**, 571, 389 – 394.
[22] Kravets, V. G.; Grigorenko, A. N.; Nair, R. R.; Blake, P.; Anissimova, S.; Novoselov, K. S.; Geim, A. K.; *Physical Review B*, **2010**, 81, 155413 - 155416.
[23] Weber, J. W.; Calado, V. E.; van de Sanden, M. C. M.; *Applied Physics Letters*, 2010, **97**, 91903 - 91904.
[24] Prato, M.; Moroni, R.; Bisio, F.; Rolandi, R.; Mattera, L.; Cavalleri, O,; Canepa, M.; J.

Appendix 3: Semi-Automated Sonochemical Synthesis of Graphene by Continuous Addition of Aqueous Surfactant

*This work was presented at the 14th European Conference on Organised Films in 2015.

Semi-Automated Sonochemical Synthesis of Graphene by Continuous Addition of Aqueous Surfactant

[1]Walch, N J., [1]Davis, F., [2]Nabok, A & [1]Higson, S P J.

[1]Cranfield Biotechnology Centre, Cranfield University, College Road, Cranfield, MK43 0AL, UK

[2]Materials and Engineering Research Institute, Sheffield Hallam University, Howard Street, Sheffield, S1 1WB, UK

A novel apparatus is described for the continuous addition of surfactant during graphene synthesis which produces pristine graphene flakes. The presence of graphene has been verified by Raman spectroscopy and AFM.

Introduction

Since its initial discovery and development by Novoselov *et al.* (2004), graphene has been of great interest to the scientific community due to its interesting optical and electrical properties. Graphene is defined as a single layer of sp^2 hybridised carbon with no 3rd dimension. The aromatic structure of graphene is responsible for the electrical properties of the material as the flipping of π-bonds between adjacent carbon atoms can be used to transmit an electrical current. Because of this electrical activity in particular, graphene is being examined as a base material in a number of different applications including sensors, the use in flexible electronics (Sharma & Ahn, 2013) and graphene based printable inks for printed electrical circuits (Torrisi *et al.*, 2012).

Graphene has reportedly been produced by a number of different methods, however the method chosen for this research was by sonochemical exfoliation. This is achieved by sonication of an aqueous suspension of graphite powder in the presence of a surfactant, as reported by Notley *et al.* (2012). A downside of this method is that the surfactant must be added slowly to maintain a constant surface tension of 41 mJ m^{-2} or significant yields of graphene will not be produced. This is a time consuming and labour intensive process. A semi-automated method to alleviate some of these issues is described here.

Apparatus

The function of the apparatus (schematic shown in Figure 1) for the production of graphene is explained thusly. The aqueous suspension of graphite is placed into the reactor (E). The graphite is kept in suspension throughout the procedure using a magnetic stirrer (G). The ultrasonic probe (D) operating at a power of 50 W, penetrates approximately 1 cm into the graphite suspension. The surfactant solution (A) is pumped into the reactor via a peristaltic pump (B). The reservoir containing the surfactant and the tubing carrying it to the reactor are heated to 60ºC in a water bath (C) to prevent precipitation of the surfactant from solution. A water trough (F) is used as a heat sink to dissipate any heat produced in the reactor during synthesis, as the ultrasonic probe can reach temperatures of 100ºC during continuous operation. The heat sink is stirred continuously, also using the magnetic stirrer (G), to maximise cooling efficiency.

A sampling loop (H) continuously cycles the liquid contents of the reactor through a photometric flow cell (I) which determines the concentration of graphene by measured absorbance at 650 nm. The concentration data is then recorded using a data logger.

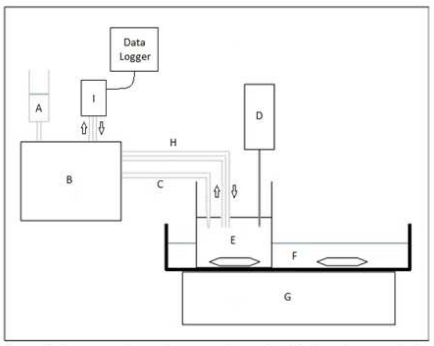

Figure 1 – Apparatus for semi-automated sonochemical graphene synthesis.

Methodology

Graphene was prepared using the apparatus described in Figure 1 before analysis. Particle sizing was performed using dynamic light scattering and concentration was determined using absorbance at 650 nm with an extinction coefficient of 13.9 mg^{-1} mL^{-1} cm^{-1} (Notley *et al.*, 2012). Graphene suspension with no unbound surfactant was obtained by washing the remaining graphite with distilled water after the initial graphene suspension had been removed. This pure graphene suspension was then freeze dried and placed into a vacuum oven to remove all traces of water. The dry sample was analysed using Raman spectroscopy to verify the presence of graphene and then by ^{1}H-NMR to show the binding relationship between the surfactant and the graphene surface.

Results

Graphene was synthesised using graphite suspensions of 10 - 50 % using either sodium dodecyl sulfate (SDS) or cetyl trimethylammonium bromide (CTAB) as the surfactants. The concentration of the final graphene solution obtained from each synthesis was determined by spectrophotometry (Figure 2).

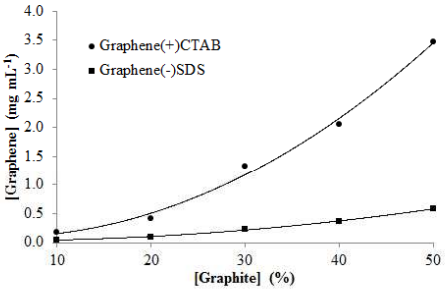

Figure 2 – Effect of initial graphite suspension concentration on final graphene concentration.

The size of the graphene flakes was determined using dynamic light scattering (DLS). The results showed that the graphene(-)SDS had a mean size of 214.2 ± 10.4 nm with a polydispersity of 0.405 ± 0.037. The graphene(+)CTAB had a mean size of 264.5 ± 5.0 nm with a polydispersity of 0.264 ± 0.023. High resolution images of the graphene flakes were obtained using atomic force microscopy (AFM), which are shown in Figure 3.

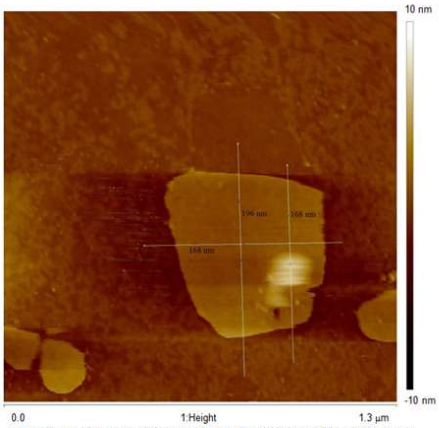

Figure 3 – Atomic force micrograph of a deposited thin film of graphene.

The sample was also analysed using Raman spectroscopy (Figure 4) which, when compared to the spectrum for graphite, was used to verify the presence of graphene.

The spectrum for graphene shows a change in the ratio of peaks D : G, and the D` peak is more pronounced when compared to the graphite spectrum. Additionally the peak labelled 2D is slightly broader and less intense. This is indicative of graphene flakes with a high number of edge defects.

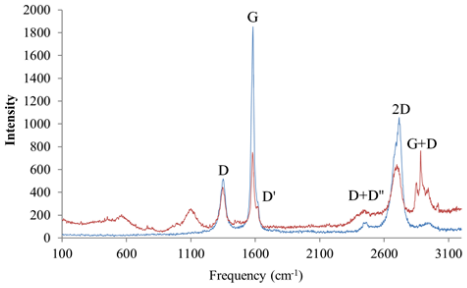

Figure 4 – The Raman spectra of graphene (red) and graphite (blue).

The ^{1}H-NMR of the graphene-surfactant complex, when compared to the ^{1}H-NMR of the surfactant alone (Figure 5), shows shifting of the peaks representing hydrogens involved in the complexation interactions. The data shows a peak shift towards the right (upfield) for almost every peak. This is a shielding effect caused by the delocalised electrons in the graphene sheet which occurs when the surfactant's protons are in close proximity and involved in Van-der-Waals interactions with the graphene. This suggests that the hydrophobic chains of each surfactant lie flat against the graphene sheet with the exception of carbon-1, which is pulled away from it by the polar head group and therefore does not undergo as much of a shielding effect in the SDS-graphene complex.

Additionally, for the CTAB-graphene complex, two of the methyl groups on the quaternary amine are interacting with the graphene sheet. This is shown by the splitting of the peak representing them into three peaks. This interaction causes the CTAB to lie much flatter against the graphene than SDS, resulting in the polar head being pulled closer to the sheet. This is why the peak for carbon-1 in the CTAB-graphene complex is displaced further towards the right than its equivalent in the SDS stabilised graphene.

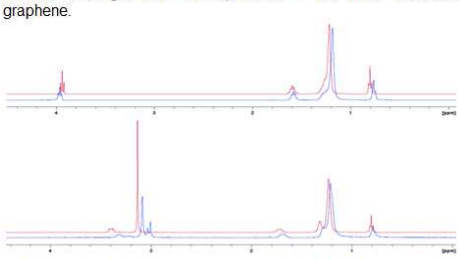

Figure 5 – The ^{1}H-NMR, in D_2O, of the graphene-surfactant complexes (blue) for SDS (top) and CTAB (bottom) stabilized graphene compared with the surfactant alone (red).

Conclusions

The novel apparatus was used to great effect as a method for producing high concentrations of graphene in a manner that was not labour intensive. The graphene flakes produced had a relatively uniform size distribution and a high number of edge defects. This makes them useful for a number of future applications, such as the enhancement of electrochemical based sensors, which are currently being assessed in on-going studies.

Acknowledgements

The authors would like to acknowledge Dr Isaac Chang and Dr Shei Su of the University of Birmingham for Raman measurements and Kevin Osborne at Sheffield Hallam University for the NMR data.

References:

Notley, S M. (2012) *Highly concentrated aqueous suspensions of graphene through ultrasonic exfoliation with continuous surfactant addition,* Langmuir, **28,** (40), pp 14110-3.

Novoselov, K S., Geim, A K., Morozov, S V., Jiang, D., Zhang, Y., Dubonos, S V., Grigorieva, I V & Firsov, A A. (2004) *Electric field in atomically thin carbon films,* Science, **306,** (5696), pp 666-9.

Sharma, B K. & Ahn, J. (2013) *Graphene based field effect transistors: Efforts made towards flexible electronics,* Solid-State Electronics, **89,** pp 177-88.

Torrisi, F., Hasan, T., Wu, W., Sun, Z., Lombardo, A., Kulmala, T S., Hsieh, G., Jung, S., Bonaccorso, F., Paul, P J., Chu, D & Ferrari, A C. (2012) *Inkjet-printed graphene electronics,* ACS Nano, **6,** (4), pp 2992-3006.